University of Alberta

Methods to Control Molecular Structure and Function in Supramolecular Chemistry

by

Tyler B. Norsten ©

A thesis submitted to the Faculty of Graduate Studies and Research in partial fulfillment
of the requirements for the degree of
Doctor of Philosophy

Department of Chemistry

Edmonton, Alberta

Fall 2001

National Library
of Canada

Acquisitions and
Bibliographic Services

395 Wellington Street
Ottawa ON K1A 0N4
Canada

Bibliothèque nationale
du Canada

Acquisitions et
services bibliographiques

395, rue Wellington
Ottawa ON K1A 0N4
Canada

Your file Votre référence

Our file Notre référence

The author has granted a non-exclusive licence allowing the National Library of Canada to reproduce, loan, distribute or sell copies of this thesis in microform, paper or electronic formats.

The author retains ownership of the copyright in this thesis. Neither the thesis nor substantial extracts from it may be printed or otherwise reproduced without the author's permission.

L'auteur a accordé une licence non exclusive permettant à la Bibliothèque nationale du Canada de reproduire, prêter, distribuer ou vendre des copies de cette thèse sous la forme de microfiche/film, de reproduction sur papier ou sur format électronique.

L'auteur conserve la propriété du droit d'auteur qui protège cette thèse. Ni la thèse ni des extraits substantiels de celle-ci ne doivent être imprimés ou autrement reproduits sans son autorisation.

0-612-69839-4

Canada

University of Alberta

Library Release Form

Name of Author: Tyler B. Norsten

Title of Thesis: Methods to Control Molecular Structure and Function in Supramolecular Chemistry

Degree: Doctor of Philosophy

Year this Degree Granted: 2001

Permission is hereby granted to the University of Alberta Library to reproduce single copies of this thesis and to lend of sell such copies for private, scholarly or scientific research purposes only.

The author reserves all other publication and other rights in association with the copyright in the thesis, and excepts as herein before provided, neither the thesis nor any substantial portion thereof may be printed or otherwise reproduced in any material form whatever without the author's prior written permission

Tyler Norsten

Box 7644
Bonnyville, AB
T9N 2H9

28
September 2001

University of Alberta

Faculty of Graduate Studies and Research

The undersigned certify that they have read, and recommend to the Faculty of Graduate Studies and Research for acceptance, a thesis entitled Methods to Control Molecular Structure and Function in Supramolecular Chemistry submitted by Tyler B. Norsten in partial fulfillment of the requirements for the degree of Doctor of Philosophy.

Associate Professor Neil R. Branda

D. L. J. Clive

Professor Derrick Clive

Martin Cowie

Professor Martin Cowie

Assistant Professor Dennis Hall

E. E. Knaus

Professor Edward Knaus

D. L. J. Clive

Professor Reginald Mitchell

In memory of my mother

Rosemarie Norsten

March 16, 1945, July 13, 2001

Abstract

Specific approaches used to control molecular structure and function are discussed. The first approach utilizes self-assembly synthesis to position large photoactive building blocks into well-defined supramolecular architectures. The assemblies were constructed for applications in synthetic light harvesting.

Anionic porphyrins and cationic iron(terpyridine)s that contain complimentary hydrogen bond surfaces were designed and synthesized . The combination of ion pairing and cooperative hydrogen bonding afforded highly stable well-ordered complexes. Steady-state fluorescence experiments showed that the fluorescence of the porphyrin was quenched by the iron(terpyridine) upon complex formation. Possible modes of fluorescence quenching are discussed.

The second approach focuses on the use of photochromic molecular switches, which are molecules that interconvert between two isomers in response to a light stimulus. The spectroscopic changes that accompany the structural transformations of the photochromes are applied to develop photochromic-based materials for information processing.

Porphyrins were covalently and non-covalently appended to dithienylethene photochromes. The emission properties of the porphyrins within the hybrid systems could be regulated by controlling the state (*open* or *closed*) of the dithienylethene photochrome.

This formed the basis of a write-read-erase storage device that employs changes in emission intensity as the readout process.

Photochromic chiral dithienylethenes formed optically pure helicates in a spontaneous stereoselective self-assembly process. The rigid positioning of the photochrome within the helicate resulted in the preferential formation of only one of the possible stereoisomers during the *ring-closing* photochromic reaction. The two-states of the photochrome exhibited large variations in their ORD spectra. This optical rotation formed the basis for a non-destructive write-read-erase system.

A dithienylethene photochrome was incorporated into a helicene backbone. The twisted structure of a [7]-thiahelicene could be turned "on" and "off" by alternate irradiation with UV and visible light. Attempts were made to form the extended [9]-thiahelicene system but it was found to be non-photochromic.

Dithienylethenes were derivatized with 2-aminopyridine. The fluorescence and redox properties of the resulting molecules could be modulated by controlling the state (*open* or *closed*) of the photochrome. A non-photochromic macrocycle containing two dithienylethene moieties was isolated and characterized by X-ray crystallography.

Preface

Outline of Thesis and Allocation of Work Described

The body of this thesis is divided into two units separated on the basis of the distinct mechanism used to control molecular structure and function. Bracketing this body of work is a detailed introduction to the thesis including a description of the general approaches to the control of molecular structure and function and specific concepts that are applied throughout and a conclusion that ultimately ties the separate approaches together.

The thesis units open with an introduction detailing selected examples showing the control of molecular structure and function setting the stage for the chapters that follow. All of the chapters are formatted identically and commence with a specific introduction to that chapter followed by a paper as it appears in published or submitted form. The paper is then followed by a detailed discussion of the work highlighting its impact and relevance to the area. Also discussed in this section is pertinent information that was not included in the body of the paper. Finally, each chapter ends with an experimental section detailing applicable procedures and apparatus. The references are located directly following the experimental sections at the end of each chapter. The thesis concludes with a appendices that detail some unpublished work and any relevant data.

The following is a list of published or submitted papers that are discussed in this thesis:

1) *A Remarkably Stable Hydrogen Bonded Porphyrin•Iron(Terpyridine) Ion Pair* Tyler B. Norsten, Kelly Chichak and Neil R. Branda *Chem. Commun.* In print

2) *Strong and Directed Association of Porphyrins and Iron (Terpyridine)s using Hydrogen-Bonding and Ion Pairing* Tyler B. Norsten, Kelly Chichak and Neil R. Branda *Tetrahedron.* Accepted for publication.

3) *Photoregulation of Fluorescence in a Porphyrinic Dithienylethene Photochrome* Tyler B. Norsten and Neil R. Branda *J. Am. Chem. Soc.* **2001**, *123*, 1784.

4) *Axially Coordinated Porphyrinic Photochromes for Non-destructive Information Processing* Tyler B. Norsten and Neil R. Branda *Adv. Mater.* **2001**, *13*, 347.

5) *Nondestructive Data Processing Based on Chiroptical 1,2-Dithienylethene Photochromes* Elisa Murguly, Tyler B. Norsten and Neil R. Branda *Angew. Chem. Int. Ed.* **2001**, *40*, 1752.

6) *Reversible [7]-Thiahelicene Formation Using a 1,2-Dithienylcyclopentene Photochrome* Tyler B. Norsten, Andrea Peters, Robert McDonald, Meitian Wang, Neil R. Branda *J. Am. Chem. Soc.* **2001**, *123*, 7447.

In the cases where T. B. Norsten is cited as the first author, I was responsible for writing the manuscript and N. R. Branda was responsible for editing the written manuscript. The one instance where I am a second author (entry 5), I contributed equally to the writing of the manuscript.

In the cases where T. B. Norsten and N. R. Branda are the only authors all work described in the manuscript was preformed by T. B. Norsten. In the other cases the allocation of work is specified below.

- *A Remarkably Stable Hydrogen Bonded Porphyrin•Iron(Terpyridine) Ion Pair* Tyler B. Norsten, Kelly Chichak and Neil R. Branda *Chem. Commun.* In print.

  All work described in this manuscript was preformed by T. B. Norsten. K. Chichak worked on a preexisting system and had intellectual input into the system described in the manuscript.

- *Strong and Directed Association of Porphyrins and Iron (Terpyridine)s using Hydrogen-Bonding and Ion Pairing* Tyler B. Norsten, Kelly Chichak and Neil R. Branda *Tetrahedron.* Accepted for publication.

  All work described in this manuscript was preformed by T. B. Norsten with the exception of the 4 synthetic steps required to transform **8** into **11** which were performed by K. Chichak.

- *Nondestructive Data Processing Based on Chiroptical 1,2-Dithienylethene Photochromes* Elisa Murguly, Tyler B. Norsten and Neil R. Branda *Angew. Chem. Int. Ed.* **2001**, *40*, 1752.

  All synthetic transformations and the initial CD and ORD studies were performed by T. B. Norsten. E. Murguly was responsible for the ^{1}H NMR,UV-Vis, and ORD studies described in the manuscript.

- Reversible [7]-Thiahelicene Formation Using a 1,2-Dithienylcyclopentene

Photochrome Tyler B. Norsten, Andrea Peters, Robert McDonald, Meitian Wang, Neil R. Branda *J. Am. Chem. Soc.* **2001**, *123*, 7447.

All work described in this manuscript was preformed by T. B. Norsten with the exception of the synthetic steps required to transform, **4** into **1a**, **5** into **2** and **6** into **3a** which was performed by A. Peters. A. Peters also responsible for the Single point energy calculations. The crystal structures of **1a** and **1b** were solved by R.

Table of Contents

Unit 1 - Chapter 1 - Methods to Control Molecular Structure and Function in Supramolecular Chemistry **1**

1.1.1 Levels of Controlling Molecular Structure 2

    1.1.1.1 Level 1 - Synthetic Control 3

    1.1.1.2 Self-Assembly Synthesis 3

    1.1.1.3 Level 2 - Post-Synthetic Control 5

1.1.2 Summary and Overview 9

1.1.3 Notes and references 10

Unit 2 - Introduction - Controlling Molecular Structure by Self-Assembly Synthesis: Self-Assembling Photoactive Complexes **12**

2.1 The Photosynthetic Reaction Center 12

2.2 References 14

Chapter 2 - Hydrogen Bond Directed Self-Assembly of Porphyrin•Iron (Terpyridine) Ion Pairs **15**

2.2.1 Photochemical Pathways 16

    2.2.2.1 Photoluminescence 16

    2.2.2.2 Energy *vs.* Electron Transfer 18

2.2.2 A Selected Example of a Supramolecular Photoactive Complex 21

2.2.3 A Novel Diatopic Approach to Assembling Large Photoactive Complexes 23

2.2.4 **Paper** A Remarkably Stable Hydrogen Bonded Porphyrin•Iron(Terpyridine) Ion Pair 25
2.2.5 **Paper** Strong and Directed Association of Porphyrins and Iron(Terpyridine)s using Hydrogen Bonding and Ion Pairing 30
2.2.6 Results and Discussion 59
    2.2.6.1 Determination of Association Constants 59
    2.2.6.2 X-ray Crystallographic Analysis of an Iron(Terpyridine) Complex 61
    2.2.6.3 Stern-Volmer Quenching Analysis 63
    2.2.6.4 Modes of Fluorescence Quenching 64
2.2.7 Conclusion 67
2.2.8 References 67

Unit 3 - Introduction - Controlling Molecular Structure and Function with Photochromic Molecules **75**
3.1 Photochromism: Memories and Switches for Non-Destructive Readout 75
3.2 Choice of Photochrome 77
3.2 Ring-Closure of a Dithienylethene 81
3.3 Non-Destructive Detection Techniques for Photochromic Systems 83
3.4 References 87

Chapter 3 - Fluorescence-Based Detection for Non-Destructive Readout **89**
3.3.1 Introduction to Fluorescence-Based Detection 89

3.3.2 **Paper** Photoregulation of Fluorescence in a Porphyrinic Dithienylethene Photochrome **92**
3.3.3 Results and Discussion 97
  3.3.3.1 Synthesis of Photochromes 97
  3.3.3.2 Photophysical Studies: Observation of Indirect Ring-Opening 100
  3.3.3.3 Possible Mode of Indirect Ring-Opening 102
3.3.4 Conclusion 106
3.3.5 Experimental 107
3.3.6 References 113

Chapter 4 - Phosphorescent-Based Detection for Non-Destructive Readout **117**
3.4.1 Back to the Drawing Board: Re-designing our Original System 117
3.4.2 **Paper** Axially Coordinated Porphyrinic Photochromes for Non-Destructive Information Processing **121**
3.4.3 Results and Discussion 126
  3.4.3.1 Synthesis of Axially Coordinated Porphyrinic Photochromes 126
  3.4.3.2 Electronic Communication Between Porphyrins: The Need for a Control Compound 130
  3.4.3.3 Separation of the Active Photochromic Absorption and Porphyrinic Emission Bands 132
3.4.4 Conclusion 133
3.4.5 Experimental 134

3.4.6 References 138

Chapter 5 - Chiroptical-Based Detection for Non-Destructive Readout 142

3.5.1 Chiroptical Methods: Optical Rotatory Dispersion and Circular Dichroism 142

3.5.2 Chirality: Optically Active Chromophores 144

3.5.3 Examples of Chiroptical Photochromes for Non-Destructive Readout 147

3.5.4 **Paper** Non-Destructive Data Processing Based on Chiroptical 1,2 Dithienylethene Photochromes **152**

3.5.5 Results and Discussion 159

  3.5.5.1 Synthesis of Chiral Photochromes 159

  3.5.5.2 X-ray Crystallographic Analysis of the Enantiomeric Helicates 159

  3.5.5.3 Analysis of ORD and CD Spectra 160

3.5.6 Conclusion 163

3.5.7 Future Outlook: A Spontaneously Resolved Photochromic Helicate 164

3.5.8 Experimental 167

3.5.9 References 178

Chapter 6 - Photochromic Control of Helical Topology 183

3.6.1 Dithienylethenes and Helicenes 183

3.6.2 **Paper** Reversible [7]-Thiahelicene Formation using a 1,2-Dithienylcyclopentene Photochrome **187**

3.6.3 Results and Discussion 192

3.6.3.1 Synthesis of Photochromes 192

3.6.3.2 Fluorescence Analysis 194

3.6.3.3 Helical Chirality 195

3.6.3.4 Inhibition of Photochromism: UV-Vis Analysis 197

3.6.4 Conclusion 197

3.6.5 Experimental 199

3.6.5 References 212

Unit 4 - Chapter 7 - Conclusion 217

Appendix I - Photochromic Dithienylalkene Pyridin-2-ylamides 219

I.1 Synthesis of Photochromes 219

I.2 X-ray Crystallographic Analysis 221

I.3 Spectroscopic Analysis of the Photochromes 223

I.3.1 ^{1}H NMR Spectroscopic Analysis 223

I.3.2 UV-Vis Spectroscopic Analysis 224

I.3.3 Fluorescence Analysis 225

I.4 Characterization of the Macrocycle 227

I.5 Electrochemical Analysis 229

I.6 Conclusion 231

I.7 Experimental 231

I.8 References 240

Appendix II - Selected ITC Data 241

18a + 13 242

18a + 7a 243

18a + 7c 244

18b + 7a 245

20a + 7a 246

20a + 7c 247

20b + 7a 248

7a into DMSO 249

Zn17a + 7a 250

Appendix III - Selected ^{1}H NMR Data 251-293

List of Tables

Chapter 2

Table 1 Calorimetric Data 41

Table 2.1 Redox Potentials 65

Chapter 3

Table 3.1 Examples of Photochromic Molecules 79

Chapter 4

Table 1 ^{1}H NMR Data 123

Chapter 5

Table 1 Diastereoselectivities of Photochromic Process 156

Appendix I

Table 1 Selected Spectroscopic Data 225

List of Figures

Chapter 1

Figure 1. A Classification of Photochemical Pathways 10

Unit 2 - Introduction

Figure 2.1 Molecular Structure of the Photosynthetic Reaction Center 13

Chapter 2

Figure 2.2 Photochemical Decay Pathways 17
Figure 2.3 Energy and Electron Transfer Quenching Mechanisms 19
Figure 2.4 A Supramolecular Photoactive Complex 22
Figure 2.5 A Diatopic Approach to the Formation of a Photoactive Complex 24

Paper **A Remarkably Stable Hydrogen Bonded Porphyrin•Iron(Terpyridine) Ion Pair**

Figure 1 Plot of Stern-Volmer Fluorescence Quenching 28

Paper **Strong and Directed Association of Porphyrins and Iron(Terpyridine)s using Hydrogen-Bonding and Ion Pairing**

Figure 1 Schematic Representation of Complexes **1** and **2** 32
Figure 2 Optimized Structure of Complex **1** 36
Figure 3 ^{1}H NMR Spectra of **7a**, **7a** + **18a**, **13**, and **13** + **18a** 37
Figure 4 Proposed Structure of the Complex Between **7a** + **20b** 39
Figure 5 The Molecular "Brake" 40
Figure 6 Calorimetric Titration Curves 42
Figure 7 Plot of Inverse Stern-Volmer Quenching 45

Figure 2.6 Raw Data and the Corresponding Integrated Binding Curve for a Typical Calorimetric Titration 60
Figure 2.7 Raw Data and the Corresponding Integrated Binding Curve for a Typical Fluorescence Quenching Titration 61
Figure 2.8 X-Ray Crystal Structure of an Iron(Terpyridine) 62
Figure 2.9 UV-Vis and Fluorescence Spectroscopic Comparison Between the Components in Complex 1 64
Figure 2.10 Possible Modes of Fluorescence Quenching 66

Unit 3 -Introduction

Figure 3.1 Molecular Orbital Diagram for a the Ring-Closing Process of Dithienylethene 82

Chapter 3

Figure 3.2 Schematic Representation of an Emission-Based Molecular Switch 88

Paper **Photoregulation of Fluorescence in a Porphyrinic Dithienylethene Photochrome**

Figure 1 UV-Vis Spectra of 1 and 2 under Irradiation 94
Figure 2 Modulated Emission Signal of 1 95

Figure 3.3 Absorption and Emission Spectra of 1 under irradiation at 313 nm 101
Figure 3.4 Emission Spectra 1 101
Figure 3.5 Absorption and Emission Spectra of 1 under irradiation at 430 nm 102

Chapter 4

Figure 4.1 Electron-Rich Derivatized Ring-Closed Dithienylethenes 117

Figure 4.2 An Axially Coordinated Ruthenium Porphyrin 118

Paper **Axially Coordinated Porphyrinic Photochromes for Non-Destructive Information Processing**

Figure 1 UV-Vis Spectrum of **1** under Irradiation 124
Figure 2 Emission Spectra and Modulated Emission Signal of **1** 125

Figure 4.3 Carbohydrate Porphyrin Dimers 131
Figure 4.4 Separation of UV-Vis Absorption and Emission Bands 133

Chapter 5

Figure 5.1 UV-Vis and ORD Spectra of 3-Methylketone 143
Figure 5.2 Examples of Chiral Chromophores 145

Paper **Nondestructive Data Processing Based on Chiroptical 1,2-Dithienylethene Photochromes**

Figure 1 X-Ray Crystal Structure of Copper (I) Complex 154
Figure 2 UV-Vis Spectra Comparing Complexes 155
Figure 3 ^{1}H NMR Spectra of Diastereoselectivity 156
Figure 4 ORD Spectra of *Open/Closed* Forms with Copper 157
Figure 5 Modulation of Optical Rotation 158

Figure 5.3 X-Ray Crystal Structures of Enantiomeric Helicates 161
Figure 5.4 CD Spectra of *Open/Closed* Forms with and without Copper 162
Figure 5.5 UV-Vis and ORD Spectra of *Open/Closed* Forms with and without Copper 163
Figure 5.6 A Homochiral Hydrogen Bonded Helix 165
Figure 5.7 X-Ray Crystal Structure of $\mathbf{Cu_2(10)_2}$ 167

Chapter 6

Figure 6.1 Photochromic Control of Crystal Surface Structure 185

Figure 6.2 Self-Assembly of a Helicene 186

Paper **Reversible [7]-Thiahelicene Formation Using a 1,2-Dithienylcyclopentene Photochrome**

Figure 1 UV-Vis Spectra of **1** under Irradiation 189
Figure 2. X-Ray Crystal Structure of **1** *open* and *closed* 189
Figure 3 X-Ray Crystal Structure of **2** and **3b** 191

Figure 6.3 Extended Aromatic Sideproduct 192
Figure 6.4 Emission Spectrum of **1** under Irradiation 195
Figure 6.5 Schematic Representation of all [7]-helicenes 196
Figure 6.6 UV-Vis Spectra of **2**, **3a** under Irradiation and **3b** 198
Figure 6.7 Schematic Representation of Chiral Derivatized Photochromic Helicenes 198

Appendix I

Figure 1 X-Ray Crystal Structure of **1** 221
Figure 2 X-Ray Crystal Structure of **3***(closed)* 222
Figure 3 Quenching Mechanism in a Bis-Dithienylethene 223
Figure 4 UV-Vis Spectra of **3**, **5** and **6** 224
Figure 5 Emission Spectra and Modulated Emission Signal of **6** 226
Figure 6 X-Ray Crystal Structure of Macrocycle **4** 228
Figure 7 Cyclic Voltammograms of **8** and **6***(open)* and **6***(closed)* 230

List of Schemes

Chapter 2

Paper **A Remarkably Stable Hydrogen Bonded Porphyrin•Iron(Terpyridine) Ion Pair**

Scheme 1 Synthesis of Complex **1** 26

Paper **Strong and Directed Association of Porphyrins and Iron(Terpyridine)s using Hydrogen-Bonding and Ion Pairing**

Scheme 1 Synthesis of Iron(Terpyridine)s **7a**, **7b** and **7c** 33

Scheme 2 Synthesis of Xanthene Iron(Terpyridine) **13** 34

Scheme 3 Synthesis of *C*2 Porphyrins **Zn17a**, **18a** and **18b** 35

Scheme 4 Synthesis of *C*4 Porphyrins **20a** and **20b** 35

Chapter 3

Paper **Photoregulation of Fluorescence in a Porphyrinic Dithienylethene Photochrome**

Scheme 1 Synthesis and Photochromism of Porphyrinic Photochromes **1** and **2** 93

Scheme 3.1 General Synthesis of Perfluorinated Dithienylethenes 97

Scheme 3.2 Synthesis of Photochrome **4** 98

Scheme 3.3 Detailed Synthesis of Porphyrinic Photochromes **1** and **2** 99

Scheme 3.4 Synthesis of Porphyrin **3** 100

Chapter 4

Paper **Axially Coordinated Porphyrinic Photochromes for Non-Destructive Information Processing**

Scheme 1 Synthesis of Axially Coordinated Porphyrinic

Photochrome **1a** 123

Scheme 4.1 Synthesis of Photochrome **2** 127
Scheme 4.2 Synthesis of Photochrome **8** 127
Scheme 4.3 Synthesis of $Ru_3(CO)_{12}$ and Ru(TTP)(CO)(EtOH) 128
Scheme 4.4 Synthesis of Photochromes **1a** and **3** 129

Chapter 5

Paper **Nondestructive Data Processing Based on Chiroptical 1,2-Dithienylethene Photochromes**

Scheme 1 Synthesis of Helicates $\mathbf{Cu_2(1a)_2}$ and $\mathbf{Cu_2(2a)_2}$ 153

Scheme 5.1 Synthesis of Chiral Photochromes **1a** and **2a** 160
Scheme 5.2 Synthesis of Helicate $\mathbf{Cu_2(10)_2}$ 166

Chapter 6

Paper **Reversible [7]-Thiahelicene Formation Using a 1,2-Dithienylcyclopentene Photochrome**

Scheme 1 Synthesis and Photochromism of Photochrome **1** and Synthesis of Compounds **2**, **3a** and **3b** 188

Scheme 6.1 Detailed Synthesis of Photochrome **1** 193
Scheme 6.2 Detailed Synthesis of Photochromes **2** and **3a** 193

Appendix I

Scheme 1 Synthesis of 2-Aminopyridyl Derivatized Photochromes 220

List of Equations

Chapter 1

Equation 1.1 An Example of a Redox-Switch 6

Equation 1.2 An Example of a Thermochromic Compound 8

Equation 1.3 Schematic Representation of a Photochromic Compound 9

Unit 3 - Introduction

Equation 3.1 A Dual-Mode Molecular Switch 85

Chapter 3

Equation 3.2 Fluorescence Changes in a Photochromic Polythiophene 90

Equation 3.3 Fluorescence Changes and Quenching Pathway in a Porphyrinic Dithienylethene Photochrome 103

Equation 3.4 Possible Mechanism of Indirect Ring-Opening for Porphyrinic Photochrome **1** 104

Chapter 4

Equation 4.1 Fluorescence Changes in a Tungsten Carbonyl•Dithienylethene Photochromic Complex 119

Chapter 5

Equation 5.1 Self-Assembly of a Stereospecific Helicate 146

Equation 5.2 Photochromic Interconversion of a Sterically-Overcrowded Alkene 148

Equation 5.3 Stereospecific Ring-Closing of a Dithienylethene Photochrome 149

Equation 5.4 Photochromic Interconversion of a Chiral Dithienylethene Photochrome 150

Equation 5.5 Photochromic Interconversion of a Chiral Dithienylethene Photochrome 150

List of Abbreviations

Bn	benzyl
Bu	*n*-butyl
CD	circular dichroism
CIS	complex induced shift
de	diastereomeric excess
eT	electron transfer
ET	energy transfer
DMF	dimethylformamide
DMSO	dimethylsulfoxide
ee	enantiomeric excess
Et	ethyl
Hex	*n*-hexyl
HOMO	highest occupied molecular orbital
HMTA	hexamethyltetraamine
i-Pr	isopropyl
IR	infrared
ITC	isothermal titration calorimetry
LUMO	lowest unoccupied molecular obital
Me	methyl
mp	melting point
MO	molecular orbital
MS	mass spectrometry

n	refractive index
NBS	N-bromosuccinimide
NMR	nuclear magnetic resonance
nOe	nuclear Overhauser enhancement
OAc	acetate
ORD	optical rotatory dispersion
Ph	phenyl
PPh_3	triphenylphosphine
py	pyridine
rt	room temperature
t-Bu	*tert*-butyl
TEA	triethylamine
Tf	trifluoromethanesulfonyl
TFA	trifluoroacetic acid
THF	tetrahydrofuran
TIPS	triisopropylsilyl
TMS	trimethylsilyl
TTP	tetratolylporphyrin
UV-Vis	Ultraviolet - Visible

Unit 1 - Chapter 1 - Methods to Control Molecular Structure and Function in Supramolecular Chemistry

The ability that biological systems display in controlling their structure both at the molecular and polymolecular levels is inspirational. From self-replication to cellular respiration, the evidence of this control is clearly apparent in the diversity of the functions that these systems manifest. Although many of these architectures are vast on a molecular scale and appear quite complex, they are governed by a set of covalent and non-covalent interactions that serve to unite the molecular components into the desired molecular formations. We are just starting to be able to manipulate the interactions between molecules to the same level reached by synthetic chemists with the covalent bond. This understanding of polymolecular phenomenon grew out of a branch of modern chemical research that is appropriately termed "molecular recognition". Molecular recognition chemistry is dedicated to understanding the rules that govern non-covalent interactions.[1] The primary motivation here is the prospect that molecular recognition by design could lead to structurally diverse materials with new and interesting functional properties that cannot be achieved at the single molecule level.

1.1.1 Levels of Controlling Molecular Structure

From a design point of view there are several levels at which molecular shape and structure can be controlled. Synthetic chemistry is the starting point to build molecular structure. This structural information may be designed to be significant within the confines of a given molecule such as the *intramolecular* interactions necessary to produce the secondary structure in protein α-helices. Alternatively, this information can be designed to extend beyond the molecular level to yield higher ordered polymolecular architectures such as protein quaternary structure. This type of polymolecular structural control is a result of *intermolecular* interactions. Often times the properties of these superstructures can be vastly different from the individual components, which makes the assembly of such structures from a materials point of view very appealing.

The next higher level to controlling structure and function is post-synthetic. After a molecule has been synthesized and its atomic skeleton has been dictated structural control remains accessible by using molecular switches, which through the application of external stimuli such as temperature, light or current, regulate the molecule's geometry and thus its properties. These levels of control are not completely detached but are interwoven, each building upon its predecessor. The following section of this thesis takes aim at describing this hierarchy of structural control and the functional utility that accompanies each level.

1.1.1.1 Level 1 - Synthetic Control

Organic synthesis has in the past, and will continue to be an invaluable tool to generate diverse molecular structures. Its merits are seen most clearly in the domain of pharmaceutical chemistry, where it continues to be the principal instrument used to generate increasingly complex molecular structures for use in drug search efforts. However this multi-step approach becomes quite cumbersome and inefficient when generating large and complex molecules. A more effective strategy to creating large complex structures is through the process of "self-assembly". In this approach, easy to synthesize small building blocks are encoded with the necessary information to spontaneously assemble into more complex supramolecular structures.

1.1.1.2 Self-Assembly Synthesis

Control of supramolecular structure via a self-assembly process stems from the rational design of its component building blocks. The design strategy should involve the appropriate geometric placement and choice of the *molecular recognition elements* onto the building block such that this synthetic molecular programming translates its "code" into the supramolecular realm. Furthermore, the ideal synthon should be obtainable in the minimum amount of synthetic steps and should upon mixing afford a single higher ordered architecture. Of course there may be several kinetically labile supramolecular orientations available to the synthon during the self-assembly process, however if properly designed the thermodynamically most stable structure(s) should dominate. This thermodynamic control is the all-important "self-correcting" mechanism that rids the system of any unwanted kinetically formed sideproducts.

The molecular recognition elements refer to the intermolecular forces that can be used to "glue" together two or more molecules. These intermolecular forces are typically referred to as "non-covalent" and include such interactions as electrostatic (ion-ion, ion-dipole and dipole-dipole), coordination bonding, hydrogen bonding, π-π stacking, hydrophobic effects and dispersion forces. Coordination bonding (sometimes referred to as dative bonding) may or may not be classified as a non-covalent interaction depending on the company you are in, but for the purposes of this discussion it has been classified as such. Some of these forces unite molecules in what appears to be a haphazard fashion. For instance ion pairing is a strong intermolecular force but lacks any directionality which results in unordered aggregates. Others, such as hydrogen bonding, tend to align the molecular components in a highly ordered fashion due to the directionality of the recognition sites.[2] These non-covalent forces are characterized by varying degrees of "stickiness" which ultimately affects the stability of the resulting supramolecular structure. On their own these forces are typically quite weak as compared to covalent bonding, but when applied in a cooperative fashion the stability of the resulting complexes increases substantially. Consequently, all of the factors described above must be carefully considered when designing synthons capable of generating highly ordered supramolecular architectures.

1.1.1.3 Level 2 - Post-Synthetic Control

As the name suggests, post-synthetic control is the ability to control molecular structure and function after synthesis is complete. This control is typically triggered by an external stimulus, the most common being light, temperature, protons or electricity. Such control mechanisms are not predisposed to all molecular systems but must be designed into the molecular system during the synthesis stage. The term *molecular switch* has been coined for a class of compounds that exhibit this type of control as they are able to reversibly alternate between two or more structurally distinct and stable isomeric forms in response to an external stimulus.[3]

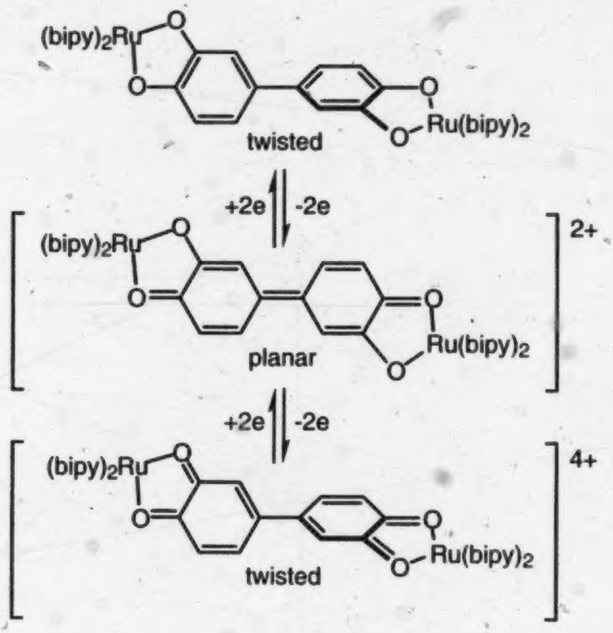

Equation 1.1. An example of a redox switch.

Molecules whose structure can be controlled by the addition or removal of electrons are appropriately termed redox switches as the oxidation/reduction properties of the molecule are responsible for the modulation process. An example of such a system is shown in Equation 1.1. where the addition or removal of electrons is responsible for controlling molecular shape (twisted or planar).[4] Incorporation of such a system into an extended molecular wire for example offers the possibility of a redox controlled molecular circuit breaker. Since planarity is typically required to form an extended conjugated pathway, altering the conformation of the bridge between planar and non-planar structures provides accesses to both conducting and insulating states or ("less conducting states") respectively.

Molecules whose structure is controlled by changes in temperature are referred to as thermochromic compounds. An example of such a compound is shown in Equation 1.2.[5] Here, temperature is used to control the relative positioning of the electrons in the complex. At low temperatures the complex contains Co^{3+} and a catecholate ligand, but under slightly more extreme conditions the redox isomer is favored affording the reduced Co^{2+} and the oxidized semiquinone complex. This temperature induced internal electron rearrangement is due to the energetic similarities between the metal-based (Co^{2+}/Co^{3+}) and ligand-based (catechol/semiquinone) interconversions. In this case both states exhibit very different magnetic and spectroscopic properties.

The addition or removal of protons to a system can also be used as a mechanism to reversibly control structure. These systems are referred to as pH switches and are used abundantly by nature to control biological structure and function.[6] For purposes of this discussion it is deceptive to group in pH switches with the other molecular switches because pH control typically requires the physical addition of reagents to affect molecular structure and as such it cannot be rigidly defined as a post-synthetic control mechanism.

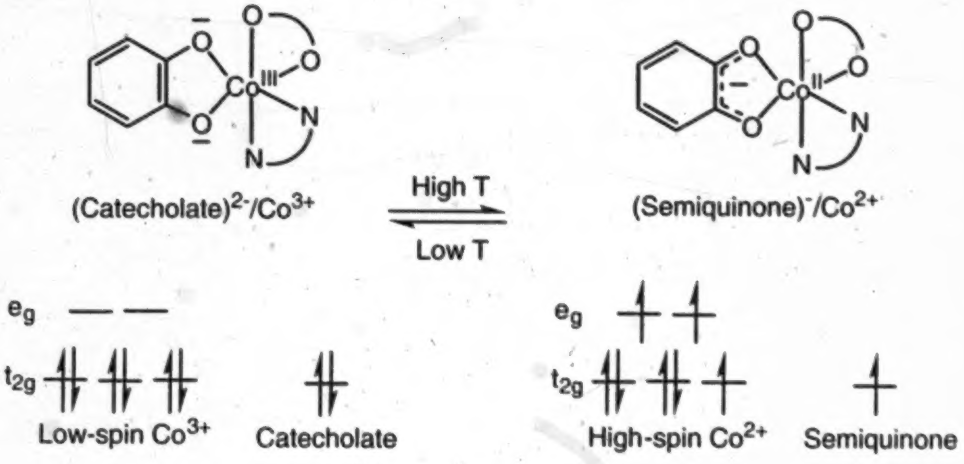
(Catecholate)2-/Co3+
High T
Low T
(Semiquinone)-/Co2+
eg
t2g
Low-spin Co3+
Catecholate
High-spin Co2+
Semiquinone

Equation 1.2. An example of a thermochromic compound. N and O are various bidentate ligands. Counterion is BF_4.

This thesis will focus on the use of light to control the structure of photochromic compounds. Photochromism[7] is defined as a reversible phototransformation of a chemical species between two isomeric forms having different absorption spectra (Equation 1.3). Modern day lasers provide a convenient means to regulate the intensity and wavelength of light while fiber optic technology provides the capability to transport and efficiently focus light.[8] As such, light energy is by far the most common and unarguably one of the most useful external control mechanisms available.

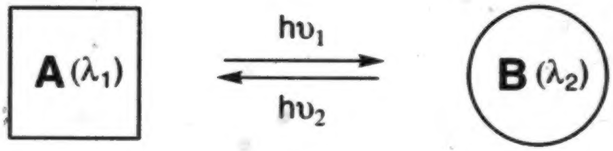

Equation 1.3. Schematic representation of a photochromic compound

1.1.2 Summary and Overview

The absorption of light energy by ground state species leads to excited state species. Depending on the molecular system the deactivation of the excited state can result in a number of both photochemical and structural transformations. Several of the possible deactivation pathways for excited state species are shown in Figure 1.1. The following Chapters will highlight how these pathways can be used in unison or in concert to control molecular structure and function. For example, Chapter 2 describes the self-assembly of photoactive complexes and discusses the resulting luminescence behavior in terms of electron and energy transfer mechanisms. Unit 3 focuses on the use of light to regulate the structure of photochromic compounds. Within Unit 3, Chapters 3 through 5 discuss the use of photochromes as memory devices, while Chapter 6 describes the photoregulated control of helical molecular morphology. All projects described in these chapters have been published. The thesis closes with Appendix I which describes an unpublished body of work where a photochrome is used to regulate the redox properties within a single system.

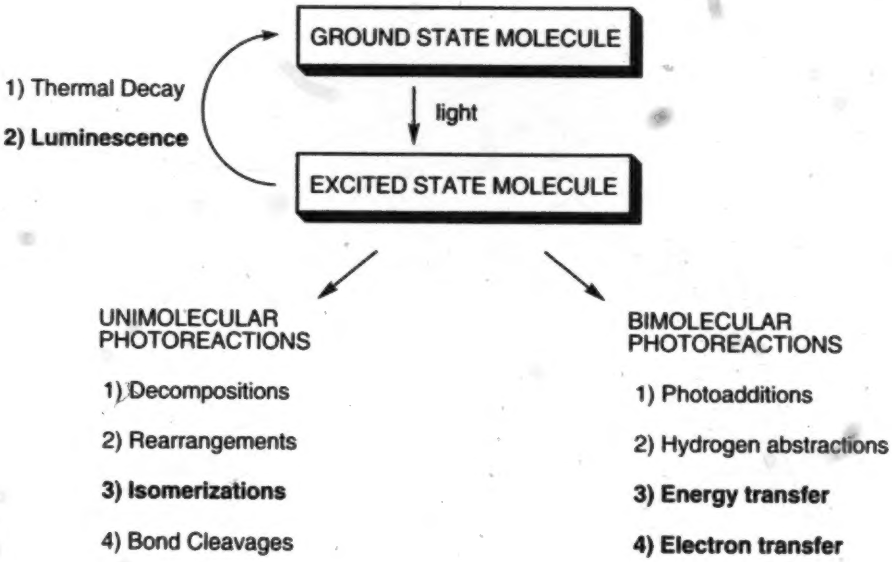
GROUND STATE MOLECULE
light
EXCITED STATE MOLECULE
1) Thermal Decay
2) Luminescence
UNIMOLECULAR PHOTOREACTIONS
1) Decompositions
2) Rearrangements
3) Isomerizations
4) Bond Cleavages
BIMOLECULAR PHOTOREACTIONS
1) Photoadditions
2) Hydrogen abstractions
3) Energy transfer
4) Electron transfer

Figure 1.1. A classification of photochemical pathways. The mechanisms in bold face are pertinent to the work discussed in this thesis.

1.1.4 Notes and references

1. *Chem. Rev.* **1997**, *97*, inclusive

2. For a survey of self-assembling systems employing multiple directed hydrogen bonding sites see: Zimmerman, S. C.; Corbin, P. S. *Structure and Bonding*, **2000**,

96, 63.

3. Ward, M. D., *Chem. Ind.* **1997**, *16*, 640.

4. Joulie, L. J.; Schatz, E.; Ward, M. D.; Weber, F.; Yellowslees, L. J. *J. Chem. Soc., Dalton Trans.* **1994,** 799.

5. Jung, O.-S.; Jo, D. H.; Lee, Y-A.; Conklin, B. J.; Pierpont, C. G. *Inorg. Chem.* **1997**, *36*, 19.

6. Bissel, R. A.; Cordova, E.; Kaifer, A. E.; Stoddart, J. F. *Nature*, **1994**, *369*, 133.

7. Irie, M. *Chem. Rev.* **2000**, *100*, inclusive.

8. Kawata, S.; Kawata, Y. Chem. Rev. **2000**, *100*, 1777.

Unit 2 -Introduction - Controlling Molecular Structure by Self-Assembly Synthesis: Self-Assembling Photoactive Complexes

2.1 The Photosynthetic Reaction Center

The existence of a photosynthetic reaction center was initially postulated in 1932 but it was not until the 1970's that the complex was isolated from the purple photosynthetic bacterium *Rhodobacter* (*Rb.*) *sphaeroides*.[1] Over a decade later the molecular structure of *Rb. sphaeroides*[2] was solved by X-ray crystallography and it showed that the various cofactors are positioned within the constructs of a complex protein scaffold (Figure 2.1). The entire assembly is precisely positioned within the cell membrane so that the light harvestingunits D_M and D_L are located towards the outer membrane wall and can efficiently collect light energy and subsequently channel the photoinduced charge along an assembly line of progressively better electron acceptors ($B_A \Rightarrow \phi_A \Rightarrow Q_A$).[3] These processes are designed to shuttle the photoinduced charge towards the interior of the cell creating a long-lived charge separated state. This relocated charge is ultimately used to drive various endothermic biochemical processes.

The most remarkable feature of this chain of events is the quantum efficiency that the system displays. The absorption of only *one* photon results in the formation of *one* charge separated pair. This results in a quantum yield close to the maximum value of unity, a feat unmatched in model systems. It is the specific spatial arrangement of the chromophores, a consequence of supramolecular positioning within the protein backbone, that is absolutely crucial for the rates and specificities of the electron transfer reactions.

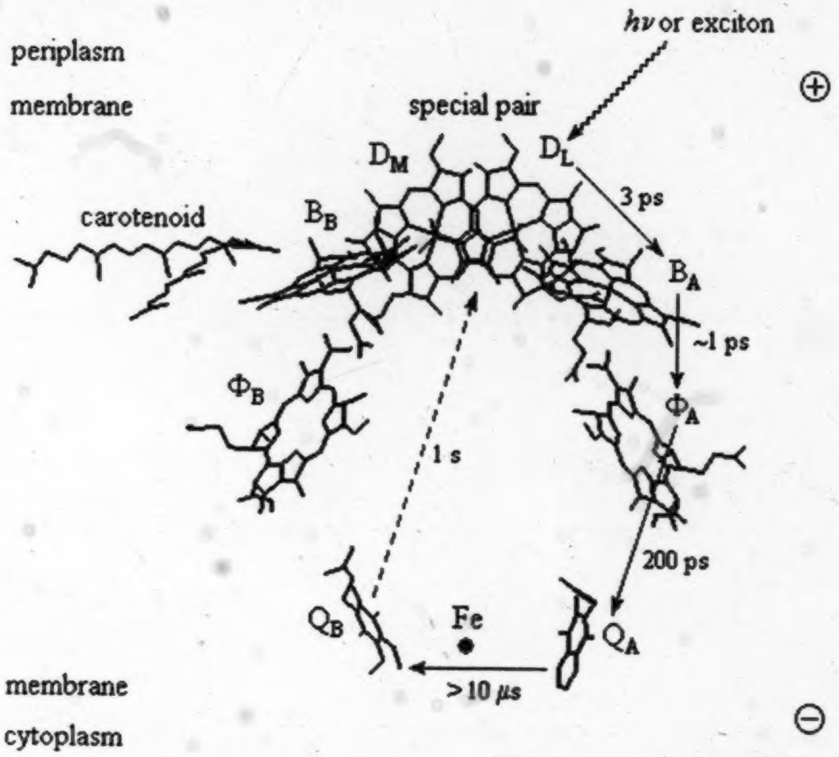

hν or exciton
periplasm
membrane
⊕
special pair
D_M
D_L
carotenoid
B_B
3 ps
B_A
~1 ps
Φ_B
Φ_A
1 s
200 ps
Q_B
Fe
Q_A
> 10 μs
membrane
cytoplasm
⊖

Figure 2.1. Molecular structure of the photosynthetic reaction center. D_L and D_M make up the bacteriochlorophyll light harvesting "special pair". Once activated this dimer can transfer its excited state energy to the bacteriochlorophyll monomer B_A, the bacteriopheophytin ϕ_A and the primary acceptor ubiquinone Q_A and secondary acceptor Q_B. The primary energy pathway is through the A-branch. It is thought that the high spin Fe^{2+} atom wedged unsymetrically between the quinones serves to stabilize the charge in the core region.

The motivation behind the design and study of synthetic supramolecular photoactive complexes is the realization of nanosized light harvesting devices that could match or possibly even out perform the system nature has evolved. The following Chapter consists of a brief discussion on photochemical pathways which is followed by a set of papers that describe both the self-assembly and resulting photochemistry of large non-covalent photoactive arrays.

2.2 Notes and references

1. Feher, G. *Photochem. Photobiol.* **1971**, *14*, 373.
2. (a) Komiya, H.; Yeates, T. O.; Rees, D. C.; Allen, J. P.; Feher, G. *Proc. Natn. Acad. Sci. USA.* **1988**, *85*, 9012. (b) Feher, G.; Allen, J. P.; Okamura, M. Y.; Rees, D. C. *Nature*, **1989**, *339*, 111.
3. Moser, C. C.; Keske, J. M.; Warncke, K.; Farid, R. S.; Dutton, L. P. *Nature*, **1992**, *355*, 796.
4. Ward, M. D *Chem. Soc. Rev.* **1997**, *26*, 365.

Chapter 2 - Hydrogen Bond Directed Self-Assembly of Porphyrin•Iron (Terpyridine) Ion Pairs

From studying the photosynthetic reaction center, it is readily apparent that structure is intimately related to function. As such, two structural characteristics that are crucial for any bimolecular photochemical reaction to proceed are proximity and orientation between reacting centers. If the distance between the two chromophores is too large the transfer of excited state energy is physically impossible. Furthermore, the centers undergoing the reaction must be positioned properly to efficiently "trap" the incoming energy.

As was established in Chapter 1, the use of non-covalent interactions to arrange molecules is an efficient way to generate large ordered molecular arrays. As such, much research has been dedicated to programming these molecular recognition elements onto photoactive building blocks in an effort to create synthetic light harvesting systems.[1] Non-covalent cohesive forces are an effective way of bringing together and aligning photoactive molecules in an effort to create functional light harvesting devices. With a global fuel crisis looming large in the next century, these systems offer the possibility of tapping into an unlimited source of fuel.

Once a photoactive complex is assembled, it is necessary to study its photophysical characteristics to ascertain its excited state pathways. The resulting photophysical studies ultimately determine the efficiency by which a complex is able to "harvest" light. In more scientific terms, it measures the lifetime of the charge-separated state; the longer the lifetime, the better. The following sections describe some common deactivation pathways and techniques used in studying excited state molecules.

2.2.1 Photochemical Pathways

2.2.1.1 Photoluminescence

All molecules are capable of electronic transitions in which an electron is promoted from a ground state energy level to a higher-energy level. An excited state molecule can return to its ground state through a variety of different mechanistic steps. However, in most instances the excited state collapses back to the ground state with the evolution of heat by a nonradiative vibrational relaxation process (e.g. T in Figure 2.2). Such molecules have little value in the study of intermolecular electron and energy transfer pathways.

Luminescent molecules on the other hand tend to have very long lived excited states. The primary deactivation pathway here is characterized by the emission of photons to the surrounding media. For example fluorescent molecules have excited-state lifetimes ranging from 10^{-9} to 10^{-5} seconds and will typically emit energy from the first excited singlet state (S_1). Molecules that phosphoresce however have excited-state lifetimes on the order of 10^{-4} to 10 seconds or more. This extended lifetime is a consequence of intersystem crossing resulting in a "spin-flip" of the excited electron. Triplet/singlet

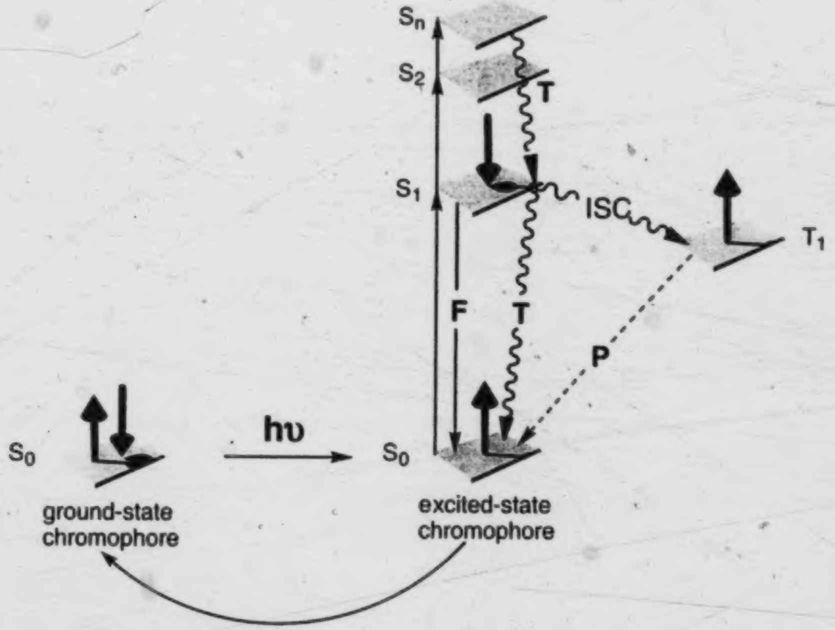
Sn
S2
T
S1
ISC
T1
F
T
P
S0
hυ
S0
ground-state chromophore
excited-state chromophore

Figure 2.2. A state energy diagram. S_0, S_1...S_n refer to the ground state, first excited singlet state and so on. ISC (intersystem crossing) leads to T_1, the first excited triplet state. **T** is a radiationless decay pathway. **F** and **P** are fluorescent and phosphorescent emission respectively.

transitions are much less probable (they are referred to as spin forbidden transitions) and as such emission may persist for some time after irradiation has been discontinued (Figure 2.2). If the lifetime of the excited state is long enough so as to permit intermolecular interactions to occur before deactivation is complete the transfer of excited state energy can occur. The loss of luminescence is the tell-tale sign that the excited state complex is being *quenched* by another species rather than undergoing radiative decay.

2.2.1.2 Energy *vs.* Electron Transfer

Quenching is defined as the deactivation of an excited molecule by an external component. The two primary quenching pathways are energy and electron transfer. The mechanistic differences between the two are illustrated schematically in Figure 2.3.

Photoexcited species have the unique property of being both better at accepting and donating electrons than their corresponding ground state counterparts. As a consequence the excited electron can collapse down into the LUMO of a nearby electron-poor species resulting in an oxidized chromophore and reduced quencher. This is referred to as oxidative electron transfer.

Alternatively, if an electron-rich species is proximal it can donate an electron to the remaining hole in the lower energy level of the excited-state chromophore resulting in a reduced chromophore and oxidized quencher, a process known as reductive electron transfer.[2]

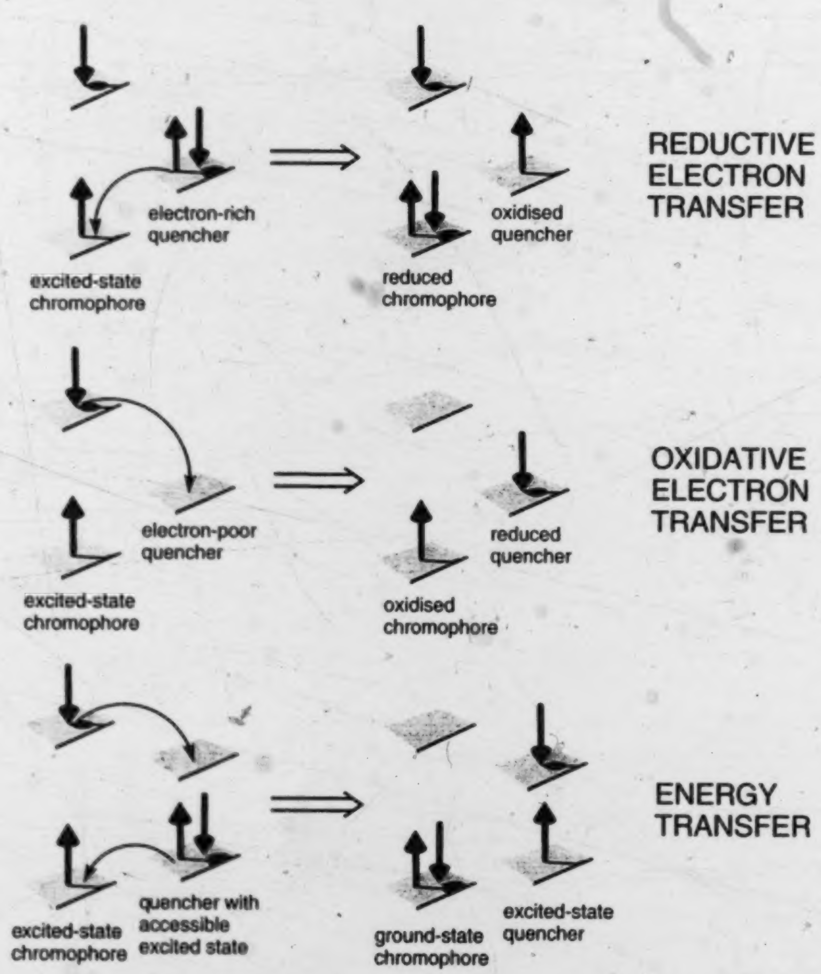
electron-rich quencher
excited-state chromophore
oxidised quencher
reduced chromophore
REDUCTIVE ELECTRON TRANSFER
electron-poor quencher
excited-state chromophore
reduced quencher
oxidised chromophore
OXIDATIVE ELECTRON TRANSFER
quencher with accessible excited state
excited-state chromophore
excited-state quencher
ground-state chromophore
ENERGY TRANSFER

Figure 2.3. Energy and electron transfer quenching mechanisms of a photoexcited chromophore.

Energy transfer in contrast, involves no net electron transfer. Specifically, it is known that both dipole-dipole interaction (Forster)[3] and exchange (Dexter)[4] mechanisms are possible for singlet-singlet energy transfer. The Dexter mechanism is depicted in Figure 2.3. Here electrons are exchanged either simultaneously or in a stepwise manner between the excited-state chromophore and quenching species. This results in the quencher now occupying an electronically excited state, a result of a double electron transfer between the donor and the acceptor species. Subsequent luminescence from the quencher excited state is an obvious sign that an energy transfer mechanism is in effect. However, if the decay pathway is non-radiative as is the case in most systems (such as our system in the paper following this discussion), the absence of luminescence will neither confirm nor deny the existence of an energy transfer process.

Nonetheless, for energy transfer to occur in any capacity there must be adequate overlap between the emission band of the donor species and the absorption band of the quenching species. This is referred to as the spectral overlap integral and is but one of the critical determining factors influencing an energy transfer mechanism.[5]

Steady state fluorescence spectroscopy is typically the first step in studying potential systems capable of generating charge separation because the simple observation of fluorescence quenching immediately signals success. Subsequent research however, is required to determine *how* successful a system is (by measuring the lifetime of the charge separated state) and by *what* mechanism it operates (energy or electron transfer). Since the lifetimes and spectroscopic characteristics between the excited-states of electron and energy transfer mechanisms are unique, time-resolved spectroscopic techniques such as transient absorption spectroscopy and time-resolved fluorescence spectroscopy are the tools of choice used to discern a given mechanistic pathway.

2.2.2 A Selected Example of a Supramolecular Photoactive Complex

In general the most common synthetic donor/acceptor duo studied is that of the porphyrin chromophore and the quinone quencher because the photochemical characteristics of this combination is well understood from studying the natural photosynthetic systems. Of these systems, one of the most successful from a design point of view, was reported by Hayashi, Ogoshi and coworkers.[6] They take a diatopic approach to the formation of a porphyrin-quinone dimer employing both multipoint hydrogen bonds and π-π stacking interactions. Here a tetramethoxy quinone can strap intimately across the face of a phenoxy-naphthalene porphyrin as shown in Figure 2.4. The association constant between these two moieties was exceedingly strong ($K_a = (6.1 \pm 1.1) \times 10^5\ M^{-1}$ in toluene) due to the multipoint hydrogen bonding present.

Furthermore, the forward and backward electron transfer rate constants reported in this non-covalently bound system were at least as large as those found in covalently bridged porphyrin-quinone systems.[7] This alone testifies to the usefulness of a molecular recognition-based approach to assemble complex photoactive architectures.

Figure 2.4.

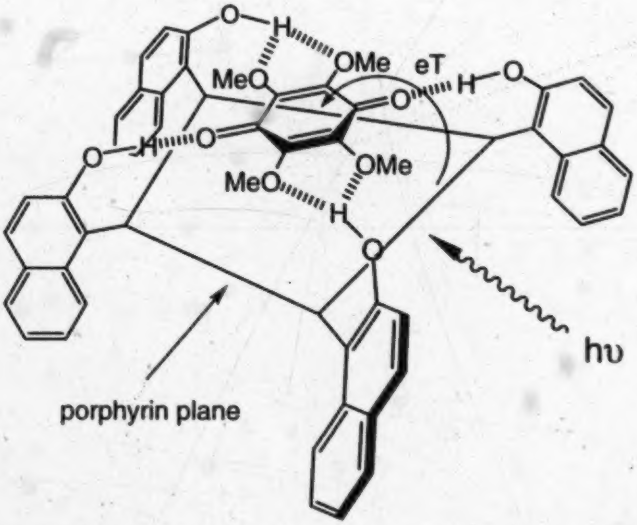

A drawback to this system, however, is that it only functions in nonpolar media such as toluene. The assembly breaks apart in more polar media that can better solvate the hydrogen bonding surfaces between the host and the guest. This is somewhat surprising because in total six hydrogen bonds must be disrupted to displace the quinone from its nest. The hydrogen bonds between the two components in this system however are electrically neutral and as a result there is little electrostatic glue holding the two species together. A better approach (if synthetically possible) would be to use oppositely charged complimentary hydrogen bonding motifs. This would create a more robust complex as the electrostatic attraction between the two components would necessarily be greater.

2.2.3 A Novel Diatopic Approach to Assembling Large Photoactive Complexes

This Chapter consists of two publications. The first paper (Section 2.2.4) is our preliminary result describing a non-covalent diatopic approach to the formation of a large photoactive complex. Both directional hydrogen bonding and electrostatic attraction (ion pairing) are used to effectively glue together two distinctly different chromophores (Figure 2.5)

The subsequent manuscript (2.2.5) is a follow up to our preliminary result and describes in detail both the associative and photophysical characteristics of the complexes. The diatopic motif used is unprecedented in that it employs remote ion pairing attractive forces between a charged chromophore **1** and a pair of oppositely charged hydrogen bond acceptors on chromophore **2** (Figure 2.5). Once together the hydrogen bond acceptors on chromophore **2** align the two chromophores in an intimate arrangement by forming directional hydrogen bonds to the neutral complimentary hydrogen bond donors on chromophore **1**. This yields a highly stable neutral photoactive complex that is held together by both cooperatively hydrogen bonding and ion pairing interactions.

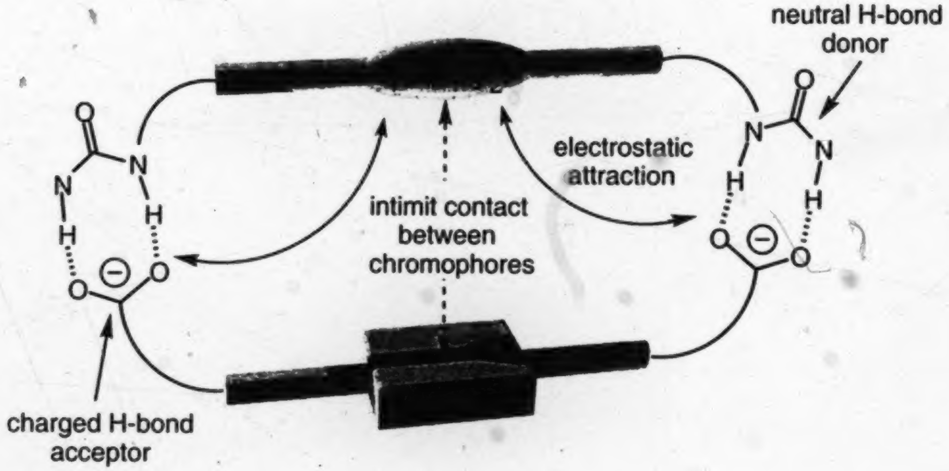

neutral H-bond donor
electrostatic attraction
intimit contact between chromophores
charged H-bond acceptor
O
N
N
H
H
O
O
⊖

Figure 2.5. Schematic representation of the non-covalent approach and resulting structure of our photoactive complex.

2.2.4 - Paper - A Remarkably Stable Hydrogen Bonded Porphyrin Iron(Terpyridine) Ion Pair

Tyler B. Norsten, Kelly Chichak and Neil R. Branda
Chem. Commun. **2001**, 1794

Even in highly competitive solvents such as DMSO, strong bimolecular association ans subsequent fluorescence quenching result from the combination of hydrogen bonding and ion pairing between a porphyrinic bis(carboxylate) dianion and an iron(terpyridine) bis(urea).

In naturally occurring light harvesting systems, the relative orientation and proximity of the photoactive components play fundamental roles in the effective operation of the system. These complex molecular devices rely primarily on non-covalent interactions to place the chromophores in the most productive locations in order to facilitate beneficial electronic communication. Accordingly, significant efforts have been devoted to develop artificial multi-component photoactive arrays, with a particular emphasis on those involving porphyrins.[8-14] Because the photochemical characteristsics are ultimately governed by the assemblies' topology, their fabrication hinges on the tailoring of productive supramolecular interactions such as the coordination bonding,[9,10] ion pairing,[11] π–π-stacking[12,13] and/or hydrogen bonds.[10,14] The hydrogen bond is a particularly serviceable driving force to align building blocks due to its directionality and ease of tailoring. This is especially true when several hydrogen bonds are united into a single multipoint recognition site. The utility of the hydrogen bond is diminished, however, in polar competitive solvents that can better solvate the hydrogen bonding surface. The implementation of cooperative or ionic hydrogen bonding motifs, where the hydrogen bond partners are of opposite charge, can often overcome these destructive solvation effects.[15] Strong complexation is especially critical in order to study energy/electron transfer processes at the low concentrations required to effectively evaluate energy/electron transfer processes using luminescence spectroscopy without having to add excessive quantities of quencher.

We describe here the synthesis and characterization of the novel non-covalently bound porphyrinic assembly **1**. The building blocks were designed to harness the

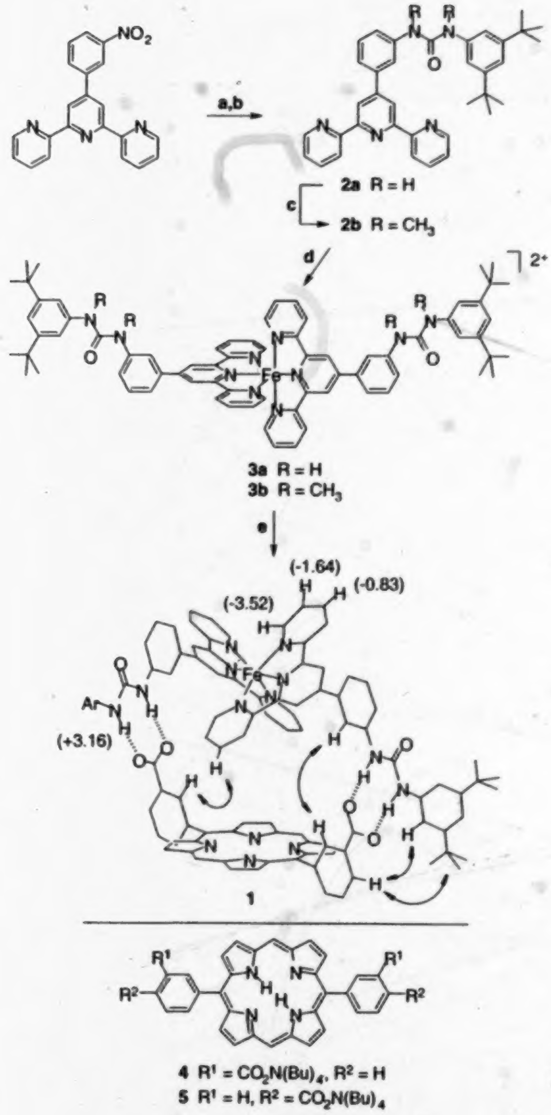

NO$_2$
a,b
2a R = H
2b R = CH$_3$
c
d
2+
3a R = H
3b R = CH$_3$
e
(-1.64)
(-0.83)
(-3.52)
(+3.16)
1
4 R^1 = CO$_2$N(Bu)$_4$, R^2 = H
5 R^1 = H, R^2 = CO$_2$N(Bu)$_4$

[a] Reaction conditions: (a) $SnCl_2{\bullet}2H_2O$, EtOH; (b) triphosgene, CH_2Cl_2, then 3,5-di-*tert*-butylaniline, 78% for three steps; (c) NaH, CH_3I, DMF, 50°C, 99%; (d) $Fe(H_2O)_6(BF_4)_2$, acetone, quantitative; (e) **4**, CH_3OH, 97%.

beneficial recognition attributes of both the ion-pairing and the hydrogen bonding interactions. The first interaction is provided by attraction between the Fe^{2+} dication complex **3a** and the porphyrinic bis(carboxylate) dianion **4**. The carboxylate groups on the porphyrin serve a dual role in that they also act as charged hydrogen-bond-acceptor sites for the neutral bidentate urea hydrogen-bond-donors on the iron(terpyridine) fragment. The result is the self-assembly of the neutral complex **1**, which retains both its structural integrity and topology even at low concentrations in polar solvents such as DMSO.

Assembly **1** was prepared by mixing an equimolar mixture of building blocks **3a** and **4** in methanol (Scheme 1). The neutral complex precipitates from the solution and is easily isolated in high purity and in nearly quantitative yield. Owing to the charges balancing in the final complex, 2 equivalents of $[Bu_4N][BF_4]$ were produced in the reaction and were washed away during the filtration. The integration of signals in the ^1H NMR spectrum of the isolated solid supports the claim that the 1:1 complex is the product of the self-assembly process. Electrospray mass spectrometry confirmed this claim as peaks at *m/z* 1738.7 and *m/z* 880.3 corresponding to $[M+Na]^+$ and $[M+2Na]^{2+}$, respectively, were observed.

Assembly **1** is freely soluble in highly polar solvents such as DMSO and DMF, but is only sparingly soluble in all other common organic solvents. GCOSY and T-ROESY experiments aided in assigning the protons of complex **1**. The complex induced shift (CIS) values for complex **1** in the ^1H NMR spectrum in DMSO-d_6 and the observed intermolecular nuclear Overhauser enhancements (nOe's) are highlighted in Scheme 1. Both experiments support the proposed structure of **1**, where **3a** is straddling across the porphyrin macrocycle and not lying to its side. The significant downfield shift ($\Delta\delta > 3$ in DMSO-d_6) observed for the urea N–H's in assembly **1** is indicative of effective hydrogen-bonding even in such a polar and competitive solvent. The role of the hydrogen bonds is also to steer the iron(terperidine) fragment into a position where it lies directly over the porphyrin plane. This guidance is successful as diagnosed by the upfield shifts observed for the hydrogen atoms of **3a** lying directly over the porphyrin plane and within the shielding region of the macrocyclic ring ($\Delta\delta$ are as large as -3.52). The signals for the four hydrogen atoms on the terminal pyridine ring of the **3a** are unique in that they appear as broad peaks in the spectrum. We attribute this to the fact that **3a** can be thought of as a 'spit on a barbecue' in which the terpyridine can slowly rotate above the porphyrin ring. The terpyridine protons can, therefore, range in distance from 3.5 to 14.5 Å[16] from the plane of the porphyrin at any given moment affording a variety of possible conformers that can exist within NMR time-scale. Variable temperature NMR experiments failed to alter the shape of these broadened signals.

The strength of the binding between **3a** and **4** was too large to be accurately measured by ^1H NMR spectroscopy even in DMSO-d_6. Isothermal titration calorimetry (ITC) experiments in DMSO, however, indicated a binding stoichiometry of 1:1 for **3a** and **4** and an impressive value for the association constant (K_a) of $(2.47 \pm .44) \times 10^6$ M^{-1}. When the ITC experiments were repeated replacing **3a** with the *N,N'*-dimethylated analogue **3b**, that can only associate through ion-pairing, the heat released upon binding was so small that the association constant was impossible to estimate. The titration of **5** with **3a** also revealed a similar trend, despite the fact that the **3a•5** complex can be isolated as a solid in a similar fashion as for **1**. In this case, the hydrogen bonds are not suitably positioned to operate in unison and direct the formation of a strapped 1:1 complex. Although, the ^1H NMR spectrum in DMSO-d_6 does reveal a 1:1 stoichiometry between **3a** and **5**, the signals for the urea N–H protons shift only 1 ppm downfield, and there is no observable shift of the signals corresponding to the C–H protons on the iron(terperidine) fragment. This indicates that **3a** does not reside over the plane of **5** and the 1:1 complex should really be thought of as an aggregate $(\mathbf{3a•5})_n$. These experiments clearly highlight that ion pairing contributes to the association of **1**; however, the cooperative hydrogen bonds aid in aligning the building blocks into close proximity so that these ion pairing attractive forces can be maximized.

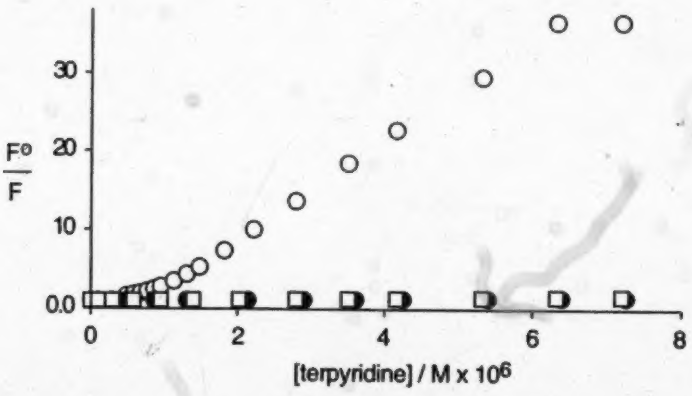

Figure 1. Stern-Volmer quenching when **4** is titrated with **3a** (○), and with **3b** (☐), and when **5** is titrated with **3a** (●) (λ_{ex} = 415 nm, λ_{em} = 633 nm). All titrations were preformed in deoxygenated DMSO. Concentrations: [**4**] and [**5**] = 1.0×10^{-6} M, [**3a**] and [**3b**] = 2×10^{-5} M.

The relative positioning of **3a** and **4** within **1** has a significant impact on the photophysical behavior of the final assembly. Studies using steady-state fluorescence spectroscopy to monitor the changes in the emission intensities of DMSO solutions of **4** and **5** as the porphyrins were treated with aliquots of **3a** are shown in Fig. 1. The immediate quenching of the fluorescence of **4** is most likely a direct result of the straddling nature of the iron(terpyridine) fragment which positions the two chromophores into the most intimate arrangement possible and ensures maximum through-space communication. The fluorescence quenching of porphyrin **4** by **3a** is clearly a result of both strong bimolecular association and optimal spatial positioning of the two chromophores. The *N,N'*-dimethylated analog **3b**, on the other hand, only slightly quenched the fluorescence of **4** in a dynamic, collision-based process. A similar low level of quenching was obtained when porphyrin **5** was titrated with **3a**. Despite the fact that both hydrogen-bonding and ion-pairing are present in the $(\mathbf{3a}\bullet\mathbf{5})_n$ polymolecular assembly, the terpyridine fragment cannot form a strapped arrangement and any through-space communication between the chromophores is significantly reduced. Impressively, similar photophysical behavior of assembly **1** was observed in a 10% H_20/acetonitrile solution attesting to the strength of the association between building blocks **3a** and **4** even in an aqueous environment.

2.2.5 - Paper - Strong and Directed Association of Porphyrins an Iron-(Terpyridine)s using Hydrogen-Bonding and Ion Pairing

Tyler B. Norsten, Kelly Chichak and Neil R. Branda

Tetrahedron. In press

Abstract—The combination of cooperative hydrogen bonding and ion pairing between cationic iron(II)terpyridines and anionic porphyrins yielded remarkably stable neutral complexes even in the highly competitive solvent DMSO. Isothermal titration calorimetry (ITC) was used to compare association constants, enthalpies and entropies of binding between various combinations of the two molecular components that make up the complexes. The rotor-like motion of the iron(terpyridine) fragment over the plane of the porphyrin was slowed by the installation of a molecular "brake," which was achieved by taking advantage of the additional intermolecular contacts between Lewis basic nitrogen atoms on a pyrazyl-modified iron(terpyridine) and a zinc atom located within the porphyrin. Steady-state luminescence studies highlighted that, as expected, the fluorescence quenching of the porphyrin is maximized in the cases where the iron(terpyridine) is strapped the most tightly across the macrocycle.

1.Introduction

The efficient collection of solar energy is the primary task of natural light harvesting systems such as those found in plants, photosynthetic algae and cyanobacteria. These complicated photo-sensitive assemblies are responsible for initiating a cascade of energy and electron transfer reactions, ultimately affording usable forms of chemical fuel. The key to the successful operation of these assemblies lies in their high degree of structural organization, which ensures optimal alignment and relative proximity of the molecular components to maximize through-space communication of the chromophores. This refined architectural organization and structural integrity is a direct outcome of a multitude of contiguous non-covalent interactions.

With this in mind, significant efforts have been devoted to designing and constructing artificial multi-component photoactive arrays, particularly those involving porphyrins.[17–42] Because the photochemical behavior of the supramolecular assemblies will be dictated by their topology, design strategies must include judicial use of molecular recognition principles and, therefore, an emphasis on the logical programming of intermolecular attractions such as coordinative bonding,[18–28] ion pairing,[28–30] π–π-stacking[31] and hydrogen bonding[32–42] is paramount. Supramolecular systems that utilize only one of these interactions, however, do not take full advantage of the properties that each has to offer (expressed in their relative binding strength and directionality). Systems that fall into this category are often plagued by their functioning only in non-competitive solvents or by the generation of assemblies with ill defined topology and composition. The obvious answer to these problems is to design heterodiatopic or heteropolytopic building blocks where several different interactions are used in concert to guide the molecular recognition process and afford strong and selective complexation. The hydrogen bond is a particularly prized interaction used to unite building blocks due to its directionality and the fact that it can be placed onto a building block with a high degree of precision. The utility of the hydrogen bond is greatly reduced, however, in polar competitive solvents that can more readily solvate the hydrogen bonding surface. The implementation of cooperative, ionic hydrogen bonding motifs, where the hydrogen bond partners are of opposite charge, can often overcome these destructive solvation effects.[43–47]
The formation of highly robust supramolecular assemblies is especially critical in order to investigate energy and electron transfer processes by luminescence spectroscopy. In the absence of strong complexation, excessive quantities of the quenching component must be added to produce the observable spectroscopic response at the low concentrations demanded by this analytical technique.

We have recently reported the self-assembly of a novel non-covalently united porphyrin•iron(II)terpyridine complex **1** and how the porphyrin's fluorescence is significantly quenched by the iron(terpyridine).[48] In the present article, we expand on the synthesis, structural characterization and luminescence properties of assembly **1** and its 1:2 counterpart **2**. We designed the building blocks in order to harness the beneficial recognition attributes of both ion pairing and hydrogen bonding. The first interaction is provided by the attraction between the cationic iron(terpyridine) coordination compounds and the anionic porphyrinic carboxylates. The carboxylate groups on the porphyrin also act as charged hydrogen-bond acceptor sites for the neutral bidentate urea hydrogen-bond donors flanking the iron(terpyridine) component. The result is the self-assembly of the neutral complexes **1** and **2**, which retain both their structural integrity and topology even at low concentrations in the highly competitive solvent DMSO.

2. Results and discussion

2.1 Synthesis of the molecular components

With the exception of **12**, we prepared all terpyridine derivatives used in this study in a similar fashion from (*E*)-3-(3'''-nitrophenyl)-1-(pyrid-2'-yl)prop-2-enone (**4**)[49] (Scheme 1). For example, when *N*-(2-(pyridyl)-2-oxoethyl)pyridinium iodide (**3a**) was heated with **4**, the known 3'-(4'''-nitrophenyl)-2,2':6',2"-terpyridine (**5a**)[49] was produced. Reduction of this product with $SnCl_2$ followed by subsequent dissymmertic urea formation employing 3,5-di-*tert*-butylaniline as the amine capping agent and triphosgene as the carbonyl linking agent conveniently yielded urea **6a**. The final iron(II) coordination compound **7a** was isolated as a purple solid by treating two molar equivalents of **6a** with one equivalent of $Fe(H_2O)_6(BF_4)_2$ in acetone. Reacting urea **6a** with iodomethane in anhydrous DMF and in the presence of base cleanly afforded the *N,N'*-dimethylated analogue **7c**, which will make its appearance as a control later in this

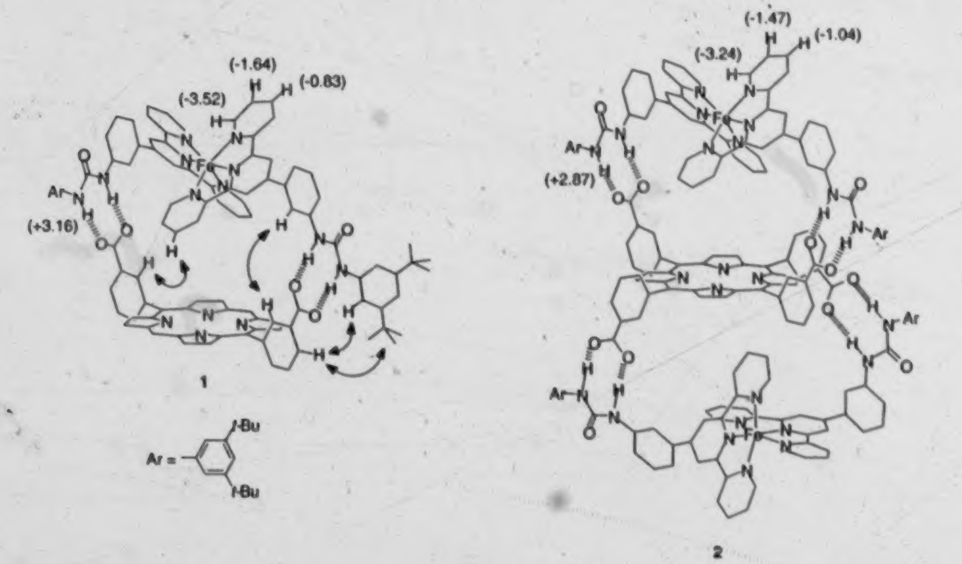

Figure 1. Schematic representation of complexes **1** and **2**. Observed intermolecular nOe's (represented as arrows) and complexation-induced chemical shifts in the ^1H NMR spectrum (shown in parentheses) are highlighted. Double bonds and carbon-bound hydrogen atoms have been removed for clarity.

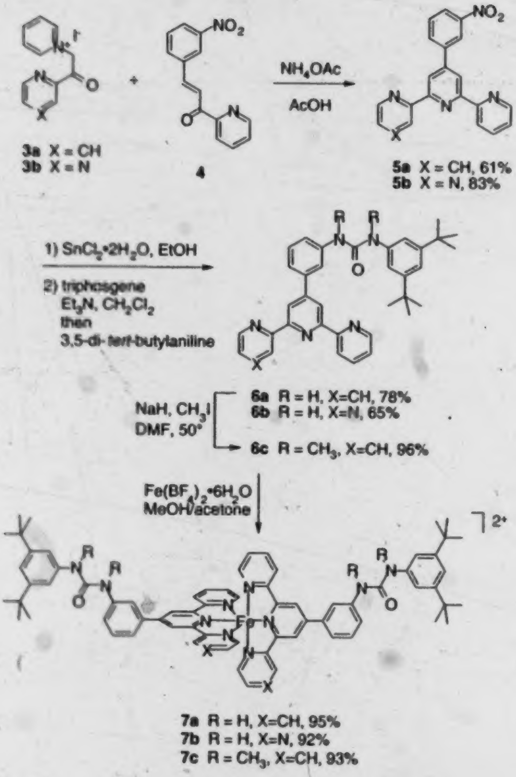
I⁻
N⁺
N
O
X
3a X = CH
3b X = N
+
NO₂
O
N
4
NH₄OAc
AcOH
NO₂
N
N
N
X
5a X = CH, 61%
5b X = N, 83%
1) SnCl₂•2H₂O, EtOH
2) triphosgene
Et₃N, CH₂Cl₂
then
3,5-di-tert-butylaniline
R
R
N
N
O
N
N
N
X
NaH, CH₃I
DMF, 50°
6a R = H, X=CH, 78%
6b R = H, X=N, 65%
6c R = CH₃, X=CH, 96%
Fe(BF₄)₂•6H₂O
MeOH/acetone
2+
R
N
R
N
O
N
N
Fe
N
N
X
X
R
N
R
N
O
7a R = H, X=CH, 95%
7b R = H, X=N, 92%
7c R = CH₃, X=CH, 93%

Scheme 1. Counterions for **7a–c** are BF_4^-.

report. The corresponding pyrazine-derivatized terpyridine **7b** was synthesized in an analogous fashion as described for **7a** from *N*-(2-(pyrazyl)-2-oxoethyl)pyridinium iodide (**3b**). The importance of this compound will also become apparent later in this article.

We also prepared the xanthene analog **13** in order to evaluate the effects (both structural and photophysical) of the relative proximity between the iron(terpyridine) and porphyrin components. The replacement of the 4'-phenyl ring in terpyridine **6a** by the extended xanthene skeleton in **12** provides a substantially deeper binding pocket (4–5 Å) in **13**, as compared to **7a** and, consequently, separates the two active components in space. The *meta*-substitution pattern between the terpyridine and urea moieties is maintained across the xanthene backbone so as not to alter the hydrogen bonding vectors involved in the association between the two chromophores. The key intermediate is the dissymetric xanthene **9**, which was conveniently prepared by a two-step nitration-

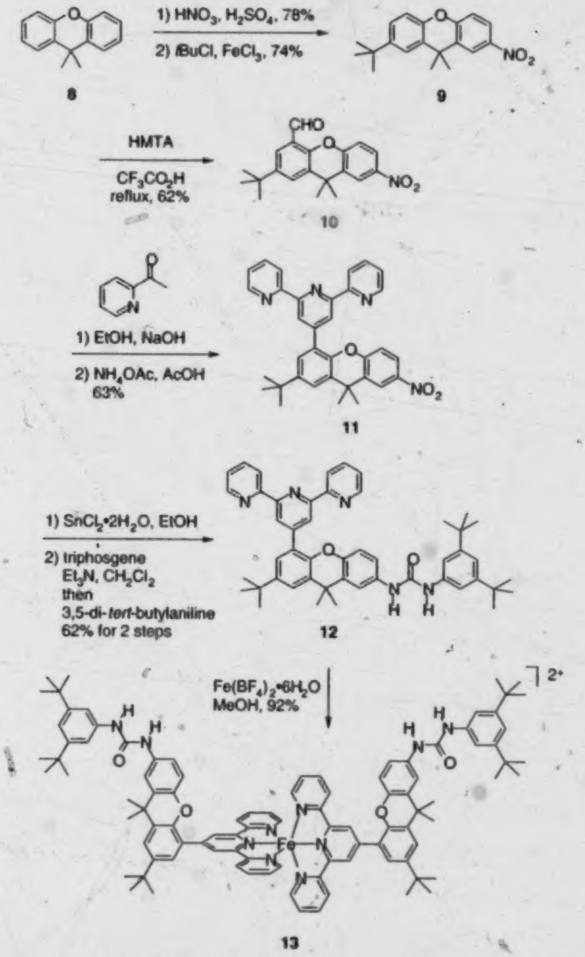
1) HNO3, H2SO4, 78%
2) tBuCl, FeCl3, 74%
8
9
HMTA
CF3CO2H
reflux, 62%
10
1) EtOH, NaOH
2) NH4OAc, AcOH
63%
11
1) SnCl2•2H2O, EtOH
2) triphosgene
Et3N, CH2Cl2
then
3,5-di-tert-butylaniline
62% for 2 steps
12
Fe(BF4)2•6H2O
MeOH, 92%
13

Scheme 2. Counterions for **13** are BF$_4^-$.

alkylation procedure. The *tert*-butyl group's role was not to enhance solubility in organic solvents as is more typical of this group. (All studies will be performed using DMSO solutions, after all.) It was incorporated to block the more reactive *para*-site on the xanthene skeleton and direct the subsequent formylation reaction (**9** → **10**) to produce the desired substitution pattern. The aldehyde was transformed in two steps to terpyridine **11** by reacting it with an excess of 2-acetylpyridine and then with tetrabutylammonium acetate. The conversion of **11** to **13** was accomplished in an identical fashion as already described for terpyridines **7a** and **7b**.

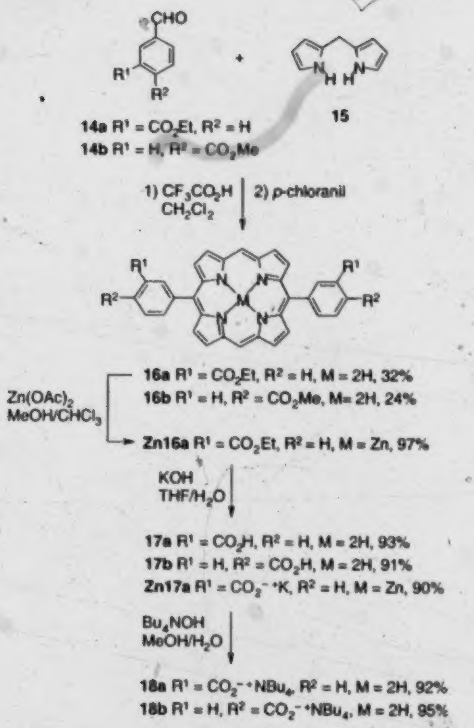
CHO
R¹
R²
+
H H
15
14a R¹ = CO₂Et, R² = H
14b R¹ = H, R² = CO₂Me
1) CF₃CO₂H 2) p-chloranil
CH₂Cl₂
R¹
R²
M
16a R¹ = CO₂Et, R² = H, M = 2H, 32%
16b R¹ = H, R² = CO₂Me, M= 2H, 24%
Zn(OAc)₂
MeOH/CHCl₃
Zn16a R¹ = CO₂Et, R² = H, M = Zn, 97%
KOH
THF/H₂O
17a R¹ = CO₂H, R² = H, M = 2H, 93%
17b R¹ = H, R² = CO₂H, M = 2H, 91%
Zn17a R¹ = CO₂⁻ ⁺K, R² = H, M = Zn, 90%
Bu₄NOH
MeOH/H₂O
18a R¹ = CO₂⁻ ⁺NBu₄, R² = H, M = 2H, 92%
18b R¹ = H, R² = CO₂⁻ ⁺NBu₄, M = 2H, 95%

Scheme 3.

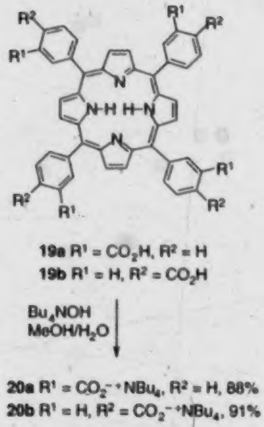
R²
R¹
N
N-H H-N
19a R¹ = CO₂H, R² = H
19b R¹ = H, R² = CO₂H
Bu₄NOH
MeOH/H₂O
20a R¹ = CO₂⁻ ⁺NBu₄, R² = H, 88%
20b R¹ = H, R² = CO₂⁻ ⁺NBu₄, 91%

Scheme 4.

All of the 5,15-*meso*-di-substituted porphyrins were synthesized by the acid-catalyzed cross-condensation[50] of the appropriately substituted benzaldehyde (**14a**[51] or **14b**) and dipyrrolemethane **15**[52] in CH_2Cl_2 (Scheme 3). Metal insertion was accomplished by treating the free-base porphyrin **16a** with $Zn(OAc)_2$. The porphyrin esters (**16**) were saponified using KOH followed by acidification to generate their corresponding carboxylic acids (**17**). The one exception is the dianion of the metalloporphyrin, which precipitated as its potassium salt (**Zn17a**) directly from the reaction mixture and was readily isolated by filtration. The tertrabutylammonium carboxylate porphyrins **18a** and **18b** were generated by treating **17a** and **17b** with 2 equivalents of a methanolic solution of tetrabutylammonium hydroxide. The corresponding derivatives of 5,10,15,20-*meso*-tetra-substituted porphyrins **20a** and **20b** were generated from the known acids (**19a**[53] and **19b**[54]) employing 4 equivalents of a methanolic solution of tetrabutylammonium hydroxide (Scheme 4).

Hydrogen-bonded complexes **1** and **2** (Figure 1) were prepared by simply mixing methanol solutions of porphyrin **18a** or **20a** with iron(terpyridine) **7a** in a 1:1 molar ratio for complex **1** and a 1:2 molar ratio for complex **2**. Complexes **1** and **2** precipitated from the reaction mixture and were easily isolated in high purity and in nearly quantitative yields. Because the association of the terpyridine and porphyrin components is accompanied by charge-balancing and the construction of neutral complexes, 2 and 4 equivalents of tetrabutylammonium tetrafluoroborate were also produced from the self-assembly reaction. These biproducts can be washed away during filtration.

Molecular modeling highlights the ideal lock-and-key fit between the two components making up complex **1** as well as the close proximity between them (Figure 2). The importance of this spatial orientation and relative arrangement will become apparent throughout this report.

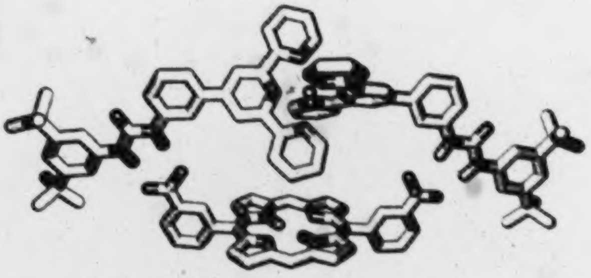

Figure 2. Optimized structure of complex **1** as predicted by molecular modeling.

2.2 ^{1}H NMR characterization of the neutral complexes 1 and 2

Complexes **1** and **2** are reasonably soluble in highly polar solvents such as DMSO and DMF but show poor solubility in other common organic solvents. The integration of the signals in the ^{1}H NMR spectrum in DMSO-d_6 corresponding to the two components that make up complex **1** yielded a clean 1:1 stoichiometry attesting to the molecular composition of the complex.[56] Upon association with the porphyrin, the signals for the protons on the terminal pyridine rings of **7a** shift significantly upfield while those for the N–H protons of the urea shift in the opposite direction (Figure 3). The ^{1}H NMR complex-induced shift (CIS) values for the urea and selected terminal terpyridyl protons are shown in Figure 1. The significant downfield shifts ($\Delta\delta$ greater than 3 ppm in DMSO-d_6) observed for the signals of the urea N–H protons are clearly a result of effective hydrogen bonding, even in such a polar and competitive solvent. The role of these hydrogen bonds is two-fold, one being to associate the two components. The second role is to steer the iron(terpyridine) fragment into a position where it lies directly over the porphyrin plane. This guidance is successful as diagnosed by the upfield shifts observed for the hydrogen atoms lying directly over the porphyrin plane and, thus, within the strong shielding region of the macrocyclic ring. GCosy and TRosey experiments aided in assigning the protons within complex **1**. Intermolecular nuclear Overhauser enhancements (n.O.e's) (highlighted by the arrows in Figure 1) support the claim that **7a** is strapped across the porphyrin ring and not straddling its side.

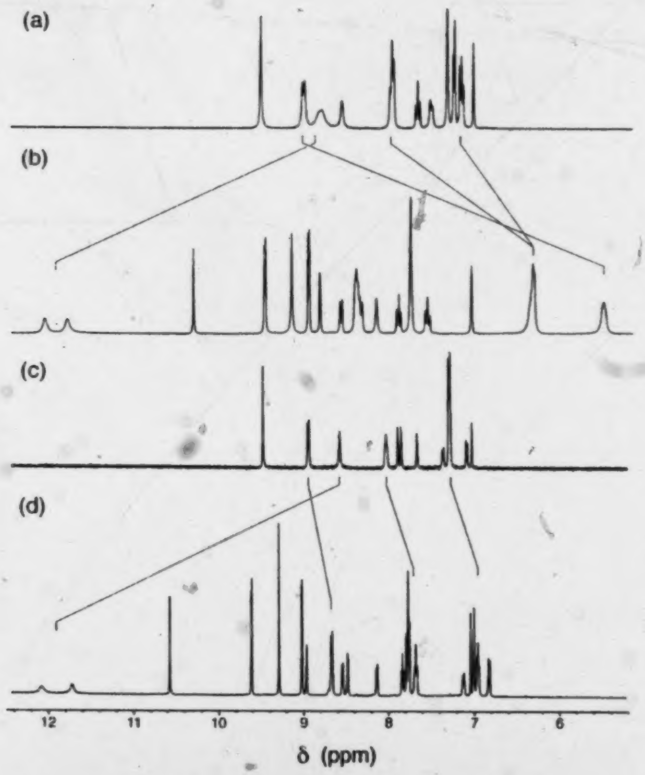

Figure 3. 300 MHz ^{1}H NMR spectra of DMSO-d_6 solutions of (a) iron(terpyridine) **7a**, (b) **7a** + porphyrin **18a**, (c) terpyridine **13**, and (d) **13** + porphyrin **18a**. Complex-induced shifts for selected hydrogen atoms are indicated by connecting lines.

The signals for the hydrogen atoms on the terminal pyridine ring of the terpyridine ligand are unique in that they also appear as broad peaks in the spectrum (Figure 3b). We attribute this to the fact that the strapped iron(terpyridine) fragment does not have the luxury to rotate freely above the porphyrin ring. The axis defined by the N–Fe–N bonds in **7a** is judged to be approximately 8.5 Å above the plane defined by the macrocycle which is not large enough to allow the terpyridine to pass over the porphyrin unencumbered. The result is that the terpyridine protons can range in distance from approximately 3.5 to 14.5 Å from the plane of the porphyrin at any given moment affording a variety of possible rotomers that can coexist within NMR time scale. Variable temperature NMR experiments failed to alter the shape of these broadened signals.

When the *para*-substituted porphyrin **18b** was exposed to iron(terpyridine) **7a**, a complex was isolated in a similar manner as already described for complex **1**. In this case, the hydrogen bonds are not suitably positioned to guide the formation of a strapped 1:1 complex, although the two components can certainly generate a polymeric array with the same 1:1 stoichiometry. The ^{1}H NMR spectrum of this complex indeed indicated a 1:1 stoichiometry, however, the signals for the N–H protons of the urea only shifted 1 ppm downfield. Also, there was no observable shifting of the terpyridine signals. These observations indicate that **7a** does not reside over the plane of porphyrin **18b** and instead suggests the existence of a polymeric aggregate $\mathbf{7a}_n \bullet \mathbf{18b}_m$. The relative positioning of the two chromophores and the inability of **18b** to form cooperative hydrogen bonds with **7a** has a significant impact on the association between the two chromophores and the nature of the fluorescence quenching as will be discussed later.

The xanthene-modified iron(terpyridine) **13** provided us a suitable model compound to evaluate the rotation of the coordination compound over the plane of porphyrin **18a**. The ^{1}H NMR of the resulting complex (Figure 3d) shows a similar downfield shifting of the signals for the urea N–H protons of **13** upon complexation to **18a** as was already observed for **7a**. However in this case, the signals corresponding to the hydrogen atoms on the terminal pyridine rings of **13** appear as sharp well-defined peaks that shift only slightly upfield. We attribute the sharpness of the signals to the fact that there is now adequate distance between the two chromophores to permit free rotation of the terpyridine rotor over the porphyrin plane. The reduced upfield shifting is easily ascribed to the fact that the pyridyl protons are lying further from the shielding region of the macrocycle.

The association of iron(terpyridine) **7a** with the tetra-substituted porphyrin **20a** resulted in the 1:2 complex **2**. Figure 1 shows how, in this case, the two iron(terpyridine) units can alternately strap across opposing faces of one porphyrin macrocycle. The CIS values in the ^{1}H NMR spectrum for the urea N–H and terpyridine protons are nearly identical to those of complex **1**. The only major difference is that the signals in the ^{1}H NMR spectrum of **2** integrate for a 1:2 stoichiometry. The addition of 2 equivalents of **7a** to a methanol solution of the *para*-substituted porphyrinic analog **20b** resulted in a precipitatethat was insoluble even in DMSO. Repeating the association experiment in DMSO-d_6 directly in an NMR tube resulted in an initial spectrum where the signals for the urea N–H protons shifted 1.5 ppm downfield without any accompanying upfield shift of the signals for the terpyridyl protons. A similar precipitate formed in the NMR tube after several hours of standing. We suggest that the result of the association of **20b** and **7a** is a 1:2 complex where the two iron(terpyridine) fragments are strapped to the side of porphyrin **20b** (Figure 4). This stoichiometry is supported by the calorimetric studies described later in this report.

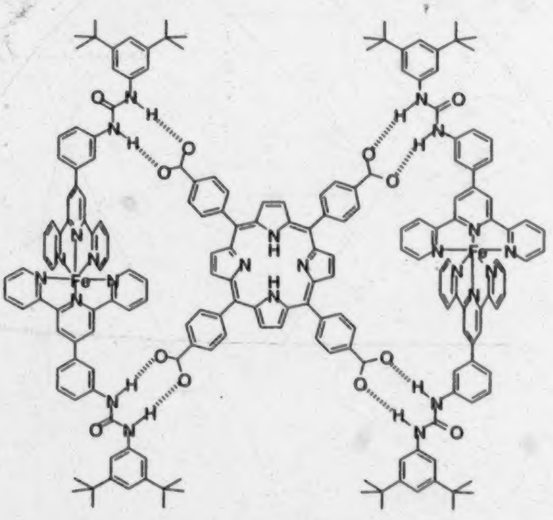

Figure 4. Proposed structure for the 2:1 complex formed when **7a** assembles with **20b**.

2.3. A molecular "brake"

In an attempt to bias the relative orientation and ultimately affect the rotation of the iron(terpyridine) fragment above the porphyrin plane, we examined the association of the pyrazine-modified coordination compound **7b** with the dianion of the metalloporphyrin **Zn17a** (Figure 5). In this molecular pair, we designed an additional recognition element expressed by the electrostatic attraction between the Lewis-acidic metal and the free nitrogen on the pyrazine, which can act as a Lewis base. The result is a molecular "brake" where the restricted rotation of the iron(terpyridine) component in **1** is even more restricted in the resulting pyrazine complex **Zn17a•7b**. As expected, in the ^{1}H NMR spectrum of **Zn17a•7b**, the signals for the urea N–H protons reside significantly downfield at 12.0 ppm and 11.6 ppm, indicative of strong hydrogen bonding between the molecular components. The orientation of the terpyridine ring is indeed biased as the furthest upfield signal corresponding to the protons of the pyrazine residue of **7b** resonates at 4.67 ppm. This value is 0.87 ppm further upfield than that of complex **1**, indicating a positive attraction between the lone pairs on the terminal nitogens and the zinc atom at the core of the porphyrin. The pyrazine signals, however, remain fairly broad, indicating that the iron(terpyridine) fragment continues to exist in a variety of slowly interconverting conformers and that, although the N → Zn coordination effectively slows the iron(terpyridine) rotor, it does not completely lock it into one conformation.

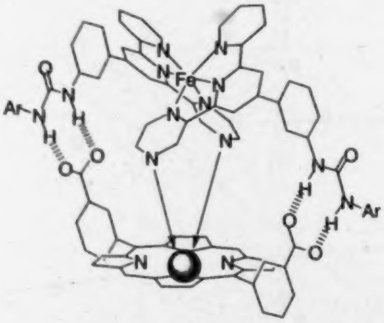

Figure 5. The molecular "brake".

2.4. Stability of the complexes

The strength of the binding between iron(terpyridine) **7a** and porphyrins **18a** and **20a** was too large to be accurately measured by ^{1}H NMR spectroscopy even in DMSO-d_6. The lack of any new or shifting absorption bands in the UV–Vis region of the spectrum during the formation of **1** or **2** also precluded this technique for the estimation of the association constants (K_a). Isothermal titration calorimetry (ITC), which measures the heat absorbed or evolved during a host-guest binding event, was employed to determine the thermodynamic parameters of the association of these high-affinity species. In addition to determining association constants, ITC conveniently provides the stoichiometry of binding as well as the enthalpy and entropy of association in a single experiment.

The integration of the heat generated as aliquots of iron(terpyridine) **7a** were added to a solution of porphyrin**18a** are plotted against the molar ratio generating the binding isotherm shown in Figure 6a. This curve fit to a one-site binding model. The steep upward sigmoidal nature of the resulting curve inflecting at a molar ratio of 1 indicates that a strong exothermic association ($K_a = 2.5 \times 10^6 \pm 4.4 \times 10^5$ M^{-1}) and 1:1

stoichiometry exists between **18a** and **7a**. Detailed calorimetric data for all titrations are collected in Table 1.

Table 1. Binding stoichiometries (N), association constants (K_a), association enthalpy (ΔH) and association entropy (ΔS) for the binding of porphyrins **13a**, **18a**, **18b**, **20a**, and **20b** with iron(terpyridine)s **7a–c** and **13** in DMSO at 25°C[a]

Entry	Components	Stoichiometry[d]	K_a (M^{-1})	ΔH (kcal mol^{-1})	ΔS (cal mol^{-1} deg^{-1})
1	**18a**[b] + **7a**	1.1 ± 0.1	$2.5 \times 10^6 \pm 4.4 \times 10^5$	–6.3 ± 0.1	8.0 ± 0.8
2	**18a**[b] + **7c**	0.1 ± 0.0	$6.9 \times 10^4 \pm 8.9 \times 10^3$	+4.3 ± 0.3	36.6 ± 1.6
3	**18b**[b] + **7a**	1.0 ± 0.1	$3.0 \times 10^4 \pm 6.1 \times 10^3$	–4.8 ± 0.0	4.6 ± 0.4
4	**18a**[b] + **13**	1.0 ± 0.1	$1.1 \times 10^6 \pm 3.0 \times 10^5$	–8.4 ± 0.2	0.3 ± 0.2
5	**Zn17a**[b] + **7b**	0.9 ± 0.1	$2.7 \times 10^6 \pm 4.4 \times 10^5$	–6.0 ± 0.1	9.1 ± 0.1
6	**20a**[c] + **7a**	2.0 ± 0.1	$2.5 \times 10^6 \pm 3.2 \times 10^5$	–5.9 ± 0.1	9.5 ± 0.4
7	**20a**[c] + **7c**	0.4 ± 0.1	$8.0 \times 10^4 \pm 3.0 \times 10^4$	+9.6 ± 2.5	64.4 ± 8.4
8	**20b**[c] + **7a**	2.1 ± 0.1	$4.3 \times 10^5 \pm 2.2 \times 10^4$	–5.4 ± 0.1	7.6 ± 0.3

[a] The data represent average values from duplicate experiments performed using fresh solutions. A typical experiment consisted of 60-70, 4 μL injections of a 1.45 mM solution of the terpyridine component into the calorimetry cell containing a 0.05 mM or 0.1 mM solution of the porphyrin component. A one-site binding model was employed for all data sets.

[b] [porphyrin] = 0.1 mM.

[c] [porphyrin] = 0.05 mM.

[d] Values represent equivalents of the terpyridine component per equivalent of the porphyrin component.

We argue that the reduced association between the two components in the corresponding xanthene complex **18a•13** is not due to any changes in hydrogen bonding, but instead, solely a result of changes in ion-pairing and solvation. We feel comfortable with this claim because the hydrogen bonding sites in **7a** and **13** are virtually identical. One reason for the lower value of K_a for **18a•13** stems from a diminished attraction of the oppositely-charged ion pairs, as the two components are now forced to reside further away from each other. This should, however, afford a less negative enthalpic term for the binding of **13** by **18a**, which was not observed (entries 1 and 4 in Table 1). An examination of the values of ΔS of association clearly show that the difference in K_a is entropically governed. The process of desolvation during a self-assembly reaction possesses an unfavorable enthalpic term (energy is required to break the bonds between the components and solvent molecules) and a favorable entropic term (there is an increase in disorder as solvent is released from the components). These arguments apply to complexes **1** and **18a•13**. In **18a•13**, because the two components are removed from each other in space, there are remaining solvent-accessible surfaces on both porphyrin faces and all around the iron(terpyridine) fragment. On the other hand, in **1** the two components are in direct contact and, in essence, solvate each other (at least on one face).

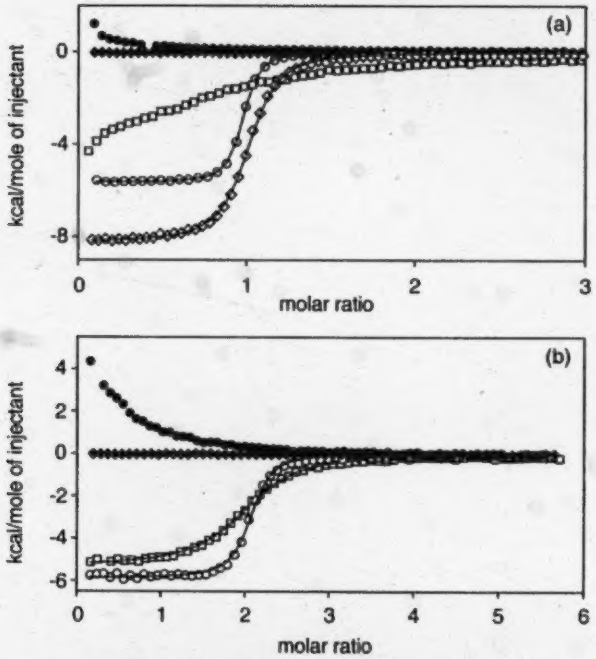

Figure 6. Heat change as iron(terpyridine)s **7a-c** and **13** are added to porphyrins **18a,b** and **20a,b** in DMSO. (a) **7a** into **18a** (○), **7c** into **18a** (●), **7a** into **18b** (□), **13** into **18a** (◊), and **7a** into DMSO (◆); (b) **7a** into **20a** (○), **7c** into **20a** (●), **7a** into **20b** (□) and **7a** into DMSO (◆). The solid lines represent the calculated isotherms.

When the hydrogen bonds are not suitably positioned to form a finite 1:1 complex, as is the case in the *para*-substituted porphyrin **18b**, the binding isotherm loses its sigmoidality and substantially flattens out. This clearly indicates that the lack of cooperative hydrogen bonding and the separation of the ion pairs in space result in a substantially weaker association between the molecular components (entry 3 in Table 1).

When hydrogen bonding is absent and association is purely ionic in nature, as is the case between porphyrin **18a** and the *N,N'*-dimethylated iron(terpyridine) **7c**, an endothermic isotherm was produced. This can be expected for ion pairing, where association is entropically driven with ΔH close to zero or positive (entry 2 in Table 1). Attempts to fit the ITC data to a one-site model resulted in a low binding stoichiometry and value of K_a. The low stoichiometries are likely a result of non-specific aggregation, typical of undefined ion pairing interactions. This data is consistent with previous ITC studies on non-specific solution based aggregation processes.[57]

When the metalloporphyrin **Zn17a** was titrated with **7a**, several of the initial points consistently deviated from the ideal single-site binding behavior. We attribute this to self-association between metalloporphyrins through the interaction of the carboxylate group and the zinc atom when low concentrations of iron(terpyridine) **7a** are present early in the titration. When these points were excluded from the curve fitting analysis, an association constant similar to that of complex **1** was obtained (entry 5 in Table 1).[45] We were surprised that, despite its having a significant impact on the dynamic nature of the terpyridine rotor, the additional N → Zn dative interaction does not seem to contribute to the stability of the supramolecular complex.

The binding isotherm for porphyrin **20a** and **7a** were fit to a two-site binding model to yield the expected 1:2 stoichiometry and two similar association constants indicative of non-cooperativity (Figure 6b and entry 6 in Table 1). It is not surprising that the two hydrogen bond chelation sites in **20a** act independently as the binding of the iron(terpyridine) component on one face of the macrocycle is not expected to have any impact on the other.

The results of the ITC experiment using the tetra-*para*-substituted porphyrin **20b** and **7a** also indicate the formation of a complex with a 1:2 stoichiometry (entry 8 in Table 1). Because the iron(terpyridine) fragment cannot strap across the face of the porphyrin macrocycle, as has already been proposed (see Figure 4), the association between **20b** and **7a** is somewhat reduced as compared to the corresponding strapped complex **2**. This is surely due to a combination of a looser fit between **20b** and **7a** (Adjacent carboxylate groups on the porphyrin do not completely span the receptor cleft provided by the **7a**.), as well as, the fact that the hydrogen bonding vectors are slightly less than ideal (90° between adjacent carboxylates for **20b**, as opposed to the more ideal 60° vectors for **20a**).

The data from the titration of **20a** with *N,N'*-dimethylated iron(terpyridine) **7c** suggest that a non-specific aggregate was produced from the self-assembly reaction as we have already argued for the association of **18a** with the same iron(terpyridine) component (entry 7 in Table 1).

Two things are evident from our calorimetric studies: (1) ion pairing significantly contributes to the association between these anionic porphyrins and cationic iron(terpyridines), however, (2) complimentary hydrogen bonding is ultimately responsible for the stoichiometic association and large exothermic response.

2.5. Fluorescence quenching behavior

The proximity and relative positioning of the two components within complexes **1** and **2** have a significant impact on the photophysical behavior of the final assemblies. Studies using steady-state fluorescence spectroscopy to monitor the changes in the emission intensities of DMSO solutions of **18a** and **20a** as the porphyrins were treated with aliquots of **7a** are shown in Figure 7.[58] The immediate quenching of the fluorescence of **18a** is clearly a consequence of both the strong association and the intimacy of the two chromophores, which ensures maximum through-space communication. The large extent of fluorescence quenching by **7a** as compared to its *N,N'*-dimethylated counterpart **7c**, which only slightly quenched the fluorescence of **18a** in a collisions-dependant process, clearly indicates that an intracomplex quenching mechanism is in effect within **1**. Although still significant, the slightly reduced fluorescence quenching observed as xanthene **13** was added to porphyrin **18a** is most likely due to a combination of the weaker association between the two components and an increase in the distance between the two chromophores. Despite the fact that both hydrogen-bonding and ion pairing are present in the $\mathbf{7a}_n\bullet\mathbf{18b}_m$ polymolecular assembly, the iron(terpyridine) fragment cannot form a cooperative hydrogen bond strapped arrangement, resulting in reduced association between the molecular components and a significant lowering of the through-space communication between the chromophores. This is reflected in the titration of **18a** with **7a**.

A dramatic decrease in fluorescence was also observed when **7a** was titrated into a DMSO solution of porphyrin **20a**. When the *para*-substituted porphyrin **20b** was titrated with **7a**, the extent of quenching response was significantly reduced, and a much shallower quenching curve was produced. We attribute this to the fact that the iron(terpyridine) component can only bind onto the side of the porphyrin and not across its face. Consequently, the distance between the two chromophores in the proposed complex (Figure 4) is greater than that in **2**.

When a sufficiently good electron acceptor is proximal, porphyrins are known to undergo rapid photoinduced electron transfer.[59] The result is a reduction in the observed fluorescence of the porphyrin because the photoexcited electron is non-emitting as it recombines with the porphyrin and relaxes back to the ground state. Alternatively, the fluorescence of a porphyrin can be quenched in an energy transfer process.[60] This requires adequate overlap between the emission band of the photoexcited molecule and absorption band of the energy acceptor molecule. Because there is minimal overlap between the porphyrin emission band and the metal-to-ligand charge transfer (MLCT) absorption band of the iron(terpyridine) in the present systems (see Supporting

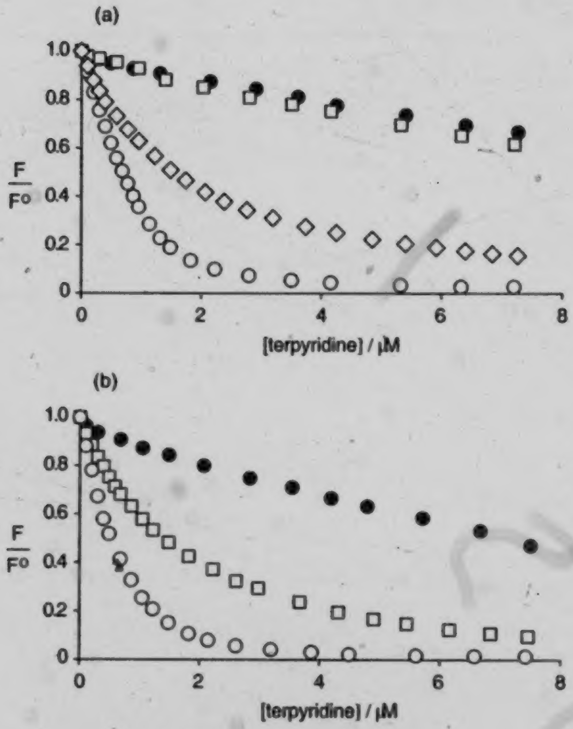

Figure 7. Inverse Stern-Volmer plots for fluorescence quenching titrations of (a) **18a** with **7a** (○), **18a** with **7c** (●), **18b** with **7a** (□) and **18a** with **13** (◊); (λ_{ex} = 415 nm, λ_{em} = 630 nm), and (b) **20a** with **7a** (○), **20a** with **7c** (●), and **20b** with **7a** (□); (λ_{ex} = 430 nm, λ_{em} = 650 nm). All titrations were performed in DMSO. [porphyrin] = 1.0×10^{-6} M, [iron(terpyridine)] = 2.0×10^{-5} M

Information), we believe that an energy transfer mechanism is not favorable, although, at this point, an energy transfer mechanism cannot be completely ruled out.

3. Conclusions

These experiments clearly highlight the need to consider a polytopic approach in self-assembly synthesis, where the advantageous features of more than one type of molecular recognition interaction can be harnessed to provide access to robust and well-ordered supramolecular assemblies. In the present cases, ion pairing certainly contributes to the stability of complexes **1** and **2**, however, it is the cooperative hydrogen bonds that, not only aid in maintaining the structural integrity of the assemblies, but are the critical element necessary to align the building blocks into the optimal spatial arrangement so that the ion pairing attractive forces can be maximized. The complexes described in this report also represent attractive architectures to investigate the through-space communication of chromophores and the motion of the building blocks within the assemblies. The ability to fine tune the photonic and dynamic behavior of the supermolecules by modifying the chromophores (varying the metal within the metallo(terpyridine) and the metalloporphyrin, for example) and/or by tailoring the size of the components (varying their proximity, for example) is paramount if supramolecular architectures are to be applied as the components of molecular machinery.

4. Experimental

4.1 General

All solvents (Caledon) were distilled prior to use with the exception of DMSO which was used as received. Solvents for NMR analysis (Cambridge Isotope Laboratories) were used as received. All synthetic precursors were purchased from Aldrich with the exception of aldehyde **14b** which was purchased from Acros.

^{1}H NMR characterizations were performed on a Varian Inova-500 instrument, working at 499.92 MHz, on a Varian Inova-400 instrument, working at 399.96 MHz, or on a Varian Inova-300 instrument, working at 299.96 MHz. Chemical shifts (δ) are reported in parts per million relative to tetramethylsilane using the residual solvent peak as a reference standard. FT-IR measurements were performed using a Nicolet Magna-IR 750 spectrometer. UV-Vis absorption measurements were performed using a Varian Cary 400 Scan spectrophotometer. Low resolution mass spectrometry measurements were preformed using an Agilent Technologies 1100 MSD with an electrospray source. High resolution measurements were preformed using a Kratos MS-50 with an electron impact source or a PerSeptive Biosystems (Mariner) MS with an electrospray source. Solutions of complex **1**, **2**, **18a•13** and **Zn17a•7a** in 10% DMF/MeOH were prepared by dissolving the isolated complexes in a minimal amount of DMF and then diluting with methanol. These solutions were infused into the electrospray source (flow rate - 30 μL/min, nebulizer pressure - 12 psi). All other electrospray data were obtained by standard injection procedures.

4.2. Synthesis of iron(terpyridine)s

4.2.1. *N*-(2-(Pyrazyl)-2-oxoethyl)pyridinium iodide (3b). A mixture of 2-acetylpyrazine (370 mg, 3.0 mmol), iodine (573 mg, 4.6 mmol) and pyridine (20 mL) was heated at reflux for 8 h. The reaction mixture was cooled to room temperature and filtered. The isolated solid was washed several times with cold pyridine and then ether. Yield 58%; mp 231-232°C; ^{1}H NMR (300 MHz, DMSO-d_6) δ 9.24 (d, *J*=1.2 Hz, 1H), 9.07 (d, *J*=2.4 Hz, 1H), 8.96 (m, 3H), 8.74 (dt, *J*=7.8, 1.0 Hz, 1H), 8.28 (dd, *J*=7.8, 6.6 Hz, 2H); ^{13}C NMR APT (75 MHz, DMSO-d_6) δ 191.0 (C), 149.6 (CH), 146.5 (CH), 146.3 (CH), 145.2 (C), 144.3 (CH), 142.9 (CH), 127.7 (CH), 66.3 (CH_2); IR (µscope) υ 3125, 3079, 2965, 2817, 1705, 1634, 1574, 1488, 1470, 1408, 1344, 1311, 1222, 1195, 1171 cm^{-1}; HRMS (ES) Calcd for $[M-I]^+$ ($C_{11}H_{10}N_3O$) 200.0818. Found: 200.0820.

4.2.2. 2,2'-Pyridine-4,3''-nitrophenyl-6,2'''-pyrazyl pyridine (5b). A mixture of **3b** (1.22 g, 3.74 mmol), dry NH_4OAc (5.4 g, 100 mmol), **4** (950 mg, 3.74 mmol), and AcOH (20 mL) was heated at reflux for 20 h. The cooled mixture was filtered and the resulting precipitate was collected by filtration and washed several times with cold MeOH. Yield 83%; mp 205-207°C; ^{1}H NMR (300 MHz, $CDCl_3$) δ 9.89 (d, *J*=0.9 Hz, 1H), 9.07 (d, *J*=1.8 Hz, 1H), 8.68 (m, 6H), 8.26 (d, *J*=8.1 Hz, 1H), 8.20 (d, *J*=7.8 Hz, 1H), 7.92 (dd, *J*=7.8, 1.8 Hz, 1H), 7.71 (t, *J*=7.8 Hz, 1H), 7.39 (ddd, *J*=7.8, 4.8, 1.2 Hz, 1H); ^{13}C NMR APT (75 MHz, $CDCl_3$) δ 156.9 (C), 153.3 (C), 154.6 (C), 150.7 (C), 149.3 (CH), 149.0 (C), 148.0 (C), 144.9 (CH), 143.7 (CH), 143.6 (CH), 140.1 (C), 137.2 (CH), 133.3 (CH), 130.2 (CH), 124.4 (CH), 123.9 (CH), 122.3 (CH), 121.5 (CH), 119.5 (CH), 119.1 (CH); IR (µscope) υ 3063, 1604, 1569, 1533, 1470, 1432, 1380, 1350, 1287, 1124, 1017 cm^{-1}; HRMS (EI) Calcd for M^+ ($C_{20}H_{13}N_5O_2$) 355.1069. Found: 355.1084.

4.2.3. 2,2'-Pyridyl-4,3''-aminophenyl-6,2'''-pyrazyl pyridine. $SnCl_2{\cdot}2H_2O$ (3.0 g, 13.6 mmol) was added to a hot (70-80°C) solution of **5b** (600 mg, 1.70 mmol) in absolute EtOH (50 mL). After stirring at 70-80°C for 2-3 h, the cooled solution was poured into an ice-cold mixture of diethylenetriaminepentacetic acid (DTPA) (4.65 g, 11.8 mmol) and H_2O (100 mL). The mixture was neutralized with saturated $NaHCO_3$, the aqueous phase was extracted with $CHCl_3$ (3 × 50 mL), and the combined organic extracts were dried over Na_2SO_4. The chloroform was removed under vacuum yielding an off-white solid. The crude amine was carried on without further purification. Crude yield 90%; mp 229-231°C; ^{1}H NMR (300 MHz, CD_2Cl_2) δ 9.86 (d, *J*=1.5 Hz, 1H), 8.78 (d, *J*=1.8 Hz, 1H), 8.73-8.69 (m, 2H), 8.67-8.62 (m, 3H), 7.91 (dt, *J*=7.8, 1.8 Hz, 2H), 7.38 (ddd, *J*=6.0, 4.8, 1.2 Hz, 1H), 7.31 (t, *J*=7.5 Hz, 1H), 7.24 (dt, *J*=7.8, 1.8 Hz, 1H), 7.20 (dd, *J*=2.4, 1.8 Hz, 1H), 6.80 (ddd, *J*=7.8, 2.4, 1.2 Hz, 1H), 3.90 (br s, 2H); ^{13}C NMR APT (125 MHz, CD$_2$Cl$_2$) δ 156.6 (C), 156.2 (C), 154.5 (C), 151.5 (C), 151.0 (C), 149.6 (CH), 147.9 (C), 145.0 (CH), 144.0 (CH), 143.9 (CH), 139.7 (C), 137.3 (CH), 130.4 (CH), 124.4 (CH), 121.6 (CH), 119.7 (CH), 119.4 (CH), 117.5 (CH), 116.1 (CH), 113.7 (CH); IR (μscope) υ 3426, 3350, 3221, 3051, 1623, 1602, 1585, 1568, 1547, 1495, 1470, 1431, 1380, 1260, 1117 cm^{-1}; HRMS (ES) Calcd for [*M*+H]$^+$ (C$_{20}$H$_{16}$N$_5$) 326.1400. Found: 326.1398.

4.2.4. Urea 6a. Triphosgene (93 mg, 0.31 mmol) was added to a solution of 4'-(3'''-aminophenyl)-2,2':6,2"-terpyridine (302 mg, 0.93 mmol) and triethylamine (212 mg, 2.1 mmol) in freshly distilled CH$_2$Cl$_2$ (50 mL). After 2 h, 3,5-di-*tert*-butylamine (229 mg, 1.12 mmol) was added and the reaction stirred for an additional 2 h. The CH$_2$Cl$_2$ was removed under vacuum, the residue was dissolved in chloroform (100 mL), and shaken with 5% HCl (100 mL). The resulting yellow precipitate was washed several times with chloroform and then suspended in fresh chloroform (100 mL). The suspension was shaken with 5% NaOH (50 mL) and the layers separated. The resulting aqueous layer was extracted once with chloroform (50 mL) and the combined organic extracts were dried over Na$_2$SO$_4$. The chloroform was removed under vacuum and the resulting residue was triturated with a minimal amount of CHCl$_3$ (2 × 5 mL) and filtered yielding a white solid. The impure mother liquor was purified by column chromatography through alumina (Act II-III) using CHCl$_3$ as the eluent. Combined yield 78%; mp 236-237°C; ^{1}H NMR (300 MHz, CDCl$_3$) δ 8.70 (m, 2H), 8.68 (s, 2H), 8.64 (d, *J*=7.2 Hz, 2H), 7.86 (dt, *J*=8.1, 1.8 Hz, 2H), 7.67-7.60 (m, 3H), 7.45 (t, *J*=8.1 Hz, 1H), 7.33 (dd, *J*=7.8, 4.8 Hz, 2H), 7.24 (m, 1H), 7.18 (d, *J*=1.2 Hz, 2H), 6.73 (br s, 1H), 6.41 (br s, 1H) 1.33 (s, 18H); ^{13}C NMR (75 MHz, CDCl$_3$) δ 155.7, 154.9, 152.7, 150.7, 149.5, 149.4, 140.9, 138.8, 138, 137.5, 129.9, 124.5, 120.9, 120.2, 119.2, 117.8, 116.2, 115.9, 113.0, 34.5, 31.2; IR (μscope) υ 3332, 3155, 3054, 2963, 2904, 2867, 1651, 1607, 1586, 1567, 1441, 1287 cm^{-1}; HRMS (ES) Calcd for [*M*+H]$^+$ (C$_{36}$H$_{38}$N$_5$O) 556.3076. Found: 556.3076.

4.2.5. Pyrazyl urea 6b. Triphosgene (110 mg, 0.37 mmol) was added to a solution of 2,2'-pyridine-4,3"-aminophenyl-6,2"'-pyrazylpyridine (360 mg, 1.11 mmol) and triethylamine (400 mg, 3.70 mmol) in freshly distilled CH$_2$Cl$_2$ (125 mL). After 5-10 minutes, 3,5-di-*tert*-butylamine (228 mg, 1.11 mmol) was added and the reaction stirred for an additional 2 h. The reaction mixture was shaken with 5% HCl (2 × 50 mL), extracted with CH$_2$Cl$_2$ and the combined organic extracts were dried over Na$_2$SO$_4$. The solvent was removed under vacuum and the resulting residue recrystallized from acetone affording a white solid. Yield 65%; mp 290-292°C; ^{1}H NMR (300 MHz, acetone-*d*$_6$) δ

9.85 (d, *J*=1.5 Hz, 1H), 8.85 (d, *J*=1.5 Hz, 1H), 8.78-8.69 (m, 5H), 8.41 (br s, 1H), 8.15 (br s, 1H), 8.09 (t, *J*=2.1 Hz, 1H), 8.01 (dt, *J*=7.8, 1.8 Hz, 1H), 7.74 (dt, *J*=7.5, 1.8 Hz, 1H), 7.55-7.46 (m, 3H), 7.43 (d, *J*=1.8 Hz, 2H), 7.11 (dd, *J*=1.5, 1.5 Hz, 1H), 1.28 (s, 18H); ^{13}C NMR (75 MHz, DMSO-d_6) δ 155.9, 154.5, 153.9, 152.7, 150.7, 149.9, 149.8, 149.3, 145.3, 144.1, 142.8, 140.9, 138.8, 137.7, 137.6, 129.9, 124.7, 121.92, 120.2, 119.4, 118.4, 118.3, 116.2, 115.9, 113.0, 34.5, 31.2; IR (µscope) υ 3329, 1952, 1650, 1602, 1586, 1567, 1468, 1440, 1379, 1362, 1293, 1227 cm^{-1}; HRMS (ES) Calcd for $[M+H]^+$ ($C_{35}H_{37}N_6O$) 557.3023. Found: 557.3025.

4.2.6. *N,N'*-Dimethyled urea 7c. A solution of **6a** (38.0 mg, 0.068 mmol) in anhydrous DMF (3 mL) was treacted with NaH (8 mg, 0.33 mmol). After 15 minutes of stirring at room temperature, iodomethane (12 µL) was added and the reaction stirred at 50°C under argon for 1.5 h. The reaction mixture was cooled to room temperature and H_2O (10 mL) was added. The mixture was extracted with EtOAc (3 × 10 mL) and the combined organic extracts were dried over Na_2SO_4. The solvent was removed under reduced pressure and the residue was purified by column chromatography (1:1 hexane/EtOAc) through Alumina (Act II-III) affording a white solid. Yield 96%; ^{1}H NMR (300 MHz, $CDCl_3$) δ 8.70 (m, 2H), 8.63 (d, *J*=8.1 Hz, 2H), 8.52 (s, 2H), 7.86 (td, *J*=7.5, 2.1 Hz, 2H), 7.41 (d, *J*=7.5 Hz, 1H), 7.33 (ddd, *J*=7.5, 4.5, 0.9 Hz, 2H), 7.17 (s, 1H), 7.14 (t, *J*=7.5 Hz, 2H), 6.95 (dd, *J*=1.8, 1.8 Hz, 1H), 6.86 (d, *J*=7.8 Hz, 2H), 6.61 (d, *J*=1.8 Hz, 2H), 3.26 (s, 3H), 3.25 (s, 3H), 1.11 (s, 18H); ^{13}C NMR (75 MHz, $CDCl_3$) δ 161.6, 156.2, 156.0, 151.3, 149.2, 146.5, 144.9, 139.1, 138.8, 129.0, 126.5, 124.5, 123.9, 121.3, 120.5, 119.3, 118.8, 39.7, 39.4, 34.7, 31.3; HRMS (EI) Calcd for M^+ ($C_{38}H_{41}N_5O$) 583.3311. Found: 583.3310.

4.2.7. 9,9'-Dimethyl-3-nitro-xanthene. A solution of 9,9'-dimethylxanthene (**8**) (2.1 g, 10.0 mmol) in glacial acetic acid (50 mL) was treated with fuming HNO_3 (700 mg) and fuming H_2SO_4 (1 mL). After stirring at room temperature for 2 h, the reaction mixture was poured over ice (200 mL) and neutralized by the careful addition of solid $NaHCO_3$. The mixture was extracted with CH_2Cl_2 (3 × 100 mL) and the combined organic extracts were dried over Na_2SO_4. The solvent was removed under vacuum and the residue purified by column chromatography through silca (50:1 hexane/EtOAc) affording a pale yellow solid. Yield 78%; mp 102–103°C; ^{1}H NMR (300 MHz, CD_2Cl_2) δ 8.37 (d, *J*=2.7 Hz, 1H), 8.10 (dd, *J*=9.0, 2.7 Hz, 1H), 7.47 (dd, *J*=7.8, 2.7 Hz, 1H), 7.26 (ddd, *J*=7.2, 1.5, 0.6 Hz, 1H), 7.16 (td, *J*=7.5, 1.5 Hz, 1H), 7.16 (d, *J*=9.0 Hz, 1H), 7.10 (dd, *J*=7.8, 1.5 Hz, 1H), 1.68 (s, 6H); ^{13}C NMR APT (125 MHz, CD_2Cl_2) δ 155.6 (C), 149.7 (C), 143.9 (C), 131.5

(C), 129.2 (C), 128.3 (CH), 126.7 (CH), 124.8 (CH), 123.8 (CH), 123.4 (CH), 117.5 (CH), 116.8 (CH), 34.7 (C), 32.8 (CH_3); IR (µscope) υ 3099, 2986, 2963, 2930, 2865, 2463, 2073, 1917, 1803, 1633, 1600, 1575, 1517, 1481, 1467, 1447, 1421, 1369, 1338, 1299, 1259, 1206, 1157, 1134, 1110, 1076, 1040 cm^{-1}; HRMS (EI) Calcd for M^+ ($C_{15}H_{13}NO_3$) 255.08954. Found: 255.08963.

4.2.8. 6-*tert*-Butyl-9,9'-dimethyl-3-nitroxanthene (9). A solution of 9,9'-dimethyl-3-nitro-xanthene (1.91 g, 7.5 mmol) in CH_2Cl_2 (50 mL) was treated with *tert*-butyl chloride (694 mg, 7.5 mmol), followed by $FeCl_3$ (catalytic). After stirring at room temperature over night, the reaction was quenched by the addition of water (100 mL), extracted with CH_2Cl_2 and dried over Na_2SO_4. Recrystallization from EtOH afforded pale yellow crystals. Yield 74%; mp 162–168°C (decomp.); ^{1}H NMR (300 MHz, CD_2Cl_2) δ 8.36 (d, J=2.7 Hz, 1H), 8.08 (dd, J=9.0, 2.7 Hz, 1H), 7.45 (d, J=2.1 Hz, 1H), 7.29 (dd, J=8.7, 2.1 Hz, 1H), 7.14 (d, J=9.0 Hz, 1H), 7.02 (d, J=9.0 Hz, 1H), 1.69 (s, 6H), 1.34 (s, 9H); ^{13}C NMR APT (125 MHz, CD_2Cl_2) δ 155.8 (C), 147.7 (C), 147.4 (C), 143.8 (C), 131.6 (C), 128.3 (CH), 125.4 (CH), 123.7 (CH), 123.4 (CH), 123.2 (CH), 117.5 (CH), 116.2 (CH), 34.9 (C), 34.9 (C), 32.9 (CH_3), 31.6 (CH_3); IR (µscope) υ 3078, 2966, 2905, 2869, 1631, 1600, 1577, 1516, 1499, 1481, 1424, 1407, 1395, 1386, 1362, 1330, 1307, 1295, 1266, 1212, 1146, 1123, 1110, 1088, 1076 cm^{-1}; HRMS (EI) Calcd for M^+ ($C_{19}H_{21}NO_3$) 311.15213. Found: 311.15131.

4.2.9. 3-*tert*-Butyl-9,9'-dimethyl-6-nitro-xanthene carboxaldehyde (10). Hexamethylenetetraamine (HMTA) (491 mg, 3.5 mmol) was added in one portion to a solution of xanthene **9** (934 mg, 3.0 mmol) in CF_3CO_2H (10 mL). After heating at reflux for 24 h, the reaction was cooled and poured into 4 M HCl (100 mL). After stirring at room temperature for 15 minutes, the mixture was extracted with CH_2Cl_2 (3 × 100 mL), the combined organic extracts were dried over Na_2SO_4 and the solvent evaporated under vacuum. Purification by column chromatography through silica (CH_2Cl_2) afforded a white solid. Yield 628 mg (62%); mp 237–239°C; ^{1}H NMR (300 MHz, CD_2Cl_2) δ 10.66 (s, 1H), 8.40 (d, J=2.7 Hz, 1H), 8.14 (dd, J=9.0, 2.7 Hz, 1H), 7.81 (d, J=2.7 Hz, 1H), 7.74 (d, J=2.7, 1H), 7.27 (d, J=9.0 Hz, 1H), 1.72 (s, 6H), 1.36 (s, 9H); ^{13}C NMR APT (125 MHz, CD_2Cl_2) δ 188.9 (CH), 154.6 (C), 149.6 (C), 147.6 (C), 144.4 (C), 131.4 (C), 129.9 (CH), 129.9 (C), 124.0 (CH), 123.9 (CH), 123.6 (C), 123.3 (CH), 117.8 (CH), 36.9 (C), 34.9 (C), 32.7 (CH_3), 31.3 (CH_3); IR (µscope) υ 3335, 3075, 2982, 2967, 2875, 2761, 1675, 1648, 1628, 1606, 1582, 1525, 1462, 1421, 1391, 1363, 1340, 1329, 1301, 1277, 1268, 1254, 1229, 1205, 1159, 1129, 1115, 1076 cm^{-1}; HRMS (EI) Calcd for M^+ ($C_{20}H_{21}NO_4$) 339.14706. Found: 339.14714.

4.2.10. Nitroterpyridine 11. A mixture of aldehyde **10** (250 mg, 0.737 mmol), 2-acetylpyridine (300 mg, 2.50 mmol), 5% aqueous NaOH (1 mL) and EtOH (3 mL) was stirred at room temperature for 15 h. The reaction was concentrated to dryness leaving a pink amphorous solid (385 mg). The pink solid (193 mg) was suspended in glacial acetic acid (1 mL), treated with excess NH_4OAc (1 g) and heated at reflux for 15 h. The reaction was cooled and diluted with 50% aqueous EtOH, affording a yellow precipitate. The precipitate was collected by vacuum filtration and washed with 50% aqueous EtOH. Recrystallization from EtOH/H_2O afforded an off-white solid. Yield 63%; mp 201–203°C; ^{1}H NMR (300 MHz, CD_2Cl_2) δ 8.72 (m, 6H), 8.40 (d, *J*=2.4 Hz, 1H), 8.06 (dd, *J*=9.0, 2.7 Hz, 1H), 7.92 (td, *J*=7.5, 1.8 Hz, 2H), 7.58 (d, *J*=2.1 Hz, 1H), 7.50 (d, *J*=2.1 Hz, 1H), 7.38 (m, 2H), 7.11 (d, *J*=9.0 Hz, 1H), 1.77 (s, 6H), 1.41 (s, 9H); ^{13}C NMR APT (125.7 MHz, CD_2Cl_2) δ 156.6 (C), 155.9 (C), 149.6 (CH), 148.1 (C), 147.7 (C), 144.8 (C), 144.0 (C), 137.2 (CH), 131.9 (C), 129.6 (C), 127.6 (C), 124.2 (CH), 123.8 (CH), 123.8 (CH), 123.1 (CH), 122.1, (CH), 121.5 (CH), 117.7 (CH), 35.4 (C), 35.1 (C), 32.4 (CH_3), 31.6 (CH_3); IR (μscope) υ 3062, 2963, 2869, 1728, 1627, 1605, 1582, 1567, 1542, 1524, 1489, 1468, 1440, 1420, 1388, 1364, 1342, 1266, 1226, 1215, 1173, 1117, 1089 cm^{-1}; HRMS (EI) Calcd for M^+ ($C_{34}H_{30}N_4O_3$) 542.23181. Found: 542.23153.

4.2.11. 4'-(3-Amino-6-*tert*-butyl-9,9'-dimethylxanthyl)-2,2':6',2''-terpyridine. This amine was synthesized using $SnCl_2$ following the same procedure used to prepare 2,2'-pyridyl-4,3''-aminophenyl-6,2'''-pyrazyl pyridine. Yield 96%; mp 130°C (decomp); ^{1}H NMR (500 MHz, CD_2Cl_2) δ 8.73 (s, 2H), 8.71 (m, 4H), 7.91 (td, *J*=7.5, 1.5 Hz, 2H), 7.53 (d, *J*=2.5 Hz, 1H), 7.43 (d, *J*=2.0 Hz, 1H), 7.36 (m, 2H), 6.81 (d, *J*=9.0 Hz, 1H), 6.78 (d, *J*=3.0 Hz, 1H), 6.51 (dd, *J*=9.0, 2.5, 1H), 3.57 (br s, 2H), 1.67 (s, 6H), 1.40 (s, 9H); ^{13}C NMR APT (125.7 MHz, CD_2Cl_2) δ 156.9 (C), 155.7 (C), 149.6 (CH), 148.8 (C), 146.7 (C), 145.7 (C), 144.0 (C), 142.9 (C), 137.1 (CH), 131.7 (C), 130.8 (C), 126.9 (C), 125.7 (CH), 124.0 (CH), 123.7 (CH), 122.2 (CH), 121.4 (CH), 117.3 (CH), 114.7 (CH), 112.2 (CH), 35.3 (C), 34.9 (C), 31.7 (CH_3), 31.7 (CH_3); IR (μscope) υ 3440, 3350, 3250, 3060, 2963, 2868, 1681, 1626, 1585, 1567, 1547, 1503, 1469, 1439, 1389, 1362, 1295, 1276, 1243, 1218, 1151, 1125, 1090 cm^{-1}; HRMS (EI) Calcd for M^+ ($C_{34}H_{32}N_4O$) 512.25763. Found: 512.25613.

4.2.12. Terpyridine 12. This urea was synthesized following the same procedure used to prepare **6b**. Purification by column chromatography (3:1 hexane/EtOAc) through

Alumina (Act II-III) afforded a white solid. Yield 65%; mp 237–239°C; ^{1}H NMR (500 MHz, CD_2Cl_2) δ 8.73 (s, 2H), 8.70 (m, 4H), 7.90 (td, *J*=7.5, 1.5 Hz, 2H), 7.53 (d, *J*=2.5 Hz, 1H), 7.48 (d, *J*=2.5 Hz, 1H), 7.45 (d, *J*=2.5 Hz, 1H), 7.35 (m, 2H), 7.20 (d, *J*=1.5 Hz, 2H), 7.18 (t, *J*=1.5 Hz, 1H), 7.14 (dd, *J*=9.0, 2.5 Hz, 1H), 6.95 (d, *J*=9.0 Hz, 1H), 6.81 (br s, 1H), 6.74 (br s, 1H), 1.67 (s, 6H), 1.39 (s, 9H), 1.29 (s, 18H); ^{13}C NMR (125.7 MHz, CD_2Cl_2) δ 156.5, 155.2, 153.8, 152.2, 149.2, 148.5, 147.9, 145.8, 145.6, 137.2, 136.9, 132.9, 131.4, 129.8, 126.7, 125.6, 123.7, 123.1, 122.1, 121.7, 121.4, 119.9, 118.8, 117.5, 116.3, 35.0, 34.9, 34.7, 31.9, 31.6, 31.4; IR (µscope) υ 3321, 3064, 2963, 2926, 2867, 1650, 1604, 1585, 1567, 1501, 1469, 1439, 1411, 1391, 1363, 1275, 1245, 1224, 1090 cm^{-1}; HRMS (ES) Calcd for $[M+H]^+$ ($C_{49}H_{54}N_5O_2$) 744.42720. Found: 744.42824.

4.2.13. General metal-coordination procedure. $Fe(BF_4)_2{\bullet}6H_2O$ (0.150 mmol) was added to a suspension of terpyridine **7a-c** or **12** (0.30 mmol) in MeOH (50 mL). The mixture immediately turned purple yielding a homogenous solution, which was further stirred for 3 h at room temperature. The volume of MeOH was reduced to 5-10 mL, at which point 5-10 mL of Et_2O was added affording a purple solid. The solid was isolated by filtration and washed times with cold acetone/Et_2O (1:4).

(7a): Prepared from **6a**. Yield 95%; ^{1}H NMR (300 MHz, acetone-d_6) δ 9.55 (s, 4H), 9.06 (d, *J*=7.8 Hz, 4H), 8.70 (s, 2H), 8.51, (br s, 2H), 8.28 (br s, 2H), 8.07 (dt, *J*=7.8, 1.2 Hz, 4H), 7.95 (d, *J*=7.8 Hz, 2H), 7.64 (m, 8H), 7.52 (d, *J*=1.5 Hz, 4H), 7.27 (m, 4H), 6.90 (d, *J*=1.5 Hz, 4H), 1.34 (s, 36H); ^{13}C NMR (75 MHz, acetone-d_6) δ 161.5, 159.3, 154.2, 153.8, 152.0, 151.9, 142.2, 140.2, 139.7, 138.3, 130.8, 128.5, 124.9, 122.5, 122.4, 121.5, 118.7, 117.3, 114.3, 35.5, 31.8; UV–Vis (DMSO) λ_{max}/nm (log ε/M^{-1} cm^{-1}) 279 (5.05), 288 (5.04), 328 (4.84), 573 (4.51); IR (µscope) υ 3381, 3078, 2962, 2904, 2867, 1698, 1606, 1548, 1495, 1440, 1396, 1298, 1217 cm^1; HRMS (ES) Calcd for $[M{-}2BF_4]^{2+}$ ($C_{72}H_{74}N_{10}O_2Fe$) 583.2667. Found: 583.2672.

(7b): Prepared from **6b** using a mixture of 1:1 MeOH/acetone instead of pure MeOH as the solvent. Yield 92%; ^{1}H NMR (300 MHz, acetone-d_6) δ 10.07 (s, 2H), 9.67 (s, 2H), 9.53 (s, 2H), 9.04 (d, *J*=7.8 Hz, 2H), 8.66 (s, 2H), 8.48 (br s, 2H), 8.30 (d, *J*=3.0 Hz, 2H), 8.25 (br s, 2H), 8.09 (t, *J*=7.8 Hz, 2H), 7.90 (d, *J*=6.6 Hz, 2H), 7.78 (d, *J*=3.0 Hz, 2H), 7.70-7.64 (m, 6H), 7.49 (d, *J*=1.5 Hz, 4H), 7.15 (dd, *J*=1.5, 1.5 Hz, 2H); ^{13}C NMR (75 MHz, CD_3CN/acetone-d_6 (1:3)) δ 161.8, 160.1, 159.1, 155.7, 154.8, 154.3, 153.3, 152.7, 150.2, 148.4, 145.3, 142.8, 140.8, 140.3, 138.7, 131.4, 129.3, 125.6, 123.9, 123.7, 123.2, 122.2, 119.4, 115.0, 35.9, 32.1; UV–Vis (DMSO) λ_{max}/nm (log ε/M^{-1} cm^{-1}) 268 (4.95), 334 (4.56), 578 (4.12); IR ($CHCl_3$, cast) υ 3288, 3074, 2962, 2865, 1695, 1607, 1552, 1495, 1468, 1439, 1413, 1393, 1300, 1217 cm^{-1}; HRMS (ES) Calcd for $[M\text{–}2BF_4]^{2+}$ ($C_{70}H_{72}N_{12}O_2Fe$) 584.2620. Found: 584.2621.

(7c). Prepared from **6c**. Yield 93%; ^{1}H NMR (300 MHz, acetone-*d*$_6$) δ 9.58 (s, 4H), 8.99 (d, *J*=8.1 Hz, 4H), 8.07 (m, 8H), 7.48 (m, 6H), 7.29 (t, *J*=7.2 Hz, 4H), 7.22 (d, *J*=7.2 Hz, 2H), 7.12 (s, 2H), 6.90 (d, *J*=1.5 Hz, 4H), 3.36 (s, 6H), 3.29 (s, 6H), 1.25 (s, 36H); ^{13}C NMR (75 MHz, acetone-*d*$_6$) δ 161.5, 160.8, 159.2, 153.8, 152.0, 150.8, 148.0, 146.0, 139.9, 137.3, 130.7, 128.6, 127.9, 125.1, 124.7, 124.2, 122.0, 120.8, 119.9, 39.8, 39.1, 35.4, 31.7; UV–Vis (DMSO) λ_{max}/nm (log ε/M^{-1} cm^{-1}) 289 (4.73), 326 (4.58), 576 (4.26); IR (μscope) υ 3080, 2962, 2902, 1662, 1617, 1593, 1541, 1447, 1409, 1287 cm^{-1}; HRMS (ES) Calcd for $[M\text{–}BF_4]^+$ ($C_{76}H_{82}N_{10}O_2Fe\ BF_4$) 1309.6000. Found: 1309.6004.

(13): Prepared from **12**. Yield 92%; ^{1}H NMR (500 MHz, acetone-*d*$_6$) δ 9.60 (s, 4H), 8.98 (d, *J*=4.8 Hz, 4H), 8.27 (br s, 2H), 8.16 (br s, 2H), 8.10 (td, *J*=8.0, 1.5 Hz, 4H), 8.01 (d, *J*=2.5 Hz, 2H), 7.96 (d, *J*=2.5 Hz, 2H), 7.78 (d, *J*=2.0 Hz, 2H), 7.60 (d, *J*=4.5 Hz, 4H), 7.51 (dd, *J*=8.5, 2.5 Hz, 2H), 7.45 (d, *J*=2.5 Hz, 4H), 7.32 (ddd, *J*=8.0, 1.5 , 1.5 Hz, 4H), 7.14 (t, *J*=1.5 Hz, 2H), 7.14 (t, *J*=2.5, 2H), 7.07 (d, *J*=9.0 Hz, 2H), 1.84 (s, 12H), 1.53 (s, 18H), 1.31 (s, 36H); ^{13}C NMR APT (125 MHz, acetone-*d*$_6$) δ 161.0 (C), 159.5 (C), 154.1 (CH), 153.9 (C), 151.9 (C), 149.7 (C), 147.3 (C), 146.9 (C), 145.9 (C), 140.5 (C), 139.9 (CH), 137.4 (C), 131.8 (C), 131.1 (C), 128.5 (CH), 127.1 (CH), 126.6 (CH), 125.6 (CH), 125.5 (C), 124.8 (CH), 124.9 (CH), 119.5 (CH), 117.4 (CH), 117.2 (CH), 117.0 (CH), 114.1 (CH), 35.8 (C), 35.5 (C), 35.4 (C), 32.6 (CH_3), 31.9 (CH_3), 31.8 (CH_3); UV–Vis (DMSO) λ_{max}/nm (log ε/M^{-1} cm^{-1}) 278 (5.20), 327 (4.89), 570 (4.51); IR (μscope) υ 3388, 3076, 2963, 2906, 2868, 1694, 1608, 1552, 1503, 1453, 1415, 1363, 1277, 1246, 1213, 1059 cm^{-1}; HRMS (ES) Calcd for $[M\text{–}2BF_4]^{2+}$ ($C_{98}H_{106}N_{10}O_4Fe$) 771.3879. Found: 771.3861.

4.3. Synthesis of the porphyrins

4.3.1. General synthesis of porphyrinic esters 16a, 16b and Zn16a. CF_3CO_2H (TFA) (1.25 equiv) was added to a solution of ethyl 3-formylbenzoate (**14a**) or methyl 4-formylbenzoate (**14b**) (1.0 equiv) and 2,2'-dipyrrolyl ketone **15** (1.0 equiv) in freshly distilled degassed CH_2Cl_2 (~5 mM). The reaction mixture was protected from light and stirred at room temperature for 18 h, at which time *p*-chloroanil (500 mg, 2.03 mmol) was added and the mixture was stirred for an additional 30 minutes. Triethylamine (3 mL) was added to neutralize the acid and the solution concentrated under vacuum to yield a purple residue. The crude residue was purified by column chromatography through silica by elution with $CHCl_3$, followed by trituration of the resulting purple solid with acetone.

(16a). Yield 32%; ^{1}H NMR (300 MHz, $CDCl_3$) δ 10.33 (s, 2H), 9.40 (d, *J*=4.8 Hz, 4H), 9.00 (d, *J*=4.8 Hz, 4H), 8.94 (s, 2H), 8.51 (d, *J*=7.8 Hz, 2H), 8.43 (d, *J*=7.8 Hz, 2H), 7.88 (t, *J*=7.8 Hz, 2H), 4.48 (q, *J*=7.0 Hz, 4H), 1.41 (t, *J*=7.0 Hz, 6H), -3.14 (s, 2H); ^{13}C NMR (75 MHz, $CDCl_3$) δ 166.9, 147.1, 145.5, 141.7, 138.7, 135.1, 132.0, 130.9, 129.6, 129.1, 127.2, 117.9, 105.6, 61.4, 14.4; UV–Vis (CH_2Cl_2) λ_{max}/nm (log ε/M^{-1} cm^{-1}) 407 (5.67), 502 (4.32), 535 (3.78), 574 (3.80), 630 (3.30); IR (µscope) υ 3272, 3102, 2982, 2937, 2906, 1722, 1579, 1412, 1365, 1299, 1272, 1239 cm^{-1}; HRMS (EI) Calcd for M^+ ($C_{38}H_{30}N_4O_4$) 606.2269. Found: 606.2269.

(16b). Yield 24%; ^{1}H NMR (300 MHz, $CDCl_3$) δ 10.36 (s, 2H), 9.43 (d, *J*=4.8 Hz, 4H), 9.04 (d, *J*=4.8 Hz, 4H), 8.50 (d, *J*=8.1 Hz, 4H), 8.36 (d, *J*=8.1 Hz, 4H), 4.14 (s, 6H), -3.13 (s, 2H); ^{13}C NMR (75 MHz, $CDCl_3$) δ 167.3, 146.7, 146.1, 145.3, 134.8, 132.0, 130.8, 129.6, 128.2, 117.9, 105.7, 52.5; UV–Vis (DMSO) λ_{max}/nm (log ε/M^{-1} cm^{-1}) 408 (5.35), 503 (3.97), 538 (3.62), 574 (3.41), 629 (3.14); IR (µscope) υ 3247, 3093, 3035, 2957, 1719, 1606, 1433, 1312, 1293, 1266 cm^{-1}; HRMS (EI) Calcd for M^+ ($C_{36}H_{26}N_4O_4$) 578.1954. Found: 578.1967.

(Zn16a). A solution of $Zn(OAc)_2$ (45 mg, 0.21 mmol) in MeOH (4 mL) was added to a solution of porphyrin **16a** (83 mg, 0.14 mmol) in $CHCl_3$ (20 mL). After heating at reflux for 40 h, the reaction mixture was cooled to room temperature and treated with $CHCl_3$ (20 mL). The mixture was washed with H_2O (25 mL) and the organic layer dried over Na_2SO_4. The solvent was removed under vacuum yielding a red solid. Yield 97%; ^{1}H NMR (300 MHz, DMSO-d_6) δ 10.42 (s, 2H), 9.54 (d, *J*=4.8 Hz, 4H), 8.89 (d, *J*=4.8 Hz, 4H), 8.73 (dd, *J*=1.8, 1.8 Hz, 2H), 8.50 (d, *J*=7.2 Hz, 2H), 8.44 (d, *J*=7.2 Hz, 2H), 8.00 (t, *J*=7.8 Hz, 2H), 4.43 (q, *J*=6.9 Hz, 4H), 1.34 (t, *J*=6.9 Hz, 6H); ^{13}C NMR (75 MHz, $CDCl_3$) δ 167.0, 150.0, 149.7, 142.9, 138.4, 134.9, 132.4, 132.1, 129.2, 128.9, 126.8, 118.9, 106.5, 61.3, 14.4; UV–Vis (CH_2Cl_2) λ_{max}/nm (log ε/M^{-1} cm^{-1}) 408 (5.62), 535 (4.21), 570 (3.38); IR (µscope) υ 1339, 3090, 2981, 2931, 1731, 1601, 1581, 1520, 1479, 1389, 1366, 1316, 1294, 1244, 1221, 1181, 1150, 1120, 1106 cm^{-1}; HRMS (EI) Calcd for M^+ ($C_{38}H_{28}O_4N_4Zn$) 668.1402. Found: 668.1399.

4.3.2. General synthesis of porphyrins 17a and 17b. An aqueous solution of KOH (4 mL, 2.0 M) was added to a solution of ester **16a** or **16b** (0.10 mmol) in THF (20 mL). After heating at reflux for 2-3 days, the mixture was cooled to room temperature and 5%

HCl was added dropwise until the pH of the solution was 3-4. The resulting precipitate was filtered and triturated with CH_2Cl_2 yielding the pure porphyrin as a purple solid.

(17a). Yield 93%; ^{1}H NMR (300 MHz, DMSO-d_6) δ 13.27 (br s, 2H), 10.68 (s, 2H), 9.69 (d, J=4.5 Hz, 4H), 9.02 (d, J=4.5 Hz, 4H), 8.76 (s, 2H), 8.55 (d, J=7.8 Hz, 2H), 8.45 (d, J=7.8 Hz, 2H), 8.02 (t, J=7.8 Hz, 2H), -3.28 (s, 2H); UV–Vis (DMSO) λ_{max}/nm (log ε/M^{-1} cm^{-1}) 408 (5.59), 502 (4.21), 538 (3.73), 574 (3.70), 629 (3.30); IR (µscope) υ 3277, 3200-2400, 1685, 1580, 1445, 1413, 1306, 1260, 1241 cm^{-1}; HRMS (ES-neg) Calcd for $[M\text{–}H]^-$ ($C_{34}H_{21}N_4O_4$) 549.1557. Found: 549.1555.

(17b). Yield 91%; ^{1}H NMR (300 MHz, DMSO-d_6) δ 10.68 (s, 2H), 9.68 (d, J=4.8 Hz, 4H), 9.05 (d, J=4.8 Hz, 4H), 8.43 (d, J=8.1 Hz, 4H), 8.41 (d, J=8.1 Hz, 4H), -3.27 (s, 2H); UV–Vis (DMSO) λ_{max}/nm (log ε/M^{-1} cm^{-1}) 410 (5.35), 505 (3.97), 539 (3.64), 577 (3.48), 631 (3.20); IR (µscope) υ 3277, 3132, 1697, 1607, 1536, 1404, 1314, 1287, 1239, 1198, 1177, 1147, 1099 cm^{-1}; HRMS (ES-neg) Calcd for $[M\text{–}H]^-$ ($C_{34}H_{21}N_4O_4$) 549.1557. Found: 549.1561.

4.3.3. Zn17a. An aqueous solution of KOH (4 mL, 2.0 M) was added to a solution of metalloporphyrin **Zn16a** (88 mg, 0.13 mmol) in THF (12 mL). After 3-4 days of heating at reflux, the reaction was cooled to room temperature and the solvent was removed under vacuum. H_2O/THF (1:4, 1-2 mL) was added to the mixture and the resulting suspension was centrifuged. The supernatant was removed and the red solid was collected and dried under high vacuum for 2 days. Yield 90%; ^{1}H NMR (300 MHz, DMSO-d_6) δ 10.34 (s, 2H), 9.47 (d, J=4.8 Hz, 4H), 8.93 (d, J=4.8 Hz, 4H), 8.67 (s, 2H), 8.27 (d, J=7.5 Hz, 2H), 8.07 (d, J=7.5 Hz, 2H), 7.67 (t, J=7.5 Hz, 2H); UV–Vis (DMSO) λ_{max}/nm (log ε/M^{-1} cm^{-1}) 397 (4.32), 417 (5.46), 511 (3.08), 548 (3.99), 585 (3.26); IR (µscope) υ 3275, 1587, 1562, 1415, 1383, 1311, 1213, 1150 cm^{-1}; HRMS (ES-neg) Calcd for $[M\text{–}2K+H]^-$ ($C_{34}H_{19}N_4O_4Zn$) 611.0692. Found: 611.0687.

4.3.4. General synthesis of porphyrins 18a,b and 20a,b. A 0.1 M methanolic solution of tetrabutylammonium hydroxide was prepared fresh by diluting 653 mg of a 40% aqueous tetrabutylammonium hydroxide solution with methanol (10 mL). This solution (2 mL for **17a** and **17b**, and 4 mL for **19a** and **19b**) were added to the porphyrin (0.1 mmol) suspended in MeOH (2 mL). After stirring at room temperature for 16 h, the solvent was removed under vacuum affording a purple oil. This oil was dissolved in methanol (0.25-0.50 mL) and diethyl ether was added until the product oiled out. The supernatant was removed and discarded and the residue was dried under high vacuum for

1 day yielding a purple solid. The resulting porphyrinic salts can be stored for up to 6 months in an anhydrous environment of $CaSO_4$.

(18a). Yield 95%; ^{1}H NMR (300 MHz, $CDCl_3$) δ 10.62 (s, 2H), 9.64 (d, *J*=4.5 Hz, 4H), 9.03 (d, *J*=4.5 Hz, 4H), 8.67 (s, 2H), 8.29 (d, *J*=7.5 Hz, 2H), 8.13 (d, *J*=7.5 Hz, 2H), 7.73 (t, *J*=7.8 Hz, 2H), 3.15 (m, 16H), 1.55 (m, 16H), 1.29 (m, 16H), 0.92 (t, J=7.2 Hz, 24H), -3.22 (s, 2H); ^{13}C NMR (75 MHz, $CDCl_3$) δ 171.6, 145.0, 139.9, 139.4, 135.8, 135.2, 131.5, 131.3, 129.1, 126.1, 120.0, 104.9, 58.7, 23.9, 19.6, 13.5; UV–Vis (DMSO) λ_{max}/nm (log ε/M^{-1} cm^{-1}) 409 (5.49), 503 (4.27), 538 (3.87), 576 (3.79), 630 (3.41); IR (µscope) υ 3280, 3087, 2960, 2874, 1607, 1587, 1567, 1467, 1358, 1257 cm^{-1}; HRMS (ES-neg) Calcd for $[M\text{–}NBu_4]^-$ ($C_{50}H_{56}N_5O_4$) 790.4327, $[M\text{+}H\text{–}2NBu_4]^-$ ($C_{34}H_{21}N_4O_4$) 549.1557 Found: 790.4335, 549.1559.

(18b). Yield 92%; ^{1}H NMR (300 MHz, DMSO-*d*$_6$) δ 10.61 (s, 2H), 9.64 (d, *J*=4.5 Hz, 4H), 9.05 (d, *J*=4.5 Hz, 4H), 8.28 (d, *J*=7.8 Hz, 4H), 8.12 (d, *J*=7.8 Hz, 4H), 3.15 (m, 16H), 1.55 (m, 16H), 1.29 (m, 16H), 0.92 (t, *J*=7.2 Hz, 24H), -3.22 (s, 2H); UV–Vis (DMSO) λ_{max}/nm (log ε/M^{-1} cm^{-1}) 410 (5.54), 504 (4.23), 540 (3.95), 579 (3.78), 633 (3.48); IR (µscope) υ 3279, 3111, 1703, 1605, 1586, 1402, 1239 cm^{-1}; HRMS (ES-neg) Calcd for $[M\text{+}H\text{–}2NBu_4]^-$ ($C_{34}H_{21}N_4O_4$) 549.1557. Found: 549.1560.

(20a) Yield 91%; ^{1}H NMR (300 MHz, DMSO-*d*$_6$) δ 8.82 (s, 8H), 8.21 (d, *J*=6.6 Hz, 8H), 8.04 (*J*=6.6 Hz, 8H), 3.14 (m, 32H), 1.55 (m, 32H), 1.26 (m, 32H), 0.92 (t, 48H), -2.89 (br s, 2H); UV–Vis (DMSO) λ_{max}/nm (log ε/M^{-1} cm^{-1}) 421 (5.65), 518 (4.20), 552 (4.00), 593 (3.70), 648 (3.78); IR (µscope) υ 3466, 3277, 3089, 2960, 2873, 1666, 1595, 1551, 1483, 1367, 1280, 1239, 1150 cm^{-1}; HRMS (ES-neg) Calcd for $[M\text{+}2H\text{–}3NBu_4]^-$ ($C_{64}H_{65}N_5O_8$) 1031.4826, $[M\text{+}3H\text{–}4NBu_4]^-$ ($C_{48}H_{29}N_4O_8$) 789.2001, $[M\text{+}H\text{–}3NBu_4]^{2-}$ ($C_{64}H_{63}N_5O_8$) 514.7363, $[M\text{+}2H\text{–}4NBu_4]^{2-}$ ($C_{48}H_{28}N_4O_8$) 394.0956. Found: 1031.4839, 789.1980, 514.7344, 394.0959.

(20b) Yield 88%; ^{1}H NMR (300 MHz, DMSO-*d*$_6$) δ 8.79 (s, 8H), 8.62 (t, *J*=7.5, 4H), 8.25 (d, *J*=7.5 Hz, 4H), 8.14-8.04, (m, 4H), 7.65 (t, *J*=7.5 Hz, 4H), -2.86 (s, 2H); ^{13}C NMR (300 MHz, $CDCl_3$) δ 171.5, 140.9, 138.9, 135.7, 134.9, 134.4, 129.1, 125.9, 125.8, 120.7, 118.2; UV–Vis (DMSO) λ_{max}/nm (log ε/M^{-1} cm^{-1}) 422 (5.64), 518 (4.11), 553 (3.90), 591 (3.48), 648 (3.60); IR (µscope) υ 3318, 2961, 2874, 1607, 1588, 1566, 1486, 1370, 1252, 1158, 1109 cm^{-1}; MS (ES-neg) Calcd for $[M\text{–}NBu_4]^-$ ($C_{96}H_{134}N_7O_8$) 1514.0, $[M\text{+}H\text{–}2NBu_4]^-$ ($C_{80}H_{99}N_6O_8$) 1271.8, $[M\text{+}2H\text{–}3NBu_4]^-$ ($C_{64}H_{64}N_5O_8$) 1030.5. Found: 1514.0, 1271.7, 1030.4.

4.4. Synthesis of the terpyridine•porphrin complexes

4.4.1. General synthesis of complexes 1 and 2. A solution of iron(terpyridine) **7a** (0.024 mmol) in MeOH (12 mL) was added porphyrin **18a** (0.024 mmol) or **20a** (0.012 mmol). A dark precipitate immediately formed. After stirring at room temperature for 2-3 h, the solution was concentrated to 1–2 mL and filtered. The filter cake was washed several times with fresh MeOH affording a purple solid.

(1). Yield 97%; ^{1}H NMR (300 MHz, DMSO-d_6) δ 12.10 (br s, 2H), 11.84 (br s, 2H), 10.35 (s, 2H), 9.52 (d, *J*=4.8, 4H), 9.20 (s, 4H), 9.00 (d, *J*=4.8, 4H), 8.87 (s, 2H), 8.62 (d, *J*=7.5, 2H), 8.44 (m, 8H), 8.20 (s, 2H), 7.94 (t, *J*=7.8 Hz, 2H), 7.80 (s, 6H), 7.60 (t, *J*=7.8 Hz, 2H), 7.09 (s, 2H), 6.37 (br s, 8H), 5.55 (br s, 4H), 1.42 (s, 36H), -3.40 (s, 2H); MS (ES) Calcd for $[M+Na]^+$ ($C_{106}H_{94}N_{14}O_6FeNa$) 1738.9, $[M+2Na]^{2+}$ ($C_{106}H_{94}N_{14}O_6FeNa_2$) 880.9. Found 1738.7, 880.7.

(2). Yield 95%; ^{1}H NMR (300 MHz, DMSO-d_6) δ 11.95 (br s, 2H), 11.48 (br s, 2H), 9.27 (s, 8H), 8.75 (s, 8H), 8.59-8.51 (m, 16H), 8.29 (br s, 8H), 8.24 (d, *J*=7.5 Hz, 4H), 7.84 (d, *J*=7.5 Hz, 4H), 7.80 (t, *J*=7.5 Hz, 4H), 7.71 (s, 8H), 7.58 (t, *J*=7.5 Hz, 4H), 7.05 (s, 4H), 6.62 (br s, 8H), 6.54 (br s, 8H), 5.82 (br s, 8H), 1.37 (s, 72H), -3.06 (s, 2H); MS (ES) Calcd for $[M+2Na]^{2+}$ ($C_{192}H_{174}N_{36}O_{12}Fe_2Na_2$) 1583.7, Found: 1583.5.

4.4.2. Xanthene complex 18a•13. A solution of the iron(terpyridine) **13** (0.002 mmol) in acetone (2 mL) was treated with porphyrin **18a** (0.002 mmol). The solution was stirred for 30 minutes and then sonicated for 10-20 seconds, at which point a dark precipitate formed. The suspension was filtered and the isolated solid was washed several times with acetone until the filtrate was colorless. Yield 91%. ^{1}H NMR (500 MHz, DMSO-d_6) δ 12.14 (br s, 2H), 11.78 (br s, 2H), 10.62 (s, 2H), 9.65 (d, *J*=4.5 Hz, 4H), 9.32 (s, 4H), 9.04 (d, *J*=4.5 Hz, 4H), 8.91 (br s, 2H), 8.69 (d, *J*=7.5 Hz, 4H), 8.56 (d, *J*=8.0 Hz, 2H), 8.50 (br s, 2H), 8.15 (d, *J*=7.5 Hz, 2H), 7.85 (t, *J*=8.0 Hz, 2H), 7.78 (m, 8H), 7.70 (t, *J*=7.5 Hz, 4H), 7.13 (d, *J*=9.0 Hz, 2H), 7.05 (s, 2H), 7.01 (two br s, 4H), 6.96 (t, *J*=5.0, Hz, 4H), 6.82 (d, *J*=9.0 Hz, 2H), 1.78 (s, 12H), 1.47 (s, 18H), 1.41 (s, 36H), -3.27 (br s, 2H); MS (ES) Calcd for $[M+Na]^+$ ($C_{132}H_{126}N_{14}O_8FeNa$) 2115.4, $[M+2Na]^+$ ($C_{132}H_{126}N_{14}O_8FeNa_2$) 1069.2. Found: 2115.8, 1069.0.

4.4.4. Pyrazine complex Zn17a•7b. A solution of iron(terpyridine) **7b** (0.006 mmol) in acetone (4 mL) was treated with metalloporphyrin **Zn17a** (0.006 mmol) dissolved in MeOH (1 mL). The reaction was stirred at room temperature for 1 h and the solvent was removed by evaporation. The residue was triturated with fresh acetone (5 mL) and filtered. The isolated solid was washed several times with MeOH until the filtrate was colorless. Yield 81%; ^{1}H NMR (500 MHz, DMSO-d_6) δ 12.06 (br s, 2H), 11.63 (br s, 2H), 10.21 (s, 2H), 9.72 (s, 2H), 9.45 (d, *J*=4.0 Hz, 4H), 9.38 (s, 2H), 9.22 (s, 2H), 8.92 (d, *J*=4.0 Hz, 4H), 8.74 (s, 2H), 8.62 (d, *J*=8.0 Hz, 2H), 8.48 (d, *J*=7.0 Hz, 2H), 8.34 (br s, 4H), 8.29 (s, 2H), 7.93 (t, *J*=7.5 Hz, 2H), 7.82 (d, *J*=7.0 Hz, 2H), 7.79 (s, 4H), 7.75 (s, 2H), 7.62 (t, *J*=7.5 Hz, 2H), 7.11 (s, 2H), 6.89 (s, 2H), 6.22 (br s, 2H), 5.49 (br s, 2H), 4.63 (br s, 2H), 1.44 (s, 36H); MS (ES) Calcd for $[M+K]^+$ ($C_{104}H_{90}N_{16}O_6FeZnK$) 1820.3, $[M+2K]^{2+}$ ($C_{104}H_{90}N_{16}O_6FeZnK_2$) 929.7. Found: 1820.4, 929.7.

4.5. Isothermal Titration Calorimetry (ITC)

All binding experiments were preformed on an Isothermal Titration Calorimeter from Microcal Inc. (Northhampton, Massachusetts). In a typical ITC experiment, a 0.10 mM solution of the porphyrin dissolved in DMSO was added to the calorimetry cell (volume=1.448 mL). A 1.45 mM solution of the iron(terpyridine) in DMSO was introduced in 60, 4 µL injections (4 minutes between injections) until a total of 240 µL of iron(terpyridine) was added. The solution was maintained at a constant operating temperature of 25°C and continuously stirred (400 rpm) to ensure rapid mixing. The data from the resulting injections were evaluated using a one-site nonlinear regression analysis in the Origin® software package.

4.6. Steady-state fluorescence titrations

Fluorescence measurements were performed using a PTI C60 photon counting spectrophotometer. In a typical experiment, the porphyrin (2.0 mL, 1.0×10^{-6} M) in DMSO was added to a quartz cuvette and the initial fluorescence profile of the porphyrin was recorded (λ_{ex} = 415 nm for **18a** and **18b**, λ_{ex} = 430 nm for **20a** and **20b**, while monitoring the fluorescence between λ = 550-800 nm). Aliquots (10–20 µL) of a DMSO solution of the iron(terpyridine) (2.0×10^{-5} M) were added to the cuvette while stirring. After each addition, the fluorescence spectrum was recorded. Upon reaching 1.5–2 equivalents of iron(terpyridine), the aliquots were increased to 50–200 µL until 1.1 mL (8-10 equivalents) was added. The raw fluorescence intensities (λ_{em} = 633 nm for **18a** and **18b**, λ_{ex} = 650 nm for **20a** and **20b**) were used to generate the inverse Stern-Volmer quenching plots.

2.2.6 Results and Discussion

2.2.6.1 Determination of Association Constants

The association ($2.5 \times 10^6\ M^{-1}$)between cationic terpyridine **7a** and anionic porphyrin **18a** is one of the strongest reported for a non-covalent porphyrin-quencher pair. Furthermore our design employing oppositely charged photoactive building blocks is substantially more robust than most current supramolecular photoactive complexes as it maintains its topology even in extremely polar media. The association was so strong that typical molecular recognition techniques used to determine association constants such as ^{1}H NMR titrations gave unsatisfactory results. Section 2.4. of the paper describes the stability of all the complexes and Figure 6 shows the integrated binding curves generated from the addition of aliquots of the terpyridine to a solution of the porphyrin. This curve is generated directly from the raw data, which measures the heat evolved with each injection of guest. To better understand how this integrated binding curve is produced a stacked plot of the raw data (top) with the resulting binding curve (bottom) for **18a** and **7a** is shown in Figure 2.6

Fluorescence spectroscopy was also used to estimate the association constant between **18a** and **7a**. Figure 2.7 shows the quenching effect that the iron(terpyridine) **7a** has on the

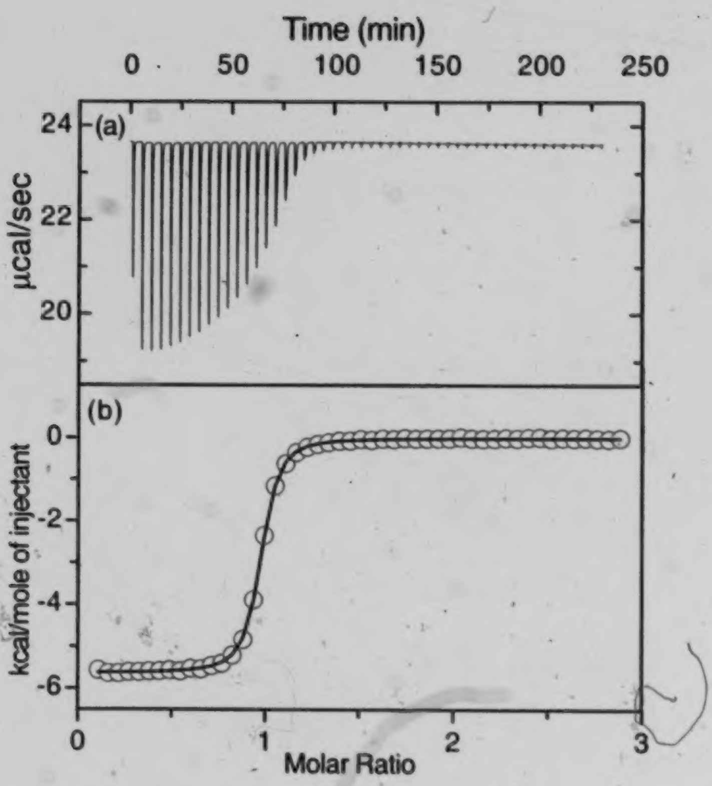

Figure 2.6. Calorimetric titration of **7a** added to **18a** in DMSO. Top panel: (a) raw data showing heat evolved with each injection of guest. Bottom panel: (b) integrated binding curve. The solid line represents a non-linear least squares fit using a 1:1 binding model.

porphyrin upon forming complex **1**. A plot of the raw fluorescence data against concentration of quencher (**7a**) added generated the binding isotherm shown in Figure 2.6. These data fit nicely to a 1:1 binding model and gave an association constant (K_a = 5.24 x 10^6 M^{-1}) that was reasonably close to that obtained by calorimetry (K_a = 2.5 x 10^6 M^{-1}). Both fluorescence titration and isothermal titration calorimetry techniques are extremely useful for determining association constants of strongly associating species. Calorimetric techniques however are generally more universal in their application because they measure purely the host-guest binding event in terms of heat absorbed or evolved. Fluorescence techniques indirectly yield an association by measuring a photochemical response (quenching) to a host-guest binding event. Hence fluorescence techniques are applicable only to luminescent systems.

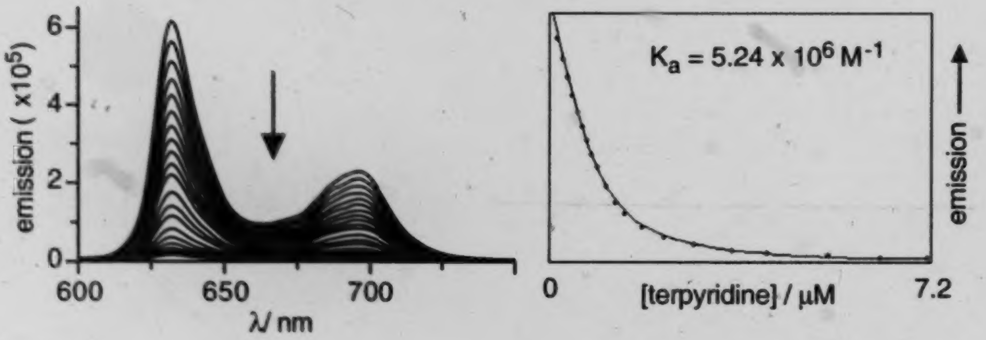

Figure 2.7. Left panel: Raw data of fluorescence titration of porphyrin **18a** (1×10^{-6} M) in DMSO as aliquots of terpyridine **7a** (2×10^{-5} M) are added. Right panel: Fluorescence titration curve for **18a** and **7a** generated directly from the raw fluorescence data. The vertical scale is in arbitrary units. **18a** was excited at 415 nm and the emission recorded at 633 nm. The curve is the best fit of the 1:1 binding isotherm used to determine the association constant.

2.2.6.2 X-ray Crystallographic Analysis of an Iron(Terpyridine) Complex

Numerous attempts were made to grow single crystals of complexes **1** and **2** for

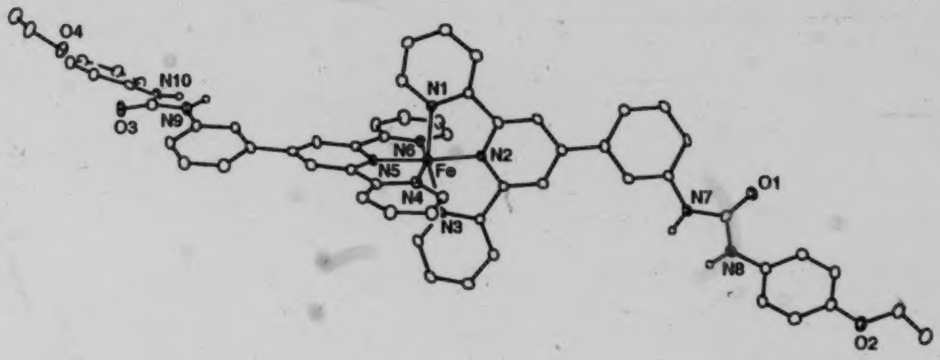

Figure 2.8. Perspective view of the $[Fe(\eta^3\text{-}\{C_5H_2N(2,6\text{-}py_2)(4\text{-}C_6H_4NHC\{O\}NHC_6H_4OEt)\})_2]^{2+}$ ion showing the atom labeling scheme. Non-hydrogen atoms are represented by Gaussian ellipsoids at the 20% probability level. Hydrogen atoms attached to nitrogens are shown with arbitrarily small thermal parameters; all other hydrogen atoms and the BF_4^- counterions are not shown.

X-ray structure determination. The solvent system was systematically varied but as only a handful of solvents could be used due to solubility reasons another approach was tested. In this approach a variation of urea **7a** was synthesized where the *tert*-butyl groups on the periphery of the iron complex were replaced by ethoxyphenyl moieties. It was hoped that this substitution would affect the crystal packing and afford suitable single crystals of the complexes. This approach also failed to yield adequate crystals of the complexes although a crystal of the ethoxyphenyl iron(terpyridine) itself was obtained. The crystals were grown by the diffusion of Et_2O into a nitromethane solution of the coordination compound. Figure 2.8 highlights how two terpyridine ligands wrap around one iron atom creating an octahedral arrangement about the core. More importantly, the iron atom serves as the glue to unite the two halves of the receptor thus creating an extended cleft functionalized with urea hydrogen bonding sites capable of binding to the carboxylate groups on the porphyrin.

2.2.6.3 Stern-Volmer Quenching Analysis

Figure 2 section 2.2.4 (page 28) shows a Stern-Volmer plot of the fluorescence quenching between a porphyrin and an iron(terpyridine). The Y-axis is the initial fluorescence divided by the observed fluorescence as quencher is added to the solution. The X-axis is concentration of quencher added. Because the initial fluorescence is divided by the observed fluorescence, quenching of fluorescence is indicated by an increase in the Y-axis as quencher is added to the solution. This plot is some-what deceiving as the numbers on the Y-axis increase due to a decrease in fluorescence.

A better way of showing fluorescence quenching between two species is to show an inverse Stern-Volmer plot. In this case the 'Y' axis is the observed fluorescence divided by the initial fluorescence as quencher is added to the solution. Here fluorescence quenching is indicated by a more appropriate decrease in the 'Y' axis. An example of an inverse Stern-Volmer plot is depicted on page 45 of section 2.2.5.

2.2.6.4 Mode of Fluorescence Quenching

A thorough review of the literature describing porphyrin photochemistry and quenching dynamics revealed that there are no reports documenting the observed quenching effect that an iron(terpyridine) ligand has on a porphyrin macrocycle. As such, the direct mode of quenching in this system is unknown. We can however hazard a hypothesis of a possible quenching mechanism by examination of both the spectral and electrochemical characteristics of the components that make up the complexes.

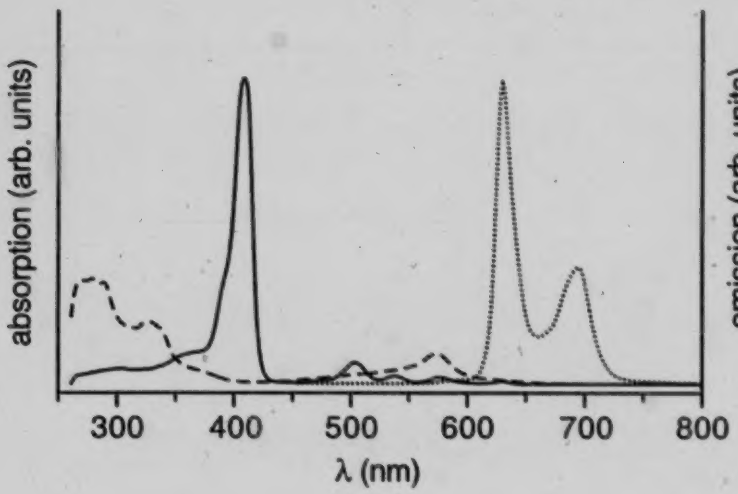

Figure 2.9. UV–Vis absorption spectrum of porphyrin **18a** (—) and terpyridine **7a** (---) in DMSO and the emission spectrum of porphyrin **18a** (···) (λ_{excit} = 415 nm). All concentrations were 1 × 10^{-6} M.

For energy transfer to be considered as a possible mode of quenching there must be adequate spectral orbital overlap between the emission band of the porphyrin and the visible MLCT absorption band of the iron(terpyridine). Close inspection of the spectral region extending from 600 nm to 615 nm reveals that there is minimal orbital overlap between these two species (Figure 2.9). However, this is a very crude approximation and on its own cannot exclude energy transfer as a possible quenching mechanism.

Alternatively, the observed quenching could be a result of a photoinduced electron transfer process. This could potentially occur via either an oxidative or a reductive electron transfer pathway. Preliminary electrochemical studies on **7a** performed in our laboratory and previous electrochemical studies on similar core iron(terpyridine) systems[61] show that the iron(terpyridine) complex is capable of behaving in dual capacities as either an oxidant or a reductant. The redox potentials for all the components of complexes **1** and **2** are compiled in Table 2.1. In an oxidative pathway, the

Table 2.1. Redox potentials for iron(terpyridine) **7a** and porphyrins **18a** and **20a**[a]

Entry	Component	Reductions[d] (eV)	Oxidations[e] (eV)
1[b]	**7a**	-1.08, -1.17	* (0.80)[*]
2[c]	**18a**	-1.08, -1.52	0.87, 0.97, 1.45, 1.80
3[c]	**20a**	-1.07	0.98, 1.14, 1.70

[a] Supporting electrolyte (0.1 M [NBu_4][PF_6]), V *vs.* Ag/AgCl, [b] [**7a**] = 5 x 10^{-4} M in deoxygenated DMSO, [c] [**18a**], [**20a**] = 5 x 10^{-4} M in deoxygenated CH_3CN, [d] Reversible processes, [e] non-reversible processes, [*] The oxidation of Fe^{II} - Fe^{III} of **7a** was unattainable due to the interference of solvent oxidation processes. The oxidation potential in brackets is representative of a typical Fe^{II} - Fe^{III} oxidation potential (in CH_3CN) seen in similar core iron(terpyridine) systems.

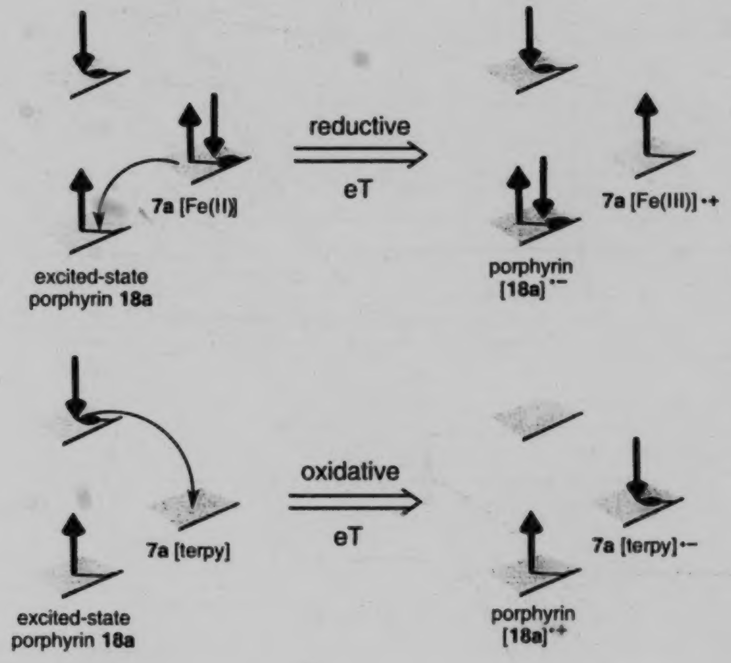
reductive
eT
7a [Fe(II)]
excited-state porphyrin 18a
7a [Fe(III)] •+
porphyrin [18a]•−
oxidative
eT
7a [terpy]
excited-state porphyrin 18a
7a [terpy]•−
porphyrin [18a]•+

Figure 2.10. Possible electron transfer fluorescence quenching mechanisms for the excited-state porphyrin **18a** and iron(terpyridine) **7a**.

photoexcited porphyrin could surrender its excited-state electron to a lower energy orbital situated on the terpyridine ligand. This is not unreasonable as **7a** is a fairly good reductant and exhibits two reversible ligand-based reductions at -1.08 and -1.17 eV respectively. The oxidative pathway would result in the formation a porphyrin radical cation species and the ligand-centered radical anion of **7a** (Figure 2.10). If, on the other hand **7a** behaved as an oxidant donating an electron to the low-lying hole on the excited porphyrin, the result would be the formation of a porphyrin radical anion species and the metal-centered radical cation of **7a**. Because the Fe(II) in **7a** surrenders an electron quite easily (0.80 eV), this may be the preferred pathway for the observed quenching process. However, this is all pure speculation at the moment and time-resolved laser experiments are required to discern between the potential pathways.

2.2.7 Conclusion

As described above the mode of fluorescence quenching of the porphyrin by the iron(terpyridine) complex is most likely due to an oxidative or reductive electron transfer mechanism. Time-resolved fluorescence measurements in conjunction with transient absorption experiments monitoring for the presence of either the porphyrin radical anion or radical cation would surely shed light on the actual quenching mechanism in effect.

2.2.8 Notes and references

1. Ward, M. D. *Chem. Soc. Rev.* **1997**, *26*, 365.

2. Kavarnos, G. J. *Fundamentals of Photoinduced Electron Transfer*; VCH: New York, NY, 1993.

3. Forster, T. *Discuss. Faraday Soc.* **1959**, *27*, 7.

4. Dexter, C. L. *J. Chem. Phys.* **1953**, *21*, 836.

5. Turro, N. J. *Modern Molecular Photochemistry*; University Science Books: Sausalito, Ca, 1991, pp 297-361.

6. Hayashi, T.; Miyahara, T.; Koide, N.; Kato, Y.; Masuda, H.; Ogoshi, H. *J. Am. Chem. Soc.* **1997**, *119*, 7281.

7. Wasielewski, M. R. *Chem. Rev.* **1992**, *92*, 435.

8. Ward, M. D. *Chem. Soc. Rev.* **1997**, *26*, 365 and references cited therein.

9. (a) Imamura, T.; Fukushima, Coord. *Chem. Rev.*, **2000**, *198*, 133. (b) Haycock, R. A.; Yartsev, A.; Michelsen, U.; Sundstrom, V.; Hunter, C. A. *Angew. Chem. Int. Ed.* **2000**, *39*, 3616. (c) Ogawa, K.; Kobuke, Y. *Angew. Chem. Int. Ed.* **2000**, *39*, 4070. (d) Chichak, K.; Branda, N. R. *Chem Commun.* **2000**, 1211. (e) Mak, C. C.; Bampos, N.; Sanders, J. K. M. *Chem Commun.* **1999**, 1085. (f) Wilson, G. S.; Anderson H. L. *Chem Commun.* **1999**, 1539. (g) Otsuli, J.; Harada, K.; Toyama, K.; Hirose, Y.; Araki, K.; Seno, M.; Taketera, K.; Watanabe, T. *Chem. Commun.*, **1998**, 1515. (h) Drain, C. M.; Nifiatis, F.; Vasenko. A.; Batteas, J. D. *Angew. Chem. Int. Ed.* **1998**, *37*, 2344. (g) Hunter, C. A.; Hyde, R. A. *Angew. Chem. Int. Ed.* **1996**, *35*, 1936.

10. Hunter, C. A.; Shannon, R. J. *Chem. Commun.* **1996**, 1361.

11. (a) Agirtas, S.; Ion, R-M.; Bekaroglu, O. *Mater. Sci. Eng. C.* **2000**, *7*, 105. (b) Lipskier, J. F.; Tran-Thi, T. H. *Inorg. Chem.* **1993**, *32*, 722.

12. Kano, K.; Minamizono, H.; Kitae, T.; Negi, S. *J. Phys. Chem A* **1997**, *101*, 6118.

13. Schneider, H-J.; Wang, M. *J. Org. Chem.* **1994**, *59*, 7464.

14. Examples of reports of multi-porphyrin arrays include: (a) Drain, C. M.; Shi, X.; Milic, T.; Nifiatis, F. *Chem. Commun*, **2001**, 287. (b) Masiero, S.; Gottarelli, G.; Pieraccini, S. *Chem. Commun.* **2000**, 1995. (c) Ikeda, C.; Nagahara, N.; Motegi, E.; Yoshioka, N.; Inoue, H. *Chem. Commun.* **1999**, 1759. (d) Drain, C. M.; Russell, K. C.; Lehn, J-M. *Chem. Commun.* **1996**, 337. Examples of porphyrin donor-acceptor hybrid arrays include: (e) Myles, A. J.; Branda, N. R. *J. Am. Chem. Soc.* **2001**, *123*, 177. (f) Berg, A.; Shuali, Z.; Asano-Someda, M.; Levanon, H.; Fuhs, M.; Mobius, K.; Wang, R.; Brown, C.; Sessler, J. L. *J. Am. Chem. Soc.* **1999**, *121*, 7433. (g) Osuka, A.; Yoneshima, R.; Shiratori, H.; Okada, T.; Taniguchi, S.; Mataga, N. *Chem. Commun.* **1998**, 1567. (h) Hayashi, T.; Miyahara, T; Norihiro, K.; Tukitoshi, K.; Masuda, H.; Ogoshi, H. *J. Am. Chem. Soc.* **1997**, *119*, 7281. (i) Arimura, T.; Brown, C. T.; Springs, S. L.; Sessler, J. L. *Chem Commun.* **1996**, 2293. (j) Kirby, J. P.; van Dantzig, N. A.; Chang, C. K.;

Nocera, D. G. *Tetrahedron Lett.* **1995**, *36*, 3477. (k) Turro, C.; Chang, K.; Leroi, G. E.; Cukier, R. I.; Nocera, D. G. *J. Am. Chem. Soc.* **1992**, *114*, 4013.

15. (a) Schmuck, C.; *Chem. Eur. J.* **2000**, *6*, 709. (b) Sebo, L.; Schweizer, B.; Diederich, F. *Helv. Chim. Acta.* **2000**, *83*, 80. (c) Linton, B.; Hamilton, A. D. *Tetrahedron* **1999**, 6027. 15. (d) Bell, T. W.; Hext, N. H.; Khasanov, A. B. *Pure Appl. Chem.*, **1998**, *70*, 2371. (d) Fan, E.; Van Arman, S. A.; Kincaid, S.; Hamilton, A. *J. Am. Chem. Soc.*, **1993**, *115*, 369.

16. These distances were estimated from the lowest energy structure of assembly **1** using computer-assisted molecular modeling

17. Ward, M. D. *Chem. Soc. Rev.* **1997**, *26*, 365 and references therein.

18. Imamura, T.; Fukushima, K. *Coord. Chem. Rev.* **2000**, *198*, 133.

19. Haycock, R. A.; Yartsev, A.; Michelsen, U.; Sundstrom, V.; Hunter, C. A. *Angew. Chem. Int. Ed.* **2000**, *39*, 3616.

20. Ogawa, K.; Kobuke, Y. *Angew. Chem. Int. Ed.* **2000**, *39*, 4070.

21. Chichak, K.; Branda, N. R. *Chem Commun.* **2000**, 1211.

22. Mak, C. C.; Bampos, N.; Sanders, J. K. M. *Chem. Commun.* **1999**, 1085.

23. Wilson, G. S.; Anderson H. L. *Chem. Commun.* **1999**, 1539.

24. Otsuki, J.; Harada, K.; Toyama, K.; Hirose, Y.; Araki, K.; Seno, M.; Takatera, K.; Watanabe, T. *Chem. Commun.* **1998**, 1515.

25. Drain, C. M.; Nifiatis, F.; Vasenko. A.; Batteas, J. D. *Angew. Chem. Int. Ed.* **1998**, *37*, 2344.

26. Hunter, C. A.; Shannon, R. J. *Chem. Commun.* **1996**, 1361.

27. Hunter, C. A.; Hyde, R. A. *Angew. Chem. Int. Ed.* **1996**, *35*, 1936.

28. Agirtas, S.; Ion, R.-M.; Bekaroglu, O. *Mater. Sci. Eng. C.* **2000**, *7*, 105.

29. Kano, K.; Minamizono, H.; Kitae, T.; Negi, S. J. *Phys. Chem A* **1997**, *101*, 6118.

30. Lipskier, J. F.; Tran-Thi, T. H. *Inorg. Chem.* **1993**, *32*, 722.

31. Schneider, H.-J.; Wang, M. *J. Org. Chem.* **1994**, *59*, 7464.

32. Drain, C. M.; Shi, X.; Milic, T.; Nifiatis, F. *Chem. Commun.* **2001**, 287.

33. Masiero, S.; Gottarelli, G.; Pieraccini, S. *Chem. Commun.* **2000**, 1995.

34. Ikeda, C.; Nagahara, N.; Motegi, E.; Yoshioka, N.; Inoue, H. *Chem. Commun.* **1999**, 1759.

35. Drain, C. M.; Russell, K. C.; Lehn, J.-M. *Chem. Commun.* **1996**, 337.

36. Myles, A. J.; Branda, N. R. *J. Am. Chem. Soc.* **2001**, *123*, 177.

37. Berg, A.; Shuali, Z.; Asano-Someda, M.; Levanon, H.; Fuhs, M.; Mobius, K.; Wang, R.; Brown, C.; Sessler, J. L. *J. Am. Chem. Soc.* **1999**, *121*, 7433.

38. Osuka, A.; Yoneshima, R.; Shiratori, H.; Okada, T.; Taniguchi, S.; Mataga, N. *Chem. Commun*. **1998**, 1567.

39. Hayashi, T.; Miyahara, T; Norihiro, K.; Tukitoshi, K.; Masuda, H.; Ogoshi, H. *J. Am. Chem. Soc*. **1997**, *119*, 7281.

40. Arimura, T.; Brown, C. T.; Springs, S. L.; Sessler, J. L. *Chem. Commun*. **1996**, 2293.

41. Kirby, J. P.; van Dantzig, N. A.; Chang, C. K.; Nocera, D. G. *Tetrahedron Lett*. **1995**, *36*, 3477.

42. Turro, C.; Chang, K.; Leroi, G. E.; Cukier, R. I.; Nocera, D. G. *J. Am. Chem. Soc*. **1992**, *114*, 4013.

43. Schmuck, C.; *Chem. Eur. J*. **2000**, *6*, 709.

44. Sebo, L.; Schweizer, B.; Diederich, F. *Helv. Chim. Acta* **2000**, *83*, 80.

45. A similar phenomenon was reported by Hamilton and coworkers for the self-association of guanidinium molecules in DMSO: Linton, B.; Hamilton, A. D. *Tetrahedron* **1999**, *55*, 6027.

46. Bell. T. W.; Hext, N. H.; Khasanov, A. B. *Pure Appl. Chem*. **1998**, *70*, 2371.

47. Fan, E.; Van Arman, S. A.; Kincaid, S.; Hamilton, A. *J. Am. Chem. Soc*. **1993**, *115*, 369.

48. Norsten, T. B.; Chichak, K; Branda, N. R. *Chem. Commun.*, 2001, 1794.

49. Mukkala, V.-M.; Helenius, M.; Hemmila, I; Kankare, J.; Takalo, H. *Helv. Chim. Acta* **1993**, *76*, 1361.

50. Lindsey, J. S.; Prathapan, S.; Johnson, T. E.; Wagner, R. W. *Tetrahedron* **1994**, *50*, 8941.

51. Schaefer, J. P.; Lark, J. C.; Flegal, C. A.; Hoing, L. M. *J. Org. Chem.* **1967**, *32*, 1372.

52. de Groot, J. A.; Koek, J. H.; Lugtenburg, J. *Recl. Trav. Chim. Pays-Bas* **1981**, *100*, 405.

53. Datta-gupta, N.; Jones, E.; Thomas, L. K.; Malakar, D. *J. Indian Chem. Soc.* **1981**, *58*, 1171.

54. Suarez, M; Salfran, E.; Rodriguez-Curiel, R. I.; Elguero, *J*, *Bull. Soc. Chim. Belg.* **1997**, *106*, 211.

55. The starting geometry of the iron(terpyridine) component was abtained from the X-ray crystal structure of the 4-ethoxyphenyl analogue of **7a** (see section 2.2.6.2. following the paper).

56. The stoichiometry of the complexes 1 and 2 were confirmed using electrospray mass spectrometry, employing continuous infusion injection (see Experimental section).

57. Corbell, J. B.; Lundquist, J. J.; Toone, E. J. *Tetrahedron Asymmetry* **2000**, *11*, 95.

58. The raw fluorescence data for the titration of 18a with 7a fit to a 1:1 binding model and gave an association constant ($K_a = 5.24 \times 10^6$ M^{-1}) that was close to that obtained for the calorimetry studies. The titration data was analyzed using Christopher A. Hunter's 1:1 complexation model program (Krebss Institute for Biomolecular Science, Department of Chemistry, University of Sheffield, UK).

59. Kavarnos, G. J. *Fundamentals of Photoinduced Electron Transfer*; VCH: New York, NY, 1993.

60. Turro, N. J. *Modern Molecular Photochemistry*; University Science Books: Sausalito, Ca, 1991, pp 297–361.

61. Constable, E. C.; Cargill Thompson, A. M. W. *J. Chem. Soc. Dalton Trans.* **1994**, 1409.

Unit 3 - Controlling Molecular Structure and Function with Photochromic Molecules

3.1 Photochromism: Memories and Switches for Non-Destructive Readout

As we move into the 21st century the world is quickly accumulating a vast amount of information. As a result, traditional storage practices used to catalog this information are being replaced by more space-effective information storage systems, the most prevalent of these being the common computer. The current objective is to develop storage systems that pack as much information as possible into the least amount of material, with the major challenge being the development of new materials and techniques that would provide a means to this end.[1] The ultimate goal here is the realization of molecular or even atomic level information storage systems.[2]

Pre-compact disk (CD) memory media was based primarily on inorganic materials and utilized magneto-optical technology as the basis for optical recording. These systems were desirable due primarily to the fact that the physical property allowing storage (ie. the magnetic alignment of molecules based on their Curie point temperatures) is reversible and the readout event could occur without disrupting the system providing a non-destructive and erasable memory medium. The ever-increasing outpour of global information, however, demanded the development of higher density data storage systems.[3] In the early to mid 1980's the development of CD technology which uses various organic dyes such as cyanine, phthalocyanine or aza dyes as the memory medium and reflected laser light as the readout source substantially improved on the information density problem, but at a cost; the inability to erase the stored data. The compact disk media that was available during this time consisted of write-once and read-only memory (WORM) and as a consequence a CD could not be used for multiple writing/erasing events. This shortfall warranted the need to develop reversible high-density optical recording media with the capacity to perform multiple read-write-erase cycles. Only very recently has an erasable CD medium become commercially available. This most recent erasable memory medium operates on detecting differences in reflectance based on phase change technology between crystalline and amorphous states of polycarbonate substrates consisting of inorganic alloys of silver, indium, germanium, tellurium and antimony.[4]

A viable alternative to employing these more expensive inorganic materials is the implementation of cheap organic based photochromes or light activated molecular switches as the memory medium. Photochromic systems are unique in that they can undergo a reversible transformation between two distinct chemical states in response to external light activation. This transformation typically results in a conformational change in the molecule and spectroscopically results in two attainable distinct absorption profiles for the two interconverting chemical species. The fact that photochromes are able to reversibly achieve two distinct states makes them readily applicable to the binary logic of computing devices. As applied to memory media, the possibility of detecting a difference between the two absorption spectra could provide a useful mechanism to read stored information. However, in order to detect an absorption difference the system must be further irradiated in a section of the spectral region that is non-photochromic. As simple as this sounds the design of such as system is yet to be realized. Irradiation for the purposes of detection on a photochromic band ultimately leads to photochemical interconversion to the other chemical species and erasure of the stored data. Consequently, one of the major hurdles that must be surmounted before a fully functional photochromic memory medium can be realized is the development of a non-destructive detection technique.

3.2 Choice of Photochrome

It may come as no surprise that the first organic based memory medium employed the use of molecular dyes, as there are literally hundreds of robust organic dyes from which to choose. In comparison, when shopping for a photochrome the shelves would appear somewhat bare as there are only a handful of known photochromic systems. Furthermore, there are even fewer that meet the strict requirements that are fundamental for practicable applications to erasable photochromic memory devices. Such requirements include:

- fatigue resistance – the ability to be subjected to numerous on/off cycles without significant degradation,
  - thermal stability – the absence of thermal interconversion between the two states,
  - detectability – the ease of identifying both photochromic states,
  - nondestructive readout – the ability to read the stored information without erasing it, and
  - multi-state photochromism – retention of photochromic ability in solid state (i.e. crystalline or thin films).

Photochromic molecules can be grouped into one of two categories. The first is made up of those that undergo reversible *cis-trans* photoisomerizations. This category includes the strained olefins, thioindigos and azabenzenes. The second class all undergo electrocyclic photocyclization reactions (*ring opening/ring closing* processes). Spirobenzopyrans, fulgides and diarylethenes are the best known members of this class.

Table 1 briefly highlights some of the drawbacks for each of the common photochromic molecules. With respect to the critical properties necessary for photochromic memory devices, the dithienylethene photochrome is the clear winner.

Table 3.1. Common Photochromic Molecules and Some of Their Properties.[†]

Reaction Type	Example	Form A	Form B	Properties
cis-trans *isomerization*	Strained olefins	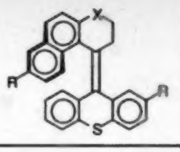	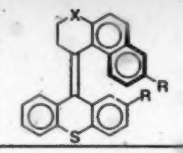	• must have optically pure starting material • slow response time
	Thioindigos	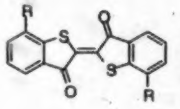	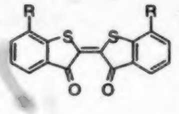	• difficult to functionalize • not thermally stable
	Azabenzenes	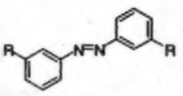	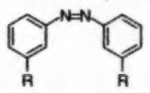	• not thermally stable
ring opening-ring closing	Fulgides	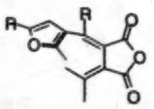	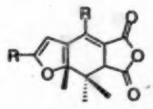	• The productive *cis* form of A isomerizes to the non-productive *trans* isomer
	Spiropyrans	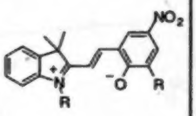	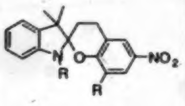	• not thermally stable • epimerization at spiro carbon center
	Dithienylethenes	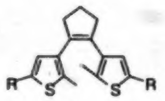	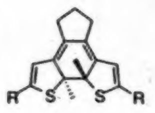	• thermally stable • easy to derivatize without loss of photochromic activity.

[†] Reprinted with permission from reference 7.

For instance, azabenzenes do not exhibit "bistability" between the two photochromic states. The *cis* form of azabenzenes is extremely susceptible to thermal reversion back to the more stable *trans* isomer.[5] The rapid degradation of this conformation limits their use as data storage devices. On the other hand, appropriately chosen dithienylethenes show no thermal interconversion even at elevated temperatures ($t_{1/2}$ = greater than 3 months at 80°C).[6a]

Spiropyrans not only show thermal reversion ($t_{1/2}$ = 10 min at 80°C) but also exhibit limited multi-cycle durability.[8] Photochromic performance of these molecules is lost after only100 colouration/decolouration cycles. In contrast, dithienylethenes show excellent fatigue resistance. In certain dithienylethene systems the *ring-closing/ring-opening* reaction cycle can be repeated more than 10^4 times without the loss of photochromic performance.[6b]

Dithienylethenes also exhibit their photochromic properties in the solid state. Reversible photochromism has been reported in sol-gel films,[9] polymer-bound thin films[10] and even in the crystalline state.[11] The dithienylethenes are clearly a versatile class of photochrome that embody the necessary requirements to be developed as materials for optical memory devices. As such this unit will describe several examples where dithienylethenes are incorporated into various chemical systems as the "logic" switch for optical memory media.

3.2 Ring-Closure of a Dithienylethene

Both the ring-opening and ring-closing reactions of dithienylethenes belong to the *electrocyclic* class of reactions. Electrocyclic reactions have several chracteristic features:

1) They require only heat or light for initiation.
2) Their mechanisms do not involve free radical or ionic intermediates.
3) Bonds are made and broken in *a single concerted step involving a cyclic transition state.*
4) The reactions are *highly stereospecific.*

In concerted reactions the molecular orbitals of the reactant are continously converted to the molecular orbitals of the product. Due to the rules of symmetry that molecular orbitals obey, restrictions exist on which molecular orbitals of the reactant may be transformed into particular molecular orbitals of the product. For the purposes of this discussion the following description will focus only on the 6π-electron system which is specific to the molecular orbital description of the dithienylethene photochrome.

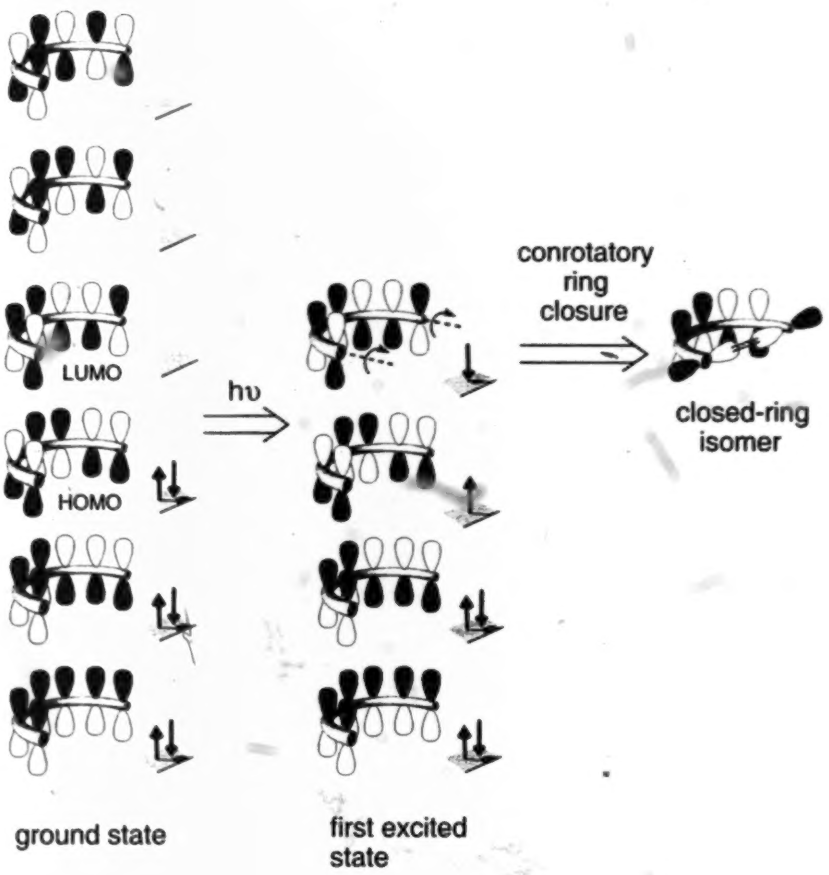
LUMO
HOMO
hυ
conrotatory ring closure
closed-ring isomer
ground state
first excited state

Figure 3.1. MO description of the photoinduced ring-closing process of a dithienylethene.

The frontier molecular orbital picture of a generic 1,3,5-hexatriene system is shown in Figure 3.1. When activated by light the HOMO promotes one of its electrons to the LUMO. This affords an excited state species. According to the symmetry of the LUMO, subsequent ring closure can only proceed in a conrotatory fashion (ie. both reacting orbitals turn the same way) to form a bonding interaction. This results in the high degree of stereospecificity observed for these types of reactions. It should be noted that in structurally unbiased substrates, the conrotatory ring closure can occur in either direction with equal probability. This has various implications with respect to the chirality of the ring-closed isomers. Chapter 5 will address the stereochemical implications of the ring closing reaction with respect to specific materials applications.

3.3 Non-Destructive Detection Techniques for Photochromic Systems

Over the past decade several strategies have been explored in an effort to develop non-destructive photochromic information storage systems. The vast majority of these studies employ a similar approach to the problem in that they focus on the detection of changes in some property of the photochromic system other than UV-Vis absorption. Non-destructive detection using UV-Vis light was however successful when used within the constructs of a gated photochromic system.

Gated photochromic systems work on the principle that in one isomeric form the photochromic properties of the system can be shutdown. This can be achieved by controlling the non-covalent interactions of a given system. For example intramolecular hydrogen bonding has been used to prevent the two carbons that make the new bond in the dithienylethene ring-closing process from approaching one another. Inhibiting intramolecular hydrogen bonding by changing solvents re-activates the photochrome.[12] Gating photochromes by changing solvents however is certainly not practical to real device applications. Alternatively, one of the isomeric forms can be rendered non-photochromic by reversible alteration of its chemical properties. This gating technique employs a dual-mode switching strategy and has been achieved using pH[13] or electrochemical[14] control mechanisms in combination with light. A unique example of a successful gated dual-mode photochromic system elegant both in its design and function is described in Equation 3.1.[14]

Irradiation of photochrome **1** with $h\upsilon_1$ results in the formation of the extended hydroquinone system **2**. Toggling between **1** and **2** is achieved via irradiation with $h\upsilon_1$ and $h\upsilon_2$ respectively providing the "write" and "erase" mechanisms. Formation of the extended hydroquinone system **2** activates the electrochromic properties of the system. Oxidation of **2** leads to the non-photochromic quinoid structure **3** and provides the critical "lock" mechanism necessary for non-destructive readout. Quinoid **3** can now be safely "read" with various wavelengths of light in a non-destructive manner and can be easily "unlocked" by reduction of **3** back to **2**. Although successful in its approach, the development of dual-mode gated photochromic systems for non-destructive read-out has

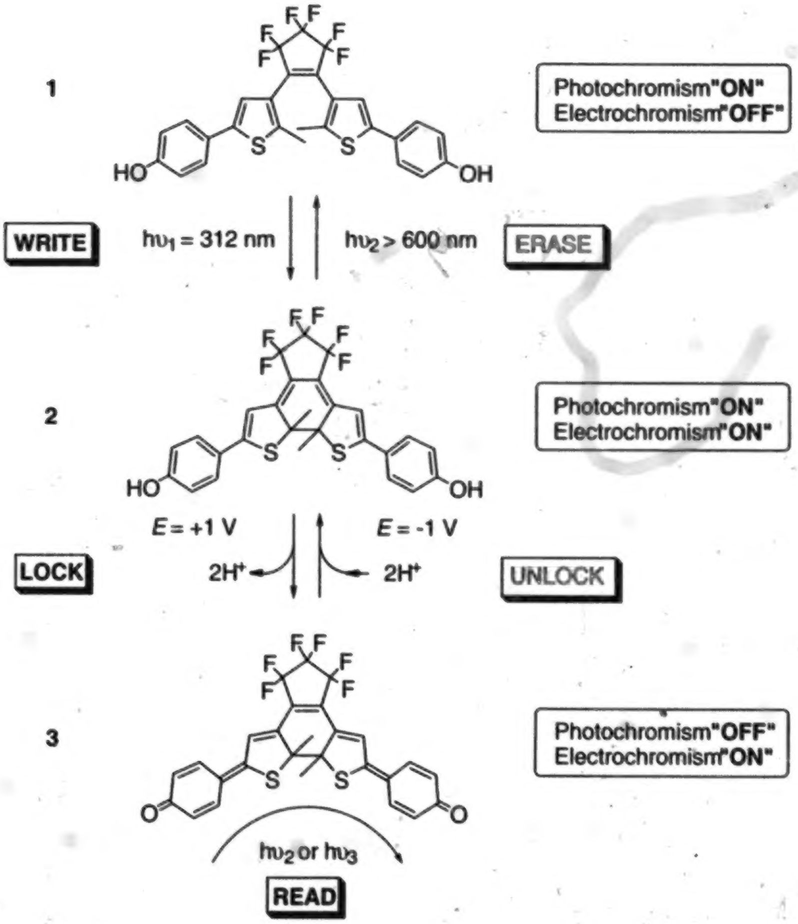
1
Photochromism"ON"
Electrochromism"OFF"
WRITE
hυ1 = 312 nm
hυ2 > 600 nm
ERASE
2
Photochromism"ON"
Electrochromism"ON"
E = +1 V
E = -1 V
LOCK
2H+
2H+
UNLOCK
3
Photochromism"OFF"
Electrochromism"ON"
hυ2 or hυ3
READ

Equation 3.1. A gated dual-mode molecular switch

largely been replaced by research on alternate-detection of physical changes that accompany the photochromic process in single-mode systems. These can include changes in optical emission, refractive index, optical rotation or infrared spectrscopy. A single-mode system offers the advantage of requiring fewer cycling steps as the need to "lock" and "unlock" the device is unnecessary. This leads to initiation of fewer chemical processes, which would ultimately result in less degradation and shorter processing times.

This Unit of the thesis compiles a collection of recently published papers, all of which focus on employing the robust dithienylethene photochrome in an effort to develop single-mode-switching devices for the purpose of non-destructive readout. In addition to the photochrome, which acts as the photo-modulator, each system employs various other chromophores. The optical properties of the chromophores are designed to respond to the reversible photo-modulation of the dithienylethene moiety ultimately providing a non-destructive detection mechanism. For instance, Chapters 3 and 4 describe how the appropriate choice of fluorescent or phosphorescent chromophores can be used for an emission-based detection system, where the emission behavior is sensitive to the state of the photochrome. Chapter 5 describes a supramolecular-based system that employs the use of chiral auxiliaries appended to a dithienylethene scaffold. In this case photochemical interconversion between the *open* and *closed* forms of the switch serves to regulate the rotation of plane polarized light offering a chiroptic-based detection system. Chapter 6 closes this section of the thesis with a paper that describes the photoregulated control of helicene backbones. Although this preliminary system has limited value as a memory device, its potential as applied other technologies will be discussed.

3.4 Notes and references

1. Jacoby, M. *C&EN*, June 12, 37.

2. Eiger, D. M.; Lutz, C. P.; Rudge, W. E. *Nature*, **1991**, *352*, 600.

3. This article describes the physical limits to high-density magnetic recording; White, R. L. *J. Magn. Magn. Mater.* **2000**, *209*, 1.

4. Gonzalez-Hernandez, J.; Chao, B. S.; Strand, D.; Ovshinsky, S. R.; Pawlik, D.; Gasiorowski, P. *Appl. Phys. Commun.* **1992**, *11*, 557.

5. F. Vögtle, *Supramolecular Chemistry*, John Wiley and Sons, New York, 1991.

6. (a) M. Irie, *Chem. Rev.* **2000**, *100*, pp1690. (b) M. Irie, *Chem. Rev.* **2000**, *100*, pp1692.

7. Murguly, E. Masters Dissertation, The University of Alberta, 2000.

8. Berkovic, G.; Krongauz, V.; Weiss, V. *Chem. Rev.* **2000**, *100*, 1741.

9. Chaput, F.; Biteau, J.; Lahlil, K.; Boilot, J. P.; Darracq, B.; Levy, Y.; Peretti, J.; Safarov, V. I.; Parent, G.; Fernandez-Acebes, A. Lehn, J-M. *Mol. Cryst. Liq. Cryst.* **2000**, *344*, 77.

10. (a) Irie, S.; Irie, M. *Bull. Chem. Soc. Jpn.* **2000**, *73*, 2385. (b) Kawai, T.; Kunitake. T.; Irie, M. *Chem. Lett.* **1999**, 905. (c) Nakashima, H.; Irie, M.; *Polym. J.* **1998**, 30, 985.
11. (a) Irie, M.; Kobatake, S.; Horichi, M. *Science*, **2001**, *291*, 1769. (b) Yamada, T.; Kobatake, S.; Irie, M. *Bull. Chem. Soc. Jpn.* **2000**, *73*, 2179.
12. Irie, M.; Miyatake, O.; Uchida, K.; Eriguchi, T. *J. Am. Chem. Soc.* **1994**, *116*, 9894.
13. Kawai, S. H.; Gilat, S. L.; Ponsinet, R.; Lehn, J.-M. *Chem. Eur. J.* **1995**, *1*, 285.
14. Kawai, S. H.; Gilat, S. L.; Lehn, J.-M. *Eur. J. Org. Chem* **1999**, *1*, 2359.

Chapter 3 - Fluorescence-Based Detection for Non-Destructive Readout

3.3.1 Introduction to Fluorescence-Based Readout

The following paper describes a new entry in the field of photochromic memory media by combining *suitably* matched fluorescent and photochromic molecules. The molecule described in the manuscript was the first emission-based system designed to allow direct irradiation of the fluorophore in a region of the UV-Vis spectrum distinct from the photochromic interconversion bands. Figure 3.2 shows a schematic representation of an emission-based system where photochemical toggling between *open* and *closed* states of a photochrome can regulate the emission intensity of an appended chromophore.

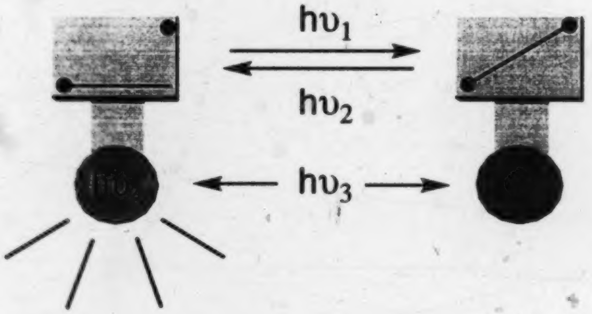

Figure 3.2. Schematic representation of an emission-based molecular switch. $h\upsilon_1$: write function, $h\upsilon_2$: erase function, $h\upsilon_3$: irradiation (input) - read function and $h\upsilon_4$: emission (output) - read function.

Equation 3.2

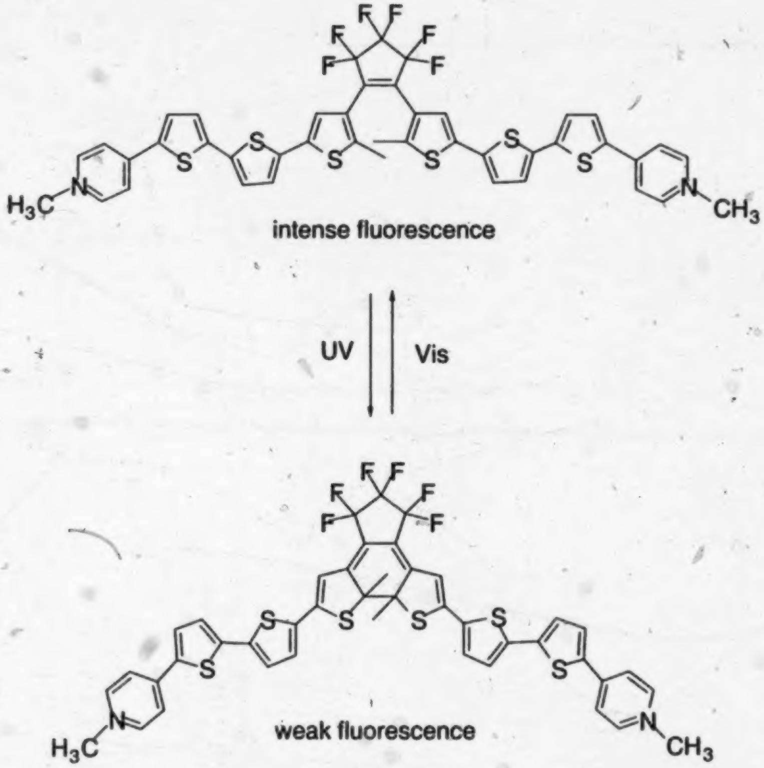

Previous to this report, all of the documented systems consisted of photochromic "write" or "erase" bands that overlapped to some extent with the fluorescent "read" bands. With respect to non-destructive readout none of the former systems behaved flawlessly, although a system reported by Lehn and coworkers based on an oligothiophene-dithienylethene hybrid system came quite close (Equation 3.2).[1] In this system a large difference in fluorescence was observed between the *open* and *closed* forms of the oligothiophene, however it was only possible to detect this change by irradiating at wavelengths where the *closed* form maintained photochromic activity. This resulted in a slow cycloreversion reaction (< 2% per 30 min) back to the original *open* state during the read-out process.

3.3.2 - Paper - Photoregulation of Fluorescence in a Porphyrinic Dithienylthene Photochrome

Tyler B. Norsten and Neil R. Branda
J. Am. Chem. Soc. **2001**, *123*, 1784.

The appeal of the reversible photocyclization reactions of 1,2-dithienylethene derivatives as applied to photonic devices such as erasable memory media and optical switches lies in their being thermally irreversible, fatigue resistant and easily monitored using UV-VIS spectroscopy.[2] Applications in information processing most often hinge upon the ease of identifying both photochromic states by measuring the spectral changes close to the absorbances that trigger the photocyclization reactions. Despite its convenience and sensitivity, this detection method can ultimately result in the interconversion of the photochrome and concomitant loss of stored information. The destructive nature of tracking photochromism using UV-Vis spectroscopy has encouraged the design of novel photochromic systems where information can be processed in a non-destructive manner.[3]

In many cases, the changes in the absorption spectra that occur during the photoisomerization reaction are accompanied by changes in other optical properties such as refractive index,[4] optical rotation[5,3c,e,f] and luminescence.[6,3b] Recording the changes in luminescence provides an alternative to UV-Vis spectroscopy as a means to process stored information while minimizing the extent at which the information is erased during the detection event. An important condition must be met, however. The wavelengths of light used to produce the luminescence (excitation wavelengths, λ_{ex}) and the resulting emission wavelengths (λ_{em}) must reside outside the spectral regions where the photochromic reactions are induced. The ability to fine tune the excitation wavelengths of porphyrins and the fact that they exhibit intense luminescence far into the visible region prompted us to investigate non-destructive information processing in porphyrin-dithienylethene hybrids.

We report herein the synthesis and optical characterization of a photochromic hybrid **1**, where porphyrin macrocycles are attached to the ends of the 1,2-*bis*-(3-thienyl)cyclopentene backbone. The relationship between the luminescence intensity of the porphyrins and the state of the photoswitch (*open* or *closed*) is clearly illustrated and provides a novel information processing system. To the best of our knowledge, this is the first example of this type of porphyrinic photochrome.

Scheme 1[a]

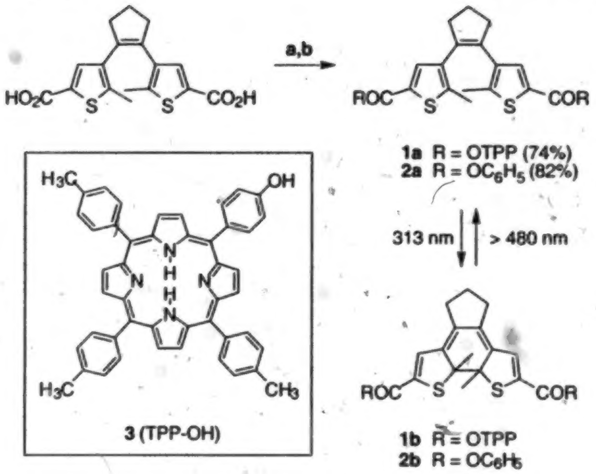

[a] Reaction conditions: (a) $(COCl)_2$, DMF, CH_2Cl_2; (b) 3, TEA, CH_2Cl_2 or phenol, NaH, benzene.

All photochromes used in these studies were prepared from readily available 1,2-*bis*-(5-carboxy-2-methyl-3-thienyl)cyclopentene[7] as shown in Scheme 1. All new compounds were characterized by ^{1}H and ^{13}C NMR spectroscopy, UV-Vis spectroscopy and mass spectrometry. The absorption spectrum of bis(porphyrin) **1a** in the UV-Vis region is essentially equivalent to the sum of the absorption spectra of the molecule's components (phenyl-functionalized photochrome **2a** and **3**) indicating there is little change in the ground state of either chromophore upon covalent linking. Irradiation[8] of **1a** at 313 nm resulted in an immediate increase in the adsorption intensity in the visible spectral region (500-625 nm) due to the appearance of the absorption bands of the *closed* isomer **1b** (λ_{max} = 560 nm for model photochrome **2b**) as shown in Figure 1. After 4 minutes of continuous irradiation (2 x 10^{-4} M, toluene-d_8), the photostationary state was reached and was identified by ^{1}H NMR spectroscopy as consisting of 69% of the closed isomer **1b**. The ease at which this photochemical ring closure occurs is impressive in light of the fact that porphyrins have been reported, on occasion, to inhibit photochromic processes.[9]

Irradiation of the closed isomer **1b** at wavelengths greater than 480 nm[8] resulted in the rapid ring-opening photoreaction and the regeneration of the original absorption spectrum corresponding to **1a**. The reversible photoisomerization reaction was also verified by monitoring the changes in the ^{1}H NMR spectrum where typical upfield shifts for the thiophene C–H signals and downfield shifts for the methyl thiophene signals were observed.[10]

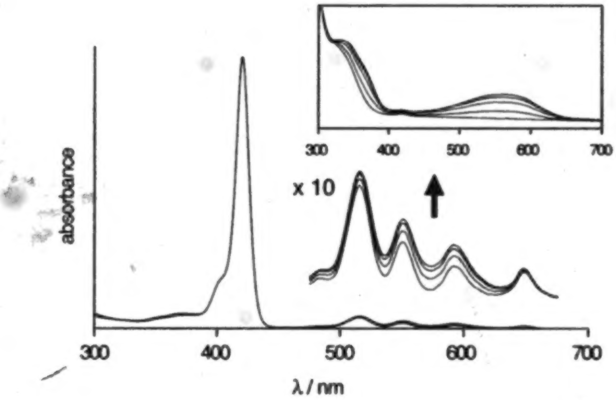

Figure 1. Changes in the UV-Vis absorption spectra of a toluene solution of **1a** (2 x 10^{-6} M) upon irradiation with 313 nm light. Irradiation periods are 0, 10, 30, and 50 seconds. The inset shows the changes for **2a** under similar conditions.

The presence of the porphyrins' Soret absorption bands centered at 420 nm allows for this chromophore to be selectively irradiated in a region of the spectrum where the 1,2-(dithienyl)cyclopentene photochromic fragment of **1a** is transparent.[11] The luminescence of the porphyrin macrocycles in **1a** and **1b** greatly depends on the state of the 1,2-(dithienyl)cyclopentene photoswitch. In the *open* form (**1a**), the porphyrins display significant fluorescence intensity at 655 nm when excited at 430 nm.[12] When the photocyclization reaction was carried out by irradiating **1a** at 313 nm, the non-fluorescent[13] *closed* form **1b** was produced. Back irradiation at wavelengths greater than 480 nm regenerated **1a** and restored the original emission spectrum. The intensity of the porphyrins' fluorescence is conveniently regulated by toggling between **1a** and **1b** by alternate irradiation at 313 nm and greater than 480 nm (Figure 2) clearly demonstrating that the hybrid **1** can act as a system for reversible data processing using fluorescence as the detection method.

Extended periods of continuous irradiation (1 hour) of a toluene solution of the photostationary state of **1** (2 x 10^{-6} M) with 430 nm light resulted in an increase (~45%) in the emission intensity at 655 nm and a corresponding decrease in absorption intensity in the visible region (500-625 nm).[14] Decomposition of the photochrome can be ruled out as a cause of these spectral changes as the resulting solutions could be taken through several photochromic cycles reproducing the original UV-Vis and fluoresence spectra.

The spectral changes are, therefore, indicative of partial cycloreversion of **1b** to **1a**. It is unlikely that this partial ring-opening is due to the *closed* isomer **1b** absorbing light at this wavelength. This is supported by the fact that the parent photochrome **2b** displayed no observable changes in the UV-Vis spectrum when irradiated at 430 nm under identical conditions.

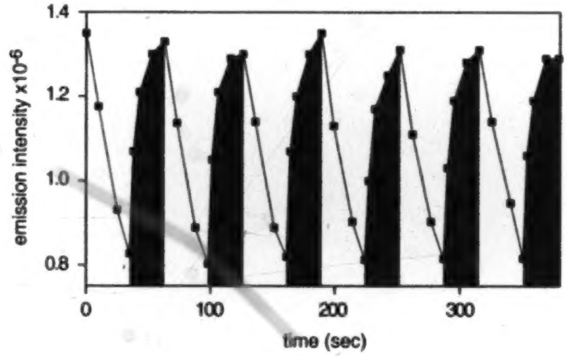

Figure 2. Modulated emission signal of a toluene solution of 1 ($2x10^{-6}$ M) during alternating irradiation at 313 nm (unshaded areas) and > 480 nm (shaded areas). All spectra were run in deoxygenated toluene (λ_{ex} = 430 nm, λ_{em} = 655 nm).

This phenomenon was also directly observed by ^{1}H NMR spectroscopy. In this experiment, a mixture of the partially closed isomers of both **1b** and **2b** were irradiated at 430 nm. After 15 hours of continuous irradiation **1b** was almost completely converted to its *open* isomer **1a**, while a minimal amount of **2b** was converted to **2a**. In light of these results, a more probable explanation for the ring-opening reaction of **1b** at 430 nm is that the porphyrins are acting as light-harvesting antennae, channeling their excited state energy towards the photochromic center. The result of this process is the photochemical regeneration of **1a**. The extent of ring-opening is significantly less for **2b** as would be expected because the porphyrins' excited state energy, in this case, must be transferred to photochrome **2b** through a diffusion controlled intermolecular process. It is obvious that this process will not be able to compete significantly with its intramolecular counterpart. The interesting photochemical characteristics displayed by **1** are strikingly similar to those found in natural light harvesting systems, where the role of the porphyrins includes acting as antennae to collect and deliver their excited state energies to the reaction centers where photochemistry ultimately takes place. Systems of this type are appealing for applications where selective irradiation of one photochrome in the presence of another is desirable. The precise nature and mechanism of this process is under investigation and the results will be reported in due time.

We have shown that the combination of porphyrins and dithienylethenes have potential in the area of optical information processing. We are currently optimizing the system by electronically fine-tuning both the porphyrin and dithienylethene chromophores.

3.3.3 Results and Discussion

3.3.3.1 Synthesis of Photochromes

Currently there are two general approaches to synthesize dithienylcyclopentene photochromic ring systems. In the original approach a pair of 2-methyl-3-bromo-thiophene moieties are fused to an octafluorocyclopentene core through the brominated thiophene and the fluorinated alkenyl positions via a lithium-halogen exchange reaction (Scheme 3.1). Due to the difficulty in controlling the exact addition of the highly volatile octafluorocyclopentene reagent this approach typically gives poor yields.

Scheme 3.1

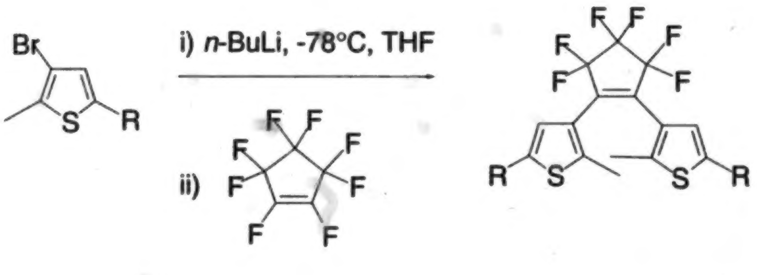

A second and more recent approach was coined by Kellogg and coworkers in response to the low yields frequently obtained by the lithium-halogen exchange methodology.[15] The key step in this approach is the titanium-based coupling reaction of a diketone to form the cyclopentene ring system affording the functional photochromic core in three simple and high yielding steps (Scheme 3.2). This general approach is substantially easier and cheaper than the original route. Furthermore, the Kellogg route provides quick access to large quantities of the photochrome.

Both the dithienylperfluorcyclopentene and the dithienylcyclopentene photochromes undergo the usual photoisomerization reactions between the open isomer and ring-closed isomer. However, the non-fluorinated form of the photochrome is not as photochemically robust as the fluorinated form.[16] In some instances, irradiation of the ring-closed form of the non-fluorinated photochrome results in photochemical degradation. In our studies we typically employ the more accessible and economical non-fluorinated version to prove our concept. The fluorinated forms can be produced when the systems are fully optimized for processing.

Scheme 3.2

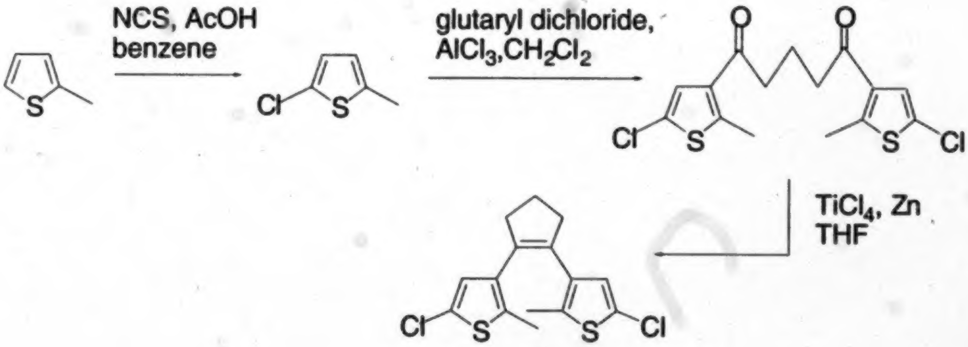

4

Taking over where the Kellogg route left off, we were able to functionalize the dichloro-photochrome **4** with carboxylic acid moieties by quenching the lithium salt with carbon dioxide (Scheme 3.3). Further elaboration of the diacid **5** afforded the dicarbonyl chloride **6**, which was the direct precursor to the porphyrin-dithienylethene hybrid **1** and the phenoic ester derivatized photochrome **2**. Porphyrin **3** (TPP-OH) was synthesized under standard Rothmund condensation conditions employing a mixture of pyrrole, 4-hydroxybenzaldehyde and 4-methylbenzaldehyde in refluxing propionic acid (Scheme 3.4).[17]

Scheme 3.3

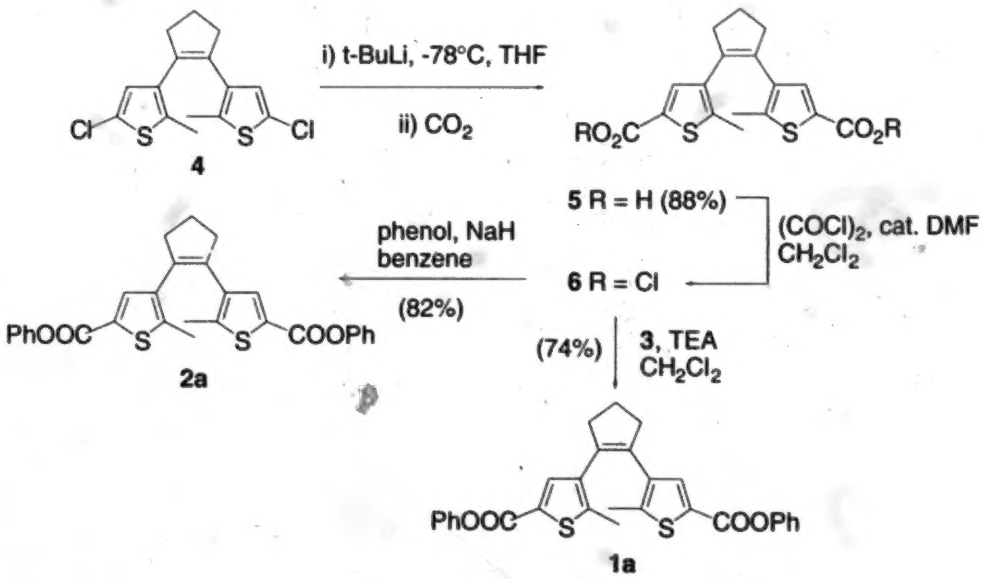

Cl
S
S
Cl
4
i) t-BuLi, -78°C, THF
ii) CO₂
RO₂C
S
S
CO₂R
5 R = H (88%)
6 R = Cl
(COCl)₂, cat. DMF
CH₂Cl₂
phenol, NaH
benzene
(82%)
PhOOC
S
S
COOPh
2a
(74%)
3, TEA
CH₂Cl₂
PhOOC
S
S
COOPh
1a

Scheme 3.4

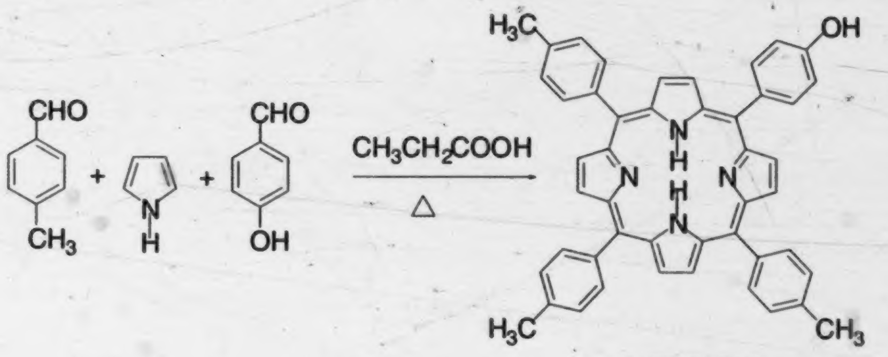

3 (TPP-OH)

3.3.3.2. Photophysical Studies: Observation of Indirect Ring-Opening

Figure 3.3 illustrates the simultaneous changes that occur in both the UV-Vis absorption and emission spectra of **1a** when irradiated with 313 nm light. Formation of the *closed* isomer **1b** is diagnosed from the increased absorption in the visible region beneath the Q-bands of the porphyrin (Figure 3.3(a)) and the corresponding decrease in the fluorescence (Figure 3.3(b)).

The relative fluorescence intensities of *open* isomer **1a**, the photostationary state and isolated **1b** (containing 2% residual **1a**) are shown in Figure 3.4. It is this change in emission intensities that provided the read-out method of the information processing system.

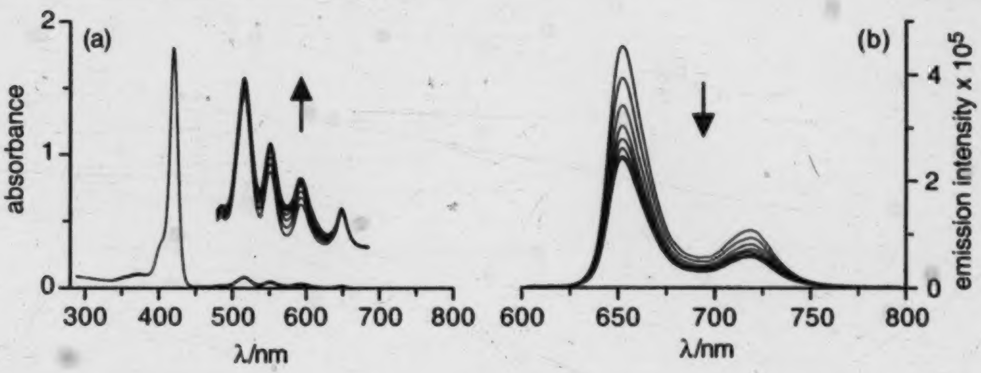

Figure 3.3. (a) Absorption spectra and (b) emission spectra of **1a** under irradiation at 313 nm in toluene (2 x 10^{-6} M). Irradiation periods are 0, 10, 20, 30, 40, 50 60 70 s. λ_{EX} = 430.

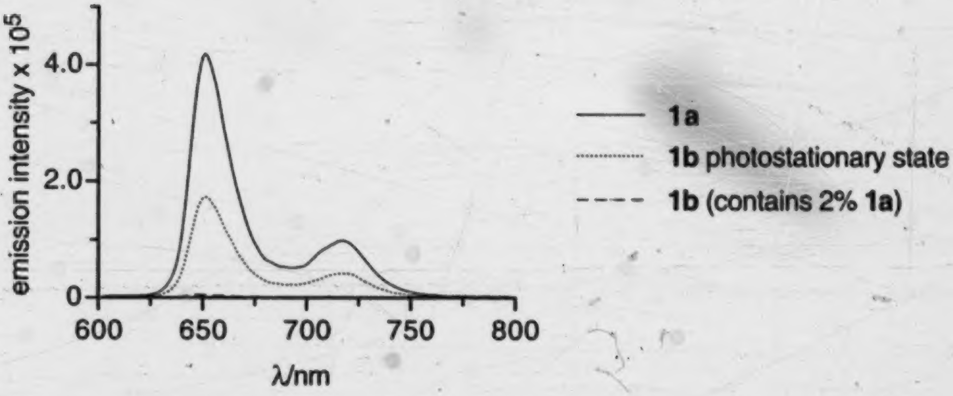

Figure 3.4. Emission spectra of **1a**, **1b** (photostationary state) and **1b** (contains 2% **1a**) in toluene (2 x 10^{-6} M). λ_{EX} = 430.

As already described, prolonged irradiation of **1b** at 430 nm results in its cycloreverting to **1a**. This was diagnosed both by UV-Vis absorption and fluorescence spectroscopies and was confirmed by ^{1}H NMR spectroscopy. Figure 3.5 clearly shows that when **1b** (at or near its photostationary state) is irradiated with 430 nm light for 30, 60 and 90 minutes the characteristic absorbance of the closed isomer **1b** slowly disappears, while the corresponding fluorescence intensity increases.

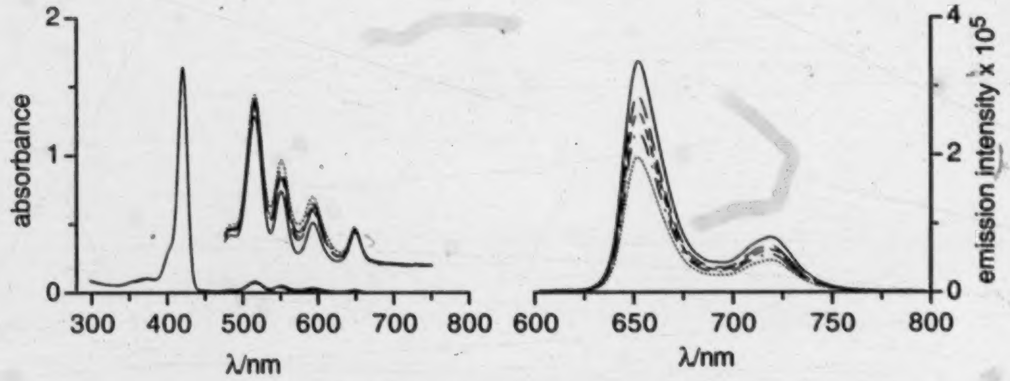

Figure 3.5. (a) Absorption spectra (b) and emission spectra of **1a** in toluene (2 x 10-6 M) before irradiation, after irradiation at 313 nm and after prolonged irradiation at 430 nm. See key (right) for irradiation periods.

—— **1a** no irradiation
·········· irr 313 nm 1.5 min
— · — irr 430 nm 30 min
- - - - irr 430 nm 1 h
— — irr 430 nm 1.5 h

3.3.3.3. Possible Mode of Indirect Ring-Opening

Subsequent to this publication, a report by Irie and coworkers employing a similar hybrid system confirmed our results (Equation 3.3).[18] They, like us, also found that the fluorescence of a porphyrin appended to a dithienylethene could be modulated by alternate irradiation with UV and visible light while irradiating at 420 nm. They attributed the quenching behavior of the *closed* isomer to an intramolecular energy transfer process between the S_1-excited state of the porphyrin and the *closed* form of the dithienylethene bridge. The authors however do not make any mention of prolonged irradiation effects while reading at 420 nm. If these studies had been performed, I believe they would have observed the similar ring-opening phenomenon that was observed in our system.

Equation 3.3

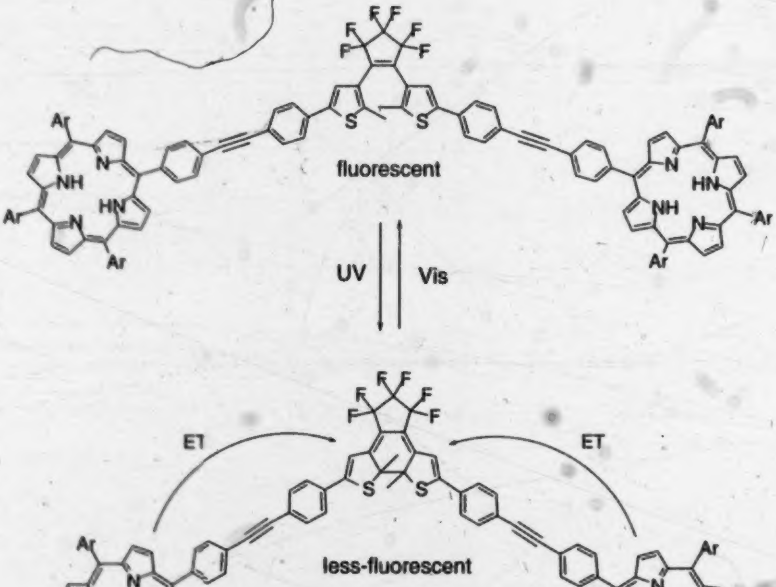
F F
F F
F F
S S
Ar
N
NH
HN
N
Ar
Ar
fluorescent
UV
Vis
ET
ET
less-fluorescent
intramolecular energy transfer

The indirect ring-opening phenomenon of **1b** may be the result of an overlapping absorption band for the *closed* form of the photochrome and emission band for the porphyrin. If this were the case, then this allows for a possible energy transfer pathway between the excited state porphyrin and the *ring-closed* dithienylethene, ultimately resulting in the observed ring opening process. Equation 3.4 provides a schematic representation of the indirect ring-opening experiment that was performed and shows a possible mechanism involved in the ring-opening process.

Equation 3.4.

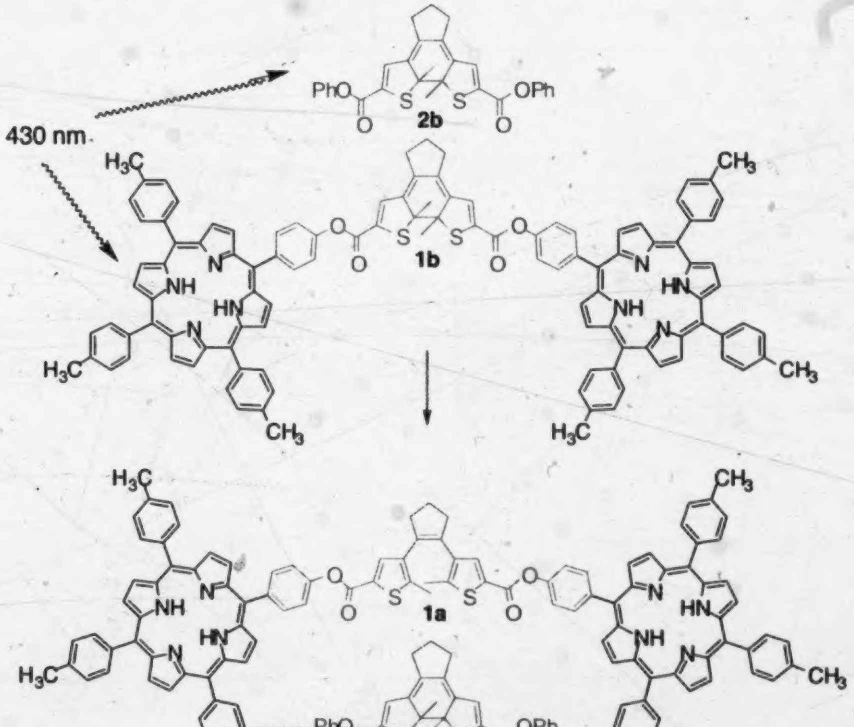

When a solution of either **2a** or **2b** is excited at 420 nm there is no change in the absorption spectrum. This indicates the absence of both the ring-opening and ring-closing photochemical transformations under these conditions. This is not unexpected as both **2a** and **2b** have no spectral absorption bands in this region. The ester linkage that connects the porphyrins to the dithienylethene photochrome in **1** effectively disrupts electronic communication between the two moieties. Hence, the UV-Vis spectral characteristics of **2a** and **2b** are a reasonable description of the spectral profiles of the photochromic portion (light colored bonds in **1a** and **1b**) that lies beneath the overpowering UV-Vis absorption bands of the porphyrins in **1** (Equation 3.4 and Figure 1). When a mixture of the *ring-closed* isomers **1b** and **2b** are irradiated at 420 nm both photochromes open. In each case, this indirect ring-opening is substantially slower than direct irradiation on the visible photochromic bands of the *ring-closed* forms. The slow ring-opening process during indirect irradiation may due to an inefficient energy transfer process, a result of a small spectral overlap integral. With respect to the indirect ring-opening process, **1b** opens at a much faster rate than **2b**. This could be due to an intramolecular energy transfer process from the appended porphyrins. The control compound **2b** may absorb some of the porphyrins excited state energy and *ring-open* through an even slower intermolecular energy transfer process.

3.3.4 Conclusion

Although this photochromic system represents the most effective emission-based information storage device at the time of publication, it ultimately suffered the same fate of its predecessors. The reading event triggered changes in the state of the photochrome. The preceding emission-based systems for non-destructive readout failed due to "readout" irradiation on a photochromic band which occurred because of insufficient separation between the UV-Vis bands responsible for both the fluorescence and photochromic processes. In this regard, the porphyrin-dithienylethene system **1** reported by us was technically sound. The destructive nature in our system stems from a process occurring between the excited state porphyrin and the *closed* form of the dithienylethene. Transient absorption spectroscopy monitoring for radical cations or anions of the porphyrins or dithienylethene directly following porphyrin irradiation, in conjunction with time resolved fluorescence experiments would shed light on the quenching mechanism.

Turning this system around and observing it from a different angle (figuratively speaking of course), one might look at this result as a success. This system is quite unique in that it allows the trigger of one switch in the presence of other very similar switches by indirect irradiation. The idea that a molecular system can "create its own energy" to work is very appealing in the area of molecular devices.

The following Chapter describes how we circumvented the undesirable ring-opening process occurring during the reading event by modifying the existing porphyrin-dithienylethene system.

4.4.6 Experimental

General: All solvents (Caledon) were distilled prior to use. Toluene used for UV-Vis spectroscopy and spectrofluorometry was deoxygenated by bubbling argon through the solvent. All other solvents were used as received. Solvents for NMR analysis (Cambridge Isotope Laboratories) were used as received. ^{1}H NMR characterizations were performed on a Varian Inova-500 instrument, working at 499.92 or on a Varian Inova-300 instrument, working at 299.96 MHz. Chemical shifts (δ) are reported in parts per million relative to tetramethylsilane using the residual solvent peak as a reference standard. Coupling constants (J) are reported in Hertz. FT-IR measurements were performed using a Nicolet Magna-IR 750. UV-Vis measurements were performed using a Varian Cary 400 Scan spectrophotometer. Fluorescence measurements were performed using a PTI C60 photon counting spectrofluorometer.

Synthesis of 5-methyl-(4[2-{2-methyl-5-carboxylic acid}-thiophen-3-yl]-cyclopent-1-enyl)-thiophen-2-carboxylic acid (5). *Tert*-butyllithium (1.7 M in hexane, 7.5 mL, 12.8 mmol) was added dropwise over 10 min to a solution of *bis*-chloride **4**[15] (1.9 g, 5.8 mmol) in anhydrous THF (130 mL) at -78°C under an argon atmosphere. The solution was stirred for a further 30 minutes at this temperature and then anhydrous CO_2 was continuously bubbled through the reaction mixture for 20 minutes, at which time the solution turned into a thick slurry. At this point THF (20 mL) was added and the reaction allowed to warm to room temperature, and stirred there for 1 hour. The THF was removed under vacuum and the residue dissolved in CH_2Cl_2 (250 mL) and shaken with 5% NaOH (2 x 250 mL). The combined aqueous layers were acidified by the dropwise addition of concentrated HCl and the resulting white precipitate was collected by vacuum filtration, triturated with cold CH_2Cl_2 (2 x 5-10mL) to remove any mono-carboxylic acid and dried affording 1.8 g of the product as a white solid. Single crystals suitable for X-ray diffraction were grown by layering a methanol solution of the **4** with H_2O.[19] Yield 88%; mp > 265°C (decomp); ^{1}H NMR (300 MHz, CD_3OD): δ 7.47 (s, 2H), 2.82 (t, *J*=8 Hz, 4H), 2.10 (q, *J*=8 Hz, 2H), 1.96 (s, 6H); ^{13}C NMR (75 MHz, CD_3OD): δ 165.2, 144.2, 138.1, 136.3, 135.7, 131.5, 39.4, 23.9, 14.8; IR (µscope) υ 2953, 2841, 2578, 1663, 1550, 1463, 1373, 1308, 1271 cm^{-1}; HRMS (EI) Calcd for M^+ ($C_{17}H_{16}O_4S_2$) 348.0490. Found: 348.0492.

Synthesis of 5-methyl-(4[2-{2-methyl-5-carboxylic acid}-thiophen-3-yl]-cyclopent-1-enyl)-thiophen-2-carbonyl chloride (6). A suspension of **5** (52 mg, 0.15 mmol) in freshly distilled CH_2Cl_2 (10 mL) was treated with anhydrous DMF (25 µL) and cooled to 0°C. Oxalyl chloride (270 mg, 2.1 mmol) dissolved in freshly distilled CH_2Cl_2 (10 mL) was added dropwise to the rapidly stirring solution over 30 minutes. A light green homogenous solution was formed after 1 hour, which was stirred at room temperature for 16 hours. The solvent was removed by evaporation yielding a green solid. The crude product was carried onto the next step without further purification. mp 115-120°C; ^{1}H NMR (300 MHz, $CDCl_3$): $\delta = 7.63$ (s, 2 H), 2.81 (t, J=8 Hz, 4H), 2.10 (q, J=8 Hz, 2H), 2.01 (s, 6H); HRMS (EI) Calcd for M^+ ($C_{17}H_{14}O_2S_2Cl^{37}Cl^{35}$) 385.9782, $[M\text{-Cl}]^+$ ($C_{17}H_{14}O_2S_2Cl^{35}$) 349.0124. Found: 385.9768 (43%), 349.0107 (100%).

Synthesis of 1a. *Bis*-carbonyl chloride **6** (12 mg, 0.03 mmol) was added to a freshly distilled solution of CH_2Cl_2 (25 mL) containing pyridine (100 mg) and 5,10,15-tris(tolyl))-20-(4-hydroxyphenyl)-porphyrin **3** (47 mg, 0.07 mmol). After stirring for 20 minutes, triethylamine (0.5 mL) was added and the solution stirred for an additional hour. The solvent was removed under reduced pressure yielding a purple residue which was purified by column chromatography (SiO_2, CH_2Cl_2) yielding 37 mg of **1a** as a purple solid. Yield 74%; mp > 300 °C; ^{1}H NMR (500 MHz, CD_2Cl_2): δ 8.89-8.84 (m, 16H), 8.27 (d, *J*=8.5 Hz, 4H), 8.09 (d, *J*=7.5 Hz, 4H), 8.03 (d, *J*=7.5 Hz, 8H), 7.92 (s, 2H), 7.66 (d, *J*=8.5 Hz, 4H), 7,58 (d, *J* =7.5 Hz, 4H), 7.50 (d, *J* =7.5 Hz, 8H), 2.89 (t, *J*=8 Hz, 4H), 2.71 (s, 6H), 2.65 (s, 12H), 2.22 (q, *J*=8 Hz, 2H), 2.21 (s, 6H), -2.85 (br s, 4H); ^{13}C NMR (75 MHz, $CDCl_3$): δ 160.7, 150.7, 144.6, 140.0, 139.3, 139.2, 137.4, 137.2, 136.9, 136.0, 135.4, 135.1, 134.6, 134.5, 128.8, 127.5, 120.4, 120.3, 120.0, 118.7, 38.9, 29.8, 23.0, 21.5, 15.3; IR (CH_3Cl, cast) υ 3316, 2921, 2852, 1726, 1505, 1471, 1444, 1401, 1349, 1265, 1194, 1166, 1109, 1019; ESMS for ($C_{111}H_{85}N_8S_2O_4$) $[M+H]^+$ 1658.6, $[M+2H]^{2+}$ 829.8.

Synthesis and isolation of 1b. *Bis*-porphyrin **1a** (4.0 mg, 0.003 mmol) was suspended in toluene (20 mL) and was gently heated until fully dissolved. The solution was diluted with toluene to 6 x 10^{-6} M. Aliquots of this solution (75 mL) were placed in a quartz tube and irradiated at 313 nm until the growing absorbances in the UV-Vis spectrum corresponding to the *closed* isomer **1b** ceased to change (about 3-4 minutes of irradiation). The toluene was removed by evaporation and to the resulting residue was dissolved in chloroform (10 mL) and treated with silica gel (100-125 mg). The chloroform was removed by evaporation and the resulting silica bound residue was placed on top of a pre-packed silica gel column (CH_2Cl_2/hexane 1:1). The column (1 cm x 30 cm) was eluted (CH_2Cl_2/hexane 2:1, 800 mL) with pressure while taking care to shield it from light. The solvent system was then changed to CH_2Cl_2 and the first three light purple fractions (0.5-1 mL each) contained **1b** with trace amounts of **1a** (2-3% as estimated by ^1H NMR). The fractions were combined and the solvent was then removed under reduced pressure yielding purple solid **1b** (0.3 mg) in 98% pure form. Yield 8%; ^1H NMR (300 MHz, $CDCl_3$): δ 8.86 (m, 16H), 8.24 (d, *J*=8 Hz, 4H), 8.08 (d, *J*=8 Hz, 12H), 7.59 (d, *J*=8 Hz, 4H), 7.54 (d, *J* =8 Hz, 12H), 7.12 (s, 2H), 2.70 (s, 18H), 2.63 (t, *J*=8 Hz, 4H) 2.30 (s, 6H), 2.03 (q, *J*=8 Hz, 2H), -2.80 (br s, 4H).

Synthesis of 5-methyl-(4[2-{2-methyl-5-carbonyl-phenyl-ester}-thiophen-3-yl]-cyclopent-1-enyl)-thiophen-2-carbonyl-phenyl-ester (2a). NaH (8 mg, 0.33 mmol) was added to a solution of phenol (10 mg, 0.11 mmol) in benzene (20 mL) and the mixture stirred for 20 minutes. 1,2-Bis(5-carbonyl chloride-2-methylthien-3-yl)cyclopentene **6** (17 mg, 0.044 mmol) was added and the mixture was stirred at room temperature for 30 minutes. H_2O (10 mL) was added and the mixture was rapidly stirred for an additional 30 minutes. The layers were then separated and the aqueous layer extracted with benzene (20 mL). The organic layers were combined and dried over anhydrous Na_2SO_4 and the resulting solution filtered. The solvent was removed under reduced pressure and the resulting residue was purified by column chromatography (SiO_2, Hexane/EtOAc 6:1) yielding 18 mg of **2a** as a white solid. Yield 82%; mp 141-142 °C; ^1H NMR (300 MHz, $CDCl_3$) δ 7.60 (s, 2H), 7.41-7.36 (m, 4H), 7.24-7.17 (m, 6H), 2.83 (t, *J*=8 Hz, 4H), 2.09 (q, *J*=8 Hz, 2H), 2.01 (s, 6H); ^{13}C NMR (75 MHz, $CDCl_3$) δ 165.4, 150.7, 144.1, 137.0, 135.7, 135.0, 129.5, 128.7, 125.9, 121.7, 38.7, 22.9, 15.0; IR ($CHCl_3$, cast) υ 2952, 2844, 1725, 1593, 1549, 1493, 1456, 1273, 1235, 1192, 1163, 1061, 1027; ESMS (EI) Calcd for M^+ ($C_{29}H_{24}S_2O_4$) 500.1116, $[M\text{-OPh}]^+$ ($C_{23}H_{19}S_2O_3$) 407.0776. Found 500.1102 (20%), 407.0776 (100%).

Synthesis of 2b. Photochrome **2a** (0.6 mg) was dissolved CD_2Cl_2 (700 µL) and placed in an NMR tube. The solution was irradiated at 313 nm for 6 minutes. This resulted in a 89% photostationary state favoring the closed isomer. No attempts were made to isolated **2b**. ^1H NMR (500 MHz, CD_2Cl_2) 7.44-7.40 (m, 4H), 7.30-7.26 (m, 4H), 7.17-7.15 (m, 2H), 6.95 (s, 2H), 2.52 (t, *J*=8 Hz, 4H), 2.05 (s, 6H), 1.92 (q, *J*=8 Hz, 2H).

3.3.5 Notes and references

1. Tsivgoulis, G. M.; Lehn, J-M. *Chem. Eur. J.* **1996**, *2*, 1399.

2. (a) Irie, M., *Chem. Rev.*, **2000**, *100*, 1685. (b) Irie, M. In *Organic Photochromic and Thermochromic Compounds*: Crano, J. C.; Gugliemetti, R. J.; Plenum Press: New York, NY, 1999; Vol. 1, Chapter 5.

3. (a) Stellacci, F.; Bertarelli, C.; Toscano, F.; Gallazzi, M. C.; Zerbi, G. *Chem. Phys. Lett.* **1999**, *302*, 563. (b) Fernandez-Acebes, A.; Lehn, J-M. *Chem. Eur. J.*, **1999**, *5*, 3285. (c) Yamaguchi, T.; Uchida, K.; Irie, M. *J. Am. Chem. Soc.* **1997**, *119*, 6067. (d) Seibold, M.; Port, H. *Chem. Phys. Lett.* **1996**, *252*, 135. (e) Yokoyama, Y.; Uchida, S.; Yokoyama, Y.; Sugawara, Y.; Kurita, Y. *J. Am. Chem. Soc.* **1996**, *118*, 3100. (f) Huck, N. P. M.; Wolter, J. F.; de Lange, B.; Feringa, B. L. *Science*. **1996**, *273*, 1686. (g) Liu, Z. F.; Hashimoto, K.; Fujishima, A. *Nature*. **1990**, *347*, 658.

4. (a) Kim, E.; Choi, K. H.; Rhee, S. B. Macromolecules, **1998**, *31*, 5726. (b) Kawai, T.; Koshido, T.; Yoshino, K. *Appl. Phys. Lett.* **1995**, *67*, 795. (c) Tanio, N.; Irie, M. *J. J. Appl. Phys.* **1994**, *33*, 1550.

5. (a) Feringa, B. L.; van Delden, R. A.; Koumura, N.; Geertsema, E. M. *Chem. Rev.*, **2000**, *100*, 1789. (b) Eggers, L.; Buss, V. *Angew. Chem. Int. Ed. Engl.* **1997**, *36*, 881. (c) Agati, G.; McDonagh, A. F. *J. Am. Chem. Soc.* **1995**, *117*,4425.

6. (a) Tsuchiya, S. *J. Am. Chem. Soc.* **1999**, *121*, 48. (b) Takeshita, M.; Irie, M. *Chem. Lett.*, **1998**, 1123. (c) Tsivgoulis, G. M.; Lehn, J-M. *Chem. Eur. J.*, **1996**, *2*, 1399. (d) Inada, T.; Uchida, S.; Yokoyama, Y. *Chem. Lett.*, **1997**, 321. (e) Seibold, M.; Port, H.; Wolf, H. C. *Mol. Cryst. Liq. Cryst.* **1996**, *283*, 75. (f) Huck, N. P. M.; Feringa, B. L. *J. Chem. Soc., Chem. Commun..*, **1995**, 1095. (g) Saika, T.; Iyoda, T.; Honda, K.; Shimidzu, T. *J. Chem. Soc., Chem. Commun.*, 1992, 591.

7. The 1,2-*bis*-(5-carboxy-2-methyl-3-thienyl)cyclopentene photochrome was synthesized from the known 1,2-*bis*-(5-chloro-2-methyl-3-thienyl)cyclopentene, see: Lucus, L. N.; van Esch, J.; Kellogg, R. M.; Feringa, B. L. *J. Chem. Soc., Chem. Commun..*, **1998**, 2313. See supporting information for details.

8. Standard lamps used for visualizing TLC plates (Spectroline E-series, 470 μW/cm^2) were used to carry out the ring-closing reaction of **1a** to **1b** and **2a** to **2b**. The ring-opening reactions were carried out using the light of a 150-W

tungsten source that was passed through a 480 nm cutoff filter to eliminate higher energy light.

9. (a) Myles, A. J.; Branda, N. R. *Tetrahedron Lett.* **2000**, *41*, 3785. (b) Hunter, C. A.; Sarson, L. D. *Tetrahedron Lett.* **1996**, *37*, 699.

10. Gilat, S. L.; Kawai, S. H.; Lehn, J.-M. *Chem. Eur. J.* **1995**, *1*, 275.

11. This claim is based on a comparison of the absorption spectra of model compounds **2a**, **2b** and **3**.

12. The monochromator of the fluorimeter (1mm slit) was employed (65-W Xenon lamp).

13. The *closed* form **1b** was isolated in 98% purity (2% residual *open* isomer **1a**, see Figure 3.4 following the paper). This sample displayed 2-3% fluorescence intensity relative to **1a** (λ_{excit} = 430 nm, λ_{em} = 655 nm) indicating that **1b** is non-fluorescent.

14. See Figure 3.5 following the paper

15. Lucus, L. N.; van Esch, J.; Kellogg, R. M.; Feringa, B. L. *J. Chem. Soc., Chem. Commun.*, **1998**, 2313.

16. Peters, A.; Branda, N. R. unpublished results.

17. Etemad-Moghadam, G.; Ding, L.; Tadj, F.; Meunier, B. *Tetrahedron* **1989**, *45*, 2641.

18. Osuka, A.; Fujikane, D.; Shinmori, H.; Kobatake, S.; Irie, M. *J. Org. Chem.* **2001**, *66*, 3913.

19. The crystal structure of **5** is discussed in detail in Appendix I

3.4.1 Back to the Drawing Board: Redesigning Our Original System

The major premises behind redesigning our original hybrid system was to electronically tune both components so that their active absorption and emission bands would not overlap with one another. The beauty of both the dithienylethene photochrome and the porphyrin chromophore is that their absorption and emission profiles can be systematically altered by changing the functional groups residing on or around their peripheries. For instance, the conjugation of electron rich substituents onto the the dithienylethene results in red-shifts for both the UV and visible absorption bands of the *ring-closed* isomer (Figure 4.1).[1]

Figure 4.1

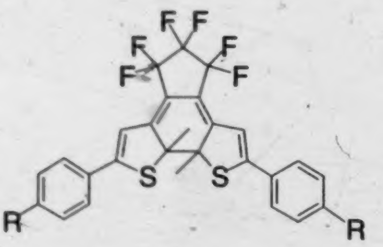

R = H, λ_{max} = 534 nm

R = CN, λ_{max} = 562 nm

R = N(Et)$_2$, λ_{max} = 597 nm

When redesigning the porphyrin fragment, we needed to look no further than some previous work performed within our own laboratory. Some of our earlier studies on the self-assembly of axially coordinated ruthenium porphyrins indicated that the placement of the ruthenium atom at the core of the porphyrin drastically effects both its absorption and emission profiles (Equation 4.2).[2] In these cases, the metallated porphyrins underwent a ruthenium-based phosphorescent emission at λ=730 nm which is 80 nm red-shifted with respect to the fluorescence of the corresponding free-base porphyrin. The incorporation of more typical porphyrin core metals such as zinc, iron or nickel into the original covalent hybrid system described in the previous Chapter was not undertaken as they typically extinguish or blue-shift the fluorescent emissive properties exhibited by the porphyrin. This would place the emission band directly over the visible absorption band of most typical *ring-closed* dithienylethenes.

Figure 4.2

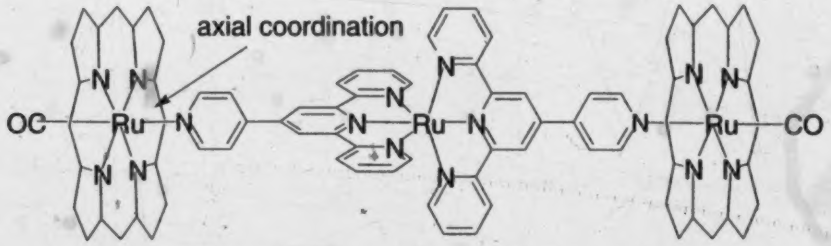

The photochromic system described in the following paper improved upon the systems reported by Lehn and coworkers, where tungsten carbonyl or ruthenium-(bipyridine) carbonyl complexes are coordinated to the peripheries of pyridyl derivatized photochromes (Equation 4.1).[3] In their studies, the authors were never able to find a band in the UV spectral region where irradiation of the fluorophore left the photochromic system undisturbed. Furthermore, the band that provided the most promising discrimination between the fluorescence and photochromic properties was of extremely high energy ($\lambda = 240$ nm). Prolonged "reading" at this wavelength would most likely result in photodegradation of the system as most organic molecules and more specifically most carbonyl coordination compounds are photochemically labile under such harsh conditions. In addition, when these systems did fluoresce, they did so in regions of the spectrum that overlapped substantially with the photochromic interconversion bands of the dithienylethenes which may have contributed to the destructive nature of the system during the reading process.

Equation 4.1

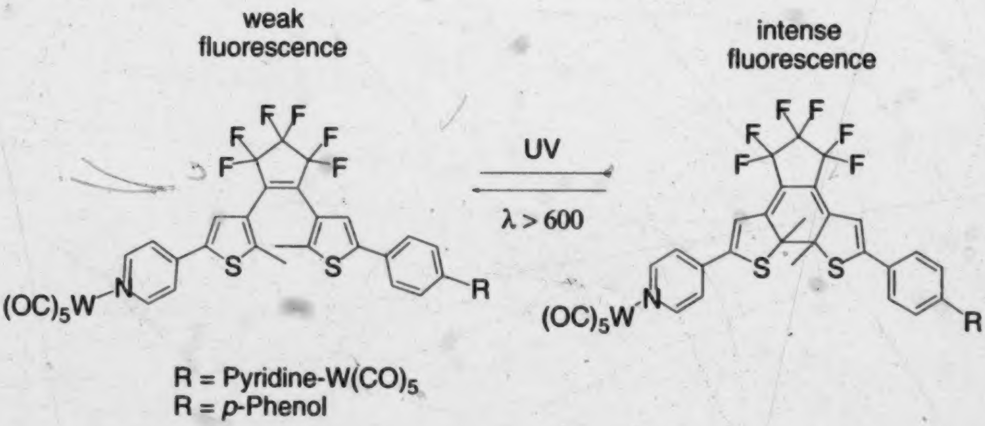

Blending of our previous knowledge of self-assembling axially coordinated ruthenium porphyrins with photochromic dithienylethene ligands would be a perfect fit from both a synthetic and spectroscopic point of view.

3.4.2 - Paper - Axially Coordinated Porphyrinic Photochromes for Non-destructive Information Processing

Tyler B. Norsten and Neil R. Branda

Adv. Mater. **2001**, *13*, 347.

Photochromic 1,2-dithienylethene derivatives have been cited as some of the most promising compounds for application to photonic devices such as erasable data storage systems and optical switches because of their thermal irreversibility and fatigue resistance.[4] The success of molecular-scale optical information processing hinges on the ease at which the detection method can read the stored information without erasing it. Photochromic molecules whose states can be identified using non-invasive detection methods form the basis of non-destructive readout devices.[5]

UV-Vis spectroscopy is by far the most common detection method used today, where the photochromic states are identified by measuring the absorption bands characteristic of the *open* and *closed* isomers. Inconveniently, these are the same absorptions that are responsible for inducing the ring-opening and ring-closing reactions of the photochrome and, as a result, measuring too close to these photochemically active absorptions eventually leads to partial erasing of the stored information. Photoluminescence has been suggested as a viable alternative for non-destructive readout, as long as changes in emission coincide with the photochromic transformation.[6,5b] In order to be formally classified as non-destructive, the productive absorption bands corresponding to the "write", "erase" and "read" processes should be adequately distant from each other so that each state can be independently accessible by irradiating in different regions of the UV-Vis spectrum. There is an additional condition that must be satisfied in the case of luminescence-based systems. The emission bands that are being measured in the read-out event should also appear far removed from all absorption bands to avoid any interconversion of the photochrome's states from the generated luminescence.

The photochromic luminescent system reported by Lehn *et al.*[5b] utilizes changes in the emission from transition metal complexes coordinated to the ends of the pyridyl-derivatized 1,2-dithienylethene **2**. A drawback of this system is that the fluorophore's excitation band cannot be independently addressed by a specific wavelength of light. The result is the partial photochemical interconversion of the photoswitch during excitation of the fluorophore. Another example was reported by our lab. When covalently attached onto the ends of the 1,2-*bis*-(3-thienyl)- cyclopentene photochromic backbone, porphyrin macrocycles luminesce with intensities that are dependent on whether the photochrome is in its *open* or *closed* state.[7] In this system, the excitation band of the flourophore is remote from the photochemically active absorption bands of the photochrome. The reported system has limited use in data processing applications, however, because excitation resulted in photochemical interconversion of the photochrome, which may be a result of the emission wavelength slightly overlapping with the active absorption band associated with the ring-opening process. This drawback can be circumvented by taking advantage of porphyrin macrocycles that phosphoresce instead of fluoresce and thus, will emit light energy far beyond the photochromically active absorption bands.

In the course of other studies, we and others have investigated the luminescence properties of ruthenium-based metalloporphyrins axially coordinated to Lewis-basic pyridyl ligands.[8] In these cases, the metalloporphyrins phosphoresced at wavelengths outside the spectral regions that would be used to carry out the photochromic reactions ("write" and "erase" processes) for most dithienylethenes,[9] when excited throughout the Soret or the Q-band regions. Here, we describe a supramolecular optical switch based on the phosphorescence of an axially coordinated ruthenium porphyrin to the pyridyl-derivatized 1,2-dithienylethene photochrome **2**. This system exemplifies the use of luminescent changes to achieve non-destructive readout.

Treatment of bis(pyridyl)photochrome **2**[6b] with two molar equivalents of Ru(TTP)(CO)(EtOH)[10] in CH_2Cl_2 followed by precipitation with hexane afforded coordination compound **1a** as a burgundy solid in high purity and in nearly quantitative yield (Scheme 1). The formation of the coordination compound is confirmed by the upfield shifts in the ^1H NMR spectrum for all thiophene and pyridine hydrogen atoms of **1a** due to their lying within the shielding cones of the porphyrin macrocycles (Table 1). ^1H NMR spectroscopy also attested to the stability of the complex as the appearance of the spectrum did not vary over concentrations ranging from 1×10^{-4} M to 6×10^{-6} M. This observation is critical as it clearly shows that the axial coordination is maintained at the low concentrations used to measure the luminescence behavior of the porphyrins.

Solutions of the *open* isomer **1a** (4×10^{-4} M in C_6D_6) were irradiated with 365 nm light[11] to generate the *closed* isomer **1b** as shown in Figure 1. After 9 minutes, the photostationary state was reached and was composed of 95% **1b** as monitored by ^1H NMR spectroscopy. The spectral trends of all photochromes are listed in Table 1.

The absorption spectrum in the UV-Vis region of both the *open* and *closed* isomers of **1** is essentially the sum of the absorption spectra of the molecule's building blocks

Scheme 1

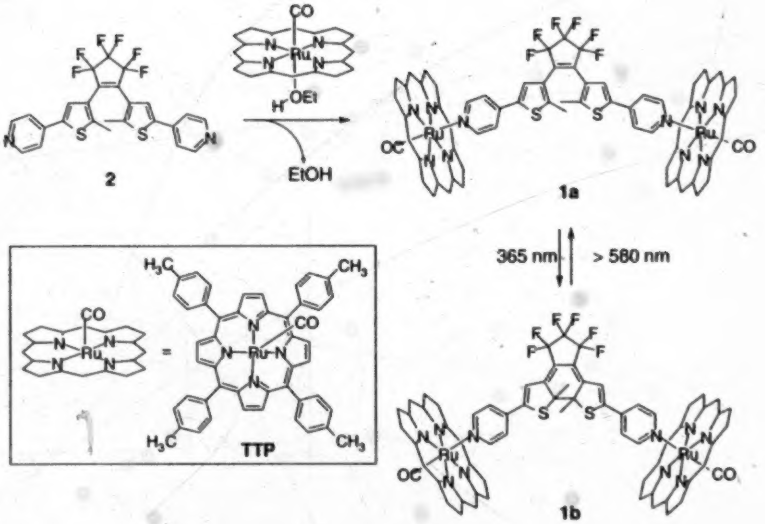

(**2(open)**, **2(closed)** and Ru(TTP)(py)(CO)[8c]) indicating there is little change in the ground state of either component upon forming the coordination compound. The high-energy absorptions responsible for conversion of **1a** to **1b** and **2(open)** to **2(closed)** ("write" band) exist below 380 nm (Figure 1). The open isomers **1a** and **2a** can be photochemically regenerated by exposing solutions of the closed isomers to visible light extending from 470-685 nm ("erase" band).

Table 1. Selected ^{1}H NMR data (300 MHz) of open and closed forms of photochromes **1-3** in C_6H_6.

Compound	δ for heterocyclic protons [ppm]			
	thiophene C-H	thiophene CH_3	pyridine α-H	pyridine β-H
1a	5.78	0,69	1.78	4.34
1b[a]	5.07	1.20	1.73	4.10
2(open)	7.29	1.60	8.45	6.82
2(closed)[a]	6.56	2.00	8.42	6.62
3(open)	6.07[b]	1.21[b]	1.82	4.46
3(closed)[a]	5.26[b]	1.60[b]	1.77	4.23

[a] Samples (10^{-3} M) were irradiated for 9 minutes (λ = 365 nm). [b] Thiophene attached to the coordinating pyridine.

Compound **1a** phosphoresces at 730 nm with varying intensities when excited throughout the UV-Vis region. The excitation wavelengths that yield the highest emission intensity exist in a narrow window of the visible spectrum between 360 and 500 nm..

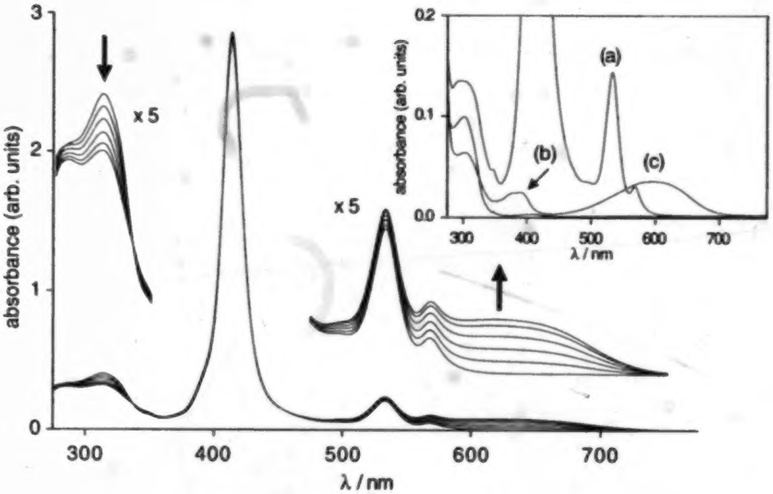

Figure 1. Changes in the UV-Vis absorption spectra of a benzene solution of **1a** (6×10^{-6} M) upon irradiation with 365 nm light. Irradiation periods are 0, 15, 45, 90, 150 and 210 seconds. The inset shows the absorption spectra of benzene solutions of *(a)* Ru(TTP)(CO)(py) at 6×10^{-6} M, *(b)* **2(open)** and *(c)* **2(closed)** at 3×10^{-6} M.

Conveniently, both **2(open)** and **2 (closed)** are transparent in this spectral region, and irradiation with light at these wavelengths has little effect on the photochemical interconversion of **1** or **2** in either direction.

The emission intensity of **1** can be modulated by photochemically toggling between **1a** and **1b**, providing a non-destructive readout method. The *open* form **1a** emits at 730 nm (Figure 2). Irradiation of **1a** at 365 nm produced the non-emitting **1b** while back irradiation at wavelengths greater than 580 nmregenerates the open form and restores the luminescence to near its original value.

Figure 2 also shows five write/erase cycles while exciting the macrocycles at 455 nm[12] and monitoring the intensity of their phosphorescence at 730 nm. Prolonged irradiation (2 hours) of solutions of **1a** and **1b** at 455 nm results in no observable spectral changes as monitored by both absorption and emission spectroscopy. This clearly demonstrates that this system is non-destructive under these conditions.

Similar experiments were performed on monoporphyrinic photochrome **3** with analogous results as those for **1**. Alternating irradiation of **3** at 365 nm and greater than580 nm resulted in a modulating emission intensity similar to that seen in **1**. This result implies that the porphyrin's emission behavior is most likely sensitive to the linearly π-conjugated chromophore created on ring closing to **1b** and not to any electronic communication between adjacent porphyrins.

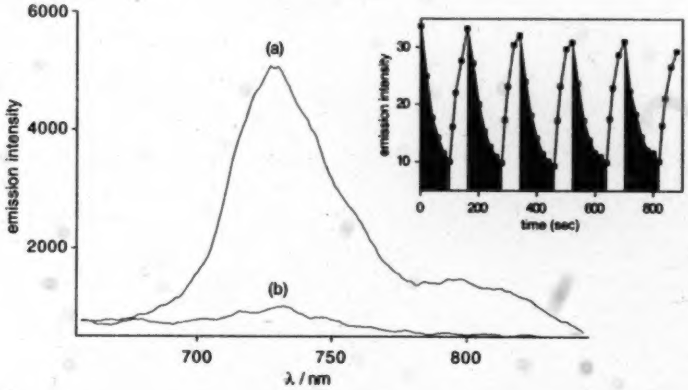

Figure 2. Emission spectra of benzene solutions (1 x 10^{-6} M) of (a) **1a** and (b) **1b**. The inset shows the modulated emission signal of benzene solutions of **1** (6 x 10^{-6} M) during alternating irradiation at 365 nm (shaded areas) and greater than 580 nm (non-shaded areas). Spectra were run in deoxygenated benzene (λ_{ex} = 455 nm, λ_{em} = 730 nm).

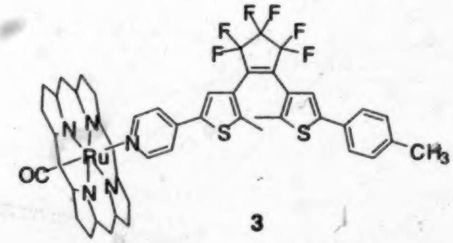

3

This body of work clearly demonstrates that when properly tuned, the optical properties of porphyrins in conjunction with dithienylethenes hold promise in the area of optical data storage devices.

3.4.3 Results and Discussion

3.4.3.1 Synthesis of Axially Coordinated Porphyrinic Photochromes

We prepared the pyridyl derivatized photochrome **2** according to the procedure previously described by Lehn and coworkers (Scheme 4.1).[13] This reaction sequence entails double bromination of 2-methylthiophene followed by selective substitution of the more reactive 2-bromo position by a boronic acid moiety. Palladium catalyzed cross coupling of the thiophene boronic acid **4** with *para*-bromopyridine afforded the pyridyl derivatized 3-bromothiophene **5**. Double addition of the lithium salt of **5** to octafluorcyclo-pentene afforded photochrome **2**. Also generated during this reaction was the mono addition adduct **6**, which was subsequently used to generate the non-symmetric control photochrome **8**.

Although Lehn and coworkers report yields as high as 67% for **2**, my best effort yielded a meager 27%. The reaction to generate photochrome **2** is quite finicky because exactly half an equivalent of octafluorocyclopentene must be added to the lithiated thiophene. This is not an easy feat as octafluorocyclopentene is extremely volatile at ambient temperatures (bp = 26 °C). In the confines of a standard laboratory, it therefore must be handled quickly and at depressed temperatures and as a result even after several attempts I was unable to achieve satisfactory yields. Nevertheless I was able to prepare ample quantities of **2** to complete the necessary photochromic studies.

Scheme 4.1

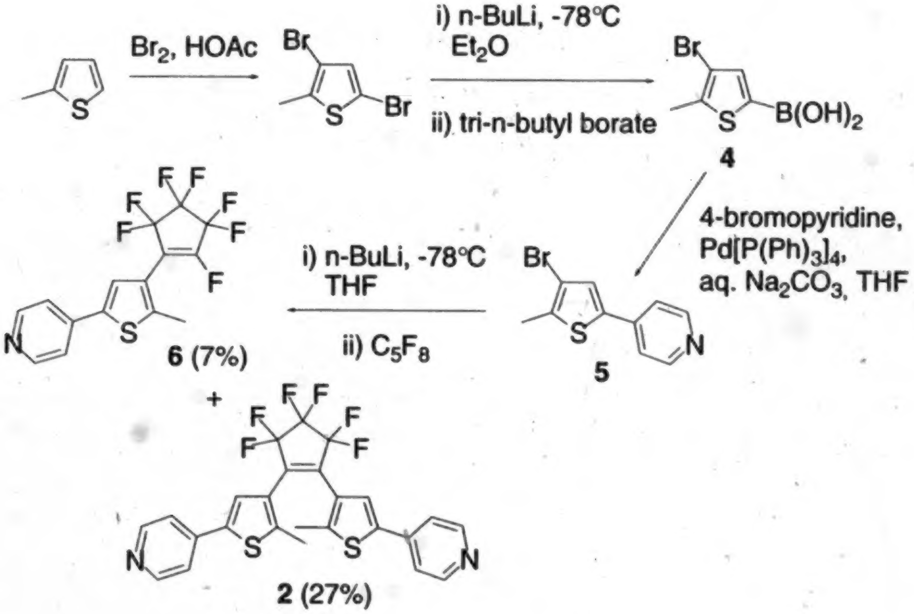

Br2, HOAc
Br
S
Br
i) n-BuLi, -78°C
Et2O
ii) tri-n-butyl borate
B(OH)2
4
4-bromopyridine,
Pd[P(Ph)3]4,
aq. Na2CO3, THF
5
N
i) n-BuLi, -78°C
THF
ii) C5F8
F
6 (7%)
+
2 (27%)

Scheme 4.2

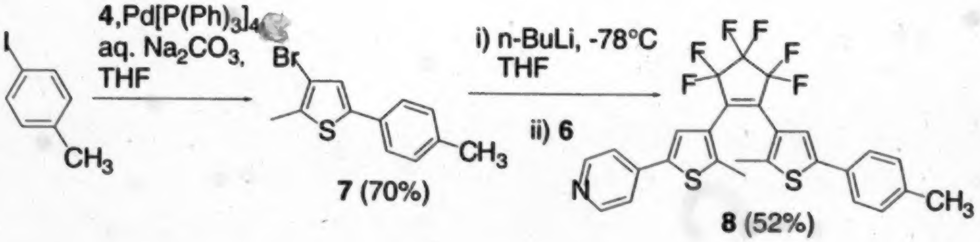

I
CH3
4,Pd[P(Ph)3]4,
aq. Na2CO3,
THF
Br
S
7 (70%)
i) n-BuLi, -78°C
THF
ii) 6
F
N
8 (52%)

The non-symmetric photochrome **8** was prepared in a similar fashion to **2** by coupling the toluene derivatized 3-bromothiophene **7** to **6** under standard butyllithium reaction conditions (Scheme 4.2).[14]

The triruthenium(0)dodecacarbonyl used to metallate the core of the tetratolyl-porphyrin (TTP) was prepared by treating $RuCl_3$ with CO in methanol according to a literature procedure.[15] The Ru(TTP)(CO)(EtOH) porphyrin used to axially coordinate to the ends of the pyridyl derivatized photochromes **2** and **8** was synthesized by refluxing TTP in the presence of $Ru_3(CO)_{12}$ (Scheme 4.3).[16]

Scheme 4.3

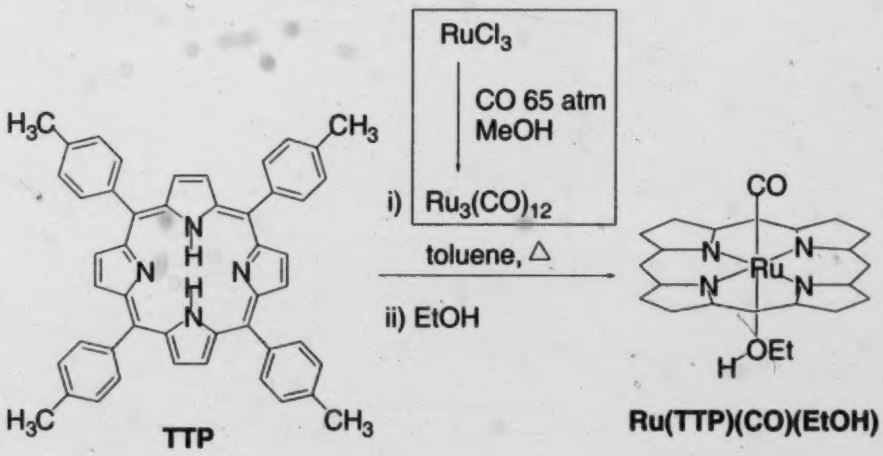
H3C
CH3
N
H
H
N
N
N
H3C
CH3
TTP
RuCl3
CO 65 atm
MeOH
i) Ru3(CO)12
toluene, Δ
ii) EtOH
CO
N
N
Ru
N
N
OEt
H
Ru(TTP)(CO)(EtOH)

Scheme 4.4

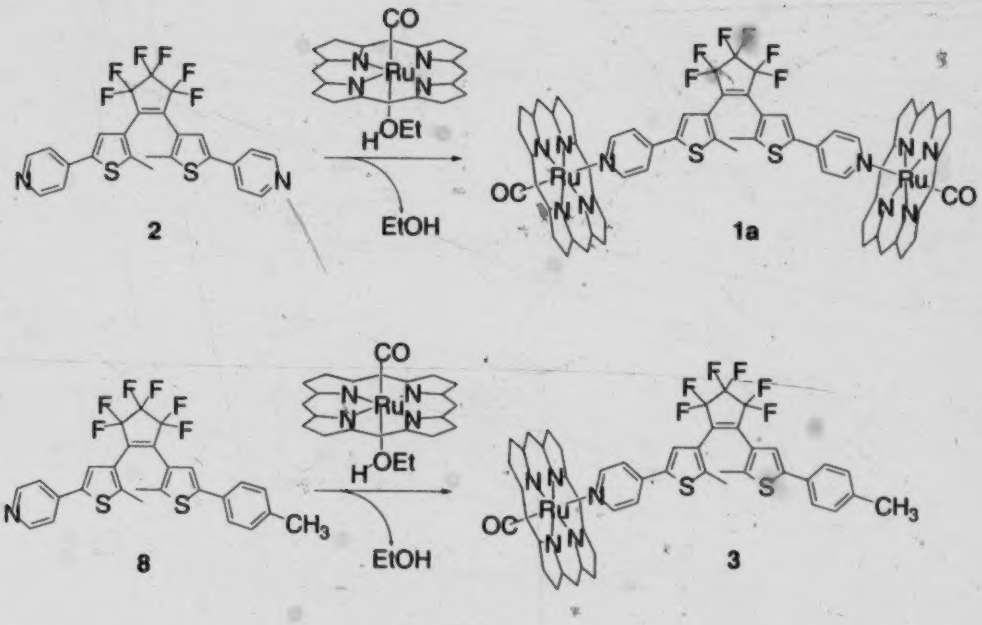

The EtOH ligand coordinated to the ruthenium atom on the Ru(TTP)(CO)(EtOH) porphyrin is easily displaced by a stronger lewis base. As such, when slightly more than two equivalents of Ru(TTP)(CO)(EtOH) is added to photochrome **2**, the pyridyl moieties quickly and quantitatively displace the labile EtOH ligands. This affords the desired coordination compound **1a**. The fact that Ru(TTP)(CO)(EtOH) is freely soluble in hexane while **1a** is not provides a convenient means to isolate **1a** in pure form. The mono porphyrinic coordination photochrome **3** was prepared in situ in an NMR tube by the addition of *exactly* one equivalent of the Ru(TTP)(CO)(EtOH) to **8** while monitoring the progress of the reaction by ^{1}H NMR spectroscopy.

3.4.3.2 Electronic Communication Between Porphyrins: The Need for a Control Compound

In nature isolated porphyrins are rare. Most often they exist in well-defined assemblies of two or more porphyrins. The porphyrin "special pair" belonging to the photosynthetic reaction center is the prototypical example of this. As described in Chapter 2, the "special pair" works in unison to trap light and subsequently shuttle the excited state energy to other nearby porphyrins.

A study by Shinkai and coworkers designed to mimic the "special pair" clearly demonstrates how proximity and orientation can effect the resulting photophysical characteristics in porphyrin pairs (Figure 4.3).[17] In this example, various carbohydrates were used as scaffolds to rigidly position porphyrin pairs in precise locations about the carbohydrate skeleton. Each carbohydrate sampled provided a unique distance and dihedral angle between the appended porphyrin pairs. Hence, the only difference between the various carbohydrate-porphyrin molecules was the relative distance and orientation between porphyrins. It was found that the relative luminescence for the various carbohydrate-porphyrin molecules was linearly correlated with the porphyrin dihedral angle. This finding clearly shows that the relative orientation plays a decisive role in the electronic properties of porphyrin dimers.

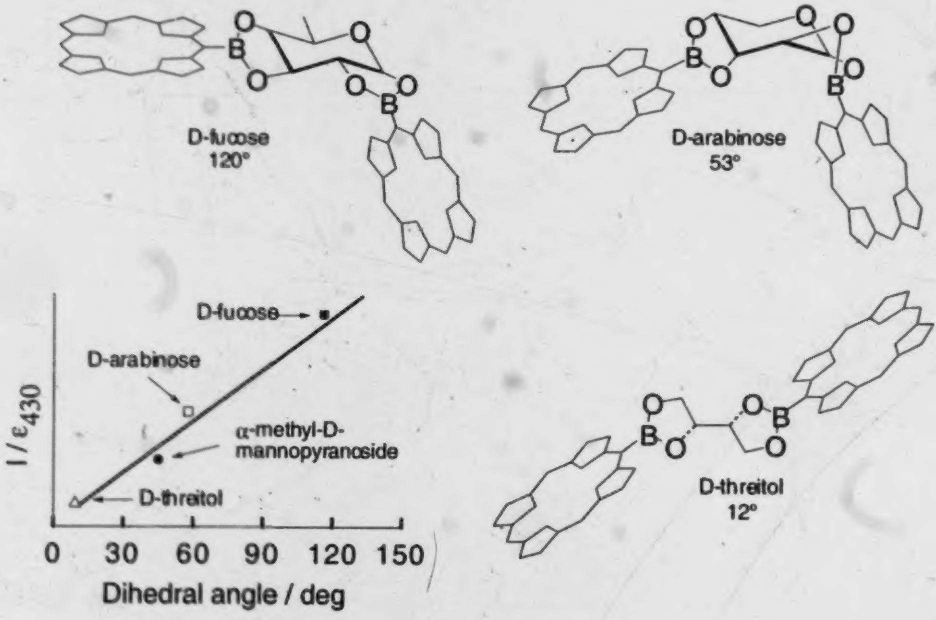

Figure 4.3. Various carbohydrate porphyrin dimers prepared by Shinkai. The graph is a plot of relative fluorescence intensities (I/ε_{430}) vs. dihedral angle of porphyrin dimers.

Our photochromic system consists of two porphyrins mounted on the ends of dithienylethene **2**. In the ring-closed form **1b** the two porphyrins are rigidly locked into a specific distance and orientation relative to one another. However in **1a** the arms of the photochrome can freely rotate affording a variety of distances and orientations between the two porphyrins. Hence, the modulating emission intensity observed for **1** could potentially be a result of the differences in porphyrin-porphyrin distance and orientation between **1a** and **1b**. To exclude the possibility of porphyrin-porphyrin *communication* the mono porphyrinic photochrome **3** was prepared. Because a similar modulation of phosphorescence was observed for **3** we concluded that the observed modulation was due to *communication* between the porphyrin and the *ring-closed* form of the dithienylethene.

3.4.3.3 Separation of the Active Photochromic Absorption and Porphyrinic Emission Bands

The primary goal of this system was to electronically tune both the lumophore and the chromophore so that their active absorption bands and emission bands were remote from one another. Figure 4.4 clearly illustrates how the write, erase and both the read excitation and read emission bands of our system (**1**) are adequately dispersed throughout the UV-Vis spectral regions. Another advantage of our system over many of the previously reported systems is that it can be read with "less harsh" light (λ = 455 nm). This would ultimately yield substantially less photodegredation over multiple read-write-erase cycles for an organic based system.

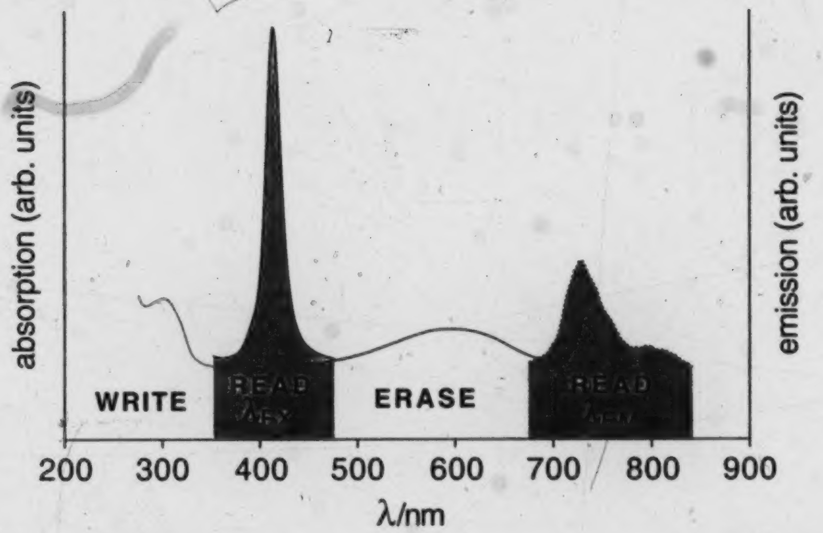

Figure 4.4. The WRITE region corresponds to the absorption profile of **2(open)**; ERASE to the absorption profile of **2(closed)**; READ λ_{EX} to the absorption profile of **1a** or **1b**; and READ λ_{EM} to the emission profile of **1a**.

3.4.4 Conclusion

If such photochromic systems are ever to be realized as functioning memory storage devices their incorporation into the solid state is the logical next step. As such there have been several examples of incorporating doped monomer[18] or polymer[19] based dithienylethenes and other photochromes[20] into thin film matrices. The results have been promising, and in most instances the photochromic properties are maintained in the solid state. Some research groups have even reported the modulation of other systemic properties such as luminescence[21] and refractive index.[22] These examples provide the necessary evidence needed to pursue solid state photochromic devices, however they were simple extensions of previous systems that were not adequate for non-destructive readout purposes. As such, future work on our system will focus on its incorporation into thin films and studying the resulting photochromic/luminescent properties.

Luminescent based detection is only one potential method for the non-destructive readout of photochromic systems. The next Chapter will discuss another useful and actively pursued alternative, which employs the use of chiral photochromes to detect differences in the rotation of linearly polarized light.

3.4.5 Experimental

General: All solvents (Caledon) were distilled prior to use. CH_2Cl_2 and benzene used for UV-Vis spectroscopy and spectrofluorometry was deoxygenated by bubbling argon through the solvent. All other solvents were used as received. See Chapter 3 for the description of apparatus used.

Synthesis of 3-bromo-2-methyl-5-(4'-tolyl)thiophene (7). Tetrahydrofuran (10 mL) and aqueous sodium bicarbonate (20% w/v), 10 mL) were added to a flask containing 3-

bromo-2-methyl-5-thiopheneboronic acid **4** (79 mg, 0.36 mmol), 4-Iodotoluene (156 mg, 0.72 mmol) and a catalytic amount of tetrakis-triphenylphosphine palladium (0). The reaction was stirred and heated at reflux under a nitrogen atmosphere for 24 hours and then cooled. The reaction was extracted with chloroform (2 x 50 mL) and the combined organic phases were dried with anhydrous Na_2SO_4 and the resulting solution filtered. The solvent was removed under reduced pressure and the product was purified by column chromatograph (SiO_2, hexane) affording 67 mg of a white solid. Yield 70%; ^{1}H NMR (300 MHz, $CDCl_3$) δ 7.38 (d, *J*=8 Hz, 2H), 7.15 (d, *J*=8 Hz, 2H), 7.04 (s, 1H), 3.39 (s, 3H), 3.34 (s, 3H); ^{13}C NMR (75 MHz, CD_2Cl_2) *δ* 141.7, 138.3, 133.7, 131.0, 130.0, 125.5, 125.3, 109.9, 21.2, 14.9; IR (CH_2Cl_2, cast) υ 2914, 1958, 1538, 1510, 1409, 1328, 1309, 1180, 1163, 1141, 1120, 1019; HRMS (EI) Calcd for M^+ ($C_{12}H_{11}SBr^{81}$) 267.9744. Found: 267.9774.

Synthesis of 1-[5'-(4"-Pyridyl)-2'-methylthien-3'-yl)]-2-[2'''-methyl-5'''-(4''''-tolyl)-thien-3'''-yl] perfluorocyclopentene (8). 3-Bromo-2-methyl-5-(4-tolyl)thiophene **7** (22 mg, 0.08 mmol) was dissolved in anhydrous THF (50 mL). The solution was cooled to -78°C and *n*-BuLi (2.5 M in hexane, 29 μl, .072 mmol) was added under an argon atmosphere and the solution stirred for a further 30 minutes. 1-[5'-(4"-Pyridyl)-2'-

methylthien-3'-yl)] perfluorocyclopentene **6** (15 mg, 0.04 mmol) dissolved in anhydrous THF (2 mL) was added to the reaction mixture. The mixture was allowed to warm to ambient temperature and stirred for 1 hour. The THF was removed under reduced pressure and the residue purified by column chromatography (SiO_2, hexane/EtOAc 1:1) affording 11 mg of a white solid. Yield 32%. ^{1}H NMR (300 MHz, CD_2Cl_2) δ 8.57 (d, *J*=6 Hz, 2H), 7.51 (s, 1H), 7.46 (s, 1H), 7.42 (d, *J*=6 Hz, 2H), 7.23 (d, *J*=8 Hz, 2H), 7.19 (d, *J*=8 Hz, 2H), 2.36 (s, 3H), 2.02 (s, 3H), 1.97 (s, 3H); HRMS (ES) Calcd for $[M+H]^+$ ($C_{27}H_{20}NF_6S_2$) 536.0936. Found 536.0936.

Synthesis of 1a. 1,2-Bis(2'-methyl-5'(pyrid-4"-yl)thienyl-3-yl)perfluorocyclopentene **2**[9b] (6.1 mg, 0.01 mmol) was dissolved in freshly distilled CH_2Cl_2 (10 mL). Ru(TTP)(CO)(EtOH) (20 mg, 0.03 mmol) was added and the mixture was stirred at ambient temperature for 30 minutes. The CH_2Cl_2 was removed under reduced pressure and the burgundy residue was then triturated several times with hexane until the washings were colorless. The solid was collected by centrifuge and dried under high vacuum for 24 hours affording a 25 mg of a burgundy solid. Yield 96%; ^{1}H NMR (300 MHz, CD_2Cl_2) δ 8.61 (s, 16H), 8.07 (dd, *J*=8, 2 Hz, 8H), 8.87 (dd, *J*=8, 2 Hz, 8H), 7.53 (d, 8 Hz, 8H), 7.45 (d, 8 Hz, 8H), 6.36 (s, 2H), 5.21 (d, *J*=7 Hz, 4H), 2.66 (s, 24H), 1.39 (d, *J*=7 Hz, 4H), 1.15 (s, 6H); ^{13}C NMR (100 MHz, CD_2Cl_2) δ 144.5, 144.4, 143.9, 139.8, 138.5, 138.2, 137.3, 137.1, 134.4, 134.2, 131.9, 127.6, 127.3, 121.9, 117.4, 21.6, 17.1; IR (CH_2Cl_2, cast) υ 3021, 2921, 2080, 2064, 1955, 1694, 1682, 1651, 1634, 1608, 1575, 1557, 1538, 1528, 1505, 1435, 1304, 1212, 1141, 1072; MS (ES) [*M* +H]$^+$ ($C_{123}H_{99}N_{10}F_6S_2O_2Ru_2$), [*M* –Ru(CO)(TTP)+H]$^+$ ($C_{78}H_{63}N_6S_2ORu$): 2119.0, 1321.0.

Synthesis of 1b. Photochrome **1a** (0.8 mg) was dissolved C_6D_6 (1 mL) and placed in an NMR tube. The solution was irradiated at 365 nm for 9 minutes. This resulted in a 95% photostationary state favoring the closed isomer. No attempts were made to isolated **1b**. ^{1}H NMR (300 MHz, CD_2Cl_2) δ 9.00 (s, 16H), 8.15 (d, *J*=8 Hz, 8H), 8.00 (d, *J*=8 Hz, 8H), 7.23 (d, 8 Hz, 8H), 7.23 (d, 8 Hz, 8H), 5.07 (s, 2H), 4.10 (d, *J*=7 Hz, 4H), 2.36 (s, 24H), 1.73 (d, *J*=7 Hz, 4H), 1.20 (s, 6H),

Synthesis of 3. 1-[5'-(4"-Pyridyl)-2'-methylthien-3'-yl)]-2-[2'''-methyl-5'''-(4''''-tolyl)-thien-3'''-yl] perfluorocyclopentene (**8**) (1-2 mg) was dissolved in CD_2Cl_2 (700 µL) and placed in an NMR tube. Small amounts of Ru(TTP)(CO)(EtOH) were added to the NMR tube until the doublet at 8.6 ppm (corresponding to the unbound pyridine α-H) disappeared. This signaled that the 1:1 axially coordinated complex between the ruthenium metallo-porphyrin and the pyridyl photoswitch was complete. The solvent was removed under reduced pressure and the residue dried under high vacuum for 24 hours affording a burgundy solid. ^{1}H NMR (300 MHz, CD_2Cl_2) δ 8.64 (s, 12H), 8.1 (dd, *J*=8, 2 Hz, 4H), 7.93 (dd, *J*=8, 2 Hz, 4H), 7.55 (d, *J*=8 Hz, 4H), 7.50 (d, *J*=8 Hz, 4H), 7.28 (d, *J*=8 Hz, 2H), 7.11 (d, *J*=8 Hz, 2H), 6.99 (s, 1H), 6.56 (s, 1H), 5.34 (d, *J*=7 Hz, 2H), 2.68 (s, 12H), 2.31 (s, 3H), 1.65 (s, 3H), 1.45 (d, *J*=7 Hz, 2H), 1.26 (s, 3H); HRMS (ES) Calcd for $[M+H]^+$ ($C_{76}H_{56}N_5F_6S_2ORu$) 1334.2868. Found: 1334.2862.

3.4.6 Notes and references

1. Irie, M.; Sakemura, K; Okinaka, M; Uchida, K. *J. Org. Chem.* **1995**, *60*, 8305.
2. Chichak, K.; Branda, N. R. *Chem. Commun.* **1999**, 523.
3. Fernandez-Acebes, A.; Lehn, J-M. *Chem, Eur. J.* **1999**, *5*, 3285.
4. (a) Irie, M., *Chem. Rev.*, **2000**, *100*, 1685. (b) Irie, M. In *Organic Photochromic and Thermochromic Compounds*: Crano, J. C.; Gugliemetti, R. J.; Plenum Press: New York, NY, 1999; Vol. 1, Chapter 5.
5. (a) Stellacci, F.; Bertarelli, C.; Toscano, F.; Gallazzi, M. C.; Zerbi, G. *Chem. Phys. Lett.* **1999**, *302*, 563. (b) Fernandez-Acebes, A.; Lehn, J-M. *Chem. Eur. J.*, **1999**, *5*, 3285. (c) Yamaguchi, T.; Uchida, K.; Irie, M. *J. Am. Chem. Soc.* **1997**, *119*, 6067. (d)

Seibold, M.; Port, H. *Chem. Phys. Lett.* **1996**, *252*, 135. (e) Yokoyama, Y.; Uchida, S.; Yokoyama, Y.; Sugawara, Y.; Kurita, Y. *J. Am. Chem. Soc.* **1996**, *118*, 3100. (f) Huck, N. P. M.; Wolter, J. F.; de Lange, B.; Feringa, B. L. *Science*. **1996**, *273*, 1686. (g) Liu, Z. F.; Hashimoto, K.; Fujishima, A. *Nature*. **1990**, *347*, 658.

6. (a) Gobbi, L.; Seiler, P.; Diederich, F. *Angew. Chem.* **1999**, *111*, 740; *Angew. Chem. Int. Ed.* **1999**, *38*, 674. (b) Takeshita, M.; Irie, M. *Chem. Lett.* **1998**, 1123. (c) Inada, T.; Uchida, S.; Yokoyama, Y.; *Chem. Lett.* **1997**, 321. (d) Tsivgoulis, G. M.; Lehn, J-M. *Chem. Eur. J.*, **1996**, *2*, 1399. (e) Seibold, M.; Port, H.; Wolf, H. C. *Mol. Cryst. Liq. Cryst.* **1996**, *283*, 75. (f) Huck, N. P. M.; Feringa, B. L. *J. Chem. Soc., Chem. Commun.*, **1995**, 1095. (g) Saika, T.; Iyoda, T.; Honda, K.; Shimidzu, T. *J. Chem. Soc., Chem. Commun.*, 1992, 591.
7. Norsten, T. B.; Branda, N. R. *J. Am. Chem. Soc.* **2001**, 123, 1784.
8. (a) Chichak, K.; Branda, N. R. *Chem. Commun.* **1999**, 523. (b) Ikonen, M.; Guez, D.; Marvaud, V.; Markovitsi, D. *Chem. Phys. Lett.* **1994**, *231*, 93. (c) Antipas, A.; Buchler, J. W.; Gouterman, M.; Smith, P. D. *J. Am. Chem. Soc.* **1978**, *100*, 3015.
9. There are several examples where the *closed* isomers of 1,2-dithienylethene derivatives absorb at wavelengths longer than 700 nm. They typically contain extended linear π-conjugation or employ a "push-pull" system on the thiophene rings

flanking the bridging ethene bond: (a) Bens, A. T.; Frewert, D.; Kodatis, K.; Kryschi, C.; Martin, H.-D.; Trommsdorff, H. P. *Eur. J. Org. Chem.* **1998**, 2333. (b) Gilat, S. L.; Kawai, S. H.; Lehn, J.-M. *Chem. Eur. J.* **1995**, *1*, 275. (c) Nakayama, Y.; Hayashi, K.; Irie, M. *Bull. Chem. Soc. Jpn.* **1991**, *64*, 789., and reference 3d.

10. The abbreviation TTP refers to 5,10,15,20-tetratolylporphyrinato dianion. (a) Funatsu, K.; Kimura, A.; Imamura, T.; Ichimura, A.; Sasaki, Y. *Inorg. Chem.* **1997**, *36*, 1625. (b) Collman, J. P.; Barnes, C. E.; Brothers, P. J.; Collins, T. J.; Ozawa, T.; Gallucci, J. C.; Ibers, J. A. *J. Am. Chem. Soc.* **1984**, *106*, 5151.
11. Standard lamps used for visualizing TLC plates (Spectroline E-series, 470 μW/cm^2) were used to carry out the ring-closing reactions of **1-3**. The ring-opening reactions were carried out using the light of a 150-W tungsten source that was passed through a 580 nm cutoff filter to eliminate higher energy light.
12. The monochromator of the fluorimeter (1mm slit) was employed (65-W Xenon lamp).
13. Gilat, S. L.; Kawai, S. H.; Lehn, J-M. *Chem, Eur. J.* **1995**, *1*, 275.
14. Kawai, S. H.; Gilat, S. L.; Lehn, J-M. *Eur. J. Org. Chem.* **1999**, 2359.
15. Bruce, M. I.; Jensen, C. M.; Jones, N. L.; Süss-Fink, G.; Herrmann, G.; Dase. V. *Inorg. Synth* **1989**, *26*, 259.

16. (a) Funatsu, K.; Kimura, A.; Imamura, T.; Ichimura, A.; Sasaki, Y. *Inorg. Chem.* **1997**, *36*, 1625. (b) Collman, J. P.; Barnes, C. E.; Brothers, P. J.; Collins, T. J.; Ozawa, T.; Gallucci, J. C.; Ibers, J. A. *J. Am. Chem. Soc.* **1984**, *106*, 5151.

17. Takeuchi, M; Chin, Y.; Imada, T.; Shinkai, S. *Chem Commun.* **1996**, 1867.

18. (a) Kasatani, K.; Kambe, S.; Irie, M. *J. Photochem. Photobio. A.: Chem.* **1999**, 11. (b) Owrutsky, J. C.; Nelson, H. H.; Baronavski, A. P.; Kim, O.-K.; Tsivgoulis, G. M.; Gilat, S. L.; Lehn, J.-M. *Chem Phys. Lett.* **1998**, 293, 555. (c) Kim, E.; Choi, K. H.; Rhee, S. B. *Macromol.* **1998**, *31*, 5726.

19. Nakashima, H.; Irie, M. *Polym. J.* **1998**, 30, 985.

20. Matsui, F.; Taniguchi, H.; Yokoyama, Y.; Sugiyama, K.; Kurita, Y. *Chem. Lett.* **1994**, 1869.

21. Kawai, T.; Kunitake, T.; Irie, M. *Chem. Lett.* **1999**, 905.

22. Yoshida, T.; Arishima, K.; Hoshino, M.; Ebisawa, F.; Sukegawa, K.; Ishikawa, A.; Kobayashi, T.; Hanazawa, M.; Horikawa, Y. *Polym. Mater. Sci. Eng.* **1996**, *75*, 368.

Chapter 5 - Chiroptical-Based Detection for Non-destructive Readout

3.5.1 Chiroptical Methods: Optical Rotatory Dispersion and Circular Dichroism

UV/Vis spectroscopy uses a beam of light that is essentially unpolarized. When considered in the context of a wave phenomenon, the electric field vectors of unpolarized light propagate in a radial fashion such that no one single direction predominates. On the other hand, linearly polarized light consists of a beam that propagates in a single direction. This is referred to as the plane of polarization. Within this same context, the propagation of circularly polarized light traces out a helix as a function of time. The resulting helix can be either right-handed or left-handed producing right or left circularly polarized light respectively.

When passed through the absorption band of an optically active medium the right- and left-handed components of circularly polarized light experience differences in absorption. This difference in absorption between right- and left-handed circularly polarized light is termed *circular dichroism* (CD) and appears as mirror image curves (or Cotton effects) in a circular dichroism spectrum.[1]

Chiral compounds also possess the unique property of rotating the plane of polarization of a linearly polarized incident light beam. As light of increasingly shorter wavelength is used, the extent of optical rotation of a compound increases. This change in optical rotation as a function of wavelength is termed *optical rotatory dispersion* (ORD).

It is important to remember that where ORD involves the measurement of a rotation, CD involves an absorption measurement. Hence CD occurs only in the vicinity of an absorption band, whereas ORD is theoretically finite throughout the spectrum. This distinction becomes paramount if these techniques are to be applied to non-destructive readout methodology.

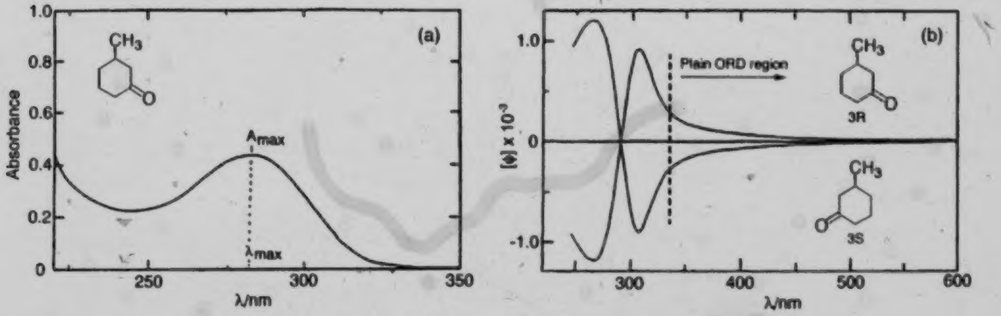

Figure 5.1. (a) UV/Vis absorptioon spectrum of 3-methylcyclohexanone and (b) ORD spectrum of the two enantiomers of 3-methylketone

The comparison between the UV absorption spectrum (Figure 5.1(a)) and the ORD spectrum (Figure 5.1(b)) of 3-methylcyclohexanone clearly illustrates the above-mentioned point. The section of the ORD curve at longer wavelengths than 340 nm, termed the *plain ORD region*, is characteristic of compounds that have no optically active absorption bands in the spectral region being measured. Within this region there is a small but clearly detectable difference in rotation between the two stereoisomeric forms. The incorporation of molecular switches into such systems would provide a convenient means to toggle between opposing rotating strengths, while providing a useful mechanism for non-destructive readout.

3.5.2 Chirality: Optically Active Chromophores

Chiral chromophores typically exhibit the strongest Cotton effects in the region of their electronic absorption bands. But, because rotatory strength falls off with through-space distance from a stereogenic center, the presence of a chiral chromophore does not predispose the molecule or molecular system to observable or detectable Cotton effects. As such, optically active chromophores have been divided into two broad classes. The first class is made up of inherently chiral chromophores which, for the purposes of this discussion I will call Class 1 chromophores. The inherent dissymmetric geometry is responsible for the optical activity of compounds belonging to this class. The second class is composed of inherently achiral but chirally perturbed chromophores, which will be referred to as Class 2 chromophores. Inherently achiral but chirally perturbed chromophores include most of the common organic functional groups. Figure 5.2 shows some examples belonging to each class.

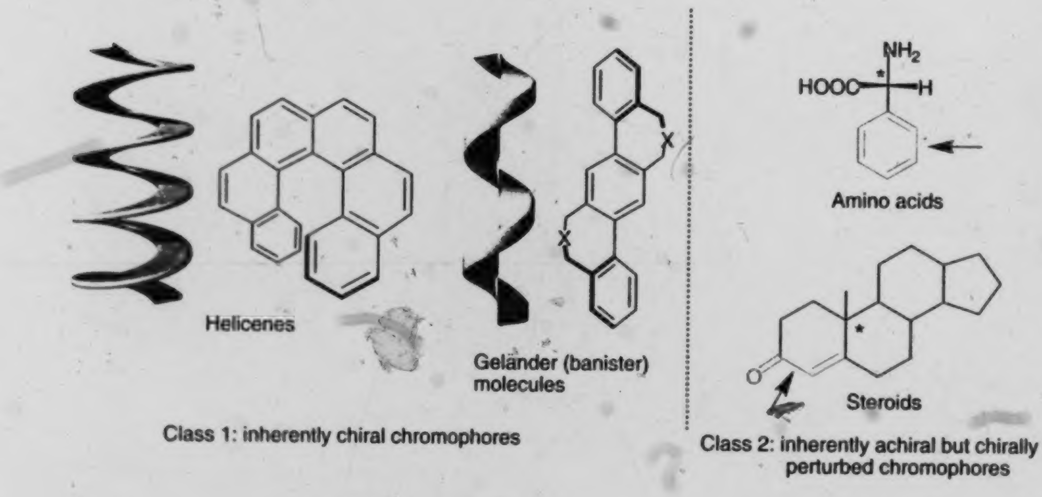
Helicenes
X
X
Geländer (banister) molecules
Class 1: inherently chiral chromophores
NH2
HOOC
*
H
Amino acids
*
O
Steroids
Class 2: inherently achiral but chirally perturbed chromophores

Figure 5.2. Some examples of Class 1 and Class 2 chiral chromophores. The arrows point to the chromophore while the (*) denotes a stereogenic center.

It is important to note that inherently chiral chromophores have large rotational strengths, whereas achiral but chirally perturbed chromophores are characterized by rather weak Cotton effects. Because of this, the majority of successful chiroptic photochromes designed for non-destructive readout belong primarily to Class 1.

An indirect way of creating an inherently chiral chromophore is through the stereoselective assembly of Class 2 chiral chromophores into well ordered noncentrosymmetric architectures. The most common example of this methodology is the supramolecular assembly of metal atoms and chiral ligands into enantiopure helicates. A specific example of this is illustrated in Equation 5.1. In this example a pair of Class 2 ligands (exhibiting relatively weak cotton effects) wind around two silver atoms forming a right-handed helicate.[2] It is the steric interactions between the chiral auxiliaries on opposing strands that initiates and amplifies the handedness of the resulting helicate. In its entirety, the newly formed helicate now adopts a Class 1 status exhibiting much stronger Cotton effects than that of its components. The formation of our photochromic helicates for non-destructive readout in the paper following this discussion is based on this type of strategy.

Equation 5.1

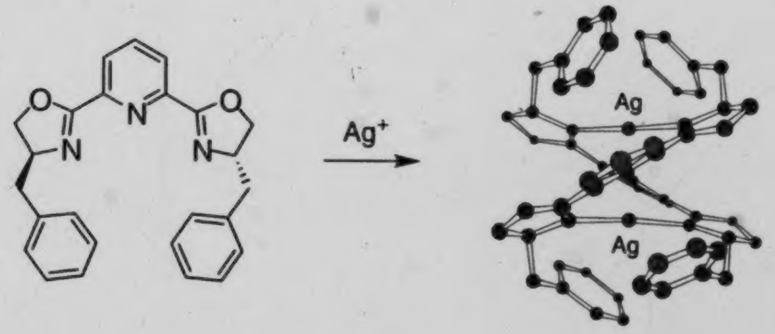

P-helicate only

3.5.3 Examples of Chiroptical Photochromes for Non-Destructive Readout

As stated above the strong rotatory power of helical molecules makes them ideally suited for information processing systems that use light outside the photochromic absorption bands. This makes for easy non-destructive detection due to the enhanced read-out signals provided by helical chirality. For example, Feringa and coworkers developed a new class of helical switch based on the twisted backbone of sterically-overcrowded alkenes (Equation 5.2).[3] It is the unfavorable steric interactions flanking the central olefinic bond that force the molecule to adopt a helical topology. When irradiated at $h\upsilon_1$ enantiomerically pure **A** undergoes a *cis-trans* isomerization which results in the formation of a specific photostationary state in favor of **B**. Subsequent irradiation at $h\upsilon_2$ results in a reversal of helicity (*M* to *P* or *P* to *M*)[4] and affords a different photostationary state in favor of **A**. The two diastereomeric states display distinctly different CD and ORD signals and there exists several regions in the ORD spectrum that can be easily accessed in a non-destructive manner. Although these systems are plagued by slow response times and low de's (diastereomeric excess) they pioneered the use of optical rotation as a non-destructive detection method.

As the previous two Chapters attest, there have been many approaches to the development of dithienylethene photochromes as applied to non-destructive readout devices. The advancement of chiroptic dithienylethenes is no exception as they are rapidly being developed for similar purposes. The *ring-closed* isomers of dithienylethene derivatives are excellent candidates for incorporation into chiroptical devices as they are necessarily chiral. A major problem however, is that the photo-induced ring-closing reaction produces equal amounts of both *R,R* and *S,S* stereoisomers (Equation 5.3), rendering the desired chiroptic readout method ineffective for the *ring-closed* form. Hence, the major driving force behind research in this area is the development systems that bias the ring-closing reaction in favor of a single stereoisomer.

Equation 5.2

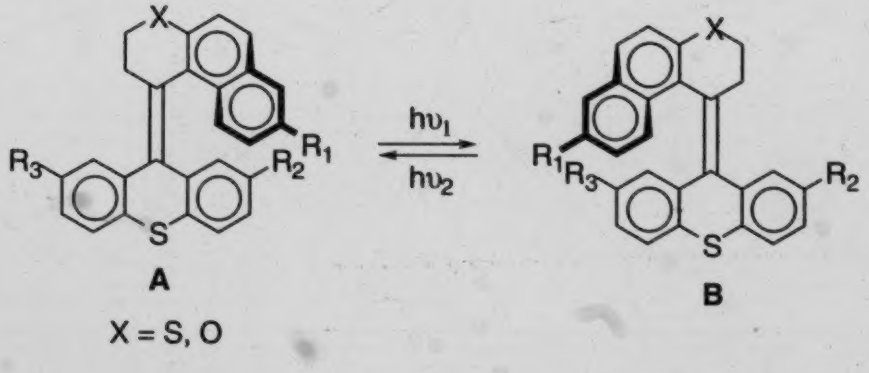

Several researchers have narrowed in on this problem employing different molecular systems yet approaching it from the same fundamental point of view. Their approach entails the incorporation of chiral substituents into the photochromic system in an attempt to bias the ring-closing process. I believe that this is a logical approach to the problem, as in most instances chirality is generated from pre-existing chirality. This is a not always the case, and an exception to this point will be discussed in my closing remarks at the end of this chapter.

Equation 5.3

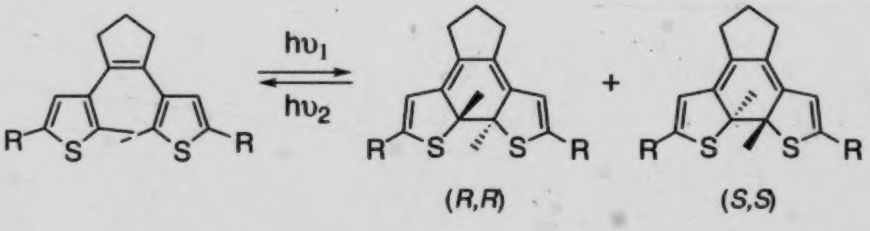

Irie and coworkers skillfully placed an optically active chiral auxiliary at the 2-position of the benzo[*b*]thiophene ring in the diarylmaleimide photochrome shown in Equation 5.4.[5] It was planned that the close proximity of the *l*- or *d*-menthyl groups to the photochromic center would affect the stereochemistry of the ring-closing process. That was indeed the case as de values as high as 86% were realized for the photocyclization process. These values were, however, only attainable under strict environmental conditions such as solvent polarity and composition (hexane/THF in 80.2:19.8) and substantially depressed temperatures (– 40 °C). Conditions such as these are not very amenable to real device applications.

Equation 5.4

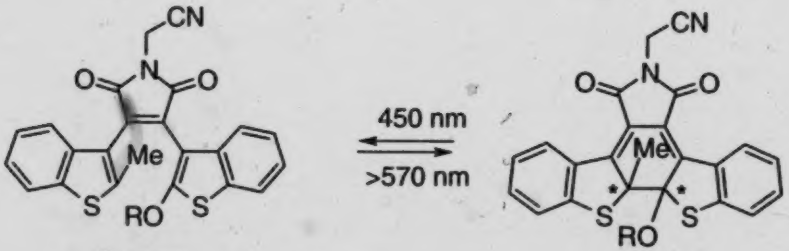
CN
N
O
O
Me
S
RO
S
450 nm
>570 nm
CN
N
O
O
Me
S
RO
S

7 *open*

R=*l* or *d*-menthyl

7 *closed*

As might be expected, the relocation of a chiral auxiliary to a remote point on the periphery of the photochromes' backbone (Equation 5.5) results in substantially reduced values of de (36%).[6] Photochrome **8** has also been introduced as a chiral dopant in an effort to modulate liquid-crystalline phases (nematic and induced cholesteric) for display technology,[7] but similar problems with low stereoselectivity during the ring-closing reaction hinders its use in these devices.

Equation 5.5

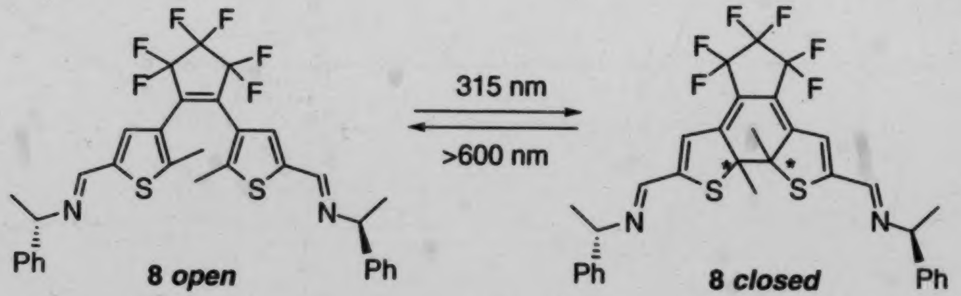
F
F
F
F
F
F
S
S
N
N
Ph
Ph
315 nm
>600 nm
F
F
F
F
F
F
S
S
N
N
Ph
Ph

8 *open*

8 *closed*

In an alternative approach to simply synthesizing chiral molecular switches containing remote stereogenic centers (or point chirality), our approach goes one step further by employing coordination chemistry to promote the stereoselective self-assembly of the chiral photochromes into enantiopure helicates, which contain an added axis of chirality. The rationalization for this strategy is two-fold: (1) Only the photocyclization of the assembled stereochemically pure helicates leads to stereochemically pure products resulting in a reversible bi-stable system where both states are inherently chiral. (2) As described earlier, the generation of helical chirality (or inherently chiral chromophores) greatly enhances the degree to which plane polarized light is rotated. This point is extremely important as this is the basis of our readout mechanism.

3.5.4 - Paper - Nondestructive Data Processing Based on Chiroptical 1,2-Dithienylethene Photochromes

Elisa Murguly, Tyler B. Norsten and Neil R. Branda

Angew. Chem. Int. Ed. **2001**, *40*, 1752.

The viability of photochromic 1,2-dithienylethene derivatives in optical device applications stems from their striking display of advantageous photochromic properties such as thermal irreversibility and fatigue resistance.[8] Their application to erasable memory media requires that both photochromic states be detected in the readout event in a facile and non-invasive manner. Typically, the readout event relies on the use of UV-Vis spectroscopy to record the spectral changes near the absorption bands corresponding to the two photochromic states. However, these are the same absorptions that induce the ring-opening and ring-closing reactions. Thus, sampling near these photoactive absorption bands inevitably causes partial switching of the photochrome and erases the stored information. This problem can be circumvented by developing photochromic systems that employ gating mechanisms[9] or systems that, upon photoisomerization, display variations in their optical properties such as refractive index,[10] luminescence,[11] or optical rotation.[12,11f] It is the detection of these accompanying changes that may ultimately lead to effective nondestructive information processing systems.

Recording changes in optical rotation is a particularly promising alternative for nondestructive readout because detection can often be performed outside the photoactive spectral regions. To enhance the readout signal in order to use this technique, two conditions must be satisfied: 1) the photochromes should exhibit significantly contrasting optical rotating strengths between their two states, and 2) the photochromic reactions should maximize the formation of only one stereoisomer.

The closed forms of 1,2-dithienylethene derivatives are chiral, making them excellent candidates for incorporation into chiroptical devices; however, the ring-closing reactions inevitably yield racemates. The presence of stereogenic centres appended onto the thiophene rings can induce stereodifferentiation in the photocyclization reaction.[13] but the restrictive environmental conditions needed to ensure high stereoselection limit the use of the existing systems.[12d,13a] Inspired by several recent examples in which remote stereogenic centres guide the creation of metallohelicates in stereochemically pure form,[14] we began to explore the unique properties of self-assembled helicates in stereoselective photochromic transformations with the goal of realizing a nondestructive *write-read-erase* system.

Herein we report the self-assembly of double-stranded stereochemically pure copper(I) helicates from chiral ligands **1** and **2** (Scheme 1). The chiral discrimination event that occurs when the chiral oxazoline auxiliaries on the periphery of the individual strands are brought into close proximity translates through the 1,2-dithienylethene backbone to ultimately dictate the handedness of the helicates. This pre-orients the thiophene rings with respect to each other so that photocyclization yields a single diastereomer. The dramatic changes in optical rotation that accompany the stereoselective photochromic process can be recorded in a nondestructive manner.

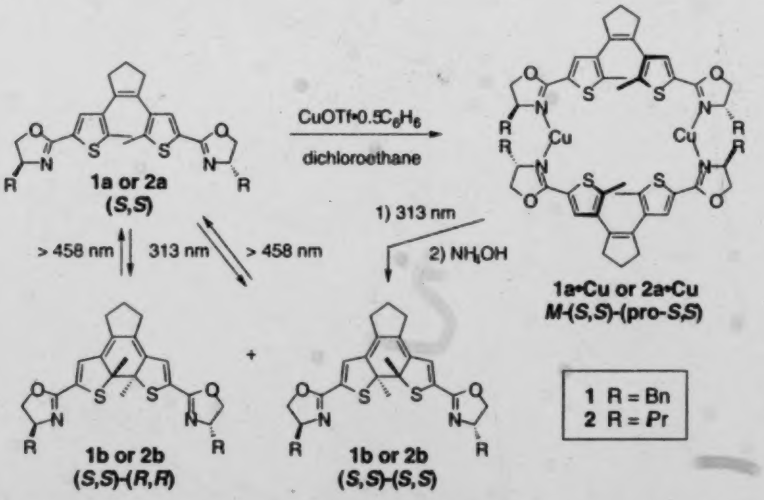

Scheme 1. Formation of ring-closed products **1b** or **2b** from photochromes **1a** or **2a** and their complexes with copper.

Both (*R*,*R*)- and (*S*,*S*)-enantiomers of photochromic bis(oxazolines) **1a** and **2a** were prepared from the known 1,2-*bis*-(5-chloro-2-methyl-3-thienyl)cyclopentene.[15] Copper(I) complexes were prepared by adding an equimolar amount of ligand **1** or **2** in deoxygenated dichloroethane to the benzene complex of copper(I) trifluoromethanesulfonate (CuOTf•0.5C_6H_6) under argon. Care was taken when handling the copper(I) reagent to ensure a moisture and oxygen free atmosphere in order to minimize the oxidation of the metal. With the exception of single crystals grown for X-ray analysis, no attempts were made to isolate the copper(I) complexes.

The electrospray mass spectra of dichloromethane solutions of freshly prepared mixtures of ligand **1a** and CuOTf•0.5C_6H_6 shows peaks at *m/z* 579.1 and 641.1 corresponding to free ligand **1a** and a mixture of the coordination compounds **$Cu_2(1a)_2$** and **Cu(1a)**, respectively. The isotopic abundance of the peak at *m/z* 641.1 shows the typical half-peak separation of a doubly charged species confirming the presence of the binuclear complex **$Cu_2(1a)_2$**. The isotopic distribution pattern verifies the presence of **$Cu_2(1a)_2$** along with mononuclear **Cu(1a)**. The ratio of **$Cu_2(1a)_2$** to **Cu(1a)** increases when the solutions are concentrated. This observation clearly emphasizes the need to control the concentration when generating the coordination compounds, a condition that will be illustrated in further studies.

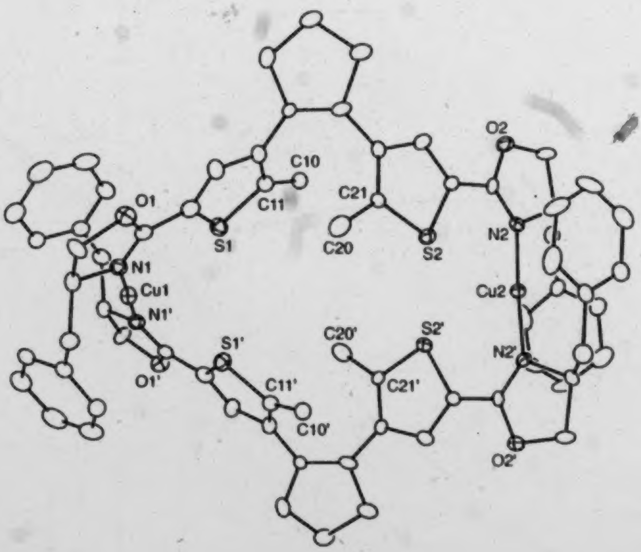

Figure 1. The structure of the copper(I) complex (*S*,*S*)-**$Cu_2(1a)_2$** in the crystal. All non-heteroatomic hydrogens and counterions have been removed for clarity. The thermal ellipsoids are drawn at the 20% probability level. The structure of the (*R*,*R*)-enantiomer is a perfect mirror image.

Single crystals of both (*R*,*R*)- and (*S*,*S*)-enantiomers of **$Cu_2(1a)_2$**•$(OTf)_2$ suitable for X-ray crystallographic analysis were obtained by layering hexane upon freshly prepared dichloromethane solutions of the copper(I) complexes. The crystal structure (Figure 1) highlights the role of the metal centers in the self-assembly process. The resulting solid-state architecture is the anticipated stereochemically pure binuclear double helix. The bis-(monodentate) oxazoline ligands coordinate to the metal centers. The two chiral auxiliaries are brought close together and can thus influence the stereochemistry of the helicate. In all cases, (*S,S*)-**1a** generates solely the *M* helix and (*R,R*)-**1a** generates solely the *P* helix. The helical handedness, in turn, biases the relative orientation of the methyl groups on the thiophene heterocycles (C10, C10', C20 and C20') and sets the carbons involved in forming the new single bond in the photoinduced ring closure (C11, C11', C21 and C21') as pro-(*S,S*) for the *M* helix and pro-(*R,R*) for the *P* helix.

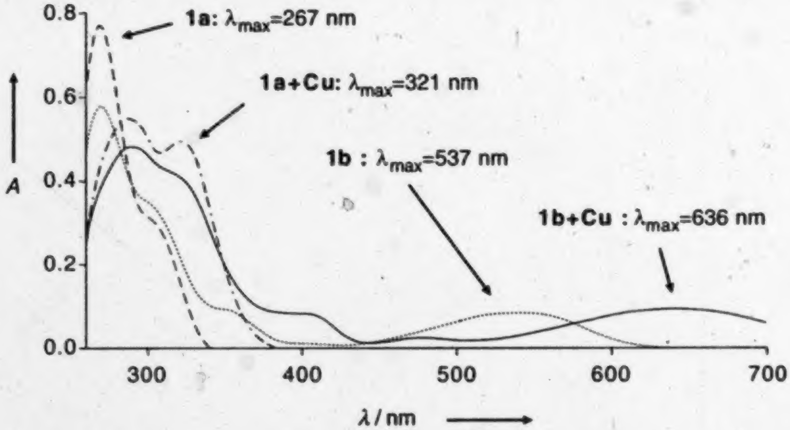

Figure 2. UV-VIS absorption spectra of photochrome **1a** and **1b** with and without CuOTF•0.5C_6H_6 (1 equiv). All spectra were run in dry degassed dichloroethane at 3.5 x 10^{-5} M.

The UV-Vis spectra of the open (**1a**) and closed (**1b**) isomers of the benzyl-substituted photochrome, and the corresponding in situ generated copper(I) complexes are shown in Figure 2, with the wavelengths of maximum absorption (λ_{max}) labeled for comparison. The ring-closed isomers were produced by irradiating dichloroethane solutions of an equimolar mixture of **1a** and CuOTf•0.5C_6H_6 with a hand-held (313 nm)[16] lamp. After irradiating for two minutes, the photostationary states were formed, which showed 90% conversion to the closed isomer by ^{1}H NMR spectroscopic analysis. Subsequent irradiation of the closed isomer at wavelengths greater than 458 nm[16] restored the spectrum to its original trace by regenerating the open isomer quantitatively. As expected, the spectral characteristics of both (*R,R*)- and (*S,S*)-enantiomers were identical.

Irradiation of the open isomer (*S,S*)-**1a** at 313 nm also produces characteristic shifts of the signals in the ^{1}H NMR spectrum. Of particular importance is the resonance assigned to the C–H protons on the thiophene rings which appears as a singlet at $\delta = 7.65$ ppm in **1a** and as two singlets of nearly equal intensity at $\delta = 6.47$ and 6.48 ppm for the

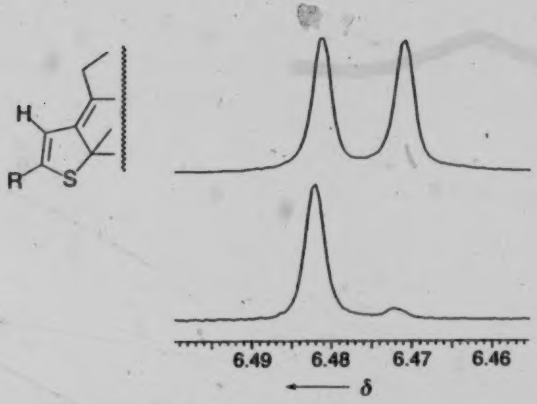

Figure 3. ^{1}H NMR (500 MHz, CD_2Cl_2) spectra of the C–H protons in **1b** generated from **1a** without $CuOTf{\bullet}0.5C_6H_6$ (top trace) and **1b** generated from **1a** with $CuOTf{\bullet}0.5C_6H_6$ after washing with NH_4OH to remove the metal (bottom trace).

corresponding ring-closed product **1b**. These two singlets (Figure 3) are clearly a result of the production of the two diastereomers in the conrotatory ring closing reaction of the 1,2-diarylethene photochrome (i.e.(*S*,*S*)-(*R*,*R*) and (*S*,*S*)-(*S*,*S*)). The relative integrations of the two singlets indicate that both diastereomeric products are being formed to nearly the same extent in the photocyclization reaction. When the photocyclization reaction of **1a** is repeated in the presence of copper(I) a major stereoisomeric product forms with a diastereoselectivity of 86% as shown by the non-equivalency of the signals in the ^{1}H NMR spectrum (Figure 3). This stereoselectivity can be best justified by invoking the existence of the helical binuclear complex **$Cu_2(1a)_2$** in solution.

Table 1. Conversions and diastereoselectivities in the photochromic processes.[a]

Entry	Photochrome	Concentration [M]	% Conversion[b]	% de
1	(*S*,*S*)-**1a** + Cu(I)	0.001	95	98
2		0.0001	94	86
3		0.00001	85	14
4	(*R*,*R*)-**1a** + Cu(I)	0.0001	92	89
5	(*S*,*S*)-**2a** + Cu(I)	0.0001	70	55
6	(*R*,*R*)-**2a** + Cu(I)	0.0001	79	49

[a] In a typical reaction, the ligand and $CuOTf{\bullet}0.5C_6H_6$ were mixed in deoxygenated dichloroethane and exposed to 313 nm light for 20 minutes. After washing with excess NH_4OH to remove the metal, the % conversions and % de's of the products were measured by ^{1}H NMR spectroscopy in CD_2Cl_2. [b] Based on the disappearance of the *open* isomers.

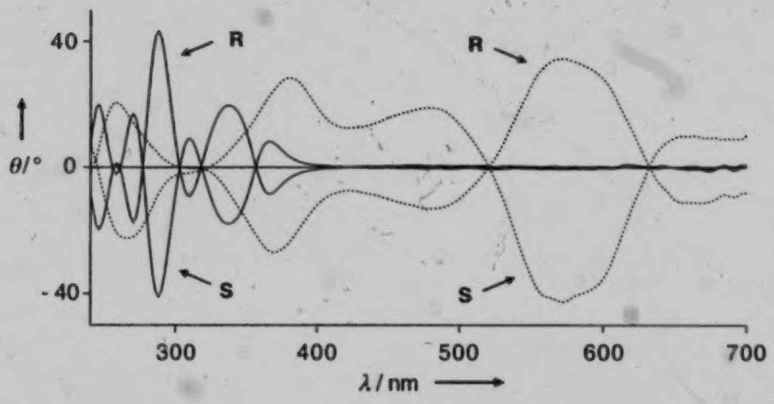

Figure 4. ORD spectra of **1a** with CuOTF•0.5C_6H_6 (—) and **1b** with CuOTf•0.5C_6H_6 (•••). All spectra were run in dry degassed dichloroethane at 2.8 x 10^{-4} M.

The results of the stereoselective ring-closing reactions are shown in Table 1. We attribute the increase in diastereoselectivity as the concentration was increased (entries 1-3) to the predominance of the binuclear complex **$Cu_2(1a)_2$** at higher concentrations.[17] The high degree of diastereoselectivity at 10^{-3} M is accompanied, however, by a coinciding increase in the amount of photochemical degradation. The diastereoselectivities were also lower when the photocyclization reactions were repeated with the isopropyl ligand **2a** (entries 5 and 6). We attribute this to the formation of a less robust coordination compound. Whether this difference in stability is due to steric and/or electronic factors is currently under investigation.

The optical rotary dispersion (ORD) spectra of the photochromic reactions are shown in Figure 4. In the presence of copper(I), both the open and closed isomers **1a** and **1b** strongly rotate light throughout the UV-Vis spectrum. There are several spectral regions where the differences in rotation between copper (I) complexes of **1a** and **1b** are dramatic and provide potential nondestructive regions for read-out. For example, the angles of optical rotation at 450 nm and 475 nm can be regulated by toggling between the copper (I) complex of **1a** and the corresponding complex of **1b** by alternate irradiation at 313 nm and at wavelengths greater than 458 nm (Figure 5), which demonstrates the utility of this system for reversible data processing. This detection method is non-invasive as illustrated by the lack of variation in the UV-Vis spectrum upon extended irradiation at 475 nm.[18]

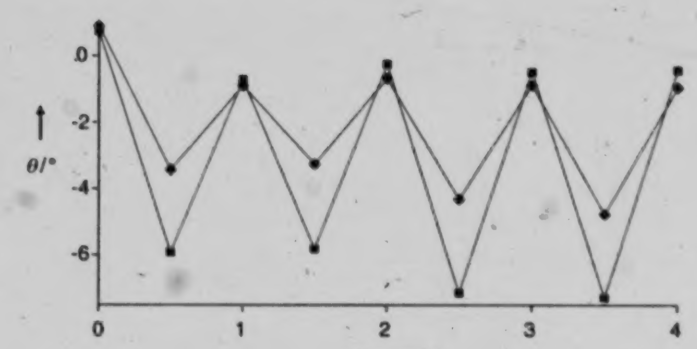

Figure 5. Modulated optical rotation at 450 nm (◆) and 475 nm (■) of a dichloroethane solution of **1a** with CuOTF•0.5C$_6$H$_6$ (2.8 x 10^{-4} M) during alternating irradiation at 313 nm and greater than 458 nm (n = number of cycles).

3.5.5 Results and Discussion

3.5.5.1. Synthesis of Chiral Photochromes

The (*R,R*) and (*S,S*) enantiomers of photochromic bis(oxazolines) **1a** and **2a** were prepared in a similar fashion from the known 1,2-bis-(5-carbonyl chloride-2-methyl-3-thienyl)cyclopentene **3**[19] as outlined in Scheme 5.1. Treatment of **3** with (*R*)- or (*S*)- 2-amino-3-phenyl-1-propanol or 2-amino-3-methyl-1-butanol under basic conditions afforded the corresponding amide alcohols **4** and **5** respectively. Conversion of **5** to the chiral oxazoline **2a** occurred in one step by treatment with thionyl chloride. A similar procedure was followed in the transformation of amide alcohol **4** to oxazoline **1**. However in this case the corresponding ring closing reaction to form the oxazoline was notably slower even at elevated temperatures. To circumvent the lengthy reaction time, the reaction was scrupulously monitored for the formation of the diamidedichloride **6**, which was typically fully formed after 90 minutes. It was possible to isolate **6** but typically it was carried on without isolation to oxazoline **1** under basic conditions.

3.5.5.2 X-ray Crystallographic Analysis of the Enantiomeric Helicates

Figure 5.3 shows a side by side comparison of the *M* and *P* double stranded photochromic helicates. The addition of **1a**-(*S,S*) and CuOTf generates exclusively the *M* helicate with a clockwise screw axis. The *P* helicate forms a counter clockwise screw axis and is generated soley from **1a**-(*R,R*) and CuOTf. The crystal structures show how the benzyl groups on opposing strands of the helicates "interact" with one another and subsequently promote the formation of stereochemically pure helicates.

Scheme 5.1

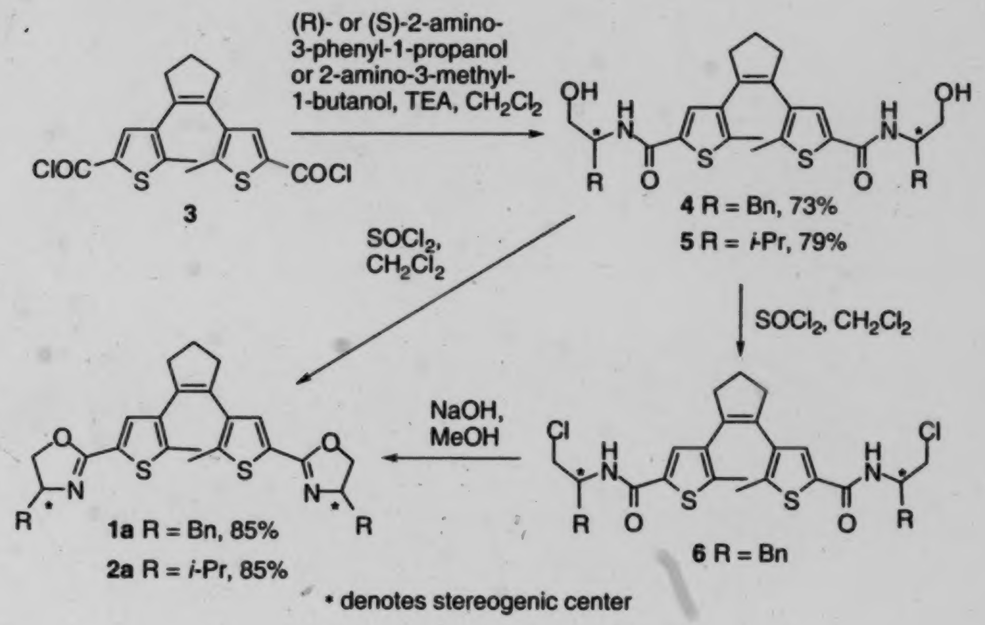
(R)- or (S)-2-amino-3-phenyl-1-propanol or 2-amino-3-methyl-1-butanol, TEA, CH_2Cl_2
ClOC
COCl
S
3
OH
H N
R
O
4 R = Bn, 73%
5 R = *i*-Pr, 79%
$SOCl_2$, CH_2Cl_2
$SOCl_2$, CH_2Cl_2
NaOH, MeOH
Cl
6 R = Bn
O
N
R
1a R = Bn, 85%
2a R = *i*-Pr, 85%

• denotes stereogenic center

3.5.5.3 Analysis of ORD and CD Spectra

The CD spectrum of the open *S*-isomer of **1a** displays a very weak positive double Cotton effect[20] while the closed form exhibits a red shifted spectrum that is of the opposite sign (Figure 5.4). As expected, the spectral characteristics of both the (*R, R*) and

(*S*, *S*) enantiomers were equal to and opposite in sign to one another. Conversely, the assembled copper helicate $\mathbf{Cu_2(1a)_2}$ in both its open and closed forms exhibits a substantial increase in both the intensity and multiplicity of the Cotton effect curves.

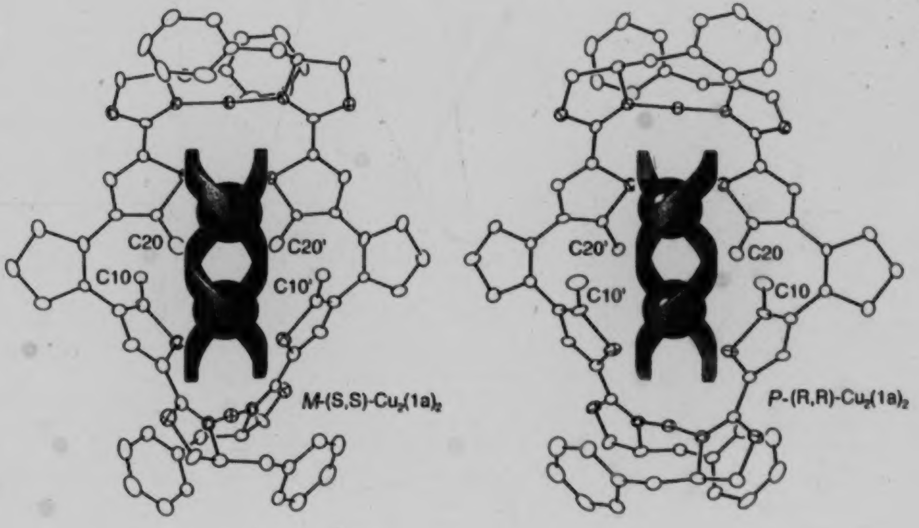

Figure 5.3. Stereochemically pure photochromic helicates in the solid state.

Figure 5.5 shows a plot of the ORD spectra of the open and closed forms of **1a** with (Figure 5.5(b)) and without (Figure 5.5(a)) copper stacked on top of the UV-Vis absorption spectra of $\mathbf{Cu_2(1a)_2}$ in both its open and closed forms (Figure 5.5(c)). Both the *open* and *closed* form of **1** without copper display relatively small optical rotatory powers, while $\mathbf{Cu_2(1a)_2}$ displays quite strong optical rotatory powers in the region spanning 230 to 360 nm. The ORD spectrum of the closed form of this complex is even more dramatic and traces out an optical rotation that spans the entire UV-Vis spectrum from 240 to 700 nm. It is, however, the region that lies between about 450 and 475 nm that is useful for non-destructive readout using ORD as the detection method. This region is the only area spanning the entire spectrum that both the open and closed forms of **$Cu_2(1a)_2$** are transparent and where large differences in rotatory power are displayed.

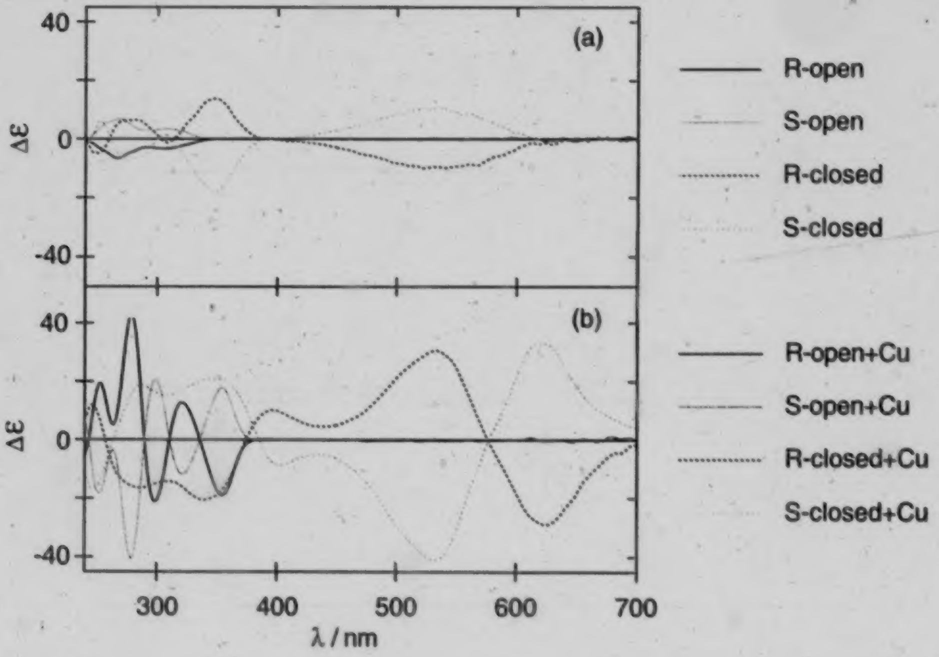

Figure 5.4. (a) CD spectra of **1a** and **1b** without $CuOTf\bullet 0.5C_6H_6$ and (b) CD spectra of **1a** and **1b** with $CuOTf\bullet 0.5C_6H_6$. All spectra were run in dry degassed dichloroethane at 2.8 x 10^{-4} M.

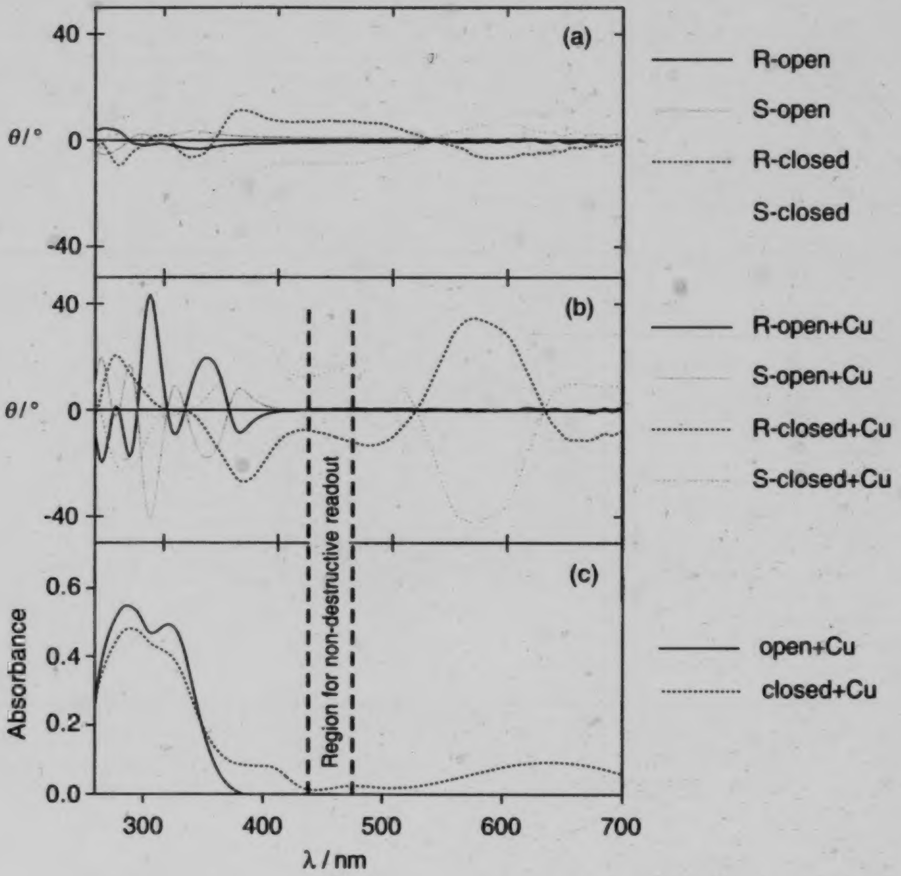

Figure 5.5. (a) ORD spectra of **1a** and **1b** without CuOTf•0.5C_6H_6, (b) ORD spectra of **1a** and **1b** with CuOTf•0.5C_6H_6 and (c) UV/Vis absorption spectra of 1a and 1b with CuOTf•0.5C_6H_6. All spectra were run in dry degassed dichloroethane at 2.8 x 10^{-4} M.

3.5.6 Conclusion

The concept of employing supramolecular chemistry to self-assemble chiroptical dithienylethenes into stereochemically pure helicates provides a useful mechanism to bias the photo-induced ring-closing reaction. Under ideal conditions, our system can afford de values as high 98%, which are the highest values ever reported for the ring-closing process of a dithienylethene photochrome. The resulting helical architecture provides large optical rotatory responses in non-photoactive regions. This response can be conveniently modulated by the fatigue resistant dithienylethene photochrome over numerous photochemical cycles while being read in a non-destructive manner.

3.5.7 Future Outlook: A Spontaneously Resolved Photochromic Helicate

> *Chirality begets chirality.*
>
> Philip Ball

The existence of enantioselectivity predisposes the existence of a chiral environment from which it was formed. Modern day chemistry attests to this as chiral catalysts are routinely used to introduce chirality into achiral systems. However one may ask, under what circumstances was the original asymmetric environment created? The origins of homochirality have yet to be strictly proven, but not for a lack of effort as there exists much literature on the topic.[21] However, certain chemical systems are challenging the notion that homochirality is necessary for the creation of chirality. One such system previously reported by us describes how the achiral dipyrrole ketone building block **9** self-assembles into a helical chiral crystalline superstructure (Figure 5.6).[22] A similar example is shown below. This work is an uncompleted extension of my studies on chiral photochromic helicates and its successful completion may shed some insight onto this rather hazy subject.

The photochromic bis(imine) **10** was synthesized by condensation of the known 1,2-Bis-(5-formyl-2-methyl-3-thienyl)cyclopentene[8] with 3,5-di-*tert*-butylaniline. By Combining **10** with an equivalent of $CuPF_6$ the doubly stranded helicate **$Cu_2(10)_2$** was formed (Scheme 5.2). This was not unexpected as the location of the coordinating nitrogen atoms in both imine ligand **10** and the oxazoline **1a** are virtually identical.

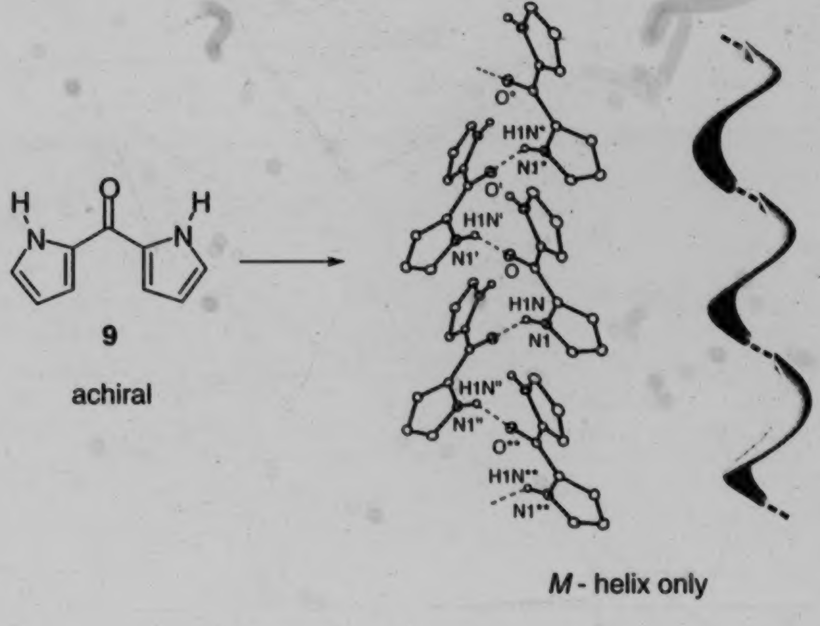

Figure 5.6. Self-assembly of homochiral supramolecular helix from an achiral building block

The existence of a helical structure was confirmed by X-ray crystallographic analysis of the assembled copper complex (Figure 5.7). The helical nature arises from the steric interactions between the *tert*-butyl groups on opposing strands of the helix. Upon closer inspection it was realized that all of the helicates within the crystal lattice were of the same handedness yielding the chiral space group *I*222. Similar to the chiral oxazoline-containing helicate the methyl groups on the thiophene heterocycles are biased in an orientation so that photo-induced ring closure would ultimately yield a single enantiomer.

Scheme 5.2.

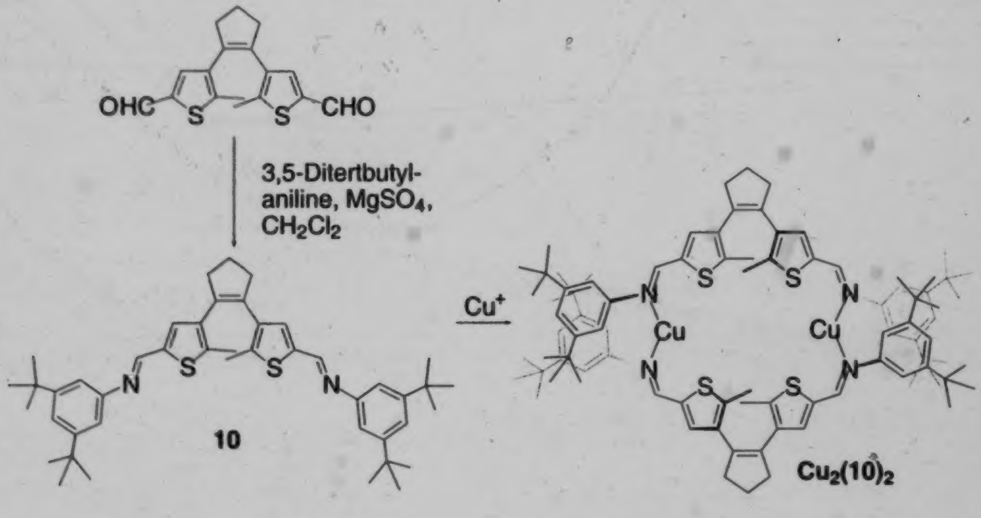

The future of this project lies in the growth, irradiation of and subsequent analysis of suitable enantiomerically pure single crystals. The prospects are exciting as the result would be the photogeneration of a stable chiral structure from purely achiral building blocks.

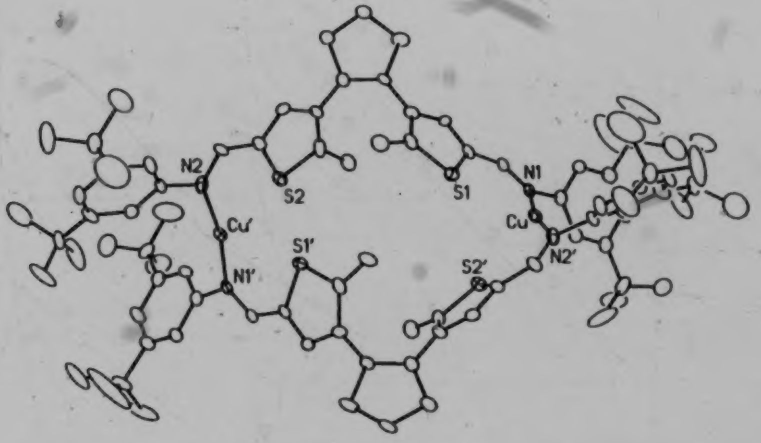

Figure 5.7. The structure of **Cu$_2$(10)$_2$** in the crystal. Carbon bound hydrogens and counterions have been omitted for clarity

3.5.8 Experimental

General: All solvents (Caledon) were distilled prior to use. Dichloroethane used for UV-Vis spectroscopy and photoisomerization reactions was deoxygenated by bubbling argon through the solvent. All other solvents were used as received. Trifluoromethanesulfonic acid copper (I) salt benzene complex was purchased from TCI America. All of the photochromic transformations were carried out under a dry argon atmosphere. CD spectra were recorded on a JASCO 7500 CD/ORD spectrophotometer. ORD spectra were obtained by utilizing the data processing unit for CD measurements.

Synthesis of 5-methyl-(4[2-{2-methyl-5-thiophene-carboxylic acid-(1-benzyl-2(*S*)-hydroxy-ethyl)-amide}-thiophen-3-yl]-cyclopent-1-enyl)-thiophen-2-carboxylic acid (1-benzyl-2(*S*)-hydroxy-ethyl)-amide (4). (S)-2-Amino-3-phenyl-1-propanol (105 mg, 0.70 mmol) and triethylamine (200 mg, 2.0 mmol) were dissolved in freshly distilled CH_2Cl_2 (25 mL) and the solution cooled to 0°C. *Bis*-carbonyl chloride (3) (127 mg, 0.33 mmol) dissolved in CH_2Cl_2 (15 mL) was added dropwise over 30 minutes. The solution was warmed to room temperature and stirred for a further 10 hours. The reaction mixture was washed with H_2O (50 mL) and the aqueous phase was extracted with CH_2Cl_2 (2 x 15 mL). The combined organic phases were washed with saturated aqueous NaCl and dried with anhydrous Na_2SO_4 and the resulting solution filtered. The solvent was removed under reduced pressure and the crude product was chromatographed through silica (1:1 EtOAc/hexane) yielding 150 mg of the product as a white solid. Yield 73%; mp 108.5-109.5°C; $[\alpha]_D^{20} = -90.0$ ($c = 0.32$ in CH_2Cl_2); a sample of the product derived from (R)-2-amino-3-phenyl-1-propanol was spectroscopically identical and possessed an optical rotation of $[\alpha]_D^{20} = +92.0$ ($c=0.24$ in CH_2Cl_2); ^1H NMR (300 MHz, CD_2Cl_2) δ 7.27 (m, 10H), 6.98 (s, 2H), 6.06 (d, *J* =8 Hz, 2H), 4.21 (m, 2H), 3.64 (m, 4H), 2.90 (d, *J* =8 Hz, 4H), 2.76 (t, *J*=8 Hz, 4H), 2.06 (q, *J*=8 Hz, 2H), 2.00 (s, 6 H); ^{13}C NMR (75 MHz, $CDCl_3$): δ 162.4, 140.6, 137.6, 136.3, 135.2, 134.0, 129.8, 129.3, 128.7, 126.8, 63.7, 53.1, 37.9, 37.2, 23.1, 14.8; IR ($CHCl_3$ cast) υ 3316, 3061, 3026, 3923, 1620, 1556, 1529, 1496, 1454, 1293,1038 cm^{-1}; HRMS (ES) for $[M+Na]^+$ ($C_{35}H_{38}N_2O_4S_2Na$) 637.2179.

Synthesis of 5-methyl-(4[2-{2-methyl-5-thiophene-carboxylic acid-(1-benzyl-2(*S*)-chloro-ethyl)-amide}-thiophen-3-yl]-cyclopent-1-enyl)-thiophen-2-carboxylic acid (1-benzyl-2(*S*)-hydroxy-ethyl)-amide (6). To a rapidly stirring solution of 1,2-bis-(5-*N*-[(2S)-(3-phenyl-1-hydroxypropyl)]amide-2-methylthien-3-yl)cyclopentene **4** (120 mg, 0.20 mmol) in CH_2Cl_2 (15 mL) cooled to 0°C was added $SOCl_2$ (100 mg, 0.85 mmol) dropwise. The solution was stirred at 0°C for 10 minutes and then allowed to warm to room temperature. After 90 minutes of stirring, the diamidodiol (R_f=0.4, SiO_2,1:4 EtOAc/hexane) was completely converted to the diamidodichloride (R_f=0.9) at which point the solvent was removed by evaporation and the pink solid residue placed under high vacuum for 3 hours. The crude product was used in the next step without further purification, mp 138.5-140.5°C; ^{1}H NMR (300 MHz, $CDCl_3$) δ 7.26 (m, 10H), 7.16 (s, 2H), 5.96 (d, *J*=8 Hz, 2H), 4.57 (m, 2H), 3.67 (dd, *J*=11 Hz , 3 Hz, 2H), 3.54 (dd, *J*=11, 3

Hz, 2H), 3.02 (dd, *J*=14, 3 Hz, 2 H), 2.93 (dd, *J*=14, 9 Hz, 2H), 2.78 (t, *J*=8 Hz, 4H), 2.06 (q, *J*=8 Hz, 2H), 1.95 (s, 6H); HRMS (ES) for $[M+Na]^+$ ($C_{35}H_{36}N_2O_2S_2Cl_2Na$) 673.1504.

Synthesis of 5-methyl-(4[2-{2-methyl-5-(4(*S*)-benzyl-4,5-dihydro-oxazole)-thiophen-3-yl}] cyclopent-1-enyl)-thiophen-2-(4(*S*)-benzyl-4,5-dihydro-oxazole) (1a). Compound **6** was taken up in MeOH (20 mL). To this was added 2 mL of an aqueous 1.3 M NaOH solution and the reaction was heated at reflux for 2.5 hours. The MeOH was removed under reduced pressure and the residue taken up in CH_2Cl_2 (15 mL). The solution was washed twice with H_2O (2 x 10 mL) and the organic layer dried with anhydrous Na_2SO_4 and the resulting solution filtered. Purification by column chromatography through silica (1:3 EtOAc/hexane) afforded 96 mg of the product as a white solid. Yield 85% from **5**; mp 92.5-94°C; $[\alpha]_D^{20} = +15.1$ ($c = 0.41$ in CH_2Cl_2); a sample of the product derived from (R)- 2-amino-3-phenyl -1-propanol was spectroscopically identical and possessed an optical rotation of $[\alpha]_D^{20} = -14.2$ ($c = 0.46$ in CH_2Cl_2); ^{1}H NMR (300 MHz, CD_2Cl_2) δ 7.27 (m, 12H), 4.50 (m, 2H), 4.32 (dd, *J*=14, 8 Hz, 2H), 4.06 (dd, *J*=14, 8 Hz, 2H), 3.08 (dd, *J*=14, 6 Hz, 2H), 2.78 (t, *J*=8 Hz, 4H), 2.75 (dd, *J*=14, 8 Hz, 2H), 2.05 (q, *J*=8 Hz, 2H), 1.94 (s, 6 H); ^{13}C NMR (75 MHz, $CDCl_3$) δ 159.5, 140.2, 138.7, 136.8, 135.1, 131.5, 129.7, 128.8, 126.7, 126.7, 72.6, 68.4, 42.0, 38.9, 23.3, 14.7; IR ($CHCl_3$ cast) υ 2918, 2843, 1644, 1494, 1477, 1453, 1439, 1354, 1019 cm^{-1}; HRMS (ES) for $[M+H]^+$ ($C_{35}H_{35}N_2O_2S_2$) 579. 2134.

Synthesis of 1(closed). Photochrome **1a** (3 mg) was dissolved in dichloroethane (6 mL) and 0.5 equivalents of CuOTf was added. The solution was irradiated for 20 minutes at 313 nm at which point 2 drops of NH_4OH were added to the solution and the solution stirred for a further 10 minutes. The solvent was washed with water and the organic layer was dried with anhydrous Na_2SO_4 and decanted and the solvent removed under vacuum. No attempt was made to isolate **1(closed)**. ^{1}H NMR (300 MHz, CD_2Cl_2) δ 7.30 (m, 6 H), 7.23 (m, 4H), 6.48 (s, 2H), 4.52 (m, 2H), 4.34 (dd, *J*=14, 8 Hz, 2H), 4.10 (dd, *J*=14, 8 Hz, 2H), 3.09 (dd, *J*=14, 6 Hz, 2H), 2.77 (dd, *J*=14, 8 Hz, 2H), 2.42 (t, *J*= 8 Hz, 4H), 1.83 (q, *J*=8 Hz, 2H), 1.99 (s, 6 H).

Synthesis of 5-methyl-(4[2-{2-methyl-5-thiophene-carboxylic acid-(1-hydroxymethyl-2(*S*)-methyl-propyl)-amide}-thiophen-3-yl]-cyclopent-1-enyl)-thiophen-2-carboxylic acid-(1-hydroxymethyl-2(*S*)-methyl-propyl)-amide (5). (S)-2-Amino-3-methyl-1-butanol (102 mg, 1.0 mmol) and triethylamine (680 mg, 6.7 mmol) were dissolved in freshly distilled CH_2Cl_2 (10 mL) and the solution cooled to 0°C. 1,2-

Bis(5-carbonyl chloride-2-methylthien-3-yl)cyclopentene (173 mg, 0.45 mmol) dissolved in CH_2Cl_2 (10 mL) was added dropwise over 30 minutes. The solution was warmed to room temperature and stirred for a further 12 hours. The mixture was diluted with CH_2Cl_2 (30 mL) and was washed with H_2O (50 mL). The aqueous phase was extracted with CH_2Cl_2 (2 x 15 mL). The combined organic phases were washed with saturated aqueous NaCl and dried with anhydrous Na_2SO_4 and the resulting solution filtered. The solvent was removed under reduced pressure and the residue was purified by column chromatography through silica (1% MeOH/$CHCl_3$ →5% MeOH/$CHCl_3$) yielding 183 mg of the product as a slightly pink solid. Yield 79% from **3**; mp 110-114°C; $[\alpha]_D^{20} = -66.6$ ($c = 0.68$ in CH_2Cl_2); a sample of the product derived from (R)-2-amino-3-methyl-1-butanol was spectroscopically identical and possessed an optical rotation of $[\alpha]_D^{20} = +62.6$ ($c = 0.71$ in CH_2Cl_2); ^{1}H NMR (300 MHz, $CDCl_3$) δ 7.06 (s, 2H), 6.23 (d, *J*=9 Hz, 2H), 3.79 (m, 2H), 3.72 (d, *J*=4 Hz, 4H), 2.95 (bs, 2H), 2.74 (t, *J*=8 Hz, 4H), 2.00 (s, 6H), 1.88 (q, *J*=8 Hz, 2H), 0.93 (t, 12H); ^{13}C NMR (75 MHz, $CDCl_3$) δ 162.6, 140.4, 136.3, 135.2, 134.2, 129.7, 63.4, 57.3, 37.8, 29.3, 23.1, 19.6, 19.2, 14.7; IR ($CHCl_3$ cast) υ 3319, 3059, 2958, 2925, 2871, 1741, 1621, 1557, 1531, 1463 cm^{-1}; HRMS (ES) for $[M+Na]^+$ ($C_{27}H_{38}O_4N_2S_2Na$) 541.2169.

5-methyl-(4[2-{2-methyl-5-(4(*S*)-isopropyl-4,5-dihydro-oxazole)-thiophen-3-yl}] cyclopent-1-enyl)-thiophen-2-(4(*S*)-isopropyl-4,5-dihydro-oxazole) (2a). To a rapidly stirring CH_2Cl_2 (10 mL) solution of **5** (177 mg, 0.35 mmol) cooled to 0° was added $SOCl_2$ (220 mg, 1.8 mmol) dropwise. The reaction was allowed to warm to room temperature and, after 45 minutes, diamidodiol **5** (R_f =0.4 amide-alcohol, silica, 1:4 EtOAc/hexane) was completely converted to the oxazoline (R_f =0.7). Cold saturated $NaHCO_3$ (5 mL) was added to the flask and the solution rapidly stirred for a further 45 minutes. The two layers were separated and the organic layer washed with saturated aqueous NaCl solution and dried with anhydrous Na_2SO_4 and the resulting solution filtered. The residual solvent was then removed under reduced pressure. The crude product was purified by column chromatography through silica (1:4 EtOAc/hexane) yielding 140 mg of the product as a white solid. Yield 85%; mp 59-62°C; $[\alpha]_D^{20} = -50.8°$ ($c = 0.26$ in CH_2Cl_2); a sample of the product derived from (R)-2-amino-3-methyl-1-butanol was spectroscopically identical and possessed an optical rotation of $[\alpha]_D^{20} = +50.6$ (c=0.65 in CH_2Cl_2); ^{1}H NMR (300 MHz, CD_2Cl_2) δ 7.24 (s, 2H), 4.35 (m, 2H), 4.01 (m, 4H), 2.77 (t, *J*=8 Hz, 4H), 2.04 (m, 2H), 1.92 (s, 6H), 1.75 (q, *J*=8 Hz, 2H), 0.98 (d, *J*=7 Hz, 6H), 0.88 (d, *J*=7 Hz, 6 H); ^{13}C NMR (75 MHz, $CDCl_3$) δ 159.0, 139.8, 136.4, 134.6, 131.1, 126.2, 72.7, 70.4, 38.7, 32.8, 22.9, 19.1, 18.1, 14.6; IR (CH_2Cl_2 cast) υ 2956, 2924, 2871, 1648, 1547, 1467, 1384, 1351 cm^{-1}; HRMS (ES) for $[M+Na]^+$ ($C_{27}H_{35}O_2N_2S_2Na$) 483.2147.

Synthesis of 2(closed). Photochrome **2a** (3 mg) was dissolved in dichloroethane (6 mL) and 0.5 equivalents of CuOTf was added. The solution was irradiated for 20 minutes at 313 nm at which point 2 drops of NH_4OH were added to the solution and the solution stirred for a further 10 minutes. The solvent was washed with water and the organic layer was dried with anhydrous Na_2SO_4 and decanted and the solvent removed under vacuum. No attempt was made to isolate **2(closed)**. ^1H NMR (300 MHz, CD_3CN) δ 6.49 (s, 2H), 4.36 (m, 2H), 4.02 (m, 4H), 2.43 (t, *J*=8 Hz, 4H), 1.94 (s, 6H), 1.82 (q, *J*=8 Hz, 2H), 1.70 (m, 2H), 0.94 (d, *J*=7 Hz, 6H), 0.85 (d, *J*=7 Hz, 6 H).

X-ray Crystallographic Analysis

General. The programs for the Bruker P4/RA/SMART 1000 CCD diffractometer operation, data collection, data reduction and absorption correction were those supplied by Bruker. The structure solution methods were obtained by the DIRDIF-96 program system; Beurskens, P. T.; Beurskens, G.; Bosman, W. P.; de Gelder, R.; Garcia Granda, S.; Gould, R. O.; Israel, R.; Smits, J. M. M. (1996), Crystallography Laboratory, University of Nijmegen, The Netherlands or by direct methods SHELX-86; Sheldrick, G. M. *Acta Crystallogr.* **1990**, *A46*, 467. The structure refinement method was obtained *SHELXL-93* program for crystal structure determination. University of Göttingen, Germany, 1993. Refinement on F_o^2 for all reflections (all of these having $F_o^2 \geq -3\sigma(F_o^2)$). Weighted *R*-factors wR_2 and all goodnesses of fit *S* are based on F_o^2; conventional *R*-factors R_1 are based on F_o, with F_o set to zero for negative F_o^2. The observed criterion of $F_o^2 > 2\sigma(F_o^2)$ is used only for calculating R_1, and is not relevant to the choice of reflections for refinement. *R*-factors based on F_o^2 are statistically about twice as large as those based on F_o, and *R*-factors based on ALL data will be even larger. The Flack parameter will refine to a value near zero if the structure is in the correct configuration and will refine to a value near one for the inverted configuration; Flack, H. D. *Acta Crystallogr.* **1983**, *A39*, 876–881. The goodness-of-fit (*S*) was calculated by: $S = [\Sigma w(F_o^2 - F_c^2)^2/(n-p)]^{1/2}$ (n = number of data; p = number of parameters varied; $w = [\sigma^2(F_o^2) + (0.1484P)^2]^{-1}$ where $P = [\mathrm{Max}(F_o^2, 0) + 2F_c^2]/3$). The final *R* indices were calculated by applying the following equations: $R_1 = \Sigma||F_o| - |F_c||/\Sigma|F_o|$; $wR_2 = [\Sigma w(F_o^2 - F_c^2)^2/\Sigma w(F_o^4)]^{1/2}$.

Cu_2[1a(R)]$_2$. $C_{74}H_{72}Cl_4Cu_2F_6N_4O_{10}S_6$(M = 1752.60); crystal dimensions 0.22 x 0.21 x 0.16 mm, orthorhombic, space group *C*222$_1$ (No. 20) $a = 11.7914(8)$, $b = 35.831(3)$, and $c = 21.4984(16)$ Å, $V = 9083.1(11)$ Å^3, $\rho_{calc} = 1.209$ g cm^{-3}, $\mu = 0.726$ mm^{-1}, $T = -80$°C; Bruker P4/RA/SMART 1000 CCD; Mo Kα radiation ($\lambda = 0.71073$ Å), scan method ϕ and ω; 25370 data measured; 9332 independent reflections. The crystal structure was solved using direct methods (*DIRDIF-96*) and refined by full-matrix least squares on F^2 (*SHELXL-93*). Final $R_1(F) = 0.0652$ (for 6582 data with $F_0^2 \geq 2\sigma(F_o^2)$), $wR_2(F^2) = 0.1938$ (on all 9332 unique data), and $S = 1.011$ for 475 parameters varied. The largest difference peak and hole in the final difference Fourier map had intensities of 0.903 and –0.621 e Å^{-3}, respectively. Flack absolute structure parameter = 0.01(2).

Cu_2[1a(S)]$_2$. $C_{74}H_{72}Cl_4Cu_2F_6N_4O_{10}S_6$(M = 1752.60); crystal dimensions 0.19 x 0.14 x 0.10 mm, orthorhombic, space group *C*222$_1$ (No. 20) $a = 11.8482(8)$, $b = 35.888(3)$, and $c = 21.3041(13)$ Å,[12] $V = 9058.6(13)$ Å^3, $\rho_{calc} = 1.285$ g cm^{-3}, $\mu = 0.789$ mm^{-1}, $T = -80$°C; Bruker P4/RA/SMART 1000 CCD[13]; Mo Kα radiation ($\lambda = 0.71073$ Å), scan method ϕ and ω; 22839 data measured; 9299 independent reflections. The crystal structure was solved using direct methods (*DIRDIF-93*)[14] and refined by full-matrix least squares on F^2 (*SHELXL-93*)[15]. Final $R_1(F) = 0.0747$ (for 3278 data with $F_0^2 \geq 2\sigma(F_o^2)$),[16] $wR_2(F^2) =$

0.2371 (on all 9332 unique data), and $S = 0.870$ for 476 parameters varied.[17] The largest difference peak and hole in the final difference Fourier map had intensities of 0.892 and –0.456 e Å^{-3}, respectively. Flack absolute structure parameter = 0.03(3).[18]

Cu$_2$[10]$_2$. $C_{92.5}H_{121}Cl_5Cu_2F_{12}N_4P_2S_4$(M = 2111.44); crystal dimensions 0.43 x 0.12 x 0.11 mm, orthorhombic, space group *I*222 (No. 23) $a = 16.1145$ (14), $b = 21.6859$ (19), and $c = 23.3041(13)$ Å, $V = 11641.3$ (17) Å^3, $\rho_{calc} = 1.148$ g cm^{-3}, $\mu = 0.637$ mm^{-1}, T = -80°C; Bruker P4/RA/SMART 1000 CCD; Mo Kα radiation ($\lambda = 0.71073$ Å), scan method ϕ and ω; 29075 data measured; 11939 independent reflections. The crystal structure was solved using direct methods/fragment search (*DIRDIF-96*) and refined by full-matrix least squares on F^2 (*SHELXL-93*). Final $R_1(F) = 0.0982$ (for 4116 data with $F_0^2 \geq 2\sigma(F_o^2)$), $wR_2(F^2) = 0.3010$ (on all 11939 unique data), and $S = 0.914$ for 535 parameters varied. The largest difference peak and hole in the final difference Fourier map had intensities of 1.119 and –0.669 e Å^{-3}, respectively. Flack absolute structure parameter = 0.01(3).

3.5.9 Notes and references

1. (a) *Optical Rotatory Dispersion and Circular Dichroism in Organic Chemistry*, G. Snatzke, Ed.; Heyden and Son Limited, Great Britian, 1967; (b) P. Crabbé, *ORD and CD in Chemistry and Biochemistry*, Academic Press Inc., New York, 1972.
2. C. Provent, E. Rivara-Minten, S. Hewage, G. Brunner, A. F. Williams, *Chem. Eur. J.* **1999**, *5*, 3487.
3. B. L. Feringa, R. A. van Delden, N. Kourmura, E. M. Geertsema, *Chem. Rev.* **2000**, *100*, 1789 and references therein.
4. For a description of *M* and *P* nomenclature, see: E. L. Eliel, S. H. Wilen, *Stereochemistry of Organic Compounds*, Wiley, New York, 1994; Chapter 14, pp 1121.
5. T. Yamaguchi, K. Uchida, M. Irie, *J. Am. Chem. Soc.* **1997**, *119*, 6066.
6. A. Fernandez-Acebes, *Chirality* **2000**, *12*, 149.
7. C. Denekamp, B. L. Feringa, *Adv. Mater.* **1998**, *10*, 1080.
8. (a) M. Irie, *Chem. Rev.* **2000**, *100*, 1685; b) M. Irie in *Organic Photochromic and Thermochromic Compounds, Vol. 1* (eds.: J. C. Crano, R. J. Gugliemetti), Plenum Press, New York, **1999**, Chapter 5.

9. (a) Kawai, S. H.; Gilat, S. L.; Ponsinet, R.; Lehn, J.-M. *Chem. Eur. J.* **1995**, *1*, 285. (b) Irie, M.; Miyatake, O.; Uchida, K.; Eriguchi, T. *J. Am. Chem. Soc.* **1994**, *116*, 9894.

10. (a) Kim, E.; Choi, K. H.; Rhee, S. B. *Macromolecules* **1998**, *31*, 5726. (b) Kawai, T.; Koshido, T.; Yoshino, K. *Appl. Phys. Lett.* **1995**, *67*, 795. (c) Tanio, N.; Irie, M. *J. J. Appl. Phys*. **1994**, *33*, 1550.

11. (a) Norsten, T. B.; Branda, N. R. *J. Am. Chem. Soc.* **2001**, *123*, 1784. (b) Norsten, T. B.; Branda, N. R. *Adv. Mater.* **2001**, *13*, 327. (c) Gobbi, L.; Seiler, P.; Diederich, F. *Angew. Chem.* **1999**, *111*, 740; *Angew. Chem. Int. Ed.* **1999**, *38*, 674. (d) Fernandez-Acebes, A.; Lehn, J.-M. *Chem. Eur. J.* **1999**, *5*, 3285. (e) Takeshita, M.; Irie, M.; *Chem. Lett.* **1998**, 1123. (f) Yokoyama, Y.; Uchida, S.; Yokoyama, Y.; Sagisaka, T.; Uchida, Y.; Inada, T. *Enantiomer* **1998**, *3*, 123. (g) Tsivgoulis, G. M.; Lehn, J.-M. *Chem. Eur. J.* **1996**, *2*, 1399. (h) Seibold, M.; Port, H.; Wolf, H. C. *Mol. Cryst. Liq. Cryst.* **1996**, *283*, 75. (i) Huck, N. P. M.; Feringa, B. L. *J. Chem. Soc., Chem. Commun.* **1995**, 1095; (j) Saika, T.; Iyoda, T.; Honda K.; Shimidzu, T. *J. Chem. Soc. Chem., Commun.* **1992**, 591.

12. (a) Feringa, B. L.; van Delden, R. A.; Koumura, N.; Geertsema, E. M. *Chem. Rev.* **2000**, *100*, 1789. (b) Yamaguchi, T.; Inagawa, T.; Nakazumi, H.; Irie, S.; Irie, M.

Chem. Mater. **2000**, *12*, 869. (c) Denekamp, C.; Feringa, B. L. *Adv. Mater.* **1998**, *10*, 1080. (d) Yamaguchi, T.; Uchida, K.; Irie, M. *J. Am. Chem. Soc.* **1997**, *119*, 6066. (e) Eggers, L.; Buss, V. *Angew. Chem.* **1997**, *109*, 885; *Angew. Chem. Int. Ed. Engl.* **1997**, *36*, 881. (f) Huck, N. P. M.; Wolter, J. F.; De Lange, G.; Feringa, B. L. *Science* **1996**, *273*, 1686. (g) Agati, G.; McDonagh, A. F. *J. Am. Chem. Soc.* **1995**, *117*, 4425.

13. (a) Fernandez-Acebes, A. *Chirality* **2000**, *12*, 149. For examples of diastereoselectivity in the crystaline state, see: (b) Kodani, T.; Matsuda, K.; Yamada, T.; Kobatake, S.; Irie, M. *J. Am. Chem. Soc.* **2000**, *122*, 9631. (c) Kodani, T.; Matsuda, K.; Yamada, T.; Irie, M. *Chem. Lett.* **1999**, 1003.
14. For recent reviews on helicates, see: (a) von Zelewsky, A.; Mamula, O.; *J. Chem. Soc. Dalton Trans.* **2000**, *3*, 219. (b) Piguet, C.; Bernardinelli, G.; Hopfgartner, G.; *Chem. Rev.* **1997**, *97*, 2005. For selected examples, see: (c) Provent, C.; Rivara-Minten, E.; Hewage, S.; Brunner, G.; Williams, A. F. *Chem. Eur. J.* **1999**, *5*, 3487. (d) Evans, D. A.; Woerpel, K. A.; Scott, M. J. *Angew. Chem.* **1992**, 104, 439; Angew. *Chem. Int. Ed. Engl.* **1993**, *31*, 430.
15. The photochromic bis-oxazolines **1** and **2** were synthesized from the known 1,2-*bis*-(5-chloro-2-methyl-3-thienyl)cyclopentene, see: Lucus, L. N.; van Esch, J.; Kellogg,

R. M.; Feringa, B. L. *Chem. Commun.* **1998**, 2313. See Supporting Information for details.

16. Standard lamps used for visualizing TLC plates (Spectroline E-series, 470 $\mu W/cm^2$) were used to carry out the ring-closing reaction of **1a** to **1b** and **2a** to **2b** with and without copper(I). The ring-opening reactions were carried out using the light of a 150-W tungsten source that was passed through a 458 nm cutoff filter to eliminate higher energy light.
17. This was already suggested by the results of the ESMS studies.
18. The monochromator of the fluorescence spectrophotometer (1 mm slit) was employed (65 W Xenon lamp).
19. L. N. Lucus, J. van Esch, R. M. Kellogg, B. L. Feringa, *Chem. Commun.* **1998**, 2313.
20. If a compound presents one or several optically active absorption bands, its ORD and CD curves will show peaks or toughs in the spectral region in which the chromophore absorbs. These curves are anomalous and called Cotton effect curves. The sign of the Cotton effect (positive or negative) is determined by whether a peak or trough, respectively, is met first when going from longer wavelengths to shorter wavelengths.
21. (a) Sowerby, S. J.; Holm, N. G.; Petersen, G. B. *Biosystems* **2001**, *61*, 69. (b) Keszthelyi, L *Orgin Life Evol. Biosphere* **2001**, *31*, 249. (c) Buschmann, H.; Thede,

R.; Heller, D. *Angew. Chem. Int. Ed.* **2000**, *39*, 4033. (d) Bailey, J.; Chrysostomou, A.; Hough, J. H.; Gledhill, T. M.; McCall, A.; Clark, S.; Menard, F.; Tamura, M. *Science*, **1998**, *281*, 672. (e) Siegel, J. S. *Chirality* **1998**, *10*, 24.

22. Norsten, T. B.; McDonald, R.; Branda, N. R. *Chem. Commun.* **1999**, 719.

Unit 3 - Chapter 6 - Photochromic Control of Helical Topology

The previous Chapters in this thesis testify to the usefulness of dithienylethenes to as internal control mechanisms activated by an external light stimulus. The dithienylethene backbone is a particularily appealing photochrome as it can be synthetically tailored to modulate a variety of desired signals, as was the case in Chapters 3 and 4 where the state of the photochrome and its corresponding electronic properties were responsible for the modulation of light and in chapter 5 where the photochrome was designed to reversibly control both the electronics and supramolecular morphology for the modulation of optical rotatory power. The present chapter endeavors to explore the use of dithienylethenes to control molecular morphology of helicene-based systems.

3.6.1 Dithienylethenes and Helicenes

A recent example by Irie and coworkers exemplifies how obtaining control over structure at the molecular level can translate into the ability to control shape on a larger scale.[1] When irradiated with UV light the flat (100) surface of the colorless single crystal (**14a**) turns blue (Figure 6.1). The color change is a result of the formation of the ring-closed isomer (**14b**). A close inspection of the crystal surface by atomic force microscopy

(AFM) reveals that a series of steps are formed. When back irradiated with visible light the steps disappear and the crystal surface is flat once again. The step height, approximately 1 nm, corresponds to one molecular layer within the crystal lattice. Irradiation of a different crystal surface (010) with UV light forms deep valleys (10 to 50 nm) that also disappear upon irradiation with visible light (Figure 6.1 - bottom). Although there have been many reported instances of photochemical transformations in the solid state they most often damage the crystal integrity in an irreparable manner. This system has the unique ability to "mend" itself in response to light activation. The surface morphological changes can be explained by the molecular structural changes of dithienylethenes regularly packed in the single crystal. The authors report that crystals of this sort could potentially act as photodriven nanoscale actuators.

Although the helicenes have been around since the mid-1950's it is not until recently that they have been exploited for the unique properties that they possess.[2] This renewed interest in helicenes is a result of new synthetic procedures and resolution techniques contributed primarily by the group of Katz.[3] These procedures have made it possible to synthesize appreciable amounts of non-racemic functionalized helicenes.

As helicenes are inherently chiral they are necessarily noncentrosymmetric and therefore possess excellent second-order non-linear optical (NLO)[4] properties.[5] Verbiest

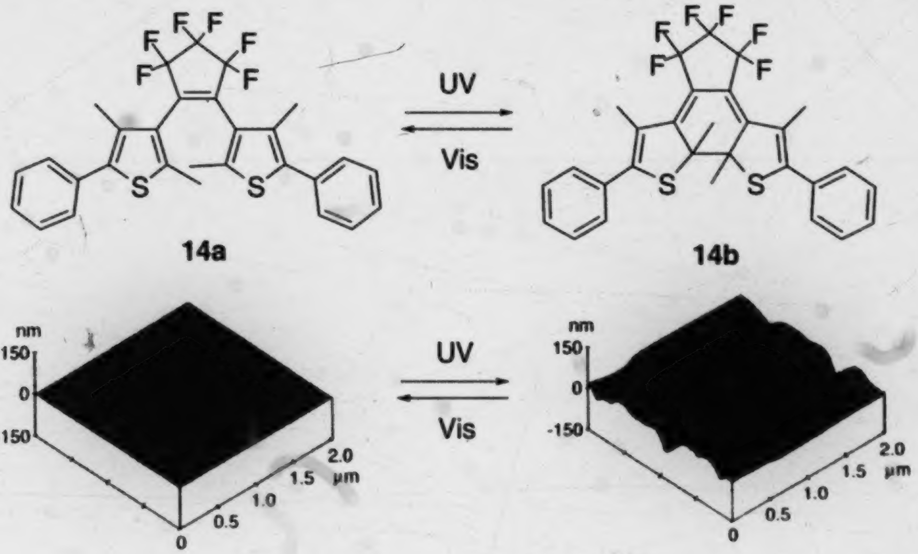

Figure 6.1. Photochromic control of dithienylethene **12** and the corresponding AFM images of the (010) crystal surface.

and Katz are currently developing several helicene containing systems as functional NLO materials.[6] For example they have shown that certain racemic and non-racemic functionalized helicene monomers are capable of self-assembling into long helical columns (Figure 6.2). The resulting NLO susceptibility of the non-racemic helical columns is about 30 times larger than that of the non-racemic material with the same chemical structure. By carefully controlling both the temperature and concentration of a related self-assembled system Katz was able to produce the first helically twisted columnar discotic liquid crystal.[7]

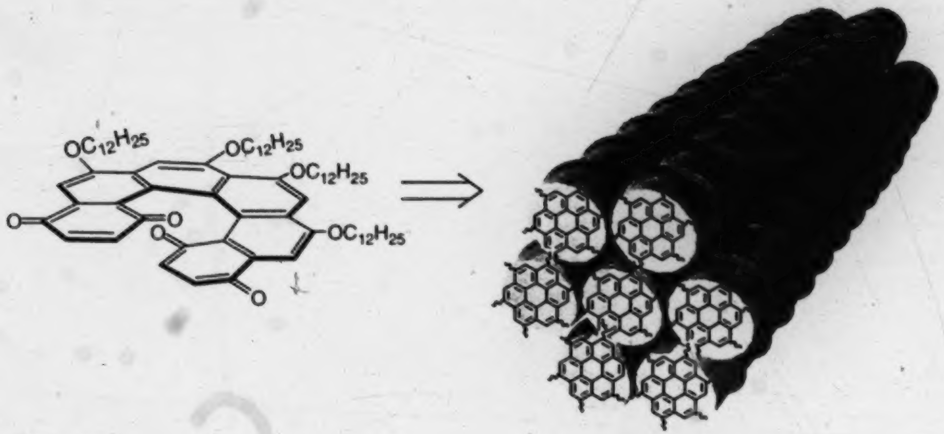

Figure 6.2. (Left) Chemical structure of the monomeric helicene and (right) schematic representation of columns of stacked helicene molecules.

As helicenes display a wide range of unique functional properties due to their twisted backbones, it would certainly be advantageous to be able to modulate the backbones in response to light activation. The following paper describes how we were able to incorporate a photo-switch directly into the helicene backbone. This was the first example of a helicene skeleton that could be turned "on" and "off" in response to an external stimulus.

3.6.2 - Reversible [7]-Thiahelicene Formation Using a 1,2-Dithienylcyclopentene Photochrome

Tyler B. Norsten, Andrea Peters, Robert McDonald, Meitian Wang, Neil R. Branda

J. Am. Chem. Soc. **2001**, *123*, 7447.

Structure is intimately related to function at the molecular level just as it is at the macroscopic level. Tailoring precise molecular architecture is, therefore, a necessity to successfully design molecules that will translate their topological properties into the nanoscale realm. Substantial ongoing research is being dedicated to the formation of molecular systems based on the helix as an architectural motif.[8] Helicenes are a specific class of helical molecules comprised of *ortho*-condensed aromatic rings that form a unique twisted non-planar π-electron system.[9] It is this inherently dissymmetric backbone that, among other features, makes helicenes structurally intriguing for application to the areas of asymmetric molecular recognition[10] and catalysis,[11] liquid crystal technology,[12] nonlinear optics[13] and as components for molecular machinery.[14]

Several groups have recently taken advantage of photochromic scaffolds to modulate helical topology,[15] most notably as potential chiroptical information storage devices.[16] However, we are unaware of any reports describing the incorporation of a photochrome directly into a helicene backbone. Here we report the first example of a [7]-thiahelicene:dithienylethene hybrid (**1**) and how the photochrome provides a convenient mechanism to modulate helical topology.

Our design involves the lesser known dithienylethene photochrome where the 3-methylthiophene heterocycles are linked to the perfluorinated cyclopentene at their 2-ring positions.[17] This particular photochrome has the structural advantage over its more commonly used 3-thienyl-linked counterpart[18] as it directs the individual naphthalene arms towards one another where photocyclization can ultimately yield a helical architecture. A rigid non-planar helical backbone is created when **1a** is converted to **1b**. The closed form represents an excellent photochromic mimic of the [7]-thiahelicene originally reported by Wynberg and coworkers.[19] Regeneration of the open form by photochemically cleaving the bridging C–C bond linking the two flanking arms of the helicene destroys the extended helicene backbone.

Scheme 1[a]

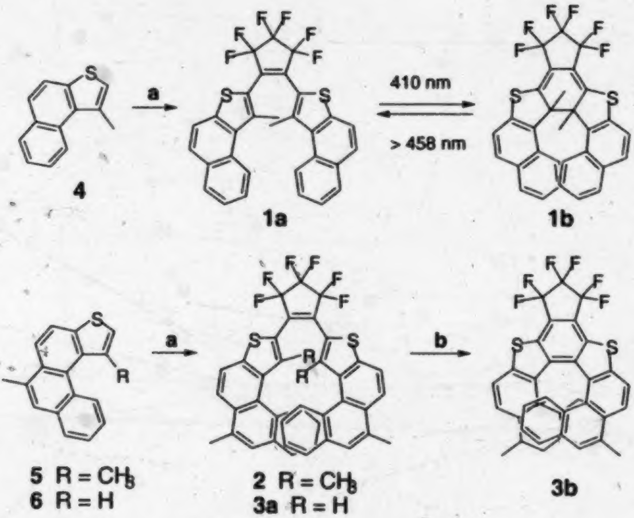

[a] Reaction conditions: (a) *tert*-BuLi, hexane (hexane/THF for 6), -78°C, then C_5F_8; (b) hυ, I_2, propylene oxide, benzene.

Photochrome **1a** was prepared by coupling the known thianapthalene **4**[20] to octafluorocyclopentene (Scheme 1). The photo-switch can be conveniently toggled between its open (**1a**) and closed (**1b**) states by alternate irradiation with appropriately tuned wavelengths of light. Irradiation of CH_2Cl_2 solutions of **1a** at 410 nm[21] resulted in an immediate increase in the absorption intensity in the visible spectral region (430-580 nm) due to the appearance of the closed isomer, **1b** (Figure 1). This photostationary state was identified by ^{1}H NMR spectroscopy as consisting of 74% of the closed isomer, **1b**. Irradiation of **1a** at wavelengths even slightly greater than or less than 410 nm resulted in a decrease in the amount of closed isomer **1b** at the photostationary state. Irradiation of **1b** at wavelengths greater than 458 nm resulted in the rapid ring-opening photoreaction and the regeneration of the original absorption spectrum corresponding to **1a**.

Single crystals of **1a** suitable for X-ray crystallographic analysis were grown by slowly cooling a hot hexane solution of the photochrome. The crystal contains the two enantiomeric forms of **1a** and consequently as a whole the crystal is racemic. When the photostationary state was treated under identical conditions, single crystals of both **1a** (yellow crystals) and **1b** (orange crystals) could be isolated. The structure of the closed isomer in the crystal (Figure 2) highlights the molecule's helical nature, which originates as a result of the steric crowding between the naphthalene arms of the helicene skeleton. The direct overlap of carbons C20 and C40 defines the 3.47 Å distance between opposing terminal benzene rings and completes one helical turn.

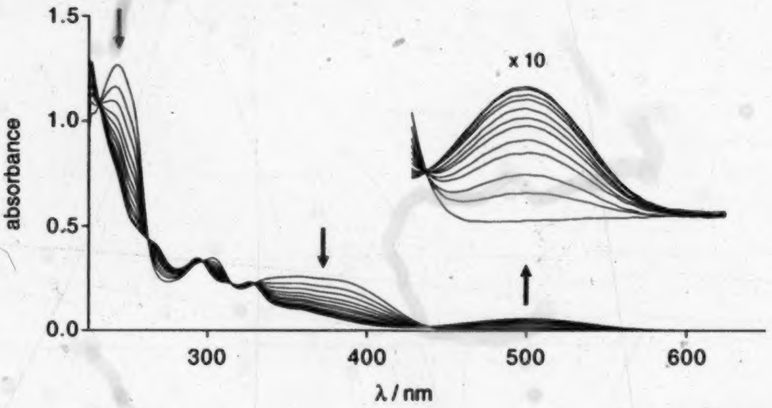

Figure 1. Changes in the UV-Vis absorption spectra of a CH_2Cl_2 solution of **1a** (2×10^{-5} M) upon irradiation with 410-nm light. Irradiation periods are 0, 5, 10, 15, 20, 25, 30, 40, 50, 60, 80 and 100 seconds.

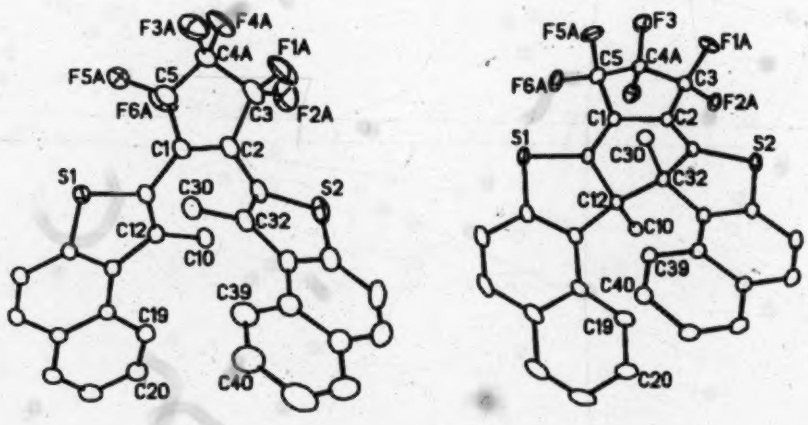
F3A
F4A
C4A
F1A
F5A
C5
F6A
C3
F2A
C1
C2
S1
C30
S2
C12
C32
C10
C39
C19
C20
C40
F5A
F3
C5
C4A
F1A
F6A
C3
F2A
C1
C2
S1
C30
S2
C32
C12
C10
C39
C40
C19
C20

Figure 2. The structures of the *open* (left) and *closed* (right) forms of photochrome **1** in the crystal. Only selected enantiomers are depicted. The thermal ellipsoids are drawn at the 20% probability level.

The conrotatory ring-closing reaction dictates that only two of the four possible stereoisomers of **1b** are produced in the photocyclization of **1a**. The four stereoisomers are a result of the creation of two stereogenic centers and a helical screw axis. This does not, however, exclude the possibility of post-cyclization epimerization of **1b** resulting in the generation of all four stereoisomers. This, however, is unlikely as previous studies on heptaheterohelicenes with similar backbones show limited racemization at ambient temperatures.[19] In the solid-state only the *P*-SS and *M*-RR stereoisomers are observed. We attribute this stereodiscrimination to be a result of the significantly enhanced stability of these two enantiomers as compared to their diastereomeric counterparts (*P*-RR and *M*-SS).[22]

The existence of only a single pair of enantiomeric products in solution was supported by the 600 MHz ^{1}H NMR spectrum of **1b** which displayed a single clean set of peaks throughout both the aromatic and aliphatic regions. All of the proton resonances in **1b** appear upfield from the corresponding signals for **1a**.

A more extended [9]-thiahelicene (**2**) was prepared by coupling [4]-thiahelicene **5** to octafluorocyclopentene as shown in Scheme 1. Photocyclization of **2** was expected to yield a [9]-thiahelicene with a substantial increase in the extent of overlap of the terminal aromatic rings. Surprisingly, no photocyclized product was detected when **2** was systematically irradiated throughout its absorbing spectral region (250–480 nm).

X-ray analysis of single crystals of **2** (Figure 3)[23] reveals that the individual [4]-thiahelicenes appended to the perfluorocyclopentene core are helical themselves due to the crowding caused by the methyl groups on the thiophene heterocycles.[24] In the event that the extended [4]-thiahelicene arms were preventing the photocyclization due to steric hindrance, **2** was irradiated in boiling decalin (b.p. = 187°C) where rapid epimerization of each arm can be expected. These experimental conditions also failed to yield any detectable photocyclized product.

When the methyl groups on the thiophene heterocycles in **2** were replaced by hydrogen atoms (**3a**), photocyclization followed by subsequent oxidative trapping afforded the non-photochromic [9]-thiahelicene **3b** in 94% yield as can be seen from the X-ray structure of the isolated product (Figure 3).[23] Compounds **2** and **3a** both absorb substantially further into the visible region (extending out to 480 nm) than the corresponding photochrome **1a**. As has previously been suggested, when the absorptions of the open and closed isomers of photochromic compounds overlap substantially and the ring-opening quantum yield is greater than the cyclization quantum yield, the presence of the closed isomer at the photostationary state will be negligible.[17a] The fact that the closed form of **3a** can be trapped in high yield as the oxidized product **3b**, strongly suggests that compound **2** suffers from the existence of a photostationary state that favors the open isomer at the expense of the closed isomer as opposed to steric inhibition of the photocylization reaction.

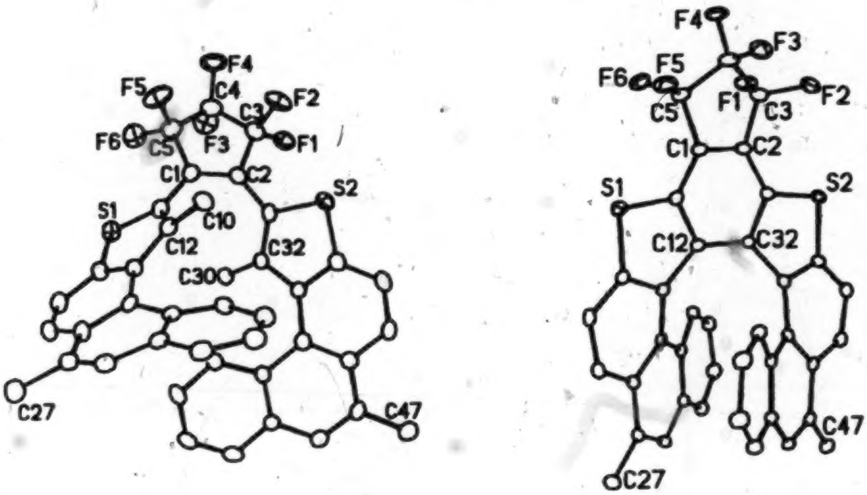
F4
F5
C4
F2
C3
F6
C5
F3
F1
C1
C2
S2
S1
C10
C12
C32
C30
C27
C47
F4
F3
F6
F5
F1
F2
C5
C3
C1
C2
S1
S2
C12
C32
C47
C27

Figure 3. The structure of the *open* form of photochrome **2** (left) and [9]-thiahelicene **3b** (right) in the crystal. The thermal ellipsoids are drawn at the 20% probability level.

The influence that remote chiral auxiliaries will have on the stereochemical ring-closing reaction of photochromic helicene precursors is currently under investigation and will be reported in due course.

3.6.3 Results and Discussion

3.6.3.1 Synthesis of Photochromes

Photochrome **1a** and parent compounds **2** and **3a** were all synthesized following the same general procedure (Scheme 6.1 and 6.2). As such only one synthesis (compound **2**) will be discussed in detail. The synthesis of **2** began with a Wittig reaction between phosphonium salt **11** and the corresponding thiophene carboxaldehyde **7** affording a mixture of the *cis*- and *trans* olefins of **12**. Irradiation of the isomeric mixture of **12** in the presence of iodine as an oxidizing agent and propylene oxide as a HI scavenger generated the desired thiaphenanthroline **5**. Addition of octafluorocyclopentene to the lithium salt of **5** resulted in the extended helicene precursor **2**.

The presence of the methyl substituent at the 3-position on the naphthalene ring of phosphonium salt **11** was designed to block photocyclization onto this position. In similar systems when this position remains unsubstituted photocyclization occurs in both directions and subsequent oxidation results in an undesirable extended aromatic sideproduct (Figure 6.3).[25]

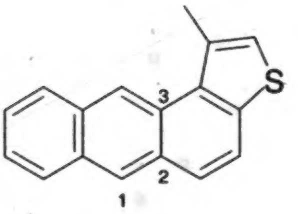

Figure 6.3.

Scheme 6.1.

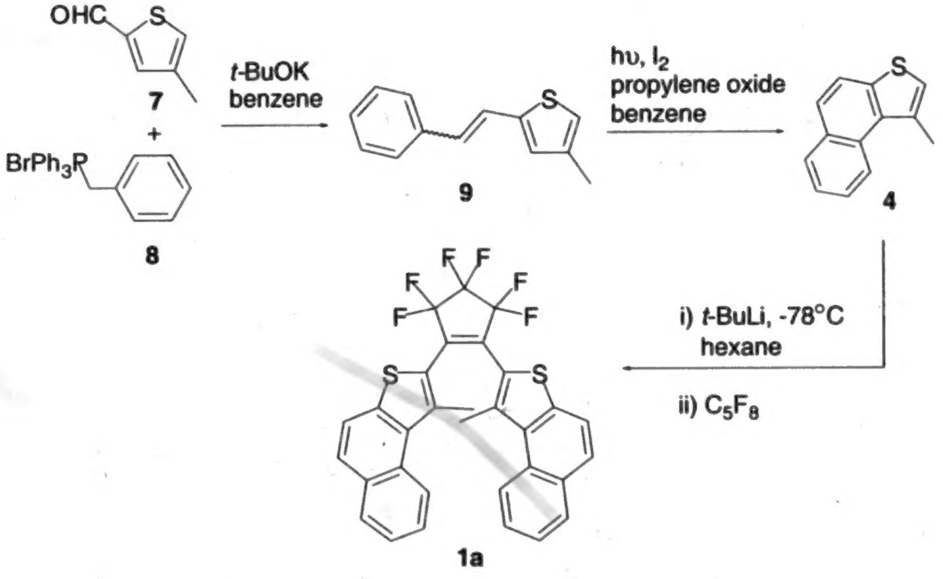
OHC
S
7
+
BrPh3P
8
t-BuOK
benzene
S
9
hυ, I2
propylene oxide
benzene
S
4
i) t-BuLi, -78°C
hexane
ii) C5F8
F F
F F
F F
S S
1a

Scheme 6.2.

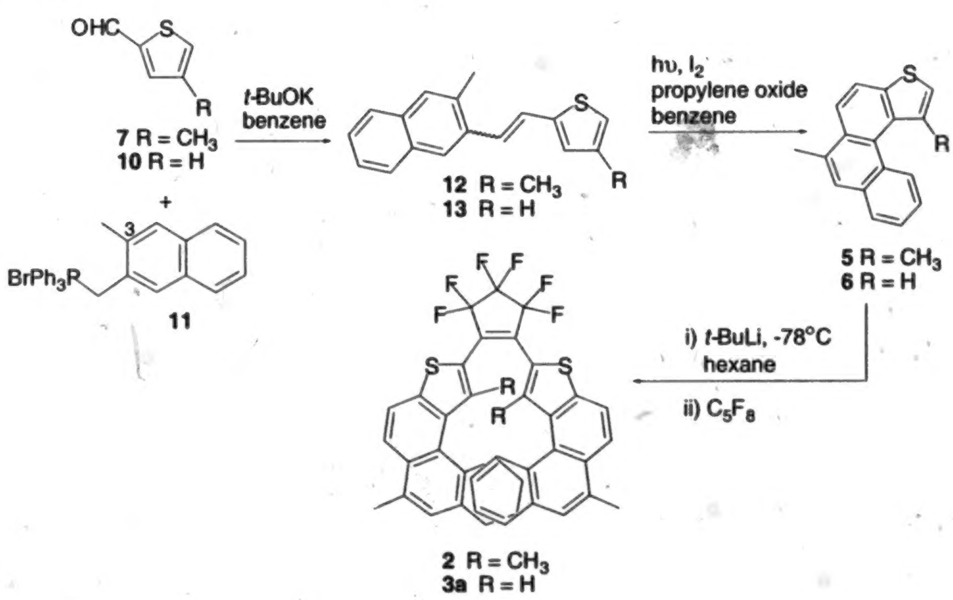
OHC
S
R
7 R = CH3
10 R = H
+
3
BrPh3P
11
t-BuOK
benzene
S
R
12 R = CH3
13 R = H
hυ, I2
propylene oxide
benzene
S
R
5 R = CH3
6 R = H
i) t-BuLi, -78°C
hexane
ii) C5F8
F F
F F
F F
S S
R
R
2 R = CH3
3a R = H

3.6.3.2 Fluorescence Analysis

In addition to the photo-modulation of helical topology, photochrome **1** was also able to modulate its emission properties. When irradiated at 375 nm the photochromic helicene precursor **1a** displayed significant fluorescence intensity at 511 nm (Figure 6.4). When the photocyclization reaction of **1a** to **1b** was carried out by irradiating **1a** at 410 nm the fluorescence intensity began to decrease. At the photostationary state the fluorescence intensity is approximately 25% of the original emission intensity which is in agreement with the photostationary state of 74% found by ^{1}H NMR studies described in the paper.

Solutions of the closed isomer **1b** are quite sensitive to stray light and if they are left unprotected from ambient lighting, the photochrome reverts back to **1a** within minutes. Attempts were made to obtain a UV-Vis and fluorescence specta of solutions prepared from the isolated crystals of **1b** but all attempts were unsuccessful as the open isomer **1a** was always observed in some capacity. The development of this system for non-destructive readout purposes was not seriously considered, as excitation experiments revealed that the absorption bands responsible for initiating fluorescence are the same bands necessary for activating the ring-closing reaction.

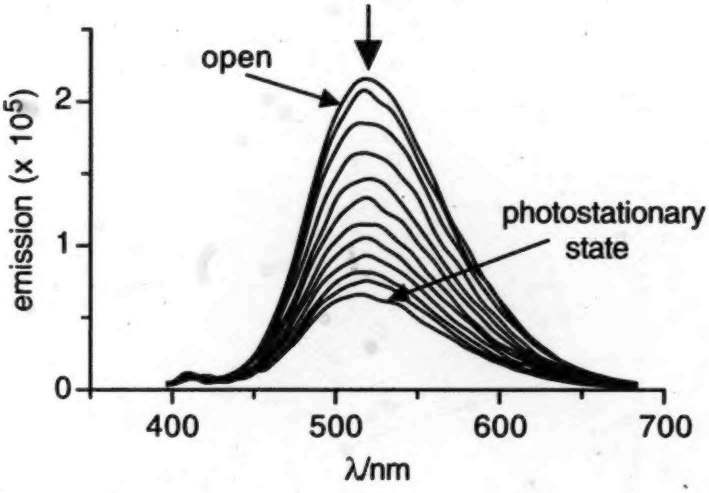

Figure 6.4. Changes in the emission spectra of a CH_2Cl_2 solution of **1a** (2×10^{-5} M) upon irradiation with 410-nm light. Irradiation periods are 0, 5, 10, 15, 20, 25, 30, 40, 50, 60, 80 and 100 seconds. $\lambda_{EX} = 375$ nm.

3.6.3.3 Helical Chirality

The presence of the ring-closed stereoisomers *P*-SS and *M*-RR of **1b** in the crystal results from the symmetry controlled conrotatory ring-closing process. The formation of their diastereomeric counterparts *M*-RR and *P*-SS are possible only under an epimerization-controlled process from the *P*-SS and *M*-RR stereoisomers where by the terminal ends of the helicene "flip" past one another (Figure 6.5). This is a common occurrence in helicene systems when there is insufficient overlap between the terminal ends of the "screw", and thermal racemization can occur quite readily under mild conditions. Although there are several factors that influence this racemizaton process, the major factor is the type and number of hetero-aromatic ring systems incorporated into the helicene backbone. Racemization is typically not seen for helicene systems with 6 or more fused rings and, therefore, is unlikely to be occurring in our system.[26] Strengthening this argument are the semiempirical AM1 calculations that estimate the observed stereoisomers to be substantially more stable than their predicted diastereomers. Hence, even if rapid epimerization was occurring the equilibrium would heavily favor the observed products.

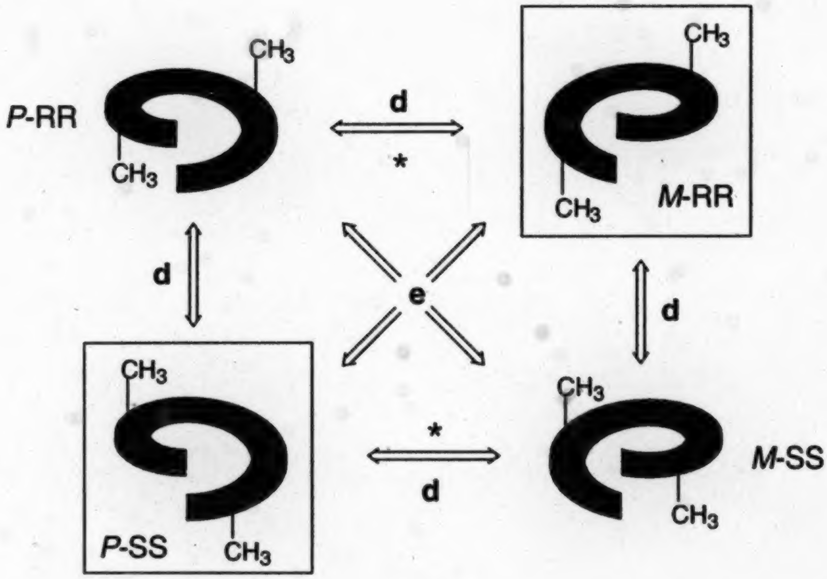

Figure 6.5. Schematic representations of all possible [7]-helicenes. The boxed structures correspondto the observed helicenes in the crystal of **1b**. Enantiomeric (e) and diastereomeric (d) relationships between helicenes are highlighted, while the (*) denotes the possible epimerization pathways.

3.6.3.4. Inhibition of Photochromism: UV-Vis Analysis

When irradiated with light in the region from 250 to 480 nm the extended helicene precursor **2** did not undergo any photochromic transformations as monitored by UV-Vis absorption spectroscopy. However, when **3a** was irradiated with UV light in the absence of an oxidizer there was some indication that the ring-closed isomer was being formed, as the absorption bands at 275 nm and 375 nm decreased (Figure 6.6), while an extremely subtle absorption appeared at longer wavelengths (475 to 500 nm). These spectroscopic changes could only be brought about by extended periods of irradiation with UV light. Back irradiation with visible light ($\lambda > 458$ nm) reversed the spectroscopic changes, but could never fully restore the spectrum to its original state. This may be due to small amounts of oxygen seeping into the system bringing about the oxidation of **3a** to **3b**. When this experiment was repeated in the presence of a strong oxidizer (I_2), **3a** was fully converted to **3b**.

3.6.4 Conclusion

Future work on this system should focus on the incorporation of chiral auxiliaries onto the termini of the helicene arms. When positioned properly, the steric interactions could influence the ring-closing reaction such that the photo-induced ring-closure would result in a single stereochemically pure helicene (Figure 6.7). Such a material would surely be useful in the areas of data storage, NLO, and liquid crystal technology.

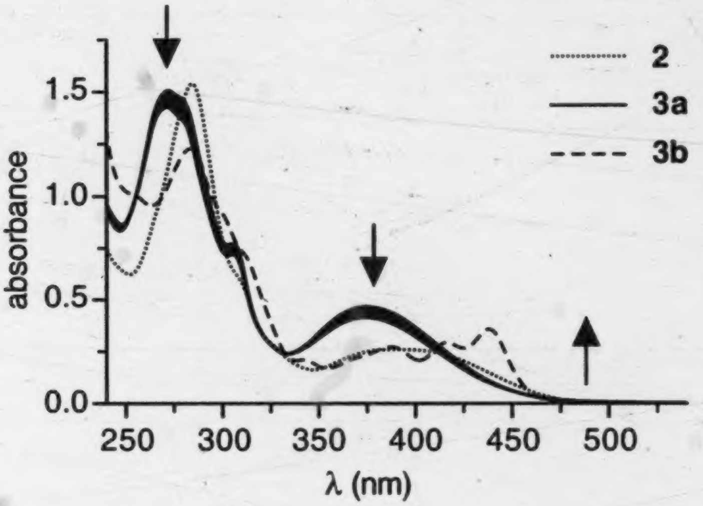

Figure 6.5. UV/Vis absorption spectra of CH_2Cl_2 solutions of **2**, **3a** and **3b** (2 x 10^{-5} M). The solution of **3a** was purged with argon and under irradiation with 410 nm light. Irradiation periods are 0, 0.5, 1, 2, 3, 5, 7, 9 and 11 min.

Figure 6.6.

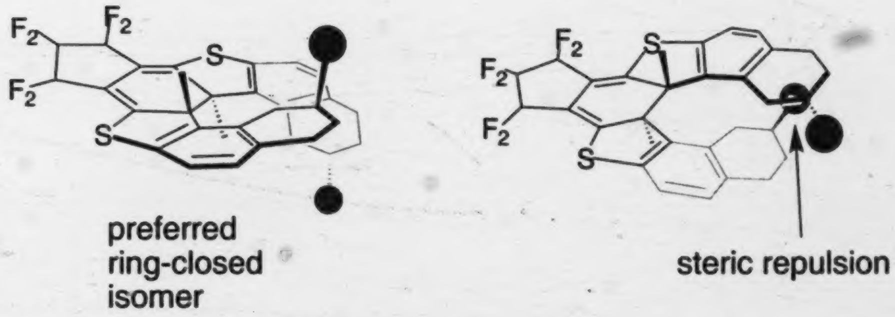
F2
F2
F2
S
S
preferred
ring-closed
isomer
F2
F2
F2
S
S
steric repulsion

3.6.5 Experimental

General: Dichloromethane used for UV-Vis spectroscopy and benzene used for photoisomerization reactions was deoxygenated by bubbling argon through the solvent. All reagents and starting materials were purchased from Aldrich or Acros Organics. 1-Methylnaphth[2,1-*b*]thiophene was synthesized employing slightly modified literature procedures as described below. In the ^{13}C spectrum of compounds **2**, **3a** and **3b** the carbons attached to the fluorine atoms as well as the sp^2 carbon atom on the cyclopentene ring are not observed due to the low intensity of the peaks resulting from the ^{13}C-^{19}F coupling.

General procedure for photocyclizations. The photoreactor was a 1.0 L cylindrical Pyrex vessel with an immersion well connected through a standard taper 50/60 ground glass joint. Attached to the upper part of the reaction vessel were gas-inlet and outlet joints, with the gas outlet leading to a silicon oil bubbler. There also was a third joint attached to the upper part of the vessel for monitoring of samples. The vessel was flat-bottomed to allow a magnetic stirring bar to rotate. The immersion well was a doublewalled Pyrex tube cooled by water and contained a Hanovia 450-W high-pressure quartz Hg-vapor lamp.

Procedure for photoirradiation in the presence of propylene oxide. Argon was bubbled through the stirred solution of the stilbene derivative and iodine in benzene for 20-30 minutes before excess propylene oxide was added. The lamp was then turned on and the argon flow was decreased but maintained throughout the procedure. The photoirradiation was monitored by the disappearance of the iodine color achieved by taking aliquots via the third joint. This typically took 2-8 hours. The resulting solutions were then evaporated under pressure to dryness.

1-methyl-naphtho[2,1-*b*]thiophene (4).[20] A solution of 4-methyl-2-styryl-thiophene (210 mg, 1.05 mmol) and iodine (265 mg, 1.05 mmol) in dry benzene (600 mL) was deoxygenated with argon for 30 minutes. Propylene oxide (4.0 mL) was added, and the solution irradiated for 5 hours. After irradiation, the solution was evaporated to dryness, and the residue taken up in CH_2Cl_2 (50 mL) and shaken with a dilute solution of sodium thiosulfate (50 mL). The CH_2Cl_2 layer was dried with anhydrous Na_2SO_4 and then filtered and the remaining solvent removed under reduced pressure affording a white residue, which was further purified by column chromatography through silica gel (hexane) to afford 175 mg of a pure white solid. Yield 85%; ^{1}H NMR (300 MHz, CD_2Cl_2) δ 8.75 (d, *J*=8 Hz, 1H), 8.02 (dd, *J*=8, 2 Hz, 1H), 7.91 (d, *J*=9 Hz, 1H), 7.78 (d, *J*=9 Hz, 1H), 7.69-7.56 (m, 2H), 7.31 (m, 1H), 2.96 (d, *J*=0.9 Hz, 3H); HRMS (EI) Calcd for M^+ ($C_{13}H_{10}S$) 198.0503. Found: 198.0496.

Synthesis of 1,2-*bis*-(methyl-naphtho[2,1-*b*]thiophen-2-yl)perfluorocyclopentene (1a). A solution of thiophene **4** (0.20 g, 1.0 mmol) in anhydrous hexane/THF (10 mL/3 mL) was treated with *tert*-butyllithium (1.7 M in hexane, 0.6 mL, 1 mmol) dropwise at -78 °C under an argon atmosphere. The solution was stirred at this temperature for 30 minutes and then octafluorocyclopentene (63 μL, 0.5 mmol) was added dropwise through a cooled gas tight syringe. At this point, the solution turned yellow/orange in color. The solution was stirred further at this temperature for 1 hour and then allowed to warm to room temperature. The reaction was quenched with H_2O and the solvent was evaporated to dryness under vacuum. The residue was dissolved in $CHCl_3$, washed with H_2O and brine and the organic layer was dried with Na_2SO_4 and filtered. The $CHCl_3$ was removed and the crude product was purified by column chromatography through silica (hexane) to afford desired product **1a** (21 mg) as a yellow solid. Single crystals suitable for X-ray diffraction were grown by slow evaporation of a hexane solution. Yield 8%; mp 212-213°C; ^{1}H NMR (300 MHz, CD_2Cl_2) δ 8.42 (m, 2H), 7.94 (m, 2H), 7.87 (d, J=9 Hz, 2H), 7.80 (d, J=9 Hz, 2H), 7.48 (m, 4H), 2.45 (s, 6H); ^{13}C NMR (125 MHz, CD_2Cl_2) δ 140.8, 138.4, 137.9 (t, J=25 Hz),133.9, 132.5, 130.9, 129.5, 127.9, 127.1, 125.8, 123.7, 123.1, 120.7, 116.2 (t, J=258, 25 Hz), 111.4 (t, J=25 Hz),18.8; IR (CH_2Cl_2, cast) υ 3054, 2986, 1615, 1587, 1557, 1511, 1436, 1339, 1272, 1243, 1196, 1129, 1056 cm^{-1}; HRMS (EI) Calcd for M^+ ($C_{31}H_{18}F_6S_2$) 568.0754. Found: 568.0745.

Synthesis of 1b. Photochrome **1a** (5 mg) was dissolved in CH_2Cl_2 (10 mL) and irradiated at 410 nm for 30 minutes. The solvent was removed under reduced pressure and the yellow/orange residue dissolved in a minimal amount of boiling hexane (2-3 mL). The solution was then slowly allowed to warm to room temperature affording both yellow crystals (**1a**) and orange crystals (**1b**). ^{1}H NMR (600 MHz, CD_3CN) δ 7.90 (d, J=8.5 Hz, 2H), 7.69 (d, J=8.5 Hz, 2H), 7.46 (d, J=8.5 Hz, 2H), 6.96 (m, 2H), 6.53 (d, J=8.5 Hz, 2H), 6.15 (m, 2H), 2.36 (s, 6H).

Synthesis of 4-methyl-2-[2-(3-methyl-napthalen-2-yl)-vinyl]-thiophene (12). To a solution of (3-methyl-2-naphthyl-methyl)-triphenyl-phosphonium bromide **11** (2.53 g, 5.09 mmol) and 4-methyl-thiophene-2-carbaldehyde **7** (640 mg, 5.1 mmol) in dry benzene (100 mL) was added potassium *tert*-butoxide (680 mg). After heating at reflux for 4 hours, the solution was cooled and the triphenylphosphine oxide was filtered off. The filtrate was evaporated to dryness and the residue purified by column chromatography through silica gel (1:10 EtoAc/hexane). The resulting residue was further purified by recrystallization from hexanes affording pale yellow leaflets (752 mg) containing 95% cis isomer. Yield 56%; mp 62-64°C; ^{1}H NMR (300 MHz, CD_2Cl_2) δ 8.01 (s, 1H), 7.82-7.79 (m, 1H), 7.74-7.71 (m, 1H), 7.63 (s, 1H), 7.42-7.39 (m, 2H), 7.24 (d, *J*=2 Hz, 2H), 6.97 (d, *J*=2 Hz, 1H), 6.83 (s, 1H), 2.56 (d, *J*=1 Hz, 3H), 2.58 (d, *J*=1 Hz, 3H); ^{13}C NMR APT (75 MHz, $CDCl_3$): δ 138.3 (C), 135.3 (C), 134.1 (C), 133.2 (C), 132.4 (C), 128.5 (CH), 128.2 (CH), 127.7 (CH), 127.7 (CH), 126.9 (CH), 125.9 (CH), 125.8 (CH), 125.4 (CH), 123.9 (CH), 123.9 (CH), 119.9 (CH), 20.5 (CH_3), 15.7 (CH_3); IR (μscope) 3048, 3014, 2994, 2945, 2921, 2858, 1792, 1661, 1632, 1613, 1594, 1546, 1496, 1439, 1377, 1359, 1334, 1314, 1272, 1233, 1202, 1182, 1151, 1131, 1086 cm^{-1}; HRMS (EI) Calcd for M^+ ($C_{18}H_{16}S$) 264.0973. Found: 264.0976.

Synthesis of 1,6-dimethyl-3-thia-cyclopenta[*c*]phenanthrene (5). A solution **12** (200 mg, 0.76 mmol) and iodine (193 mg, 0.76 mmol) in dry benzene (600 mL) was deoxygenated with argon for 30 minutes. Propylene oxide (4 mL) was added, and the solution irradiated for 1.5 hours. After irradiation, the solution was evaporated to dryness, the residue was taken up in CH_2Cl_2 (50 mL) and shaken with a dilute solution of sodium thiosulfate (50 mL). The CH_2Cl_2 layer was dried with anhydrous Na_2SO_4 and filtered and the solvent removed under vacuum affording a yellow residue, which was eluted through a plug of silica gel (hexane). The resulting solid was recrystallized from hexanes affording 145 mg of X-ray quality yellow rod-like crystals. Yield 72%; mp 125-126°C; ^{1}H NMR (300 MHz, CD_2Cl_2) δ 8.12 (d, J=8 Hz, 1H), 8.05 (d, J=8 Hz, 1H), 7.96 (d, J=8 Hz, 1H), 7.88 (dd, J=7, 2 Hz, 1H) 7.70 (s, 1H), 7.61-7.50 (m, 2H), 7.43 (d, J=1 Hz 1H), 2.81 (s, 3H), 2.48 (s, 3H); ^{13}C NMR APT (75 MHz, $CDCl_3$) δ 140.9 (C), 135.6 (C), 135.3 (C), 132.9 (C), 132.8 (C), 130.9 (C), 130.4 (CH), 128.3 (C), 127.9 (C), 126.7 (CH), 126.5 (CH), 126.3 (CH), 125.0 (CH), 123.8 (CH), 121.8 (CH), 120.7 (CH), 20.6 (CH_3), 20.0 (CH_3); IR (μscope) 3092, 3047, 2974, 2945, 2918, 1617, 1601, 1507, 1480, 1439, 1376, 1338, 1317, 1287, 1235, 1185, 1168, 1147, 1098 cm^{-1}; HRMS (EI) Calcd for M^+ ($C_{18}H_{14}S$) 262.0816. Found: 262.0819.

Synthesis of 1,2-*bis*-(1,6-dimethyl-3-thia-cyclopenta[*c*]phenanthren-2-yl) perfluorocyclopentene (2). A solution of thiophene **5** (0.13 g, 0.5 mmol) in anhydrous hexane/THF (10 mL/5 mL) was treated with *tert*-butyllithium (1.7 M in hexane, 0.4 mL, 0.66 mmol) dropwise at -78 °C under an argon atmosphere. The solution was stirred at this temperature for 30 minutes and then octafluorocyclopentene (32 µL, 0.25 mmol) was added dropwise through a cooled gas tight syringe. At this point, the solution turned yellow/orange in color. The solution was stirred at this temperature for 1 hour and then allowed to warm to room temperature. The reaction was quenched with H_2O and solvent was evaporated under vacuum. The residue was re-dissolved in $CHCl_3$, washed with H_2O and brine and the organic layer was dried with Na_2SO_4 and filtered. The $CHCl_3$ was removed under vacuum and the crude product was purified by column chromatography through silica (hexane) to afford the desired product **2** (18 mg) as a yellow solid. Single crystals suitable for X-ray diffraction were grown by slow evaporation of a hexane solution. Yield 11%; mp 250-252°C; ^{1}H NMR (300 MHz, CD_2Cl_2) δ 8.12 (s, 4H), 7.72 (d, *J*=8 Hz, 2H), 7.65 (s, 2H), 7.40 (d, *J*=8 Hz, 2H), 7.27 (dt, *J*=7, 1 Hz, 2H), 6.51 (dt, *J*=7, 1 Hz, 2H), 2.81 (d, *J*=1 Hz, 6H), 2.06 (s, 6H); ^{13}C NMR (125 MHz, CD_2Cl_2) δ 146.7, 144.0, 140.0, 137.3, 137.3, 135.8, 134.4, 132.5, 132.2, 131.5, 131.3, 131.2, 130.2, 128.2, 127.8, 125.8, 25.0, 24.9; IR (CH_2Cl_2, cast) 3046, 2925, 1600, 1439, 1338, 1273, 1127 cm^{-1}; HRMS (EI) Calcd for M^+ ($C_{41}H_{26}F_6S_2$) 696.1380. Found: 696.1379.

Synthesis of 2-[2-(3-methyl-naphthalen-2-yl)-vinyl]-thiophene (13). To a solution of (3-methyl-naphthalen-2-yl-methyl)-triphenyl-phosphonium; bromide **11** (1.24 g, 2.50 mmol) and thiophene-2-carbaldehyde **10** (290 mg, 2.59 mmol) in dry benzene (50 mL) was added potassium *tert*-butoxide (300 mg). After heating at reflux for 3 hours the solution was cooled and the triphenylphosphine oxide was filtered off. The filtrate was evaporated to dryness and the residue purified by column chromatography through silica gel (hexane) affording 358 mg of a white solid containing a 80:20 mixture of cis:trans isomers. Yield 58%; mp 110-113°C; ^{1}H NMR (300 MHz, $CDCl_3$) δ 7.98 (s, 1H), 7.80-7.76 (m, 1H), 7.72-7.69 (m, 1H), 7.60 (s, 1H), 7.41-7.36 (m, 2H), 7.40 (d, *J*=2 Hz, 2H), 7.19 (d, *J*=5 Hz, 1H), 7.10 (dd, *J*=4, 1 Hz, 1H), 7.01 (dd, *J*=5, 4 Hz, 1H), 6.92 (m, 0.2H), 6.87 (d, *J*=11 Hz, 0.2H), 6.81 (dd, *J*=4, 4 Hz, 0.2H), 6.63 (d, *J*=11 Hz, 0.2H), 2.5 (s, 3H), 2.38 (s, 0.6H); ^{13}C NMR (75 MHz, $CDCl_3$) δ 143.2, 135.3, 134.1, 133.2, 132.4, 128.2, 128.2, 127.7, 126.9, 126.3, 126.2, 125.9, 125.4, 124.5, 124.0, 123.7, 20.5; IR (*μ*scope) 3099, 3051, 3012, 2979, 2952, 1796, 1614, 1593, 1516, 1495, 1437, 1426, 1290, 1277, 1233, 1203, 1150, 1046 cm^{-1}; HRMS (EI) Calcd for M^+ ($C_{17}H_{14}S$) 250.0816. Found: 250.0814.

Synthesis of 6-methyl-3-thia-cyclopenta[*c*]phenanthrene (6). A solution of 2-(3-methyl-2-naphthalen-2-yl-vinyl)-thiophene **13** (322 mg, 1.3 mmol) and iodine (330 mg, 1.3 mmol) in dry benzene (600 mL) was deoxygenated with argon for 30 minutes. Propylene oxide (5 mL) was added, and the solution irradiated for 2 hours. After irradiation, the solution was evaporated to dryness, the residue was taken up in CH_2Cl_2 (50mL) and shaken with a dilute solution of sodium thiosulfate (50 mL). The CH_2Cl_2 layer was dried with Na_2SO_4 and filtered, and the solvent evaporated under vacuum. The resulting residue was purified by column chromatography through silica gel (hexane) to afford 252 mg of a pure white solid. Yield 80%; mp 88-89°C; ^{1}H NMR (300 MHz, CD_2Cl_2) δ 9.07 (d, *J*=8 Hz, 1H), 8.63 (d, *J*=6 Hz, 1H), 8.15 (dd, *J*=8, 1 Hz, 1H), 8.04 (dd, *J*=9, 6 Hz,1H), 7.92 (dd, *J*=8, 1 Hz, 1H), 7.77 (d, *J*=6 Hz, 1H), 7.70 (s, 1H), 7.69-7.59 (m, 2H); ^{13}C NMR (75 MHz, $CDCl_3$) δ 139.9, 135.4, 132.9, 132.7, 130.3, 129.8, 127.9, 127.1, 126.6, 126.5, 126.2, 126.0, 125.5, 121.3, 20.9; IR (μscope) 3095, 3077, 3049, 3034, 2974, 2942, 2915, 2862, 1885, 1759, 1623, 1603, 1585, 1500, 1471, 1455, 1441, 1404, 1386, 1377, 1346, 1337, 1314, 1304, 1230, 1211, 1179, 1160, 1144, 1102 cm^{-1}; HRMS (EI) Calcd for M^+ ($C_{17}H_{12}S$) 248.0660. Found: 248.0653.

Synthesis of 1,2-*bis*-(6-methyl-3-thia-cyclopenta[*c*]phenanthren-2-yl) perfluorocyclopentene (3a). A solution of thiophene **6** (0.15 g, 0.60 mmol) in anhydrous hexane/THF (10 mL/5 mL) was treated with *tert*-butyllithium (1.7 M in hexane, 0.35 mL, 0.60 mmol) dropwise at -78 °C under an argon atmosphere. The solution was stirred at this temperature for 30 minutes and then octafluorocyclopentene (37 µL, 0.30 mmol) was added dropwise through a cooled gas tight syringe. At this point, solution turned yellow/orange. The solution was stirred at this temperature for 2 hours and then allowed warm to room temperature. The reaction was quenched with H_2O and solvent was evaporated off under vacuum. The residue was dissolved in $CHCl_3$, washed with H_2O and brine and the organic layer was dried with anhydrous Na_2SO_4 and filtered. The $CHCl_3$ was evaporated removed and the crude product was purified by column chromatography through silica (hexane followed by 5 % CH_2Cl_2/hexane) to afford the desired product **3a** (24 mg) as a yellow solid. Yield 12%; mp 252-253°C; ^{1}H NMR (500 MHz, CD_2Cl_2) δ 9.08 (s, 2H), 8.82 (d, *J*=8.6 Hz, 2H), 8.15 (d, *J*=8.8 Hz, 2H), 8.04 (dd, *J*=8.6, 1.0 Hz, 2H), 7.90 (dd, *J*=8.0, 1.2 Hz, 2H), 7.73 (s, 2H), 7.56 (ddd, *J*=8.0, 7.0, 1.0 Hz, 2H), 7.40 (ddd, *J*=8.5, 7.0, 1.4 Hz, 2H), 2.82 (d, *J*=0.7 Hz, 6H); ^{13}C NMR (125 MHz, CD_2Cl_2) δ 142.6, 139.1, 133.5, 133.2, 131.9, 130.9, 129.6, 128.4, 127.7, 127.7, 127.2, 126.5, 126.4, 124.5, 121.2, 20.9; IR (CH_2Cl_2, cast) 1611, 1518, 1484, 1455, 1438, 1330, 1293, 1256, 1116, 1103 cm^{-1}; HRMS (EI) Calcd for M^+ ($C_{39}H_{22}F_6S_2$) 668.1067. Found: 668.1062.

Synthesis of helicene 3b: A solution of **3a** (6.5 mg, 0.01 mmol), iodine (9.1 mg, 0.04 mmol) and propylene oxide (0.25 mL) in dry benzene (75 mL) was placed in a quartz tube and irradiated with 313 nm light for 2 hours employing a standard hand held lamp used for visualizing TLC plates (Spectroline E-series 470 μW/cm^2). After irradiation, the solution was evaporated to dryness, the residue was taken up in CH_2Cl_2 (50mL) and shaken with a dilute solution of sodium thiosulfate (50 mL). The CH_2Cl_2 layer was dried with anhydrous Na_2SO_4 and filtered, and the solvent removed affording a yellow residue. Single crystals suitable for X-ray analysis were obtained by diffusing pentane into a benzene solution of **3b**. Yield 94%; mp >300°C; ^{1}H NMR (500 MHz, CD_2Cl_2) δ 8.12 (d, *J*=8.3 Hz, 2H), 8.02 (d, *J*=8.3 Hz, 2H), 7.26 (s, 2H), 7.23 (d, *J*=7.5 Hz, 2H), 6.89 (ddd, *J*=8.0, 7.0, 1.0 Hz, 2H), 5.99 (d, *J*=8.0, 2H), 5.73 (ddd, *J*=8.0, 7.0, 1.0 Hz, 2H), 2.65 (d, *J*=1.0 Hz, 6H); ^{13}C NMR (125 MHz, CD_2Cl_2) δ 140.4, 137.2, 131.6, 130.5, 129.7, 128.9, 128.8, 128.7, 127.4, 126.1, 125.6, 125.5, 124.2, 122.0, 119.5, 20.5; IR (CH_2Cl_2, cast) 3071, 3034, 2925, 2853, 1728, 1619, 1561, 1487, 1427, 1402, 1376, 1350, 1339, 1315, 1305, 1290, 1253, 1228, 1197, 1170, 1150, 1129, 1112 cm^{-1}; HRMS (EI) Calcd for M^+ ($C_{39}H_{20}F_6S_2$) 666.0911. Found: 668.0882.

X-ray Crystallographic Analysis.

(1a). $C_{31}H_{18}F_6S_2$ (M= 568.57); crystal dimensions 0.54 × 0.15 × 0.13 mm, monoclinic, space group *C2/c* (No. 15) $a = 28.759(3)$, $b = 17.5928(16)$, and $c = 15.3097(14)$ Å, $\beta = 90.680(2)°$, V = 7745.3(12) Å^3, $\rho_{calc} = 1.463$ g cm^{-3}, $\mu = 0.270$ mm^{-1}, $T = -80$°C; Bruker PLATFORM/SMART 1000 CCD; Mo Kα radiation ($\lambda = 0.71073$ Å), scan method ω; 20408 data measured; 8001 independent reflections. The crystal structure was solved using direct methods (DIRDIF-96) and refined by full-matrix least squares on F^2 (SHELXL-93). All hydrogens were generated in idealized positions according to the sp^2 or sp^3-hybridized geometries of their attached carbon atoms. Final $R_1(F) = 0.0868$ (for 4250 data with $F_0^2 \geq 2\sigma(F_0^2)$), $wR_2(F^2) = 0.2853$ (on all 8001 unique data), and S = 1.024 for 621 parameters varied. The largest difference peak and hole in the final difference Fourier map had intensities of 1.012 and -0.607 e Å^{-3}.

(1b). $C_{31}H_{18}F_6S_2$ (M= 568.57); crystal dimensions 0.77 × 0.12 × 0.06 mm, orthorhombic, space group *Pbca* (No. 61) $a = 14.3016(19)$, $b = 15.120(2)$, and $c = 22.865(3)$ Å, V=

4944.3(11) Å^3, ρ_{calc}= 1.528 g cm^{-3}, μ = 0.282 mm^{-1}, T = -80°C; Bruker PLATFORM/SMART 1000 CCD; Mo Kα radiation (λ = 0.71073 Å), scan method ω; 25586 data measured; 5068 independent reflections The crystal structure was solved using direct methods (SHELXS-86) and refined by full-matrix least squares on F^2 (SHELXL-93). All hydrogens were generated in idealized positions according to the sp^2 or sp^3-hybridized geometries of their attached carbon atoms. Final $R_1(F)$ = 0.0525 (for 3429 data with $F_0^2 \geq 2\sigma(F_0^2)$), $wR_2(F^2)$ = 0.1295 (on all 5068 unique data), and S = 1.022 for 377 parameters varied. The largest difference peak and hole in the final difference Fourier map had intensities of 0.325 and -0.328 e Å^{-3}.

(2). $C_{41}H_{26}F_6S_2 \bullet C_6H_{14}$ (M= 782.91); crystal dimensions 0.69 × 0.10 × 0.06 mm, monoclinic, space group $P2_1/c$ (No. 14) a = 17.542(5), b = 12.255(3), and c = 18.173(5) Å, β = 96.569(7)°, V = 3881.2(19) Å^3, ρ_{calc} = 1.340 g cm^{-3}, μ = 0.200 mm^{-1}, T = -80°C; Bruker PLATFORM/SMART 1000 CCD; Mo Kα radiation (λ = 0.71073 Å), scan method ω; 17289 data measured; 7797 independent reflections. The crystal structure was solved using direct methods/fragment search (DIRDIF-96) and refined by full-matrix least squares on F^2 (SHELXL-93). All hydrogens were generated in idealized positions according to the sp^2 or sp^3-hybridized geometries of their attached carbon atoms. Final

$R_1(F)$ = 0.0810 (for 2502 data with $F_0^2 \geq 2\sigma(F_0^2)$), $wR_2(F^2)$ = 0.1837 (on all 7797 unique data), and S = 0.911 for 499 parameters varied. The largest difference peak and hole in the final difference Fourier map had intensities of 0.353 and -0.246 e Å^{-3}.

(3b). $C_{39}H_{20}F_6S_2{\bullet}C_6H_6$ (M= 744.78); crystal dimensions 0.55 × 0.11 × 0.10 mm, monoclinic, space group $P2_1/n$ (an alternate setting of $P2_1/c$ [No. 14]), a = 7.8785(6), b = 240608(2), and c = 17.5224(14) Å, β = 97.5468(16)°, V = 3367.7(5) Å^3, ρ_{calc} = 1.469 g cm^{-3}, μ = 0.200 mm^{-1}, T = -80°C; Bruker PLATFORM/SMART 1000 CCD; Mo Kα radiation (λ = 0.71073 Å), scan method ω; 16588 data measured; 6893 independent reflections. The crystal structure was solved using direct methods (SHELXL-86) and refined by full-matrix least squares on F^2 (SHELXL-93). All hydrogens were generated in idealized positions according to the sp^2 or sp^3-hybridized geometries of their attached carbon atoms. Final $R_1(F)$ = 0.0510 (for 4873 data with $F_0^2 \geq 2\sigma(F_0^2)$), $wR_2(F^2)$ = 0.1379 (on all 6893 unique data), and S = 1.038 for 480 parameters varied. The largest difference peak and hole in the final difference Fourier map had intensities of 0.632 and -0.264 e Å^{-3}.

3.6.6 References and notes

1. Irie, M.; Kobatake, S.; Horichi, M. *Science*, **2001**, *291*, 1769.

2. Katz, T. J.; *Angew. Chem. Int. Ed.* **2000**, *39*, 1921.
3. (a) Carreno, C. M.; Hernandez-Sanchez, R.; Mahugo, J.; Urbano, A. *J. Org. Chem.* **1999**, *64*, 1387. (b) Fox, J. M.; Goldberg, N, R.; Katz, T. J. *J. Org. Chem.* **1998**, *63*, 7456. (c) Katz, T. J.; Liu, L.; Willmore, N. D.; Fox, J. M.; Rheingold, A. L.; Shi, S.; Nuckolls, C.; Rickman, B. H. *J. Am. Chem. Soc.* **1997**, *119*, 10054. (d) Dai, Y.; Katz, T. J.; *J. Org. Chem.* **1997**, *62*, 1274. (e) Liu, L.; Yang, B.; Katz, T. J.; Poindexter, M. K. *J. Org. Chem.* **1991**, *56*, 3769.
4. NLO is a branch of optics that deals with the optical properties of matter that is subjected to intense electromagnetic radiation. It is based on the principle that the induced electric polarization of certain matter is not a linear function of the external electromagnetic radiation.
5. Ashitaka, H.; Yokoh, Y.; Shimizu, R.; Yokozawa, T.; Morita, K.; Suehiro, T.; Matsumoto, Y. *Nonlinear Optics* **1993**, *4*, 281.
6. (a) Sioncke, S.; Elshocht, S. V.; Verbiest, T.; Persoons, A.; Kauranen, M.; Phillips, K. E. S.; Katz, T. J. *J. Chem. Phys.* **2000**, *113*, 7578. (b) Verbiest, T.; Elshocht, S. V.; Kauranen, M.; Hellemans, L.; Snauwaert, J.; Nuckolls, C.; Katz, T. J.; Persoons, A. *Science* **1998**, *282*, 913.
7. Nuckolls, C.; Katz, T. J. *J. Am. Chem. Soc.* **1998**, *120*, 9541.

8. (a) Cuccia, L. A.; Lehn, J.-M.; Homo, J.-C.; Schmutz, M. *Angew. Chem. Int. Ed. Engl.* **2000**, *39*, 233. (b) Grimme, S.; Harren, J.; Sobanski, A.; Vogtle, F. *Eur. J. Org. Chem.* **1998**, 1491. (c) Piguet, C.; Bernardinelli, G.; Hopfgartner, G. *Chem. Rev.* **1997**, *97*, 2005. (d) Kiupel, B.; Niederalt, C.; Nieger, M.; Grimme, S.; Vogtle, F. *Angew. Chem. Int. Ed. Engl.* **1998**, *37*, 3031.

9. (a) Caronna, T.; Sinisi, R.; Catellani, M.; Malpezzi, L.; Meille, S. M.; Mele, A. *Chem. Commun.* **2000**, 1341. (b) Rajca, A.; Wang, H.; Pink, M.; Rajca, S. *Angew. Chem. Int. Ed. Engl.* **2000**, *39*, 4481. (c) Tanaka, K.; Kitahara, Y. *Chem. Commun.* **1998**, 1141. (d) Martin, R. H. *Angew. Chem. Int. Ed. Engl.* **1974**, *13*, 649.

10. (a) Murguly, E.; McDonald, R.; Branda, N. R. *Org. Lett.* **2000**, *2*, 3169. (b) Owens, L.; Thilgen, C.; Diederich, F.; Knobler, C. B. *Helv. Chim. Acta* **1993**, *76*, 2757.

11. (a) Dreher, S. D.; Katz, T. J.; Lam, K.-C.; Rheingold, A. L. *J. Org. Chem.* **2000**, *65*, 815. (b) Reetz, M. T.; Beuttenmuller, E. W.; Goddard, R. *Tetrahedron Lett.* **1997**, *38*, 3211. (c) Terfort, A.; Goris, H.; Brunner, H. *Synthesis* **1997**, 79.

12. Nuckolls, C.; Katz, T. J. *J. Am. Chem. Soc.* **1998**, *120*, 9541.

13. (a) Sioncke, S.; Elshocht, S. V.; Verbiest, T.; Persoons, A.; Kauranen, M.; Phillips, K. E. S.; Katz, T. J. *J. Chem. Phys.* **2000**, *113*, 7578. (b) Verbiest, T.; Elshocht, S. V.;

Kauranen, M.; Hellemans, L.; Snauwaert, J.; Nuckolls, C.; Katz, T. J.; Persoons, A. *Science* **1998**, *282*, 913.

14. Kelly, T. R.; Sestelo, J. P.; Tellitu, I. *J. Org. Chem.* **1998**, *63*, 3655.

15. Dinescu, L.; Wang, Z. Y. *Chem. Commun.* **1999**, 2497.

16. (a) Murguly, E.; Norsten, T. B.; Branda, N. R. *Angew. Chem. Int. Ed. Engl.* **2001**, *40*, 1752. (b) Chen, C.-T.; Chou, Y.-C. *J. Am. Chem. Soc.* **2000**, *122*, 7662. (c) Feringa, B. L.; van Delden, R. A.; Koumura, N.; Geertsema, E. M. *Chem. Rev.* **2000**, *100*, 1789. (d) Huck, N. P. M.; Wolter, J. F.; de Lange, G.; Feringa, B. L. *Science* **1996**, *273*, 1686.

17. (a) Uchida, K.; Kido, Y.; Yamaguchi, T.; Irie, M. *Bull. Chem. Soc. Jpn.* **1998**, *71*, 1101. (b) Uchida, K.; Irie, M. *Chem. Lett.* **1995**, 969.

18. Irie, M. *Chem. Rev.* **2000**, *100*, 1685.

19. Groen, M. B.; Schadenberg, H.; Wynberg, H. *J. Org. Chem.* **1971**, *36*, 2797.

20. Tominaga, Y.; Lee, M. L.; Castle, R. N. *J. Heterocyclic Chem.* **1981**, *18*, 977.

21. The monochromatic light used to carry out the ring-closing reaction was generated from a Spectral Energy lamp (1000 W Xe/Hg source) and monochromator assembly. The ring-opening reaction was carried out using the light of a 150-W tungsten source that was passed through a 458-nm cutoff filter to eliminate higher energy light.

22. Single point energy calculations of the AM1-optimized structures of both diastereomers were performed using the GAUSSIAN 98 suite of programs and the standard 3-21G* basis set. These calculations estimate that the observed stereoisomers are more stable by 19.2 kcal mol^{-1}.

23. Single crystals of **2** were grown by slow evaporation of a hexane solution. Crystals of **3b** were grown by diffusion of pentane into a benzene solution.

24. This was previously shown to be the case for a structurally similar molecule: Musmar, M. J.; Martin, G. E.; Gampe R. T. Jr.; Lynch. V. M.; Simonsen, S. H.; Lee, M. L.; Tedjamulia, M. L.; Castle, R. N. *J. Heterocyclic Chem.* **1985**

25. Murguly, E. Masters Dissertation, The University of Alberta, 2000.

26. (a) Janke, R. H.; Haufe, G.; Wurthwein, E-U.; Borkent, J. H.; *J. Am. Chem. Soc.* **1996**, *118*, 6031. (b) Borkent, J. H.; Laarhoven, W. H. *Tetrahedron*, **1978**, *34*, 2565.

Unit 4 - Chapter 7- Conclusion

The covalent addition of atoms to form molecules is a powerful way to start to build-up molecular structure. The structural characteristics at this level provide the scaffold on which higher ordered structures can form. Self-assembly is a versatile and quick way to extend structure beyond the single-molecule level to afford larger and more complex structures. Post-synthetic control provides an external mechanism to modulate molecular structure and function.

Chapter 2 described a novel diatopic approach to assembling photoactive building blocks into large well-defined supramolecular structures. The photophysical characteristics displayed by the assembled complexes were clearly a function of the resulting molecular topology. This example demonstrated how self-assembly synthesis was used to control structure and function.

Unit 3 showed how photochromic molecules can be used to modulate molecular structure in response to light activation. Specifically, Chapter 6 demonstrated how the incorporation of a photochrome into extended polyaromatic systems provides a means to control helical topology. This shows the usefulness of post-synthetic mechanisms to control structure.

The most comprehensive example that combines both levels of control was described in Chapter 5. In this example, dative bonding was used to self-assemble optically pure photochromic ligands into stereochemically pure helicates. The weak optical rotatory properties of constituents were amplified during the self-assembly process into the strong rotatory properties displayed by the fully-assembled helicate. The rigid positioning of the photochrome within the helicate resulted in the preferential formation of one of the stereoisomers during the ring-closing photochromic reaction. Modulation between "more helical" and "less helical" structural forms was achieved by alternate irradiation with UV and visible light. The resulting structural regulation, in turn, affects the chiroptical properties of the system providing a non-destructive readout method for information storage.

Appendix I- Photochromic Dithienylcyclopentene Pyridin-2-ylamides

This chapter describes a series of dithienylethene photochromes that can reversibly change their luminescence intensities and redox properties by alternate irradiation with ultraviolet and visible light.

I.1 Synthesis of Photochromes

The pyridin-2-ylamide-functionalized dithienylethenes **3-6** were prepared from the diacid **1** as outlined in Scheme 1. The synthesis of **1** was described in Chapter 3, Scheme 3.3. The diacid **1** was converted into its corresponding acid chloride **2** which was treated with 2-aminopyridine yielding a mixture of compounds **3**, **4** and **5**. Each of these compounds can be isolated by column chromatography. Photochrome **3** was isolated as the major product along with minor amounts of the other species, **5** and the bis-dithienylethene macrocycle **4**. Alternatively, treatment of **3** with and equimolar amount of the diacid chloride of **2** in a refluxing solution of NaH and benzene afforded the macrocycle **4** in nearly quantitative yield. Bis-imide **6** was prepared in excellent yield by treating **3** with 5-methyl-2-thienyl chloride in benzene at reflux. The fluorescence and redox control compounds amide **7** and imide **8** were synthesized by treatment of 2-

aminopyridine with 5-methyl-2-thienyl chloride under similar conditions to the preparation of **3** from **2**.

Scheme 1

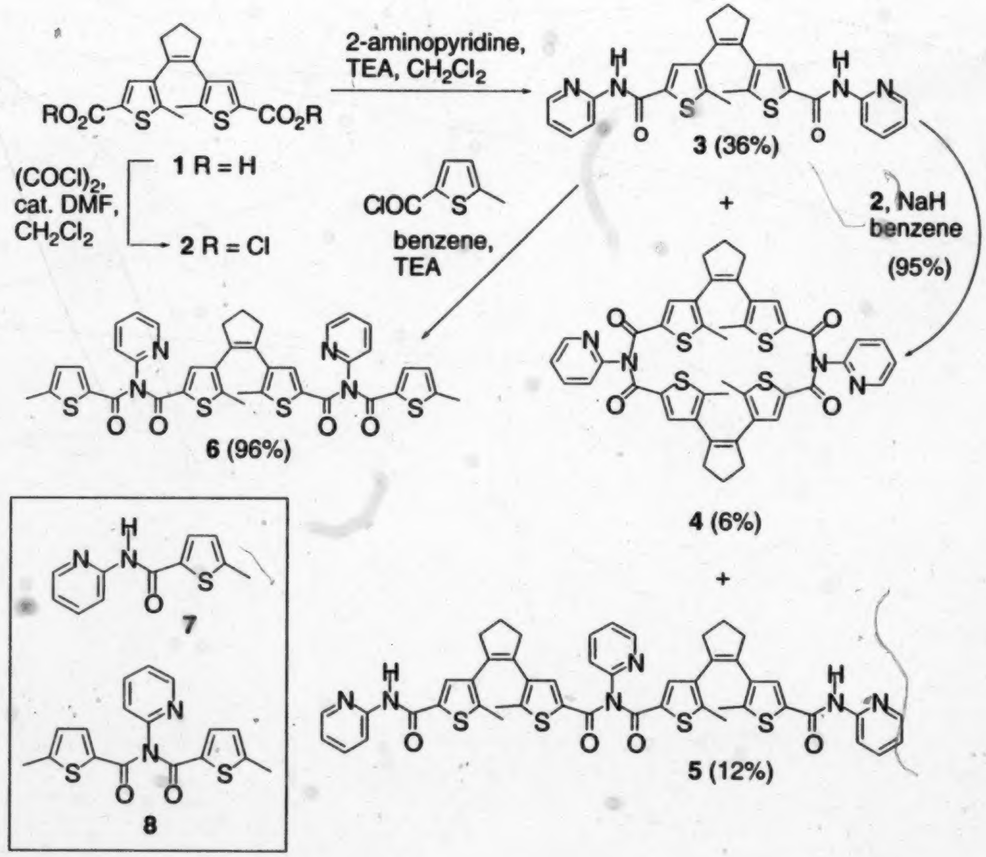
RO2C
CO2R
1 R = H
2 R = Cl
(COCl)2, cat. DMF, CH2Cl2
2-aminopyridine, TEA, CH2Cl2
3 (36%)
ClOC
benzene, TEA
+
2, NaH benzene
(95%)
6 (96%)
4 (6%)
+
5 (12%)
7
8

I.2 X-ray Crystallographic Analysis

Single crystals of **1** were obtained by layering a MeOH solution of the dicarboxylic acid with H_2O. Within the crystal lattice **1** adopts a conformation where the two thiophene rings lie in an antiparallel arrangement with respect to one another. This orients the two carboxylic acid moieties within an individual unit in opposing directions (Figure 1(a)). The result of this is a supramolecular crystal lattice comprised of hydrogen-bonded ribbons. These ribbons consist of a herringbone arrangement of alternating enantiomers of **1** (Figure 1(b)).

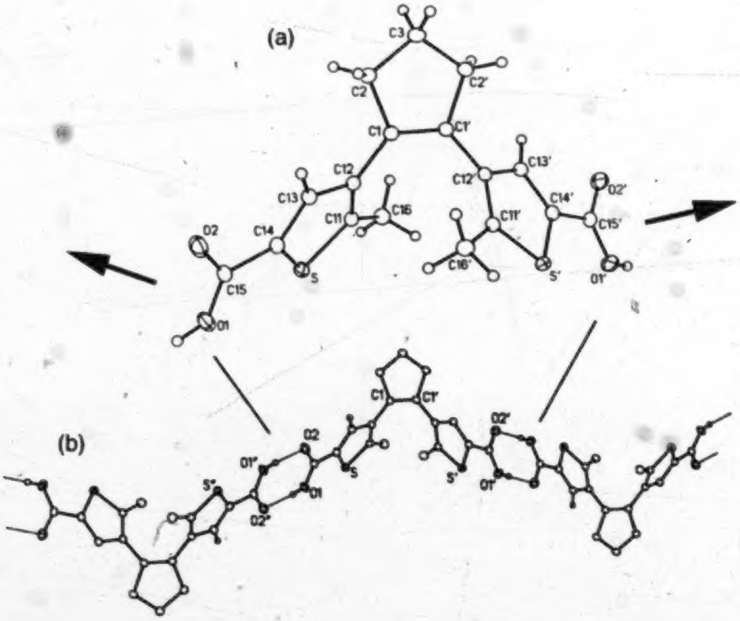
(a)
C3
C2
C2'
C1
C1'
C12
C13
C12'
C13'
C14'
O2'
C16
C11
C11'
C15'
O2
C14
C15
S
C16'
S'
O1'
O1
(b)
C1
C1'
O2'
O2
O1''
S''
O1
S
S'
O1'
O2''

Figure 1. Molecular structure of (a) **1** highlighting an individual dicarboxylic acid moiety (b) illustrating a self-assembled hydrogen-bonded ribbon of alternating enantiomers of **1**. Thermal ellipsoids at the 20% probability level.

Irradiation of a CH_3CN solution of **3(open)** with 254 nm light produces a deep red solution of **3(closed)** in near quantitative yield. Single crystals suitable for X-ray analysis were obtained by diffusion of pentane into a benzene solution of **3(closed)**. Figure 2 shows the molecular structure of **3(closed)** in the crystalline state highlighting the newly formed carbon-carbon bond between C11A and C21A. As was seen in Chapter 5, unless there is induction by a chiral auxiliary, the conrotatory ring closure of dithienylethenes results in an equal mixture of enantiomeric products. Hence for 3, both enantiomers (*R,R*) and (*S,S*) were present in the crystal lattice resulting in overall racemic crystal .

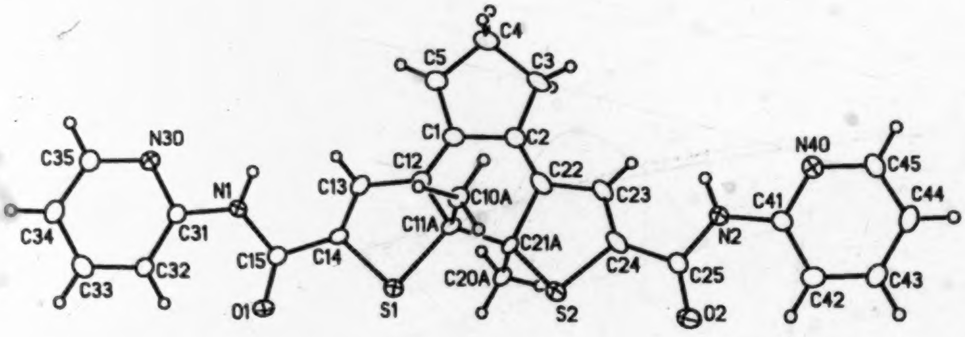
C4
C5
C3
C1
C2
N30
C35
N1
C12
C22
N40
C45
C13
C10A
C23
C41
C44
C34
C11A
N2
C31
C21A
C15
C14
C24
C32
C20A
C25
C43
C33
O1
S1
S2
O2
C42

Figure 2. Molecular structure of **3(closed)** (*R,R*) in the crystalline state. Thermal ellipsoids at the 20% probability level.

I.3 Spectroscopic and Photochemical Studies of the Photochromes

I.3.1 ^{1}H NMR Spectroscopic Analysis

Photochemical cyclization reactions of the open forms of **3**, **5** and **6** to their corresponding closed forms were followed directly by ^{1}H NMR and UV-Vis spectroscopy. Irradiation of CD_3CN solutions of **3** and **6** with 254 nm light resulted in greater than 98% conversion to the colored *closed* forms as diagnosed by ^{1}H NMR spectroscopy. The chemical shift data for all of the compounds studied are given in Table 1. Photocyclization of **5** under identical conditions to those described above resulted in cyclization of only one of the dithienylethene moieties as diagnosed by ^{1}H NMR spectroscopy. This phenomenon has been recently observed in another covalently linked bis-dithienylethene system,[1] and it has further been suggested that the newly formed *ring-closed* moiety suppresses the photocyclization of the remaining excited *open* photochrome via an energy transfer process (Figure 3).[2]

Figure 3

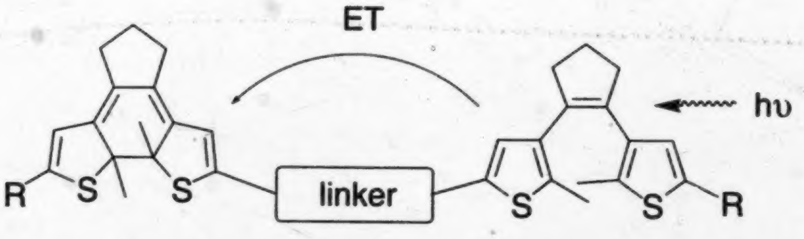

I.3.2 UV-Vis Spectroscopic Analysis Studies

The major absorptions recorded in the UV-Vis spectra of both the *open* and *closed* forms of compounds **3**, **5** and **6** are listed in Table 1. A trend that is apparent between the *closed* forms of these compounds is that the visible band is shifted to longer wavenumbers as one acyl-thiophene (in the case of **5**), and two acyl-thiophenes (in the case of **6**) are appended to the amide nitrogen atoms of compound **3** (Figure 4). This red-shifting effect caused by appending electron rich substituents to the 5-thienyl position of the colored forms of these photochromes was described in Section 3.4.1.

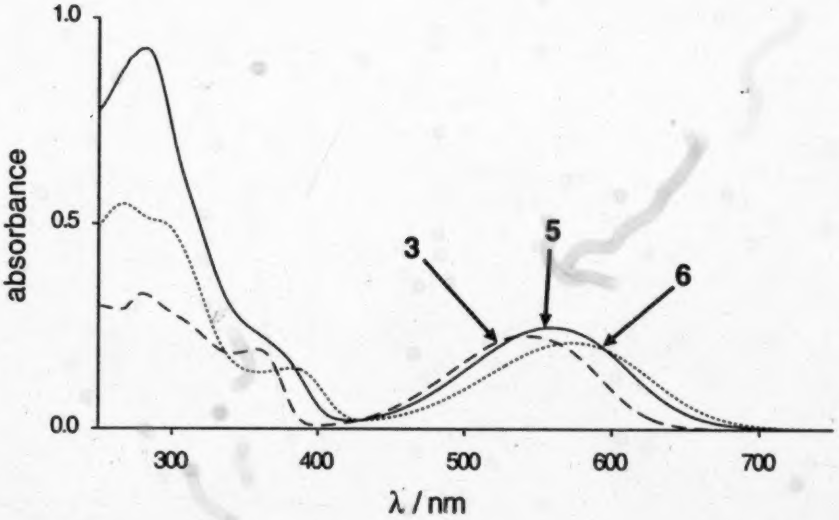

Figure 4. Absorption spectra of **3** (- - -), **5** (—) and **6** (•••) at 2 x 10^{-5} M in CH_3CN after irradiation at 254 nm for 50 sec.

Table 1. Photochemical, absorption, emission and selected ^{1}H NMR spectroscopic data for all compounds used in this study.[a]

Compound	λ_{max} [nm] log[ε/M^{-1}cm^{-1}]	Conversion [%][b]	δ [ppm] C–H	 CH$_2$[c]	λ_{emiss} [nm][d]	Relative Fluorescence Intensity[e]
3(*open*)	288 (3.35)	–	7.60	2.85	436	0.14
3(*closed*)	542 (1.14)	> 98	6.88	2.45	436	0.04[b]
4	282, 336 (4.89, 1.56)	–	6.75	2.41	481	1.0
5(*open*)	285 (5.90)	–	7.48 7.04	2.69	488	0.58
5(*closed*)	560 (1.23)	95	7.55 7.13 6.83 6.75	2.75 2.40	488	0.05[b]
6(*open*)	278 (2.63)	–	7.08	2.61	487	0.52
6(*closed*)	575 (1.05)	> 98	6.53	2.34	487	0.04[b]
7		–			505	0.20
8		–			490	0.12

[a] All spectra were recorded in deoxygenated CH_3CN or CD_3CN except for the ^{1}H NMR spectrum of **4** which was recorded in CH_2Cl_2,[b] Based on the ratio of *open* to *closed* isomers in the ^{1}H NMR spectra when solutions were irradiated with 254 nm light until the photostationary state was reached (5-10 minutes),[c] Refers to the allylic protons, [d] λ_{excit} = 300 nm, [e] Relative to the fluorescence intensity of **3**.

I.3.3. Fluorescence Analysis

The capacity to control differences in emission between the *open* and *closed* forms of a photoswitch has been shown to hold great potential in the area of optically controlled non-destructive read-write-erase information storage systems as has been already described in this thesis. The porphyrin-dithienylethene photochrome described in Chapter 3 demonstrated that it is essential for the fluorophore excitation band to be remote and independently addressable from the photochromic interconversion bands. If this prerequisite is not met, reading of information by excitation of the fluorofore inevitably results in photochromic interconversion and erasure of information.

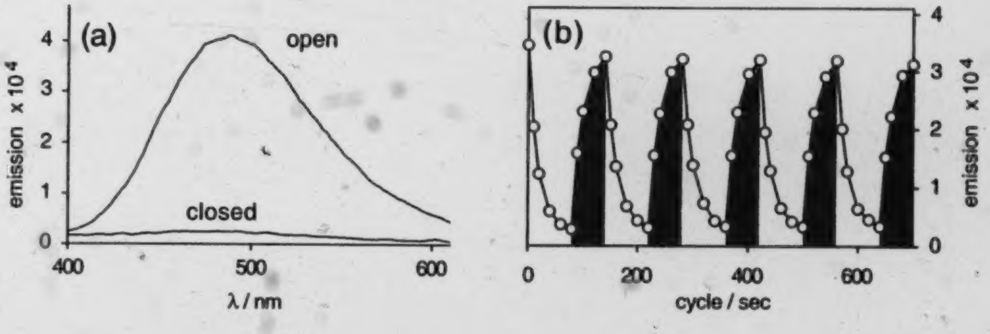

Figure 5. (a) Fluorescence emission spectra of **6** in its open and closed forms. (b) Modulated emission signal of **6** in CH_3CN (2×10^{-5} M) during alternating irradiation at 254 nm (unshaded) and greater than 450 nm (shaded) ($\lambda_{ex} = 300$ nm, $\lambda_{em} = 485$ nm).

The *open* and *closed* forms of compound **6** were found to display large differences in fluorescence intensity when excited at 260-360 nm. It was found that when excited at 300nm, the open form of **6** was strongly fluorescent while the *closed* form emitted only weakly (Figure 5(a)). This fluorescence can be conveniently modulated by alternate irradiation at 254 nm and greater than 480 nm while irradiating at 300 nm (Figure 5(b)). Similar fluorescent behavior was observed for compounds **3** and **5**. Table 1 illustrates the luminescence wavelengths and relative intensities of compounds **3-8** when excited at 300 nm. Unfortunately the absorption bands necessary to produce the fluorescence are the same bands required for the ring-closing reaction. To determine if there existed any photochromic/fluorescence discrimination within these bands, compound **6** was irradiated with light of different wavelengths between 260-360 nm. It was found that there was very little discrimination between luminescence and photochromic activity, as all the excitation wavelengths sampled resulted in ring closure and a subsequent decrease in fluorescence.

I.4 Characterization of the Macrocycle

Macrocycle **4** is comprised of two dithienylethenes scaffolds bridged by pyridin-2-ylimide linkers. The macrocycle is comprised of 20 sp^2 hybrid carbon centers and two pseudo sp^2 hybrid imide nitrogens, and as a result is expected to be quite rigid. Studies on **4** show that it is not photochromic, as its UV-Vis profile remains unchanged even after prolonged systematic irradiation throughout its absorbing spectral region. An X-ray structure of **4** (Figure 6) reveals that the thiophene rings expected to undergo cyclization lie perpendicular to one another, and it may be this type of rigid macrocyclic conformation that exists in solution preventing the photocyclization reaction from occurring. It was anticipated that prolonged irradiation at elevated temperatures may result in a conformation that is conducive to the cyclization reaction. However, irradiation of **4** in a boiling solution of decalin (b.p. = 187°C) with UV light did not result in the appearance of the visible absorption band that is diagnostic for the cyclized form.

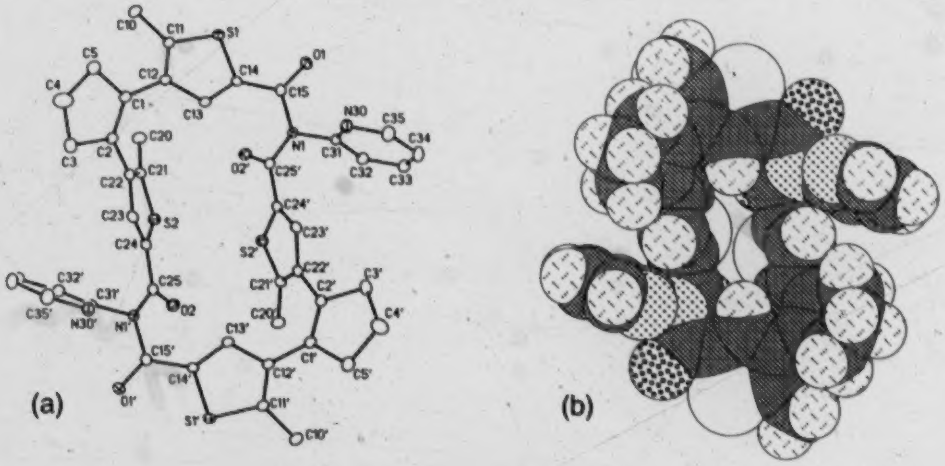
C10
C11
S1
C5
O1
C4
C12
C14
C1
C15
C13
N30
C35
C20
N1
C31
C34
C3
C2
O2'
C25'
C32
C33
C22
C21
C24'
C23
S2
C23'
C24
S2'
C22'
C3'
C32'
C25
C21'
C2'
C31'
C35'
N30'
N1'
O2
C20'
C4'
C13'
C15'
C1'
C12'
C14'
C5'
(a)
O1'
C11'
S1'
C10'
(b)

Figure 6. Molecular structure of macrocycle **4** in the crystal drawn with (a) thermal ellipsoids at the 15% probability level and (b) a space-filling representation.

I.5 Electrochemical Studies

Thiophene containing compounds such as polythiophenes and thiophene oligomers have attracted a great deal of attention because of their potential use as organic based conducting materials.[12] Photochromic molecular switches could serve as light driven circuit breakers when incorporated into such organic based molecular wires. Consequently, we turned our attention to the electrochemical properties of the oligothiophene photochrome **6**. Cyclic voltammetry experiments were performed in MeCN employing 0.1 M $Bu_4N^+ {}^-PF_6$ as the supporting electrolyte. The dithienyl-pyridyl-imide arms that flank the cyclopentene moiety were shown to be electrochemically active by model compound **8**. The cyclic voltamogram of compound **8** shows that it is reversibly reduced at -1.8 eV and irreversibly reduced at -2.3 eV (Figure 7, top trace). Compound **6** is similarly electroactive, however the open form displays an irreversible reduction at -1.7 eV followed by a reversible reduction at -2.4 eV (Figure 7, middle trace). The subsequent electrochemical properties between the open and closed forms of **6** are dramatically different. Irradiation of a solution of **6(open)** with 254 nm light leads to a dark purple solution of **6(closed)** which exhibits a reversible reduction at -0.8 eV and an irreversible oxidation at 0.7 eV (Figure 7, bottom trace). Back irradiation of **6(closed)** with visible light (> 480 nm) restores it to the original voltamogram. The dithienylethene essentially behaves as regulator, capable of interrupting conjugation between the peripheries of the switch by means of photoregulation.

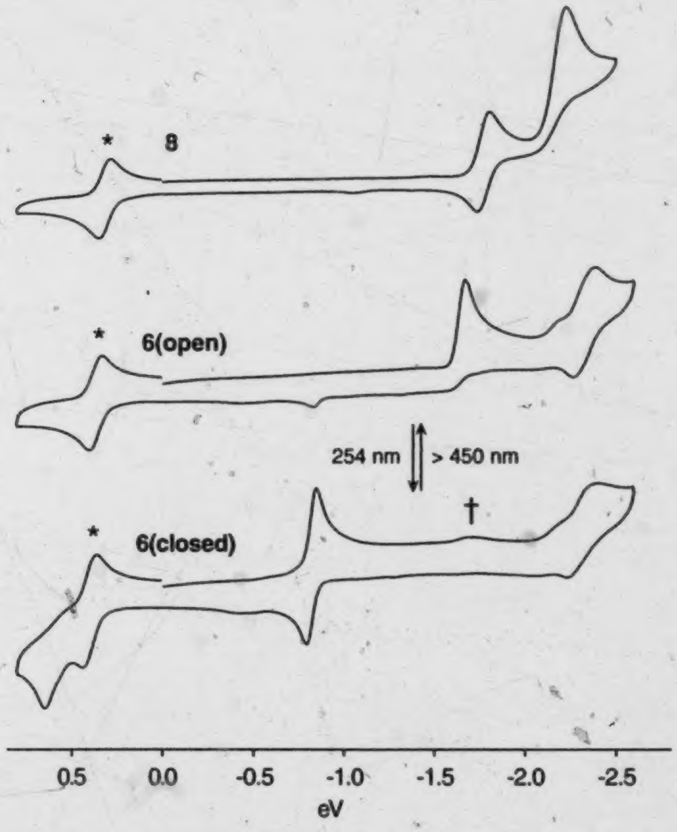

Figure 7. Cyclic voltammograms of **8** and of **6** in its open and closed forms. The closed form was generated by irradiation of ***6(open)*** at 254 nm for 30 min (CH_3CN, 0.1 M n-$Bu_4N^{+}\,{}^{-}BF_4$, scan 100 mVs^{-1}) using a glassy carbon electrode (vs Ag/Ag^{+}). The symbol [*] denotes the ferrocene/ ferrocinium redox couple, [†] denotes residual **6(open)**.

I.6 Conclusion

The types of compounds presented in this chapter are of a basic interest for the development of molecular electronic devices. They represent a new class of dithienylethenes whose photochemical and electrochemical properties can be conveniently modulated by irradiation with light. The electrochemical properties of **6** are well behaved in both its open and closed forms and the large differences between these voltamograms represent the vastly different degrees of conjugation that can be reversibly achieved by photochemical regulation of the central dithienylethene moiety. Future work on this system should involve characterizing the exact nature of both the photophysical and electrochemical properties.

I.7 Experimental

General. All solvents used for the photochemical transformations were thoroughly deoxygenated by bubbling argon through the solution. Standard lamps used for visualizing TLC plates (Spectroline E-series, 470 mW/cm^2) were used to carry out the ring-closing reactions. The ring-opening reactions were carried out using the light of a 150-W tungsten source that was passed through a 458 nm cutoff filter to eliminate higher energy light.

Synthesis of (3), (4) and (5). To a rapidly stirred solution of 2-aminopyridine (55.0 mg, 0.58 mmol) and triethylamine (80.0 mg, 0.79 mmol) in freshly distilled CH_2Cl_2 (20 mL) was added **2** (53 mg, 0.14 mmol) in small portions over 1 minute. After 1 hour, the solution was washed with 5% HCl (2 x 10 mL) and the CH_2Cl_2 layer dried with Na_2SO_4 and filtered. The solvent was removed under vacuum and the resulting residue was chromatographed through a long column of silica gel (1:1 EtOAc/Hex) affording **3**, **4** and **5**:

5-methyl-(4[2-{2-methyl-5-(carboxylic acid pyridin-2-ylamide)-thiophen-3-yl]-cyclopent-1-enyl)-thiophen-2-carboxylic acid pyridin-2-yl-amide (3). R_f (1:1 EtOAc/Hex) = 0.6; Yield 36%; mp 231-233°C; ^1H NMR (300 MHz, $CDCl_3$) δ 8.62 (bs, 2 H), 8.27 (d, *J*=8 Hz, 2H), 8.22 (d, *J*=5 Hz, 2H), 7.71 (m, 2H), 7.41 (s, 2H), 7.02 (dd, *J*=8, 5 Hz, 2H), 2.78 (t, *J*=8 Hz, 4H), 2.07 (m, *J*=8 Hz, 2H), 1.96 (s, 6H); ^{13}C NMR (75 MHz, $CDCl_3$) δ 159.9, 151.4, 147.5, 142.1, 138.7, 136.8, 134.9, 134.5, 130.3, 119.8, 114.4, 38.6, 22.9, 14.9; IR (μscope) υ 3332, 3107, 3067, 3001, 2952, 2920, 2840, 1703, 1658, 1620, 1594, 1574, 1524, 1433, 1310, 1268, 1235 cm^{-1}; HRMS (EI) Calcd for M^+ ($C_{27}H_{24}N_4O_2S_2$) 500.1341. Found: 500.1352.

Synthesis of 3(closed). Photochrome **3** (1 mg) was dissolved in CD_3CN (1 mL) and the resulting solution placed in an NMR tube. The tube was irradiated for 6 minutes at 254 nm. No attempt was made to isolate **3(closed)**. ^1H NMR (300 MHz, CD_3CN) δ 8.68 (bs, 2 H), 8.31 (d, *J*=8 Hz, 2H), 8.16 (d, *J*=5 Hz, 2H), 7.76 (m, 2H), 7.08 (dd, *J*=8, 5 Hz, 2H), 6.88 (s, 2H), 2.45 (t, *J*=8 Hz, 4H), 2.07 (m, *J*=8 Hz, 2H), 1.99 (s, 6H).

macrocycle (4). The eluted fractions from the column (1:1 EtOAc/Hex) **3** were allowed to slowly evaporate affording crystals suitable of X-ray quality analysis. Yield 6%.

Alternate synthesis of 4. A mixture of **3** (20 mg, 0.04 mmol) and **2** (15 mg, 0.04 mmol) and NaH (12 mg) in dry benzene (10 mL) was refluxed under an atmosphere of argon. After 3 days H_2O (10 mL) was added to the mixture, the layers were then separated and the benzene layer dried with Na_2SO_4 and filtered. The benzene was removed under vacuum affording a white residue that was further triturated with CH_3CN affording 30 mg of the pure macrocycle. Yield 93%; R_f (1:1 EtOAc/Hex) 0.7; ^1H NMR (300 MHz, $CDCl_3$) δ 8.44 (ddd, *J*=5, 2, 1 Hz, 2 H), 7.63 (ddd, *J*=7, 5, 2 Hz, 2H), 7.15 (dd, *J*=7, 5 Hz, 2H), 7.04 (dd, *J*=8, 1 Hz, 4H), 6.75 (s, 4H) 2.41 (m, 8H), 2.11 (s, 12H), 1.85 (m, 4H); ^{13}C NMR (75 MHz, $CDCl_3$) δ 165.7, 154.9, 149.5, 145.1, 138.2, 135.7, 7, 134.3, 134.1, 133.4, 130.1, 123.1, 122.5, 37.8, 22.9, 15.5; IR ($CHCl_3$, cast) υ 2922, 1675, 1586, 1431, 1288, 1266, 1252, 1200, 1168, 1147, 1112, 1088 cm^{-1}; HRMS (ES) Calcd for $[M+Na]^+$ ($C_{44}H_{36}N_4O_4S_4Na$) 835.1517. Found: 835.1522.

***bis*-switch (5).** R_f (1:1 EtOAc/Hex) = 0.41; Yield 12%; ^{1}H NMR (300 MHz, $CDCl_3$) δ 8.70 (bs, 2 H), 8.38 (d, *J*=5 Hz, 1H), 8.28 (d, *J*=9 Hz, 2H), 8.23 (d, *J*=4 Hz, 4H), 7.71 (m, 3H), 7.33 (s, 2H), 7.18 (s, 2H), 7.15 (m, 2H), 7.03 (m, 2H), 2.69 (m, 8H), 2.00 (m, 4H), 1.90 (s, 6H), 1.86 (s, 6H); ^{13}C NMR (75 MHz, $CDCl_3$) δ 165.4, 159.9, 153.8, 151.5, 149.3, 147.7, 144.5, 142.0, 138.6, 138.2, 136.7, 136.6, 135.1, 135.0, 134.8, 134.6, 134.3, 130.1, 122.4, 121.9, 119.8, 114.4, 38.6, 38.5, 22.8, 14.9, 14.8; IR ($CHCl_3$, cast) υ 2950, 2843, 1664, 1575, 1514, 1431, 1303, 1231, 1150 cm^{-1}; HRMS (ES) Calcd for $[M+H]^+$ ($C_{49}H_{43}N_6O_4S_4$) 907.2229. Found: 907.2232.

Synthesis of 5(closed). Photochrome **5** (1 mg) was dissolved in CD_3CN (1 mL) and the resulting solution placed in an NMR tube. The tube was irradiated for 15 minutes at 254 nm. No attempt was made to isolate **5(closed)**. ^{1}H NMR (300 MHz, $CDCl_3$) δ 8.80 (bs, 1 H), δ 8.67 (bs, 1 H), 8.36 (d, *J*=4 Hz, 1H), 8.30 (d, *J*=4 Hz, 2H), 8.15 (d, *J*=8 Hz, 1H), 8.09 (d, *J*=8 Hz, 1H), 7.84-7.72 (m, 3H), 7.55 (s, 1H), 7.30-7.25 (m, 2H), 7.13 (s, 2H), 7.12-7.05 (m, 2H), 6.83, (s, 2H), 6.75 (s, 2H), 2.75 (m, 4H), 2.40 (m, 4H), 2.06 (s, 3H), 2.00 (m, 4H), 1.89 (s, 6H), 1.80 (s, 3H).

Synthesis of 5-methyl-(4[2-{2-methyl-5-(thiophene carboxylic acid [5-methyl-thiophene-carbonyl)-pyridin-2-yl-amide)-thiophen-3-yl]-cyclopent-1-enyl)-thiophen-2-carboxylic acid-5-methyl-thiophene-2-carbonyl)-pyridin-2-yl-amide (6). To a solution of 3 (9.0 mg, 0.02 mmol) and triethylamine (18 mg, 0.2 mmol) in dry benzene (10 mL) was added 2-carbonyl chloride-5-methylthiophene (15 mg, 0.1 mmol). After 4 hours at reflux the solvent was removed by evaporation and the resulting residue was purified through silica gel (1:1 EtOAc/Hex) affording 12 mg of a white solid. Yield 93%; ^{1}H NMR (300 MHz, CD_3CN) δ 8.33 (d, *J*=5 Hz, 2 H), 7.81 (ddd, *J*=7, 5, 2 Hz, 2H), 7.33 (d, *J*=8 Hz, 2H), 7.29-7.24 (m, 4H), 7.08 (s, 2H), 6.75 (dd, *J*=4, 1 Hz, 2H), 2.61 (t, *J*=8 Hz, 4H), 2.46 (s, 6H), 1.84 (s, 6H); ^{13}C NMR (75 MHz, $CDCl_3$) δ 165.5, 165.4, 153.8, 149.8, 149.3, 144.4, 138.3, 136.6, 136.1, 134.9, 134.7, 134.6, 134.5, 126.7, 122.3, 121.8, 38.5, 22.7, 15.9, 14.8; IR ($CHCl_3$, cast) υ 3056, 2953, 2920, 2845, 1675, 1586, 1533, 1451, 1433, 1337, 1286, 1249, 1167, 1150, 1119, 1088 cm^{-1}; HRMS (ES) Calcd for $[M+Na]^+$ ($C_{39}H_{32}N_4O_4S_4Na$) 771.1204. Found: 771.1195.

Synthesis of 6(closed). Photochrome **6** (0.5 mg) was dissolved in CD_3CN (1 mL) and the resulting solution placed in an NMR tube. The tube was irradiated for 10 minutes at 254 nm. No attempt was made to isolate **6(closed)**. ^1H NMR (300 MHz, CD_3CN) δ 8.39 (d, J=5 Hz, 2 H), 7.81 (ddd, J=7, 5, 2 Hz, 2H), 7.35-7.27 (m, 6H), 6.79 (dd, J=4, 1 Hz, 2H), 6.52 (s, 2H), 2.48 (s, 6H), 2.33 (t, J=8 Hz, 4H), 1.70 (s, 6H).

Synthesis of control compounds (7) and (8). To a rapidly stirred cool solution (0°C) of 2-aminopyridine (115 mg, 1.3 mmol) and triethylamine (800 mg, 8 mmol) in freshly distilled CH_2Cl_2 (20 mL) was added a CH_2Cl_2 solution (5 mL) of 2-carbonyl chloride-5-methylthiophene (250 mg, 1.6 mmol) dropwise over 10 minutes. The solution was allowed to warm to ambient temperature and stirred for 1 hour. The mixture was washed with 5% HCl (2 x 10 mL) and the CH_2Cl_2 layer dried with Na_2SO_4 and filtered. The solvent was removed by evaporation and the resulting residue was chromatographed through a long column of silica gel (1:4 EtOAc/Hex) affording:

5 methyl-thiophene-2-carboxylic acid pyridin-2-yl-amide (7). Yellow solid. R_f (1:4 EtOAc/Hex) = 0.6; Yield 14 %; mp 89-93°C; ^1H NMR (300 MHz, CD_2Cl_2) δ 8.34 (bs, 1 H), 8.28 (d, J=5 Hz, 1H), 8.24 (d, J=8 Hz, 1H), 7.76-7.71 (m, 1H), 7.48, (d, J=4 Hz, 1H)

7.06 (ddd, J=8, 5, 1 Hz, 1H), 6.83 (dd, J=4, 1 Hz, 1H), 2.54 (s, 3H); ^{13}C NMR (75 MHz, $CDCl_3$) δ 160.0, 151.4, 147.7, 147.3, 138.6, 136.2, 129.4, 126.5, 119.8, 114.3, 15.8; IR ($CHCl_3$, cast) υ 1660, 1594, 1576, 1542, 1515, 1450, 1431, 1335, 1304, 1267, 1240, 1084 cm^{-1}; HRMS (EI) Calcd for M^+ ($C_{11}H_{10}N_2OS$) 218.0514. Found 218.0513 (31%), 185.0715 (20%), 125.0064 (100%).

5-methyl-thiophene-2-carboxylic acid (5-methyl-thiophene-carbonyl)-pyridin-2-yl-amide (8). Recrystallized from CH_2Cl_2 affording yellow platelets. R_f (1:4 EtOAc/Hex) = 0.4; Yield 24 %; mp 143-144°C; ^{1}H NMR (300 MHz, CD_2Cl_2) δ 8.40 (d, J=5 Hz, 1H), 7.80-7.74 (m, 1H), 7.31 (m, 3H), 7.24-7.19 (m, 1H), 6.70 (d, J=4 Hz, 2H), 2.29 (s, 6H); ^{13}C NMR (75 MHz, $CDCl_3$) δ 165.7, 153.9, 149.7, 149.3, 138.2, 136.0, 134.5, 126.6, 122.3, 121.8, 15.9; IR ($CHCl_3$, cast) υ 1676, 1586, 1571, 1451, 1432, 1336, 1287, 1266, 1247, 1121, 1089, 1072, 1050 cm^{-1}; HRMS (EI) Calcd for M^+ ($C_{17}H_{14}N_2O_2S_2$) 342.0497. Found: 342.0505 (13%), 185.0721 (28%), 125.0065 (100%)

X-ray Crystallographic Analysis

5-methyl-(4[2-{2-methyl-5-carboxylic acid}-thiophen-3-yl]-cyclopent-1-enyl)-thiophen-2-carboxylic acid (1). Crystals of **1** were grown by layering a MeOH solution of the photochrome with H_2O. $C_{17}H_{16}O_4S_2$ (M=348.42); crystal dimensions 0.55 × 0.24 × 0.08 mm, monoclinic, space group *C2/c* (No. 15) $a = 12.4887(16)$, $b = 8.0738(10)$, and $c = 16.554(2)$ Å, $V = 1628.1(4)$ Å^3, $\rho_{calc} = 1.421$ g cm^{-3}, $\mu = 0.344$ mm^{-1}, $T = -80°C$; Bruker P4/RA/SMART 1000 CCD; Mo Kα radiation ($\lambda = 0.71073$ Å), scan method ω; 4209 data measured; 1546 independent reflections. The crystal structure was solved using direct methods (SHELXL-86) and refined by full-matrix least squares on F^2 (SHELXL-93). Final $R_1(F) = 0.0378$ (for 1302 data with $F_0^2 \geq 2\sigma(F_0^2)$), $wR_2(F^2) = 0.1122$ (on all 4209 unique data), and S = 1.075 for 112 parameters varied. The carboxylic acid hydrogen was found to be disordered over two sites, being alternately bound to O4 and O5. The positions were generated using the following restraints: d(O1-H1O) = (d(O2-H2O) = 0.84 Å; d(H1O···O2") = d(H2O···O1") = 1.78 Å (doubly-primed atoms are related to unprimed ones via the crystallographic inversion center (1/2, 0, 0). The largest difference peak and hole in the final difference Fourier map had intensities of 0.338 and -0.227 e Å^{-3}.

[3(closed)]. Crystals of **3(closed)** were grown by diffusion of pentane into a benzene solution of the photochrome. $C_{27}H_{24}N_4O_2S_2 \bullet 0.75C_6H_6$ (M=559.20); crystal dimensions 0.20 × 0.18 × 0.16 mm, orthorhombic, space group *Pccn* (No. 56) $a = 12.3133(16)$, $b =$

19.747(3), and $c = 25.439(4)$ Å, $V = 6185.4(16)$ Å^3, $\rho_{calc} = 1.201$ g cm^{-3}, $\mu = 0.205$ mm^{-1}, $T = -80$°C; Bruker P4/RA/SMART 1000 CCD; Mo Kα radiation ($\lambda = 0.71073$ Å), scan method ω; 29038 data measured; 6345 independent reflections. The crystal structure was solved using direct methods (SHELXL-86) and refined by full-matrix least squares on F^2 (SHELXL-93). All hydrogens were generated in idealized positions according to the sp^2 or sp^3-hybridized geometries of their attached carbon atoms. Final $R_1(F) = 0.0929$ (for 2494 data with $F_0^2 \geq 2\sigma(F_0^2)$), $wR_2(F^2) = 0.3168$ (on all 6345 unique data), and S = 0.955 for 392 parameters varied. The largest difference peak and hole in the final difference Fourier map had intensities of 1.174 and -0.405 e Å^{-3}.

Macrocycle (4). Crystals of **4** were grown by allowing the collected fractions containing **4** from the column described in the synthesis of **(3)**, **(4)** and **(5)** to slowly evaporate. $C_{44}H_{36}N_4O_4S_4$ (M=813.01); crystal dimensions 0.21 × 0.15 × 0.09 mm, monoclinic, space group *C2/c* (No. 15) $a = 25.588(2)$, $b = 11.0282(10)$, and $c = 14.2192(11)$ Å, $V = 3948.2(6)$ Å^3, $\rho_{calc} = 1.368$ g cm^{-3}, $\mu = 0.290$ mm^{-1}, $T = -80$°C; Bruker P4/RA/SMART 1000 CCD; Mo Kα radiation ($\lambda = 0.71073$ Å), scan method ω; 9616 data measured; 4040 independent reflections. The crystal structure was solved using direct methods (SHELXL-86) and refined by full-matrix least squares on F^2 (SHELXL-93). Final $R_1(F)$

= 0.0447 (for 4040 data with $F_0^2 \geq 2\sigma(F_0^2)$), $wR_2(F^2) = 0.1030$ (on all 9616 unique data), and S = 0.909 for 255 parameters varied. The largest difference peak and hole in the final difference Fourier map had intensities of 0.264 and -0.247 e Å^{-3}.

I.8 References

1. Peters A.; Branda, N. R. *Adv. Mater. Opt. Electron.* **2000**, *10*, 254.
2. Kawai, T.; Sasaki, T; Irie, M. *Chem. Commun.* **2001**, 711.
3. (a) Ward, M. D. Chem. Ind. 1996, 568. (b) Tour, J. M.; Wu, R.; Schmm, J. S. *J. Am. Chem. Soc.* **1990**, *112*, 5662.

Appendix II - ITC Data

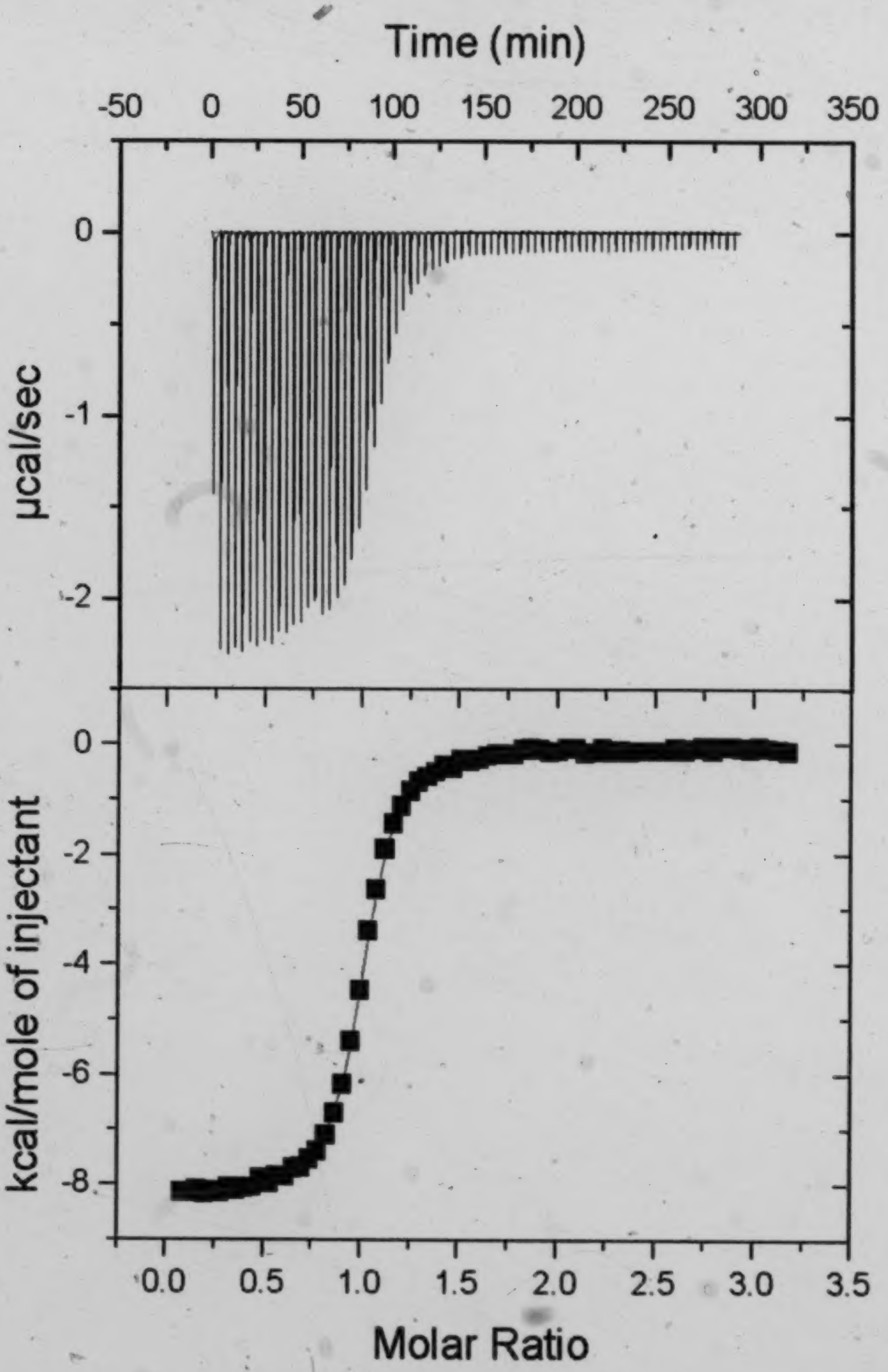
Time (min)
-50
0
50
100
150
200
250
300
350
µcal/sec
0
-1
-2
kcal/mole of injectant
0
-2
-4
-6
-8
0.0
0.5
1.0
1.5
2.0
2.5
3.0
3.5
Molar Ratio

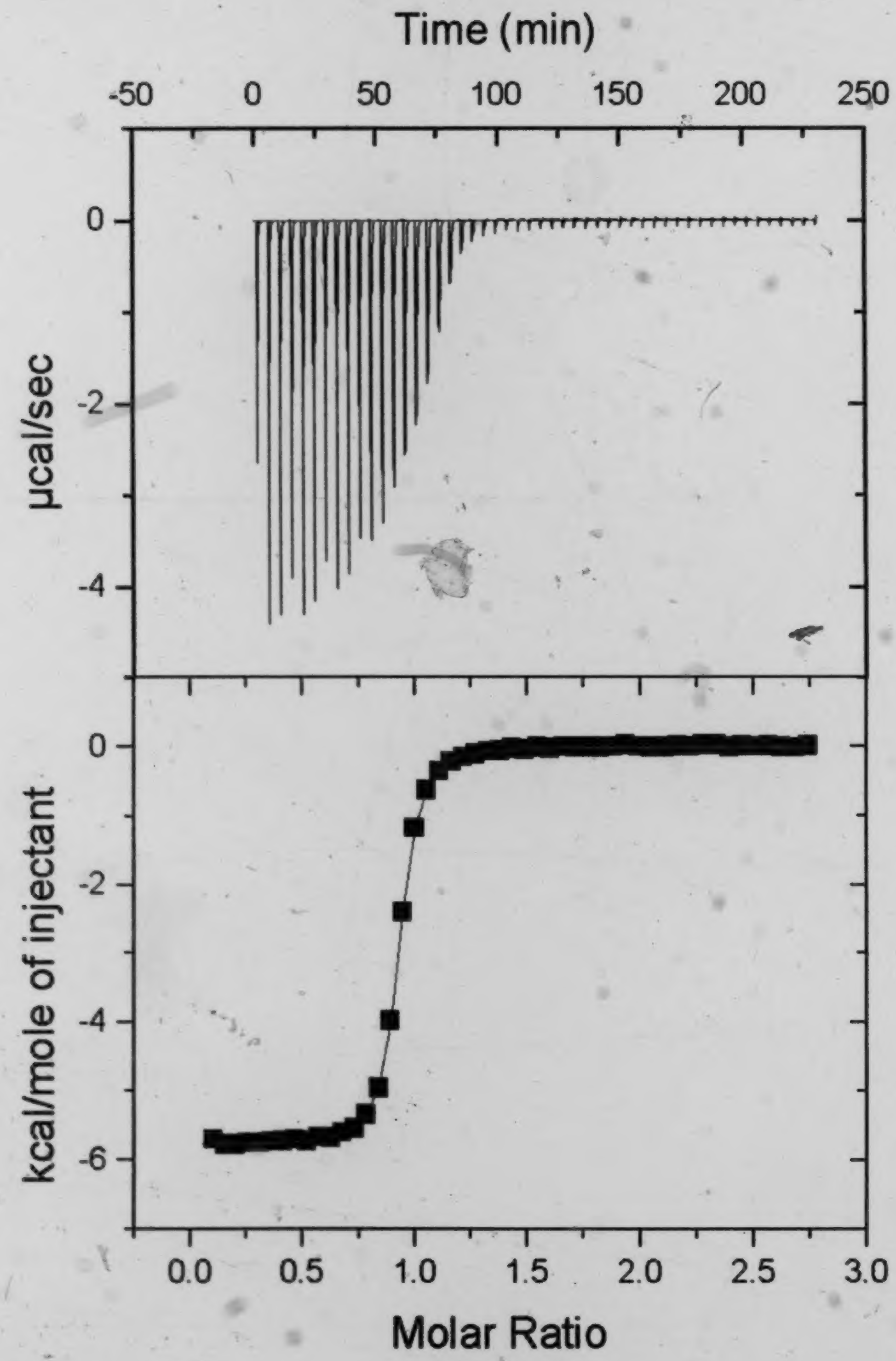
Time (min)
-50
0
50
100
150
200
250
μcal/sec
0
-2
-4
kcal/mole of injectant
0
-2
-4
-6
0.0
0.5
1.0
1.5
2.0
2.5
3.0
Molar Ratio

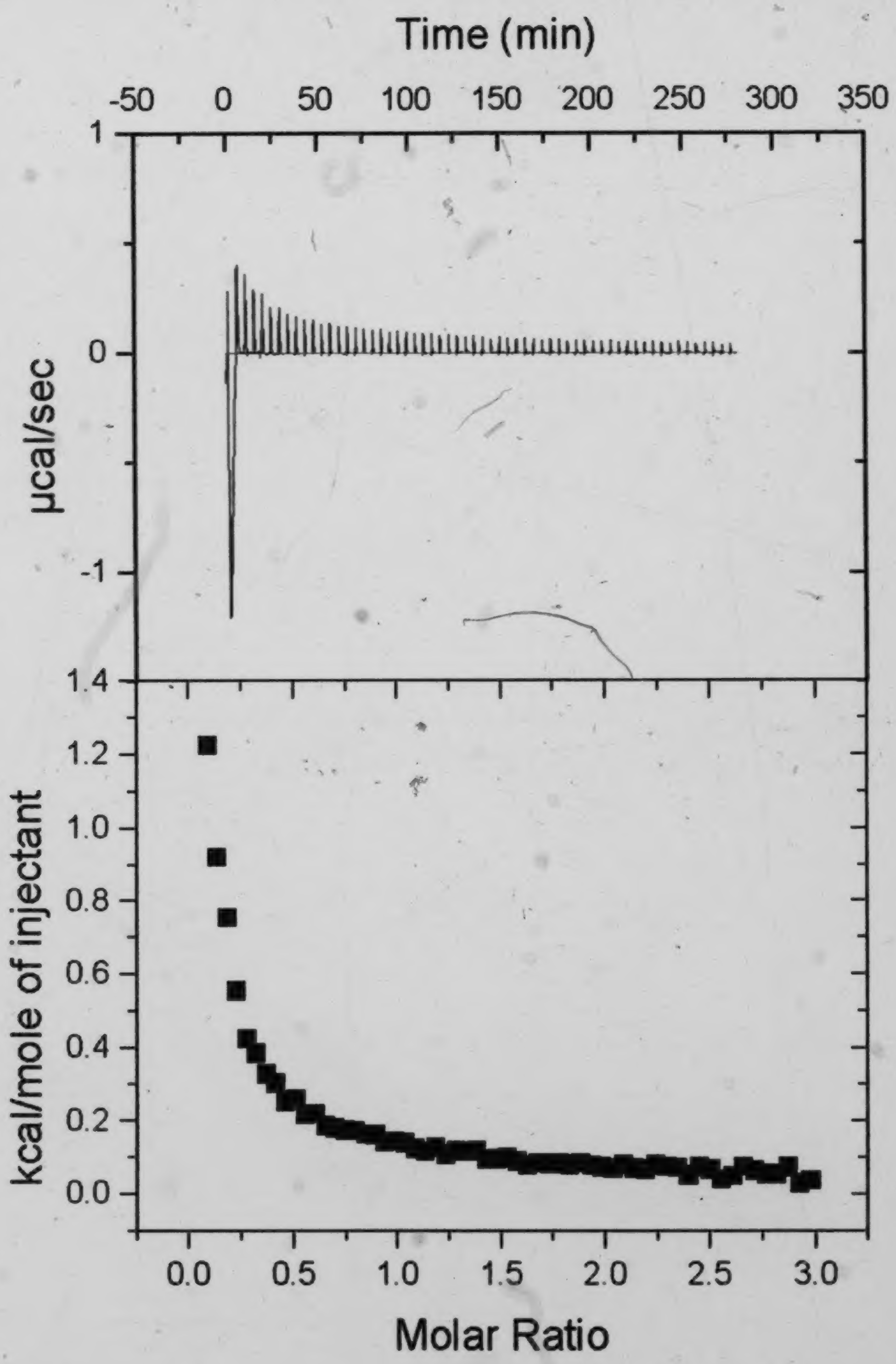
Time (min)
-50
0
50
100
150
200
250
300
350
1
0
-1
µcal/sec
1.4
1.2
1.0
0.8
0.6
0.4
0.2
0.0
kcal/mole of injectant
0.0
0.5
1.0
1.5
2.0
2.5
3.0
Molar Ratio

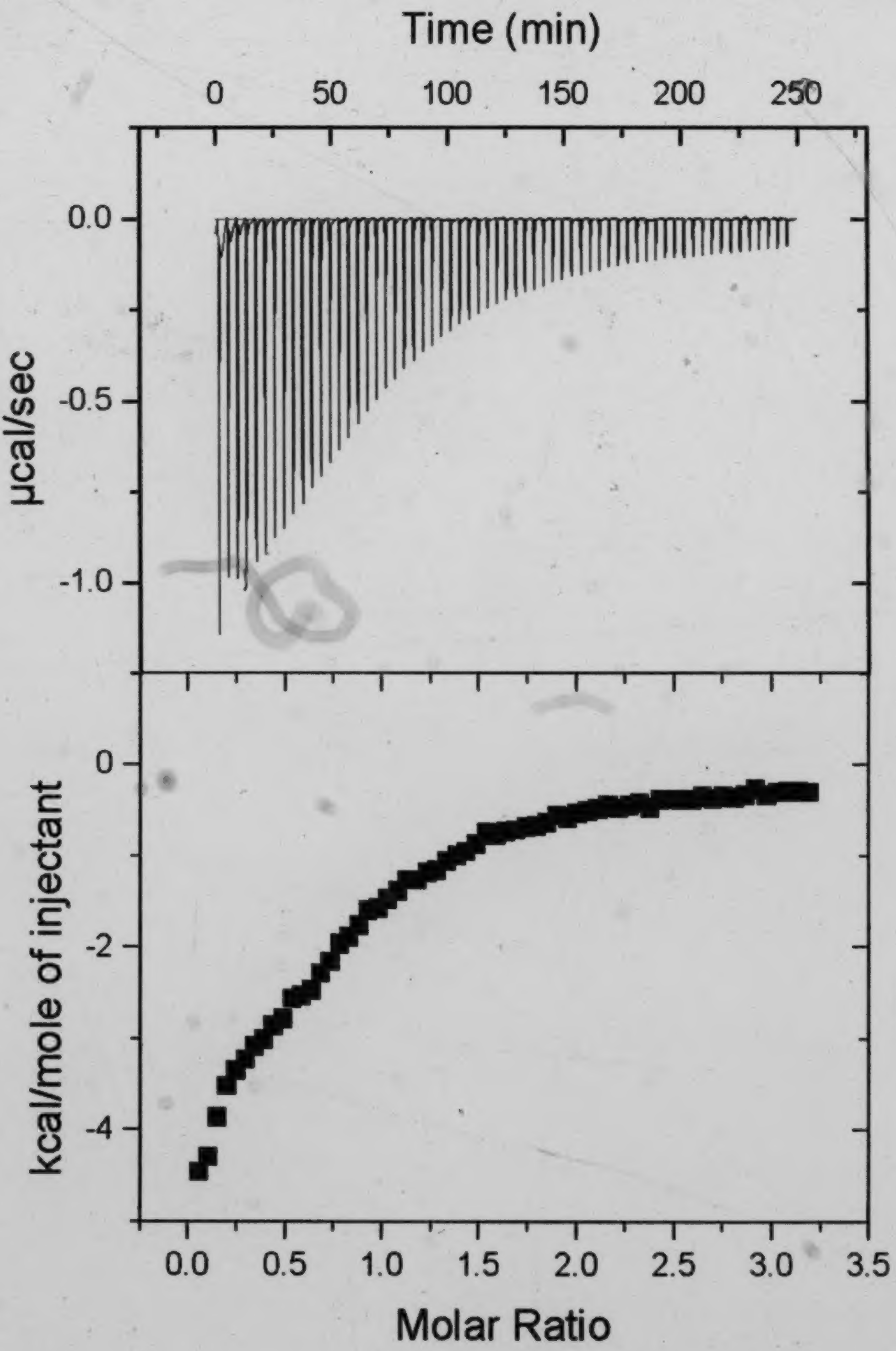
Time (min)
0
50
100
150
200
250
0.0
-0.5
-1.0
µcal/sec
0
-2
-4
kcal/mole of injectant
0.0
0.5
1.0
1.5
2.0
2.5
3.0
3.5
Molar Ratio

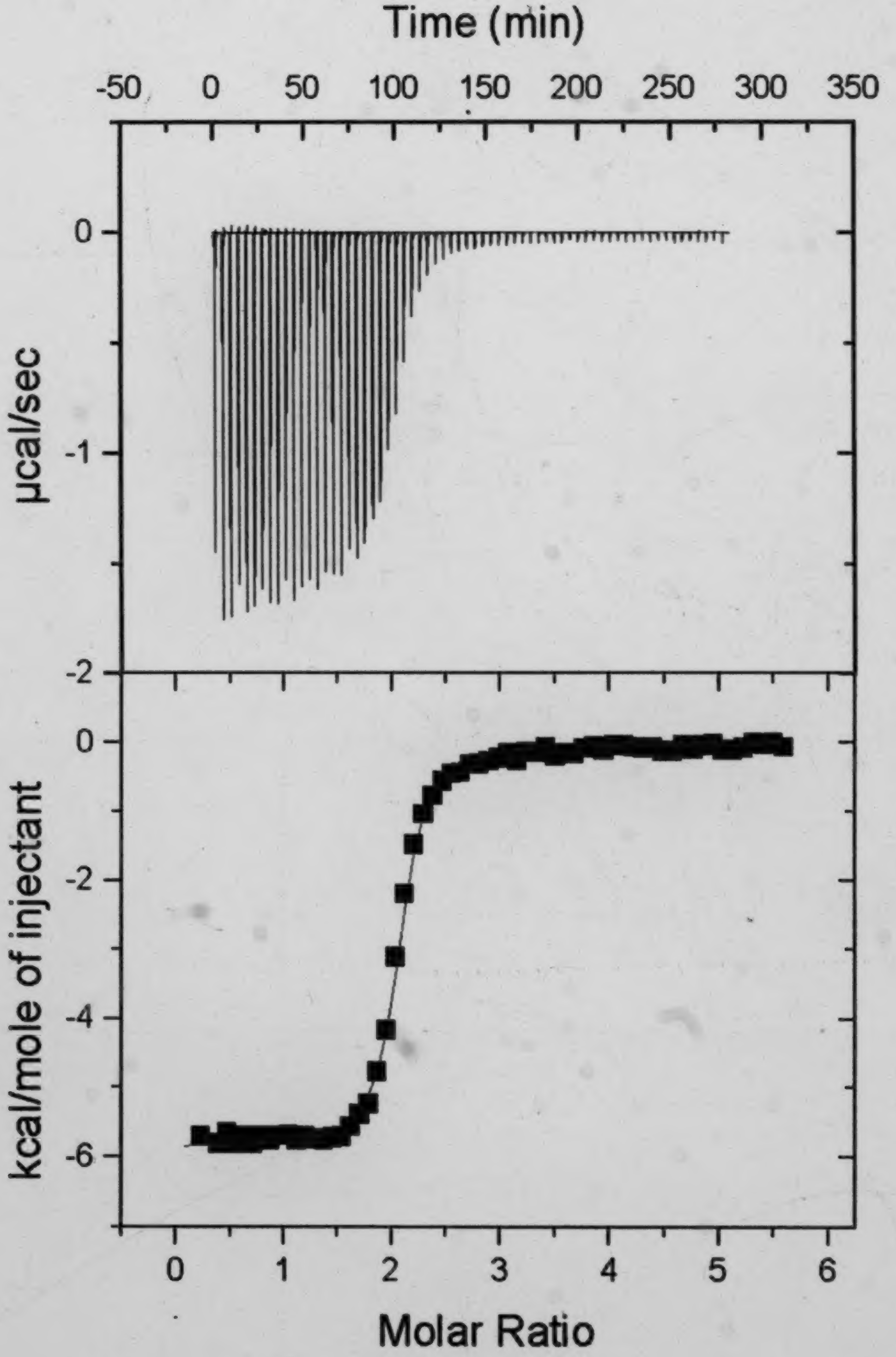
Time (min)
-50
0
50
100
150
200
250
300
350
µcal/sec
0
-1
-2
kcal/mole of injectant
0
-2
-4
-6
0
1
2
3
4
5
6
Molar Ratio

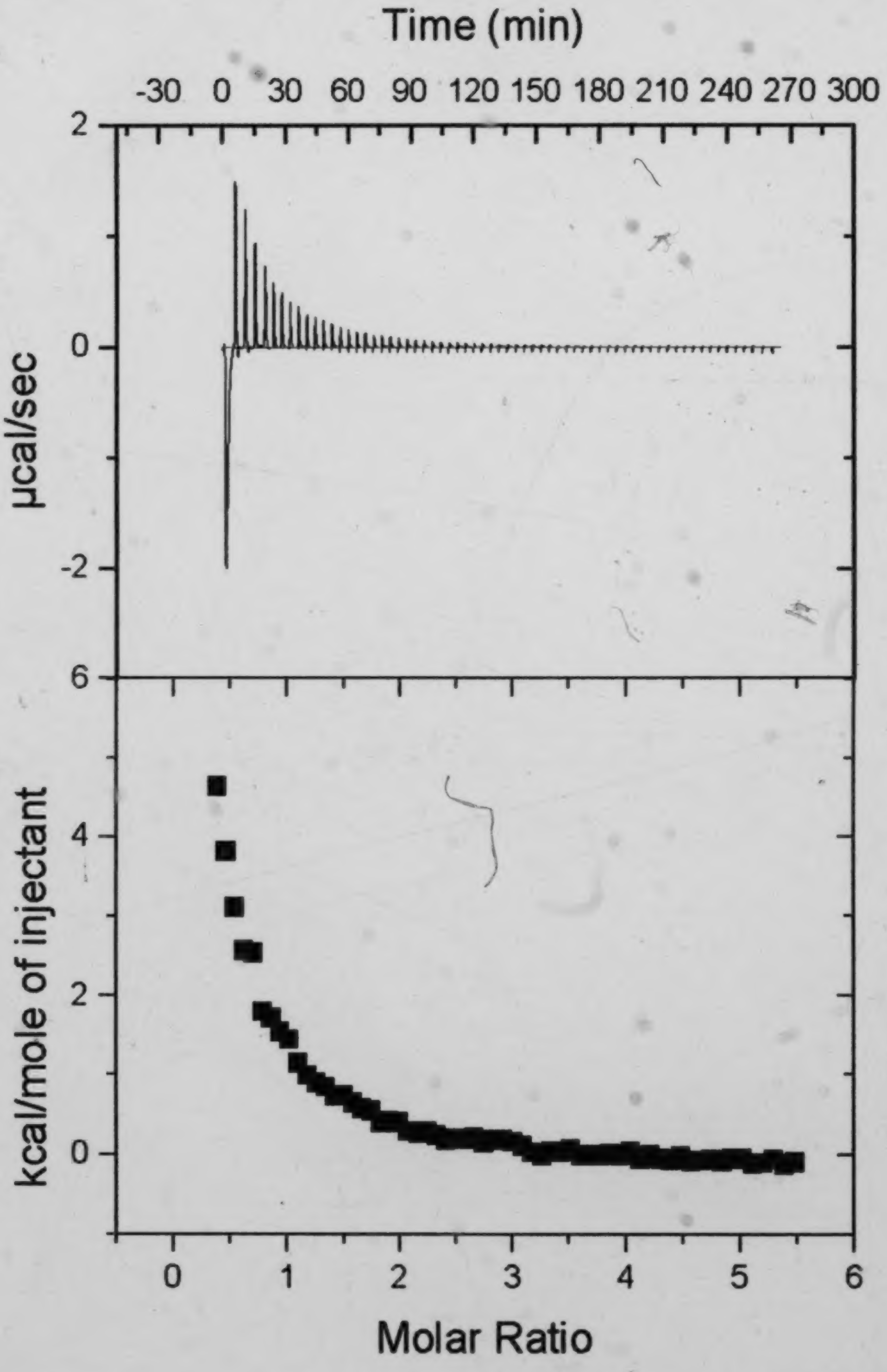
Time (min)
-30
0
30
60
90
120
150
180
210
240
270
300
2
0
-2
µcal/sec
6
4
2
0
kcal/mole of injectant
0
1
2
3
4
5
6
Molar Ratio

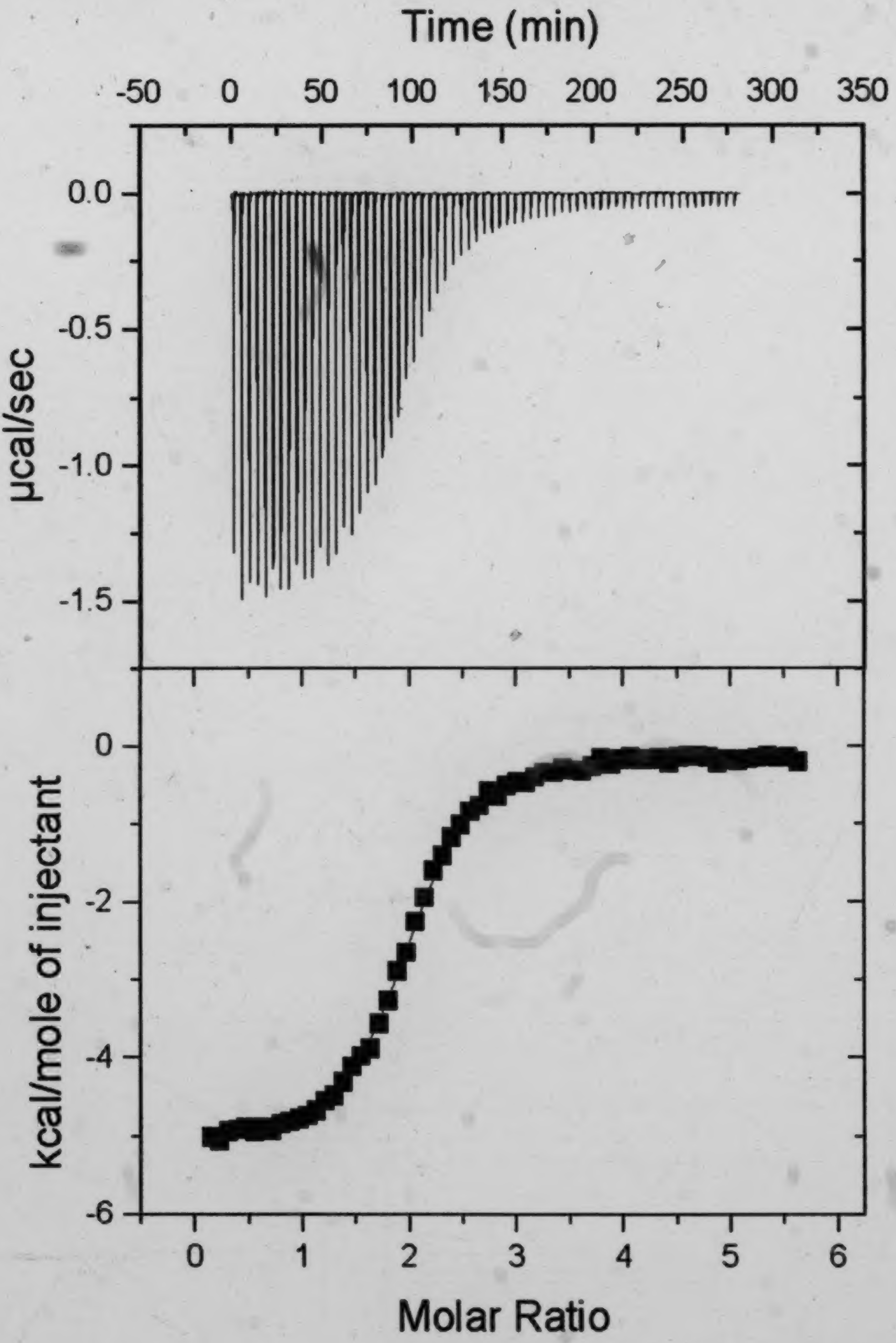
Time (min)
-50
0
50
100
150
200
250
300
350
0.0
-0.5
-1.0
-1.5
µcal/sec
0
-2
-4
-6
kcal/mole of injectant
0
1
2
3
4
5
6
Molar Ratio

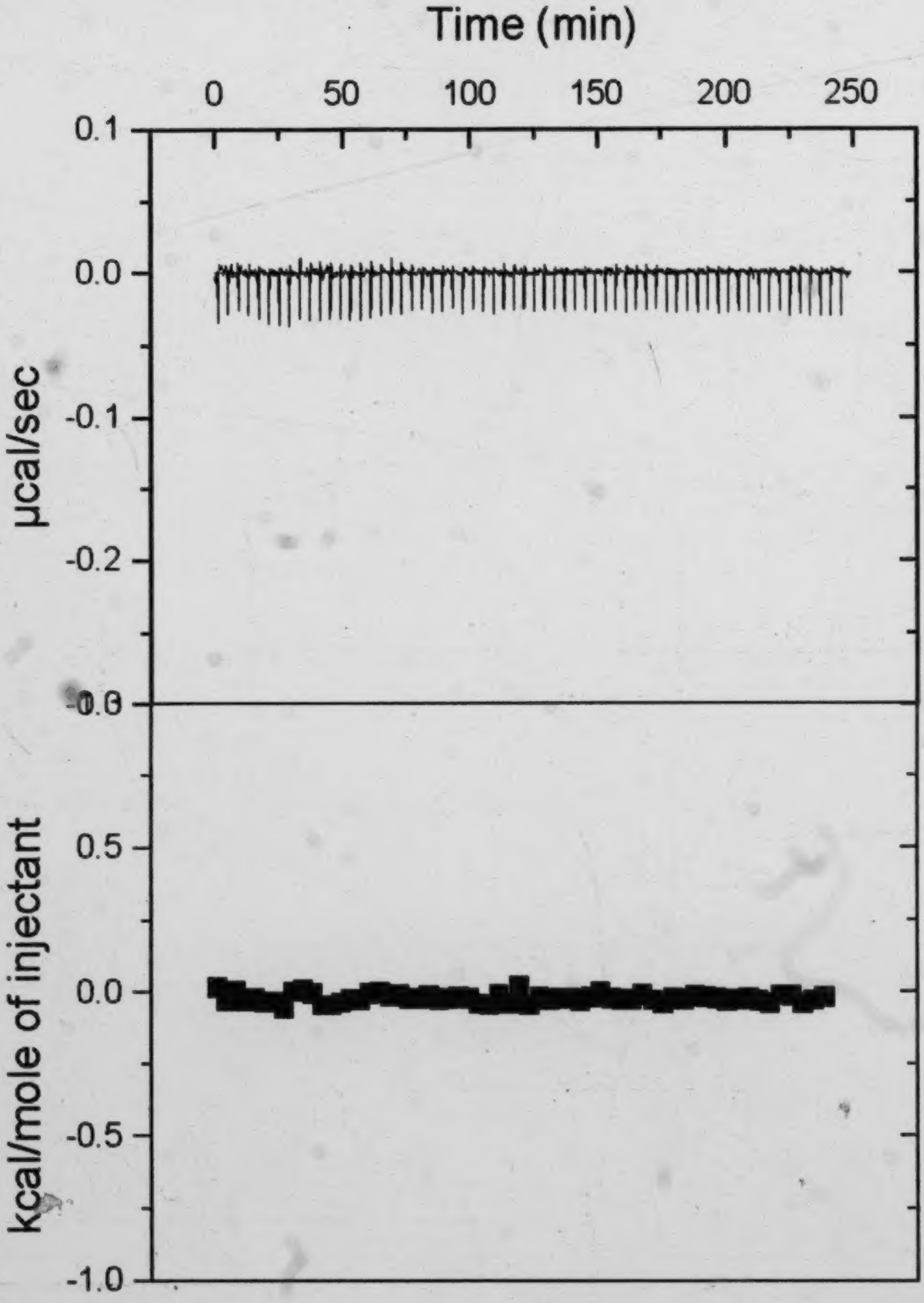
Time (min)
0
50
100
150
200
250
0.1
0.0
-0.1
-0.2
-0.3
µcal/sec
0.5
0.0
-0.5
-1.0
kcal/mole of injectant

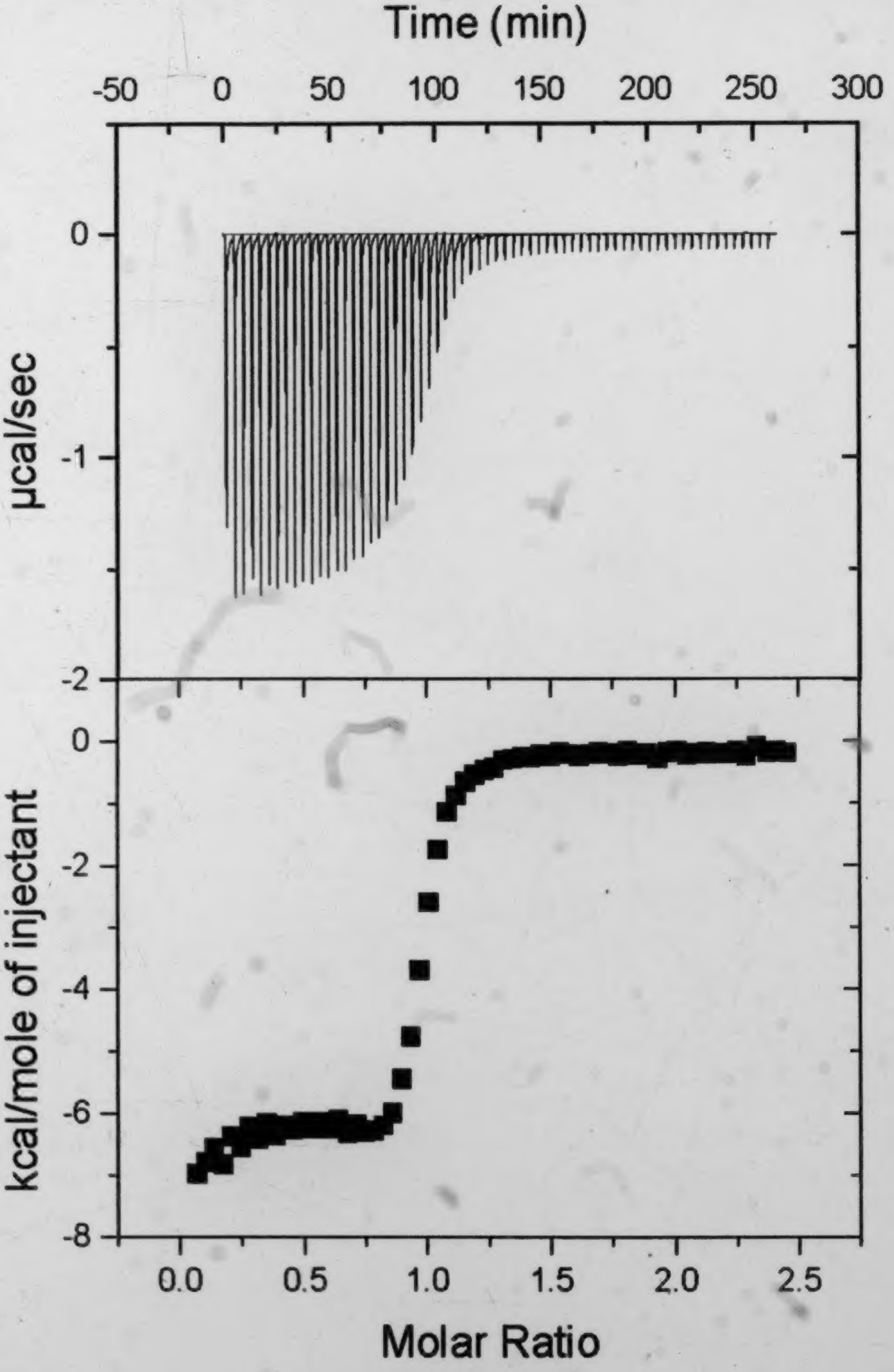
Time (min)
-50
0
50
100
150
200
250
300
µcal/sec
0
-1
-2
kcal/mole of injectant
0
-2
-4
-6
-8
0.0
0.5
1.0
1.5
2.0
2.5
Molar Ratio

Appendix III - ^{1}H NMR Data

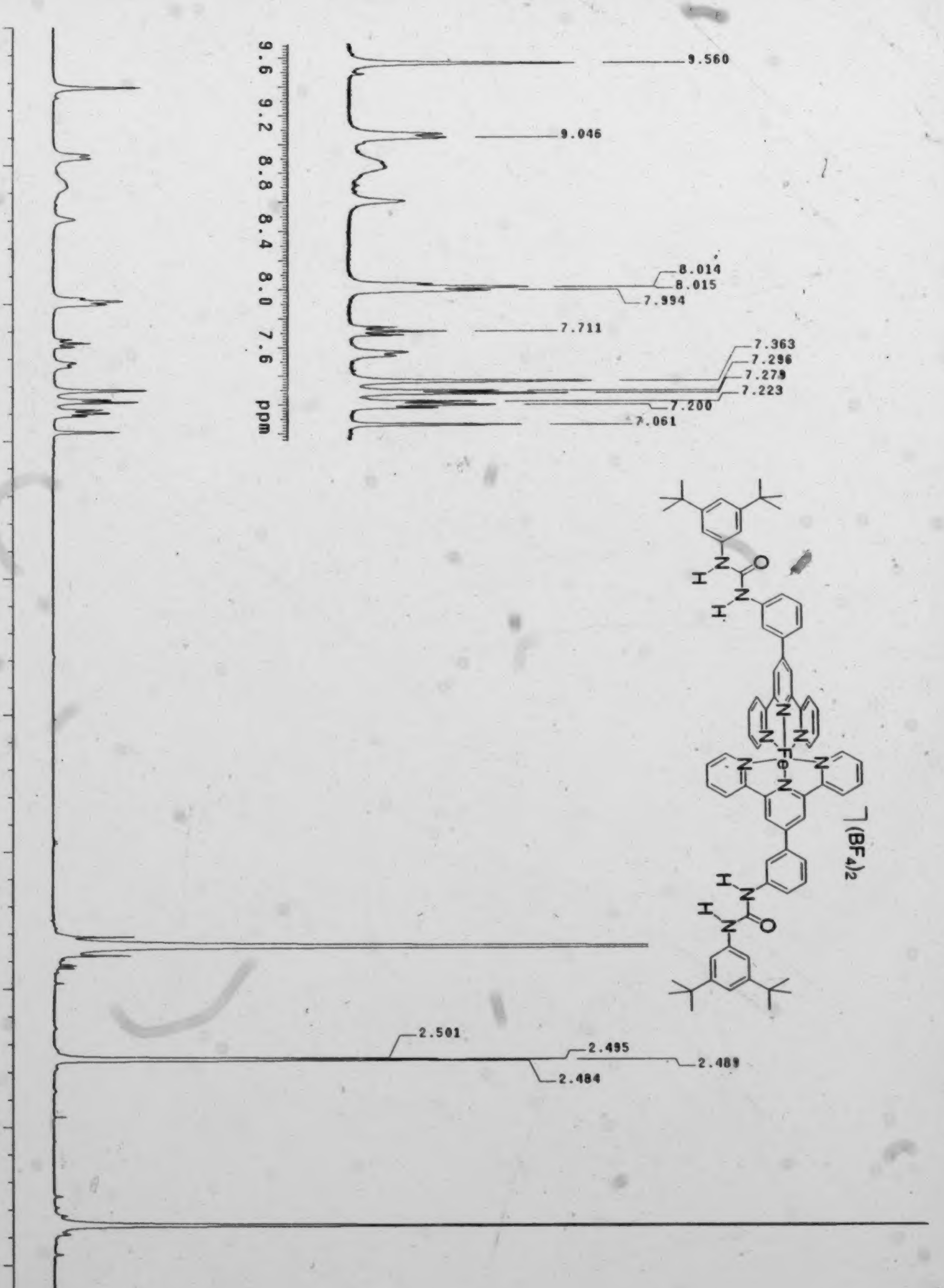
9.560
9.046
8.014
8.015
7.994
7.711
7.363
7.296
7.279
7.223
7.200
7.061
2.501
2.495
2.489
2.484
9.6
9.2
8.8
8.4
8.0
7.6
ppm
9
8
7
6
5
4
3
2
1
ppm
(BF4)2
Fe

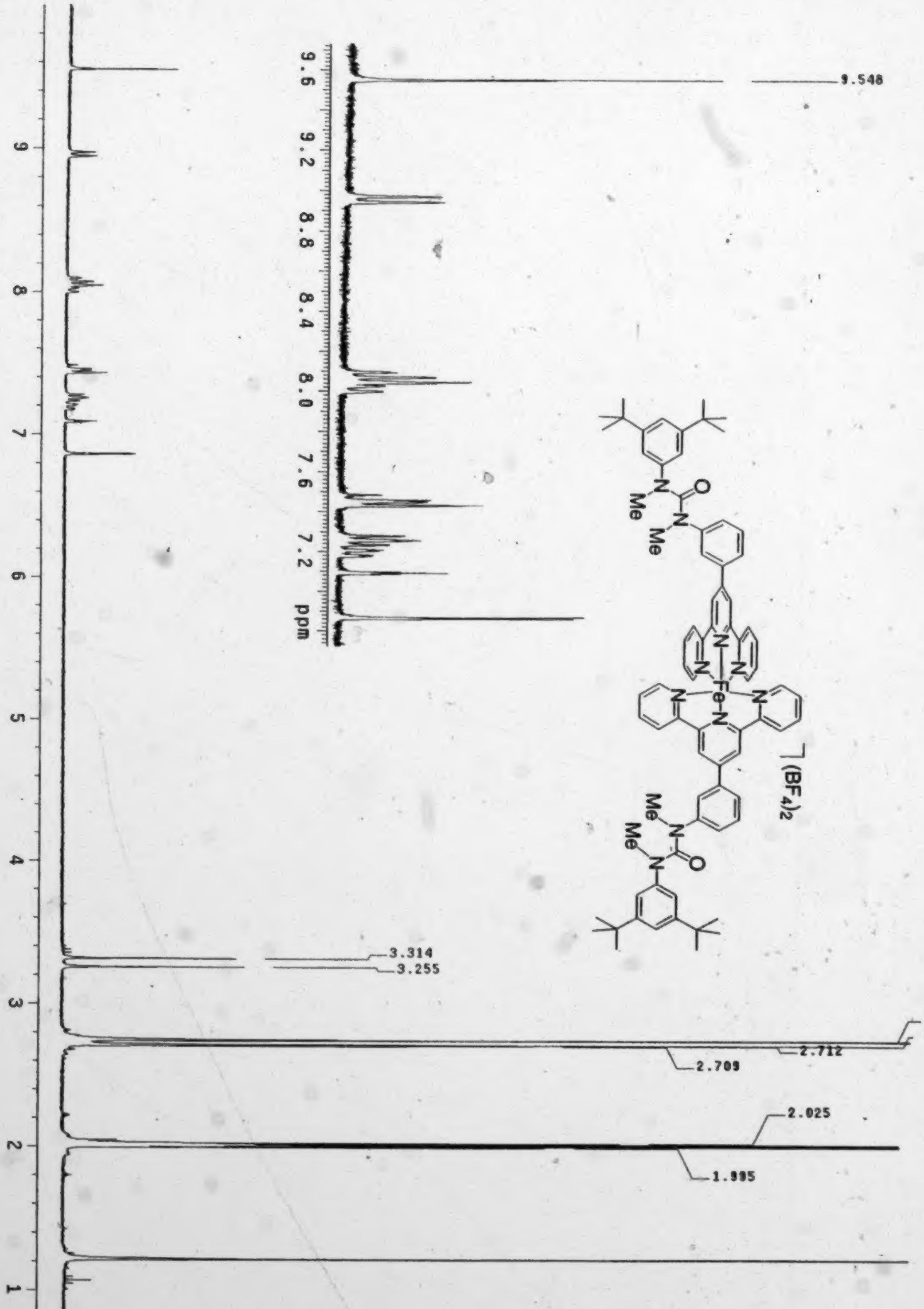
9.548
3.314
3.255
2.712
2.709
2.025
1.995
9.6
9.2
8.8
8.4
8.0
7.6
7.2
ppm
9
8
7
6
5
4
3
2
1
ppm
(BF$_4$)$_2$
Fe
N
O
Me

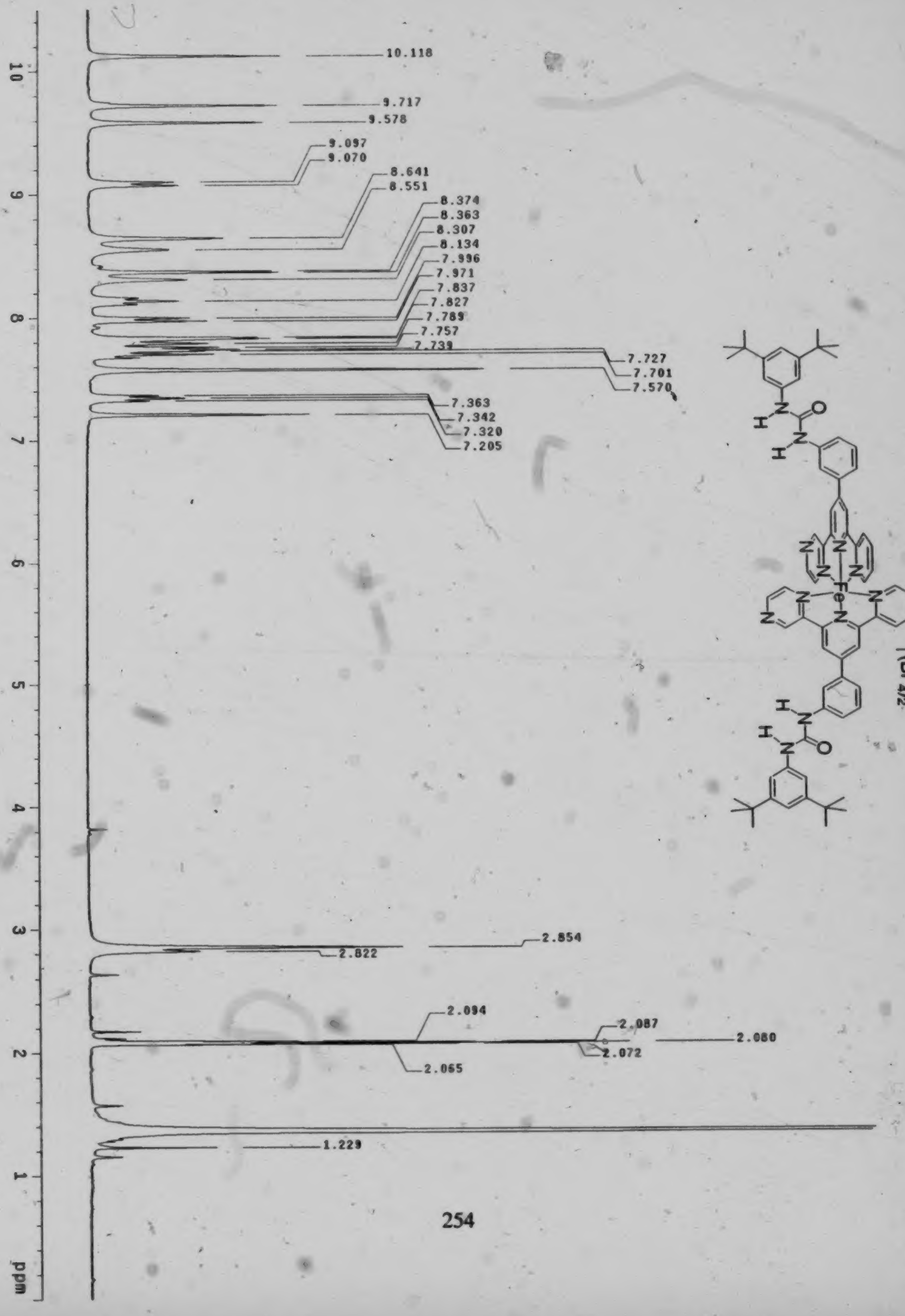
10.118
9.717
9.578
9.097
9.070
8.641
8.551
8.374
8.363
8.307
8.134
7.996
7.971
7.837
7.827
7.789
7.757
7.739
7.727
7.701
7.570
7.363
7.342
7.320
7.205
2.854
2.822
2.094
2.087
2.080
2.072
2.065
1.229
10
9
8
7
6
5
4
3
2
1
ppm
H
N
O
Fe
(BF4)2

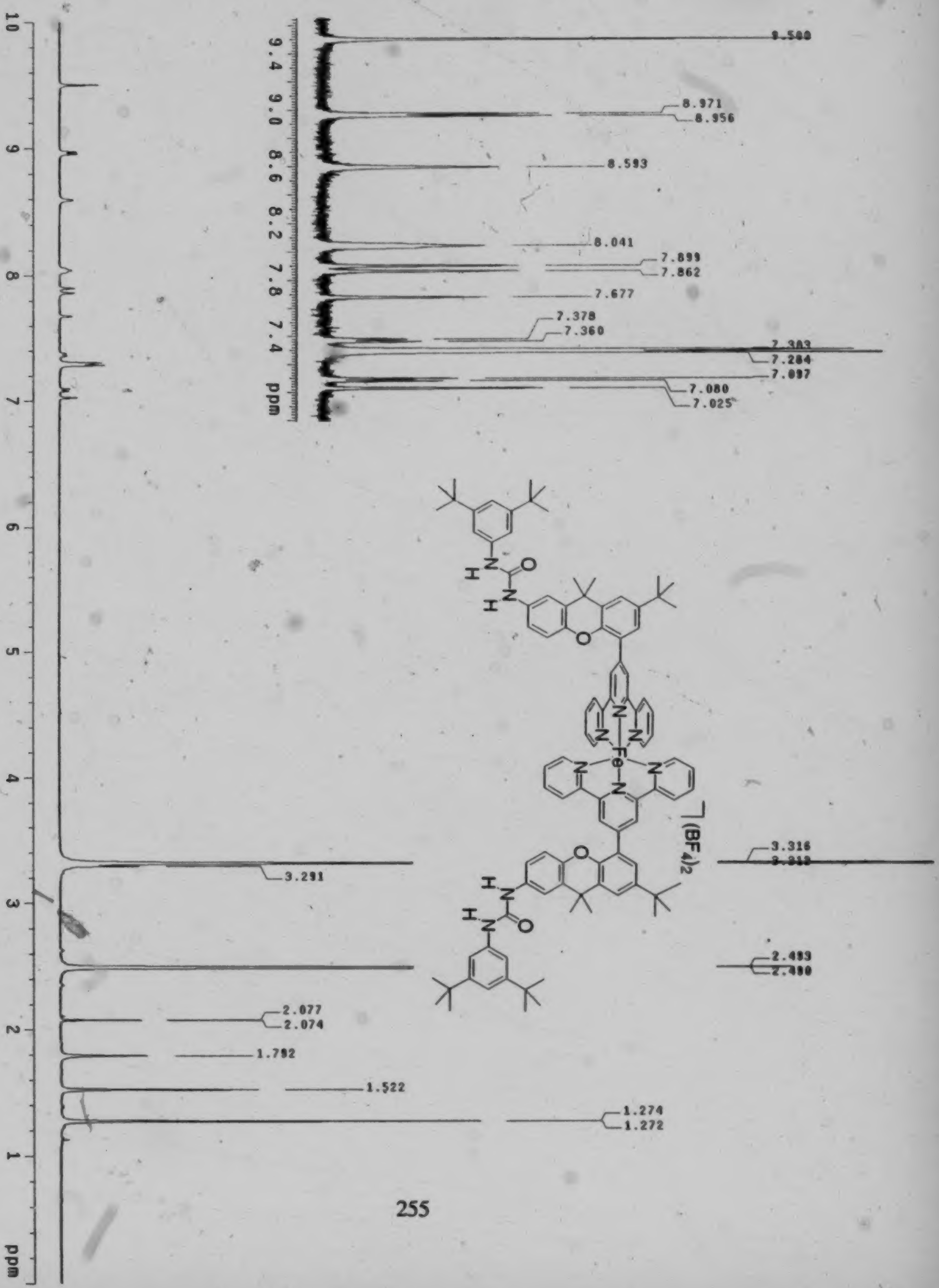

9.500
8.971
8.956
8.593
8.041
7.899
7.862
7.677
7.378
7.360
7.303
7.284
7.097
7.080
7.025
9.4 9.0 8.6 8.2 7.8 7.4 ppm
3.316
3.313
3.291
2.493
2.490
2.077
2.074
1.792
1.522
1.274
1.272
10 9 8 7 6 5 4 3 2 1 ppm
H
N
O
Fe
(BF4)2

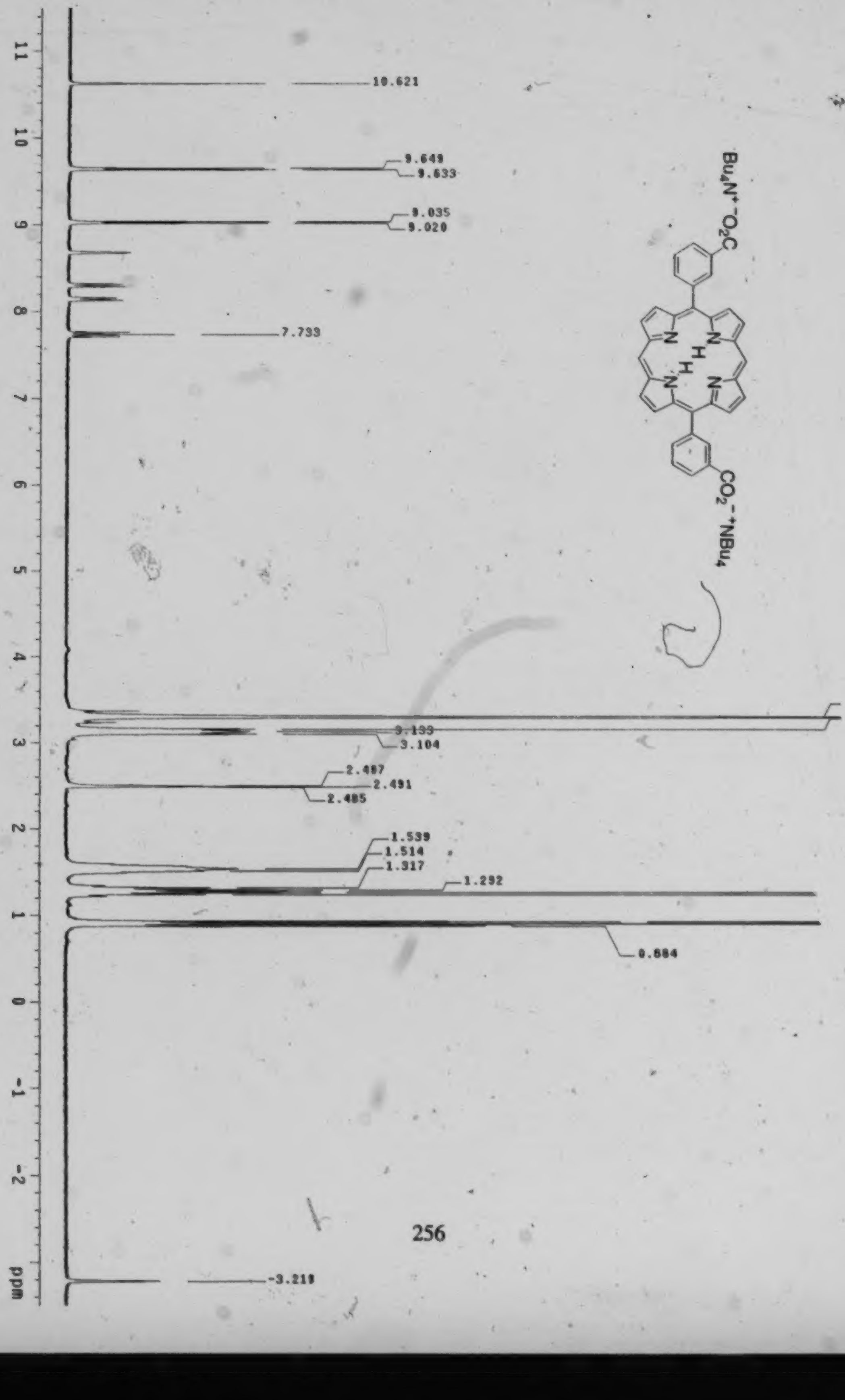
Bu$_4$N$^+$ $^-$O$_2$C
N
H
CO$_2$$^-$ $^+$NBu$_4$
10.621
9.649
9.633
9.035
9.020
7.733
3.133
3.104
2.497
2.491
2.485
1.539
1.514
1.317
1.292
0.884
-3.219
11
10
9
8
7
6
5
4
3
2
1
0
-1
-2
ppm

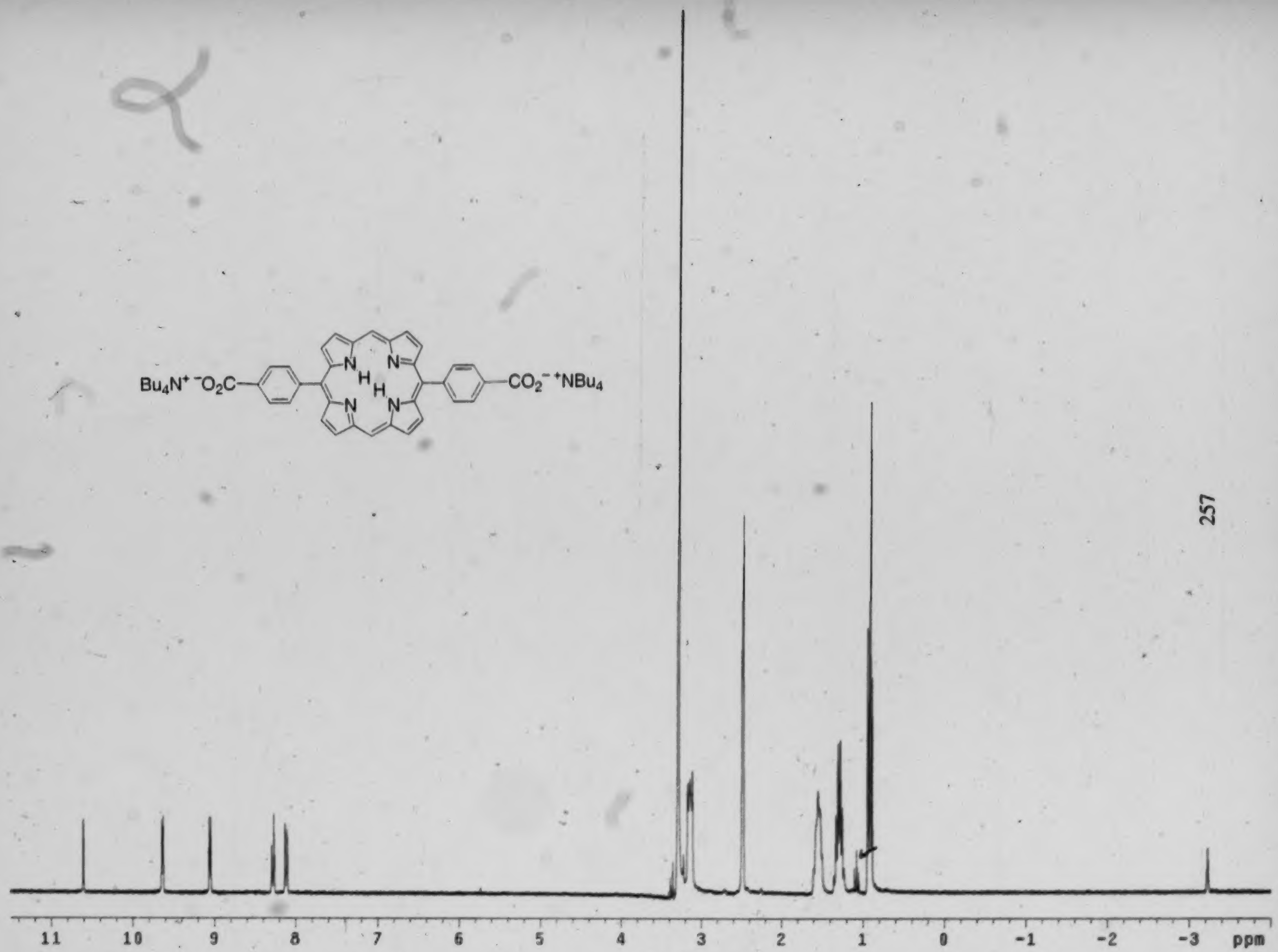
Bu4N+ -O2C
CO2- +NBu4
N
H
H
N
N
N
11
10
9
8
7
6
5
4
3
2
1
0
-1
-2
-3
ppm

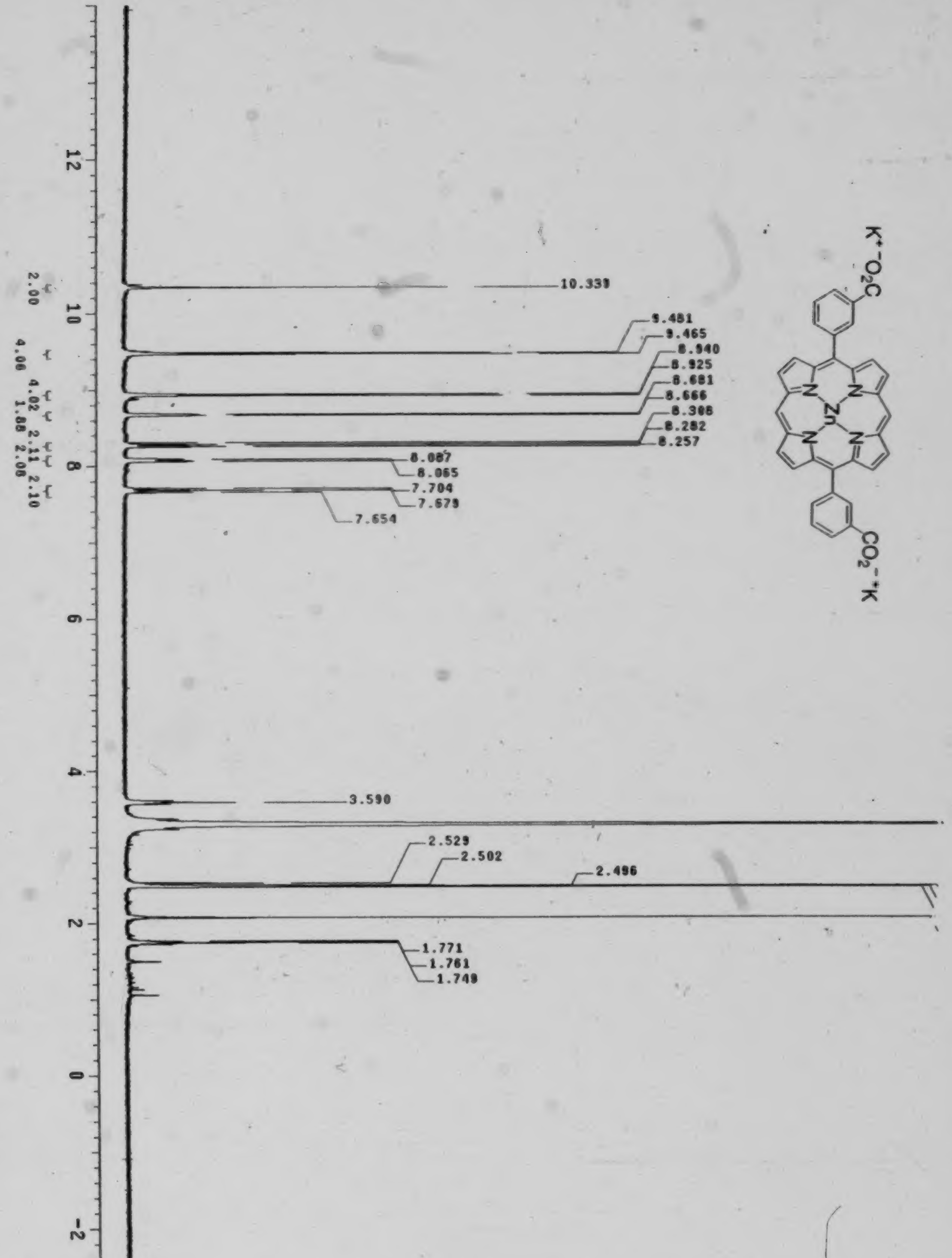
K⁺ ⁻O₂C
Zn
N
CO₂⁻ ⁺K
10.339
9.481
9.465
8.940
8.925
8.681
8.666
8.308
8.282
8.257
8.087
8.065
7.704
7.679
7.654
3.590
2.529
2.502
2.496
1.771
1.761
1.749
2.00
4.06
4.02
1.88
2.11
2.06
2.10
12
10
8
6
4
2
0
-2
ppm

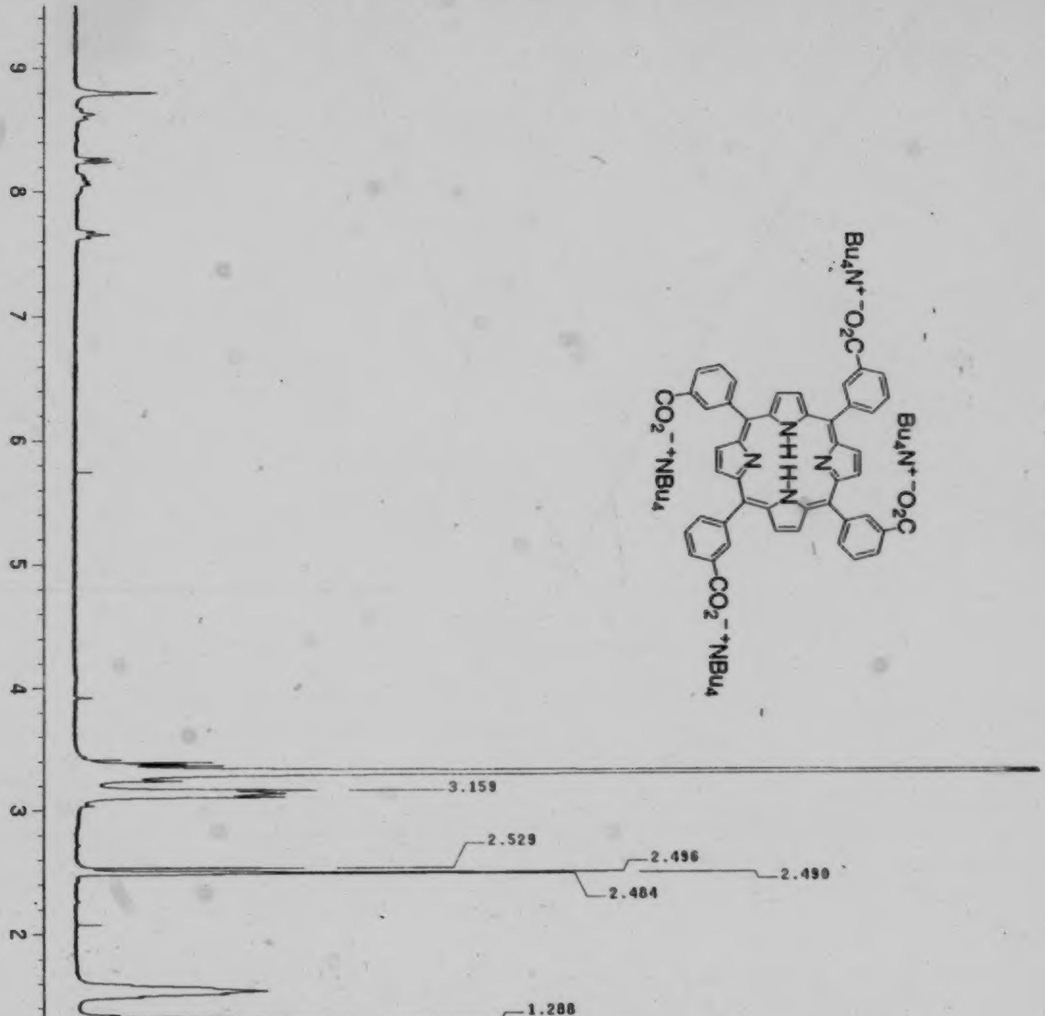
9
8
7
6
5
4
3
2
1
0
-1
-2
ppm
3.159
2.529
2.496
2.490
2.484
1.288
1.265
0.926
0.877
Bu₄N⁺ ⁻O₂C
Bu₄N⁺ ⁻O₂C
CO₂⁻ ⁺NBu₄
CO₂⁻ ⁺NBu₄
N-H
H-N
N
N

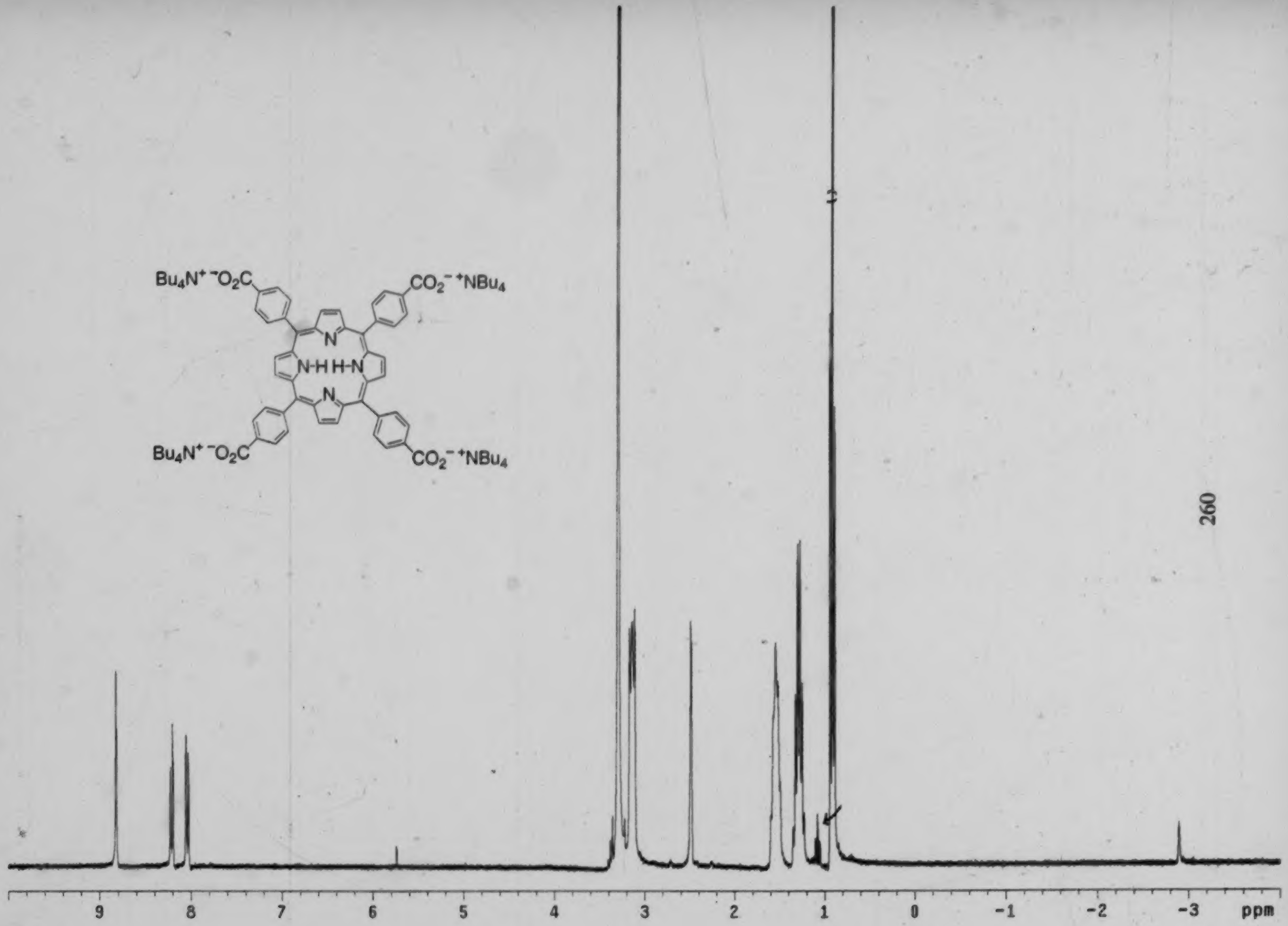
Bu$_4$N$^+$ $^-$O$_2$C
CO$_2$$^-$ $^+$NBu$_4$
N
N-H H-N
N
Bu$_4$N$^+$ $^-$O$_2$C
CO$_2$$^-$ $^+$NBu$_4$
9
8
7
6
5
4
3
2
1
0
-1
-2
-3
ppm

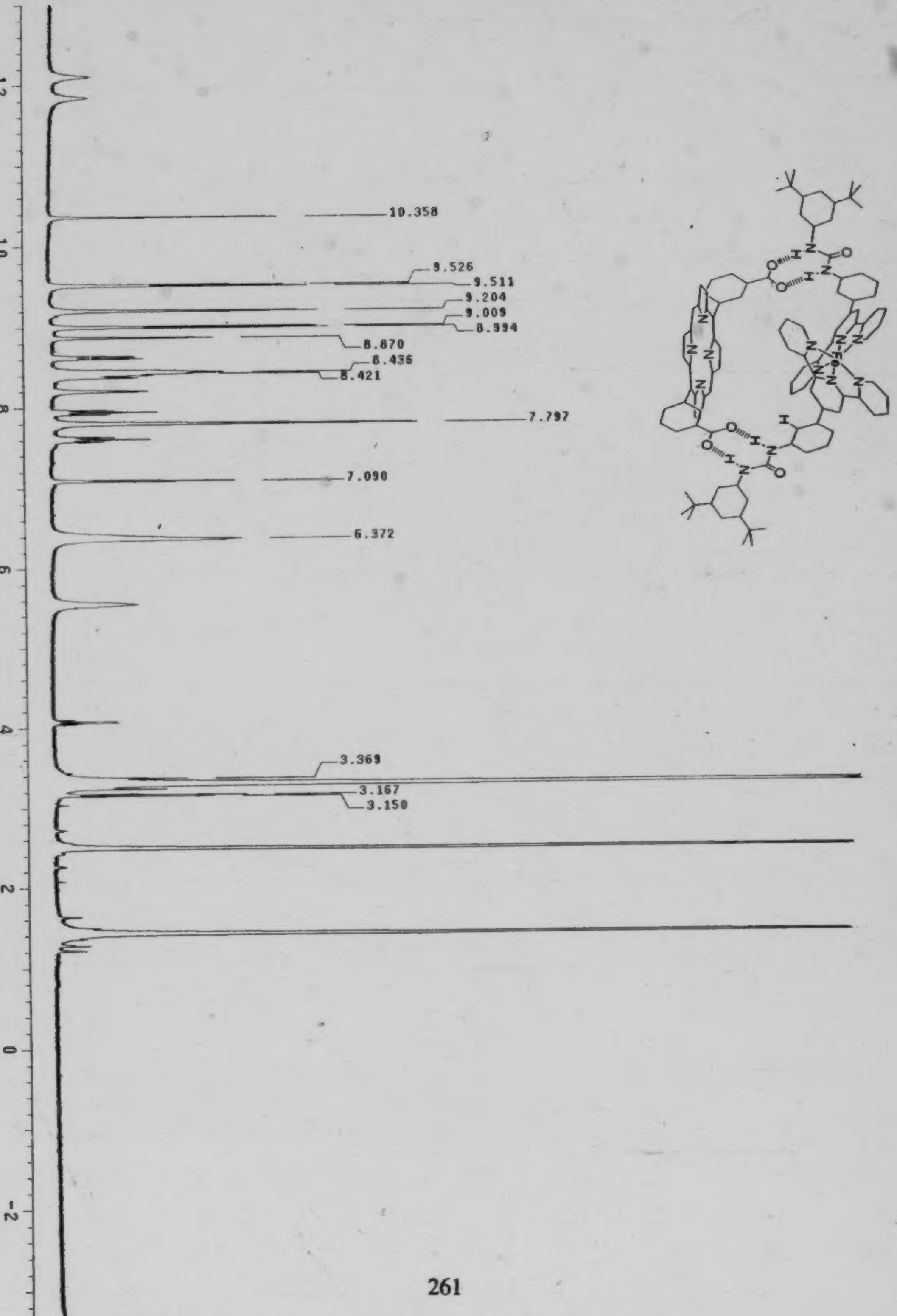
10.358
9.526
9.511
9.204
9.009
8.994
8.870
8.436
8.421
7.797
7.090
6.372
3.369
3.167
3.150
12
10
8
6
4
2
0
-2
ppm
Fe

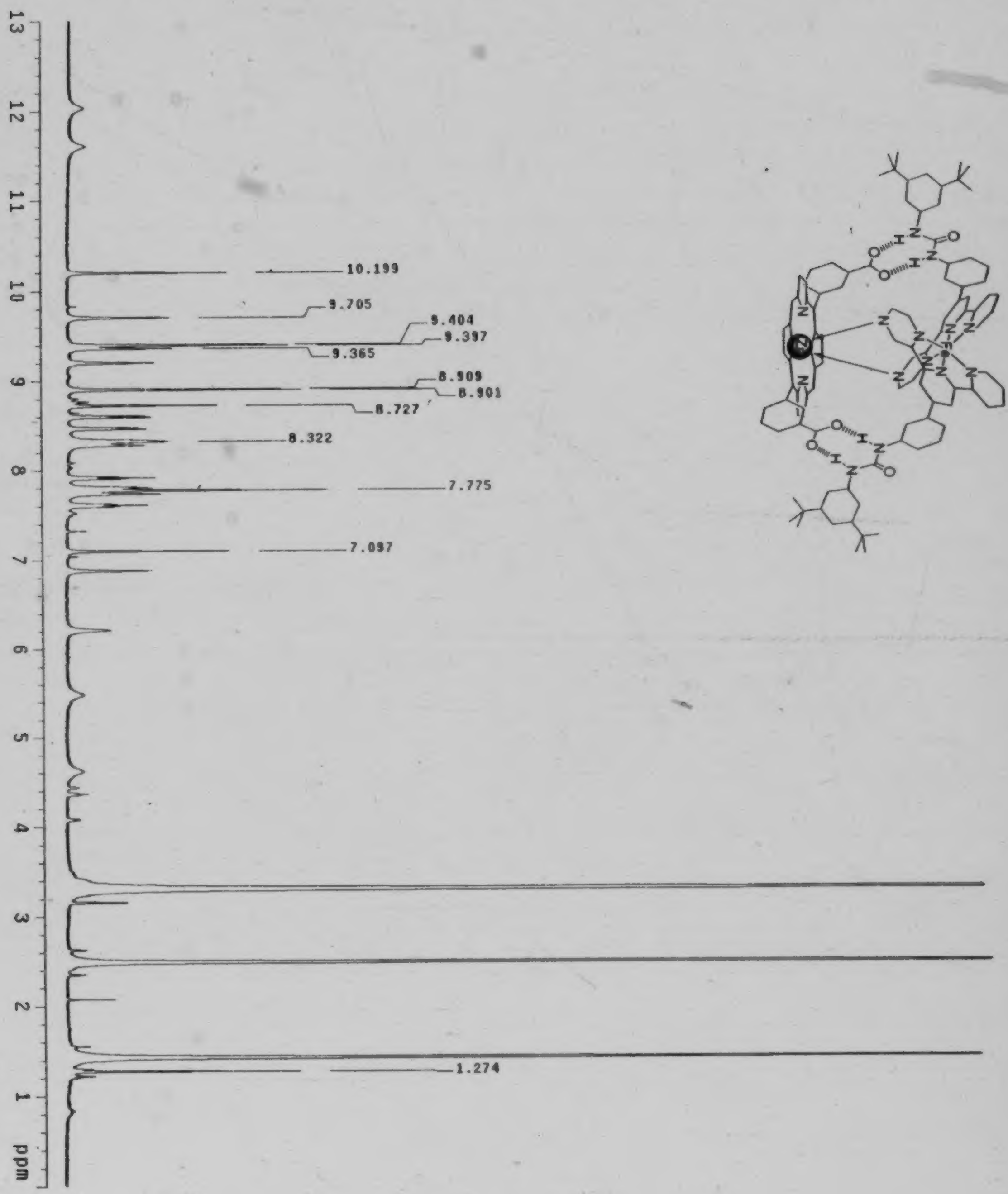
10.199
9.705
9.404
9.397
9.365
8.909
8.901
8.727
8.322
7.775
7.097
1.274
13
12
11
10
9
8
7
6
5
4
3
2
1
ppm

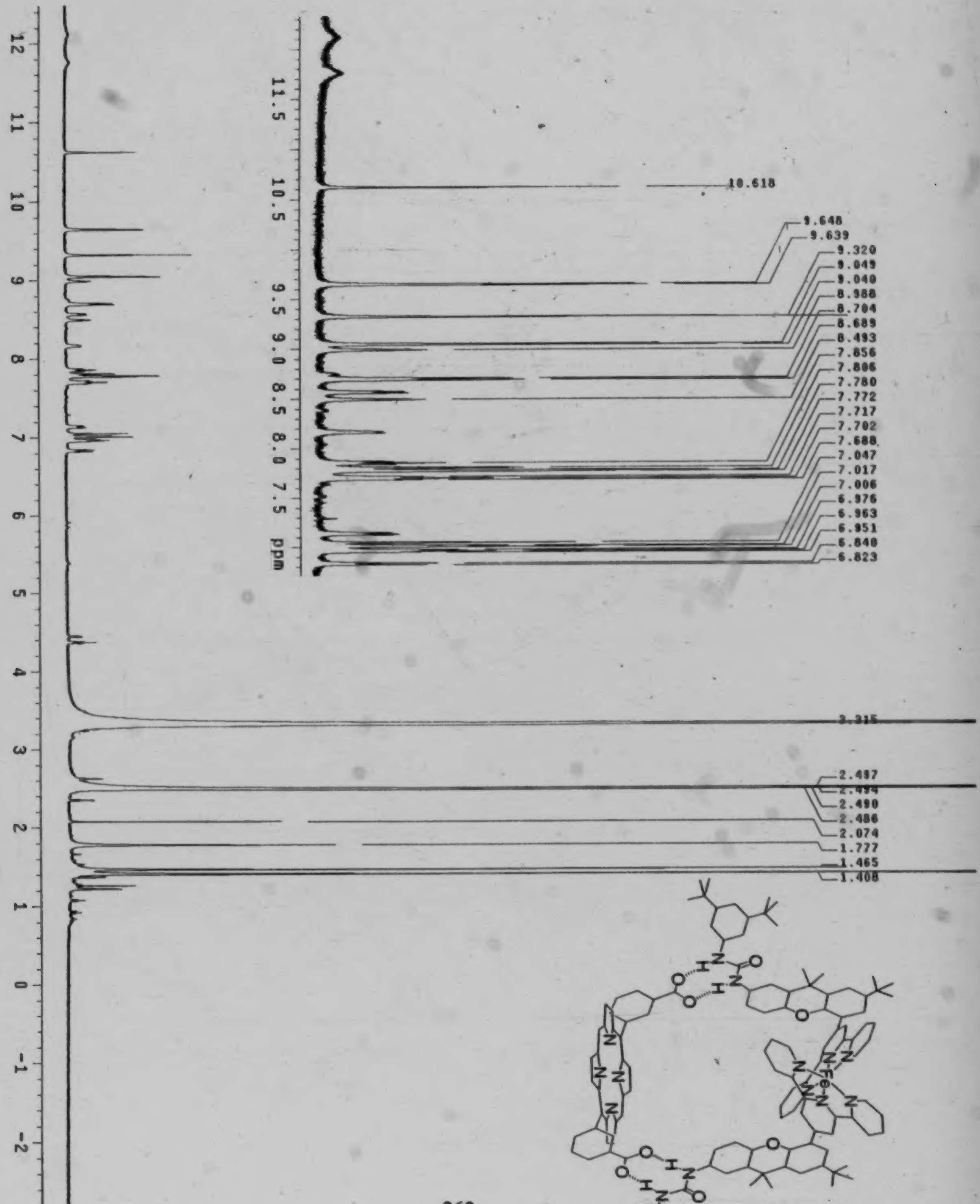

10.618
9.648
9.639
9.320
9.049
9.040
8.988
8.704
8.689
8.493
7.856
7.806
7.780
7.772
7.717
7.702
7.688
7.047
7.017
7.006
6.976
6.963
6.951
6.840
6.823
11.5
10.5
9.5
9.0
8.5
8.0
7.5
ppm
3.315
2.497
2.494
2.490
2.486
2.074
1.777
1.465
1.408
12
11
10
9
8
7
6
5
4
3
2
1
0
-1
-2
ppm
N
Fe
O
H

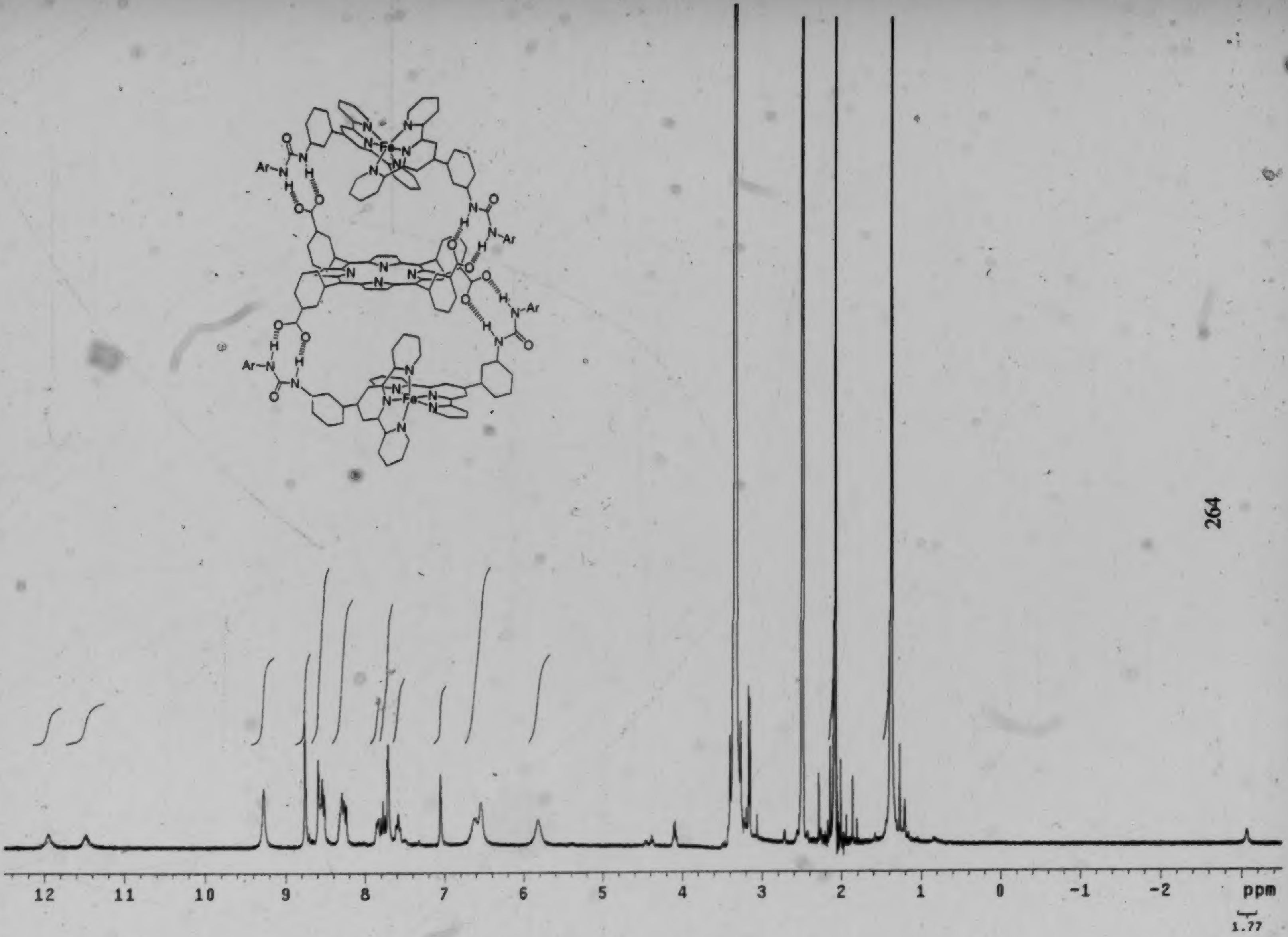
Ar
N
H
O
Fe
12
11
10
9
8
7
6
5
4
3
2
1
0
-1
-2
ppm
1.77

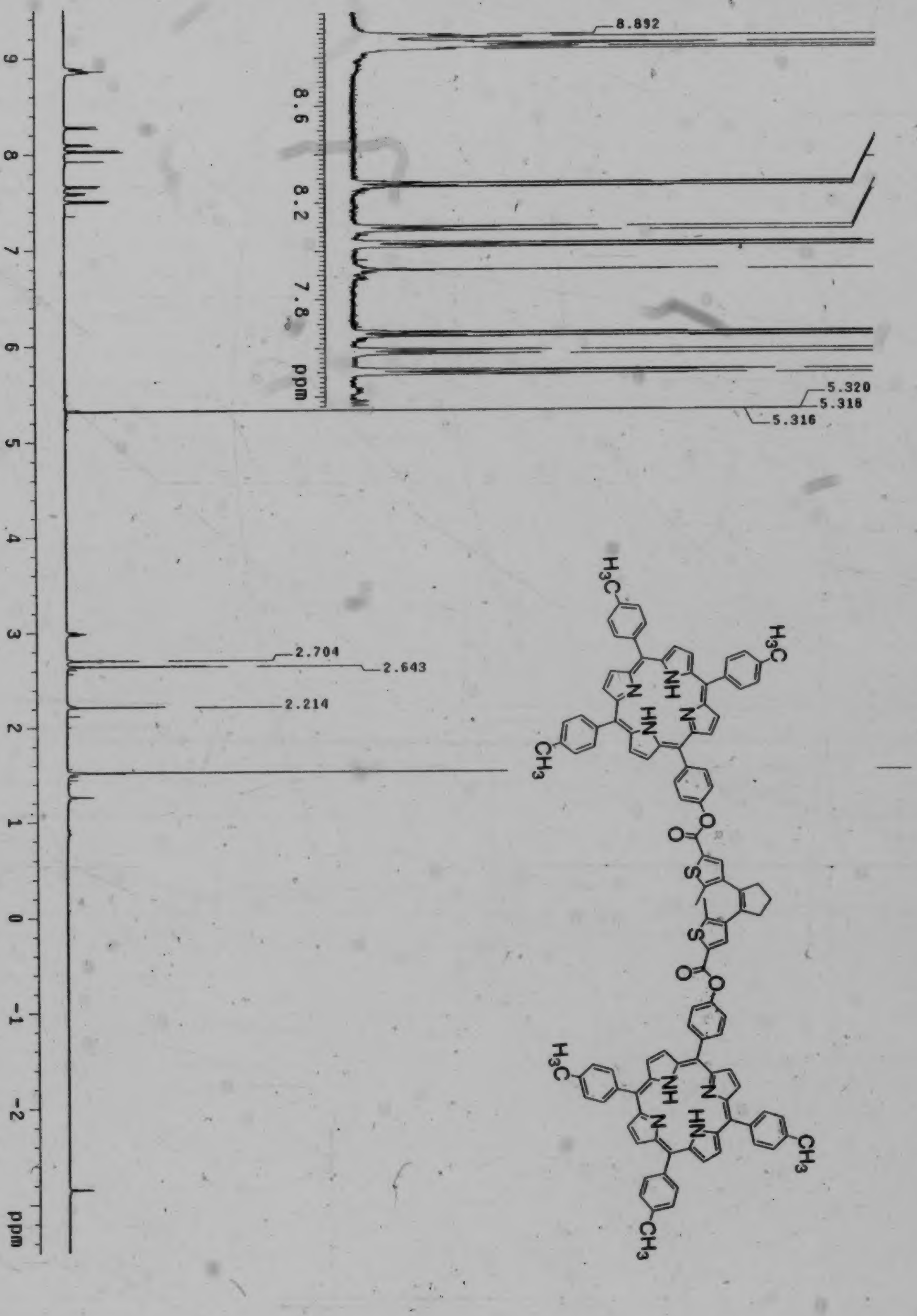8.892
8.6
8.2
7.8
ppm
5.320
5.318
5.316
2.704
2.643
2.214
9
8
7
6
5
4
3
2
1
0
-1
-2
ppm
H_3C
H_3C
CH_3
NH
HN
N
N
O
O
S
S
O
O
H_3C
NH
HN
N
N
CH_3
CH_3

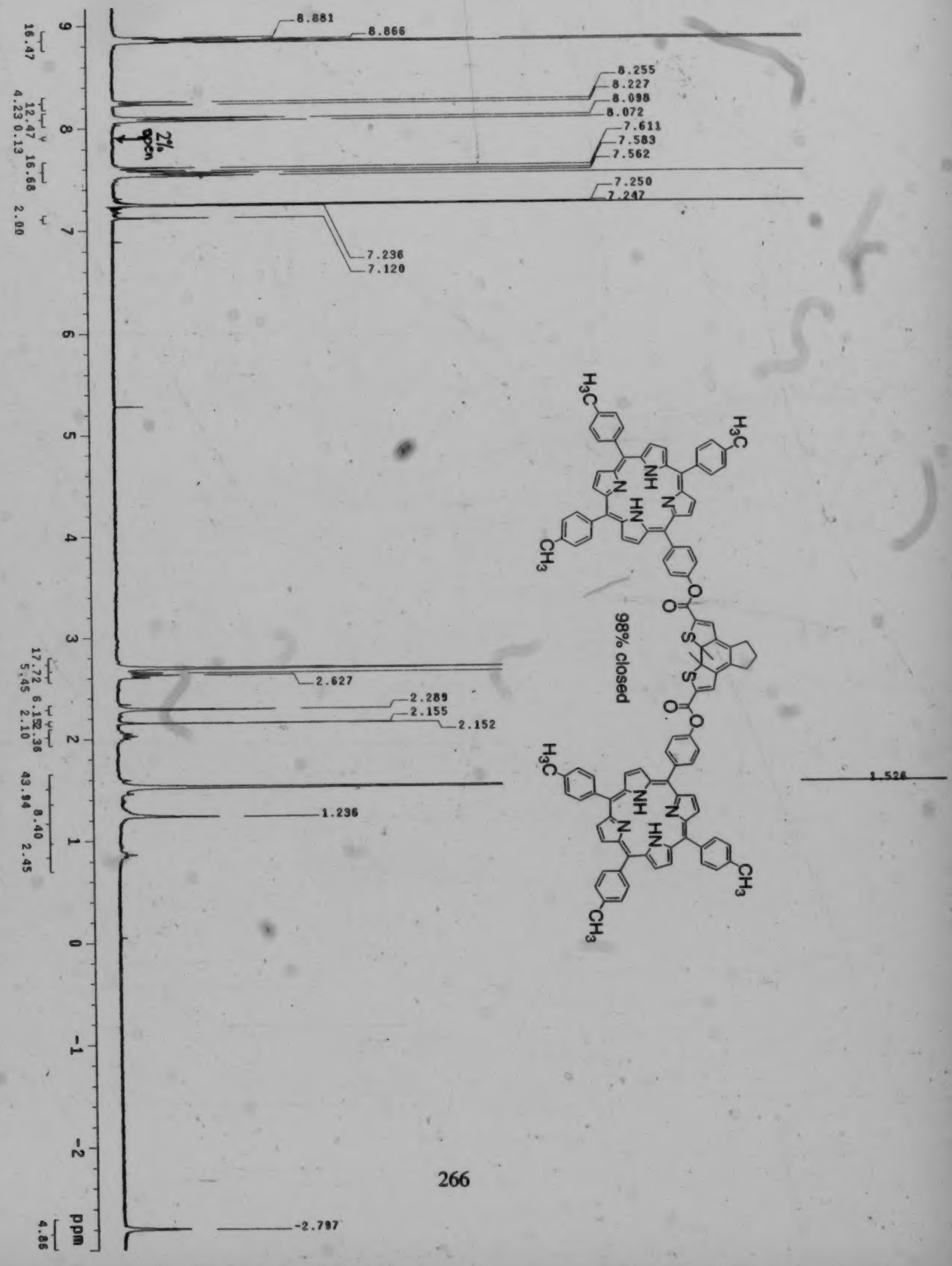

8.881
8.866
8.255
8.227
8.098
8.072
7.611
7.583
7.562
7.250
7.247
7.236
7.120
2.627
2.289
2.155
2.152
1.526
1.236
-2.797
2% open
98% closed
16.47
12.47
4.23
0.13
16.68
2.00
17.72
5.45
6.15
2.10
2.36
43.84
8.40
2.45
4.85
9
8
7
6
5
4
3
2
1
0
-1
-2
ppm
H3C
CH3
NH
HN
N
O
S

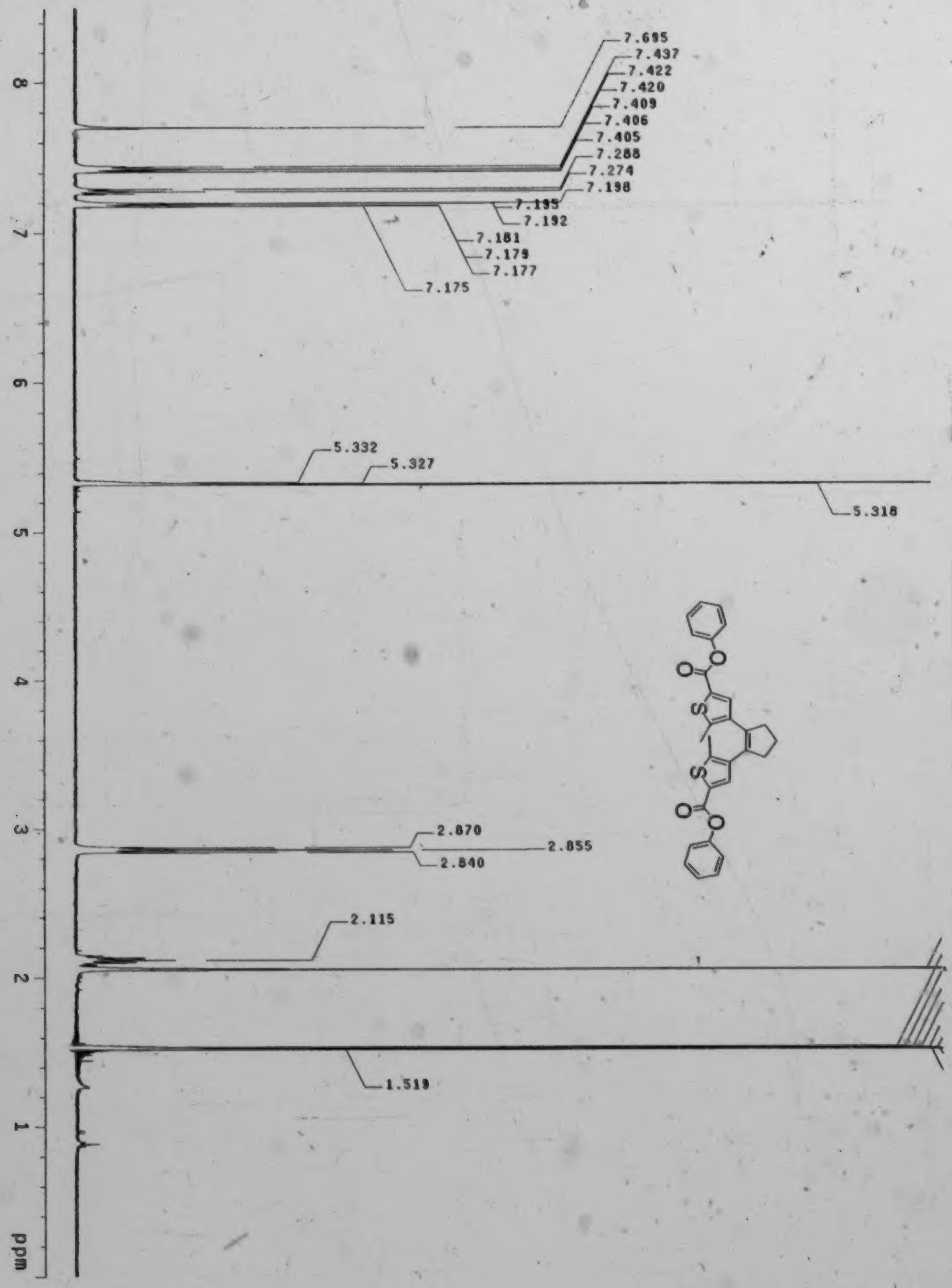
7.695
7.437
7.422
7.420
7.409
7.406
7.405
7.288
7.274
7.198
7.195
7.192
7.181
7.179
7.177
7.175
5.332
5.327
5.318
2.870
2.855
2.840
2.115
1.519
8
7
6
5
4
3
2
1
ppm
O
O
S
S
O
O

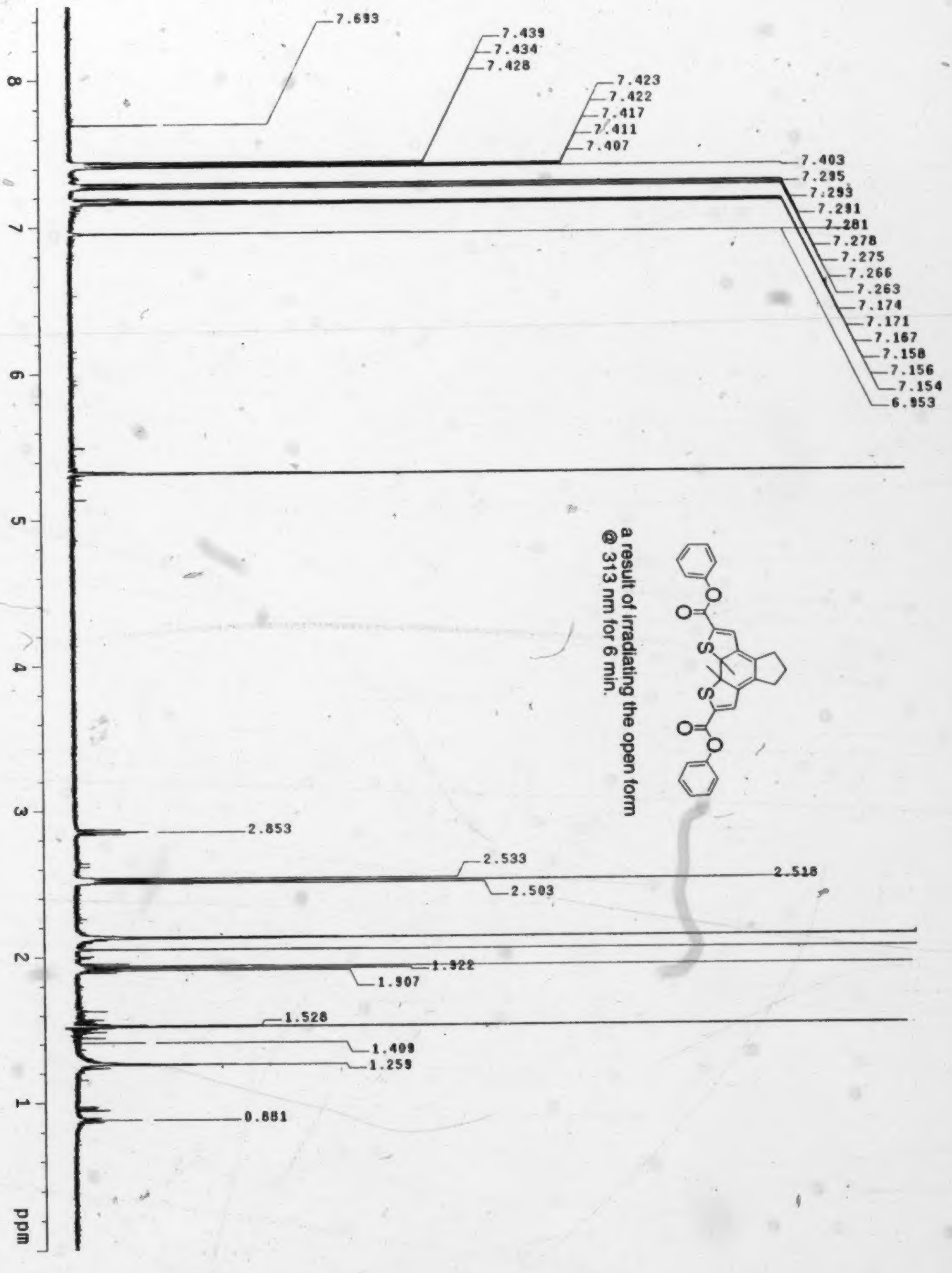

a result of irradiating the open form @ 313 nm for 6 min.

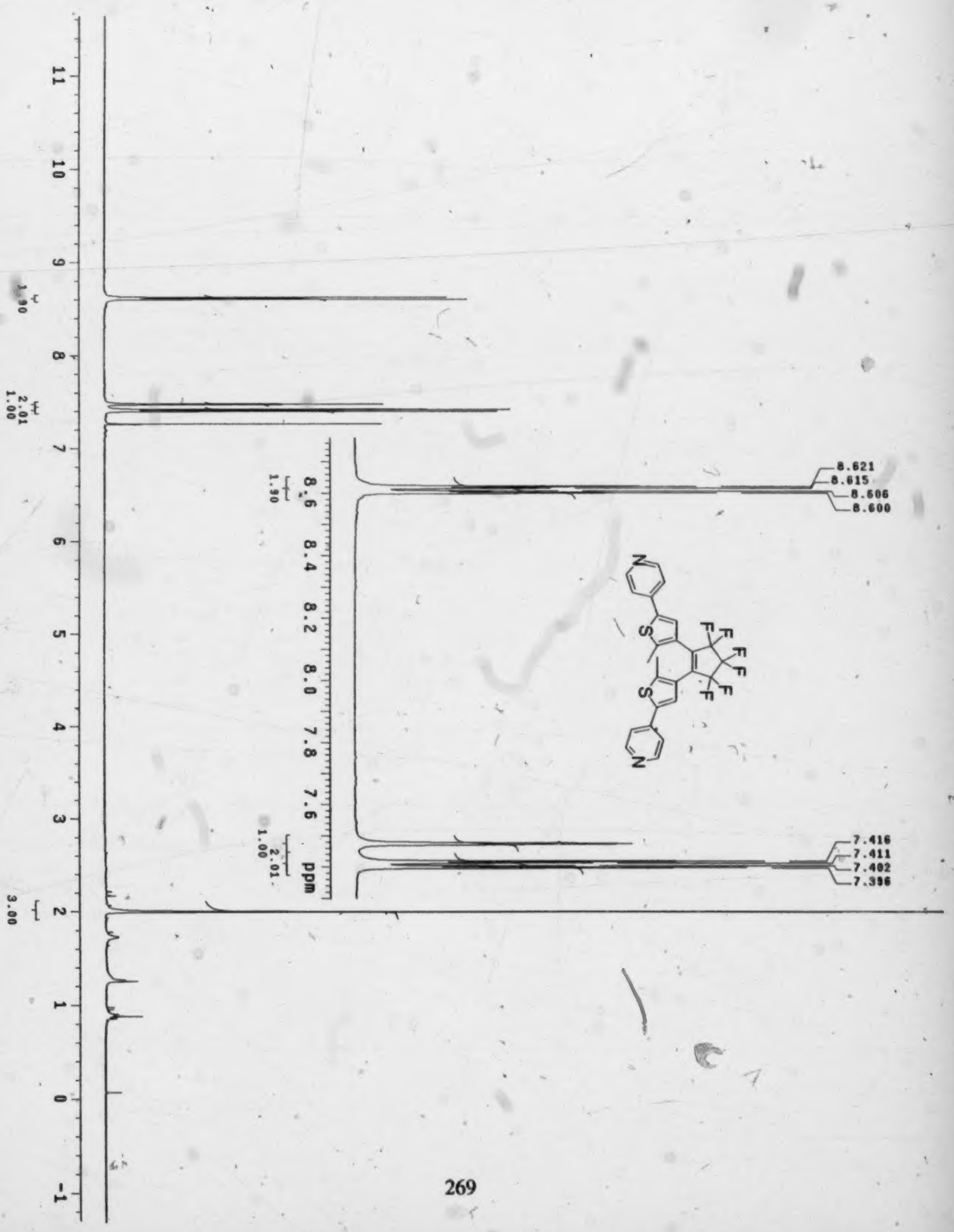
8.621
8.615
8.606
8.600
7.416
7.411
7.402
7.396
8.6
8.4
8.2
8.0
7.8
7.6
ppm
1.90
2.01
1.00
3.00
11
10
9
8
7
6
5
4
3
2
1
0
-1
N
S
F

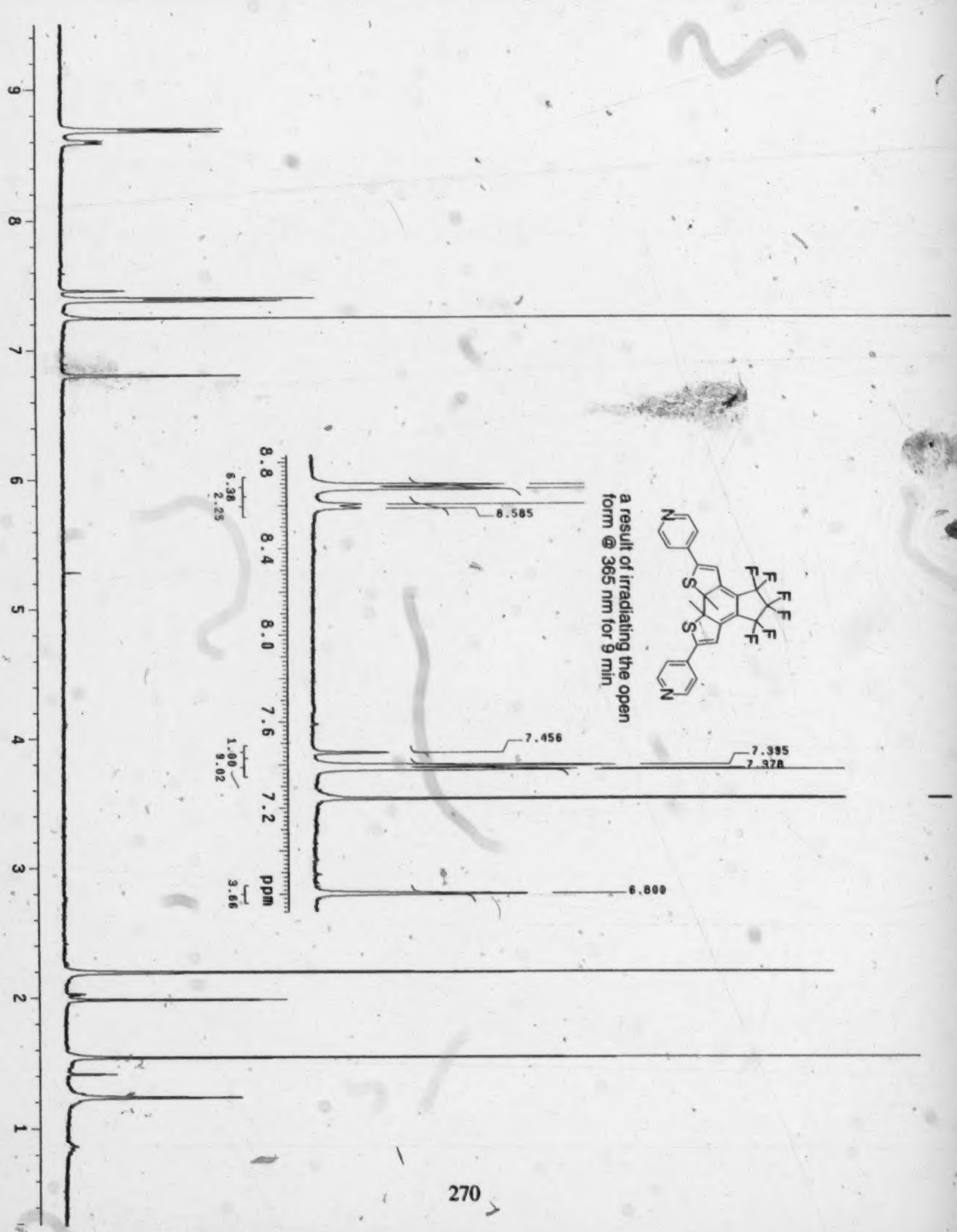

a result of irradiating the open form @ 365 nm for 9 min

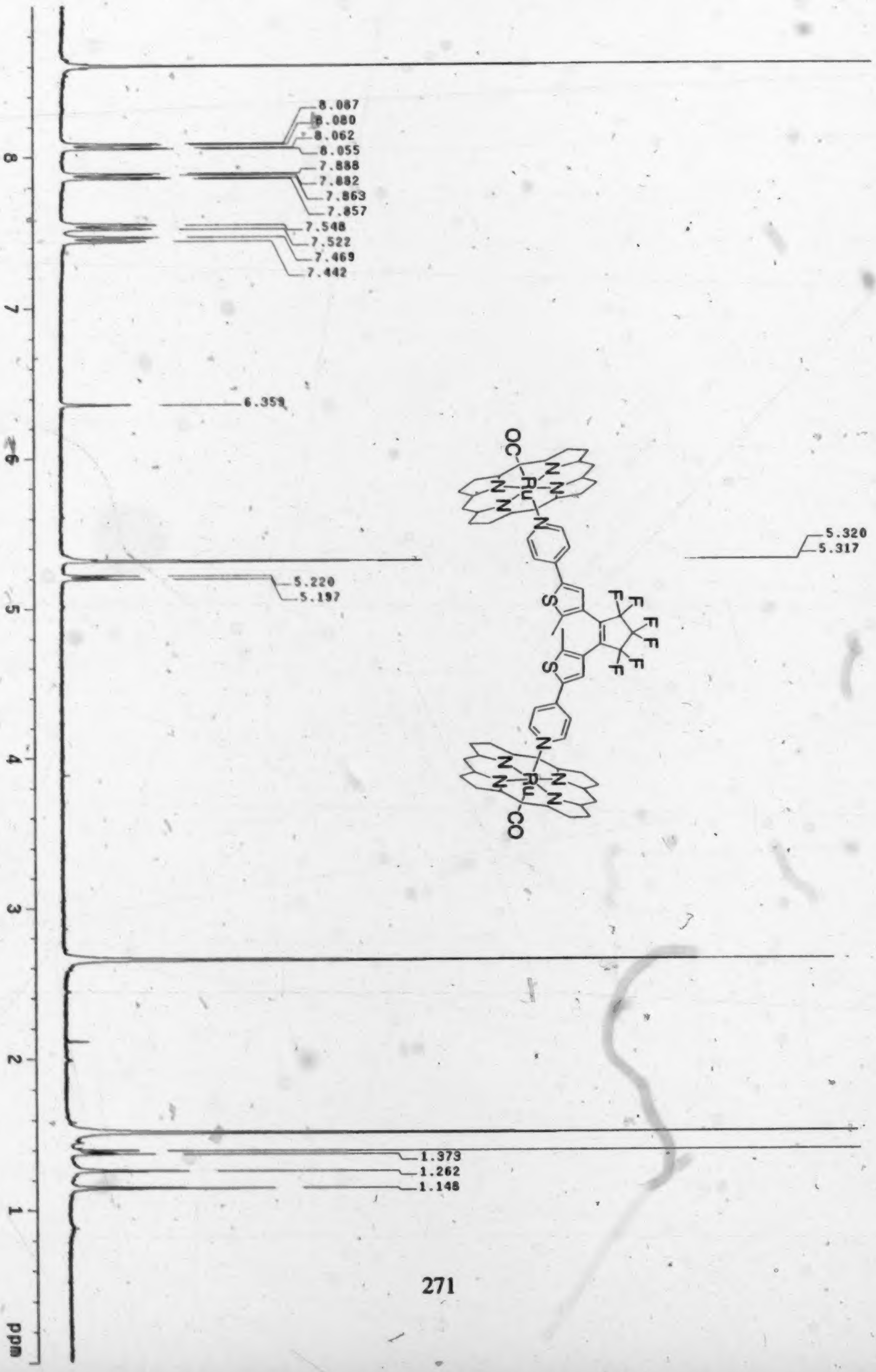
8.087
8.080
8.062
8.055
7.888
7.882
7.863
7.857
7.548
7.522
7.469
7.442
6.359
5.320
5.317
5.220
5.197
1.373
1.262
1.148
OC
N
N
Ru
N
N
N
S
F
F
F
F
F
F
S
N
N
N
Ru
N
N
CO
8
7
6
5
4
3
2
1
ppm

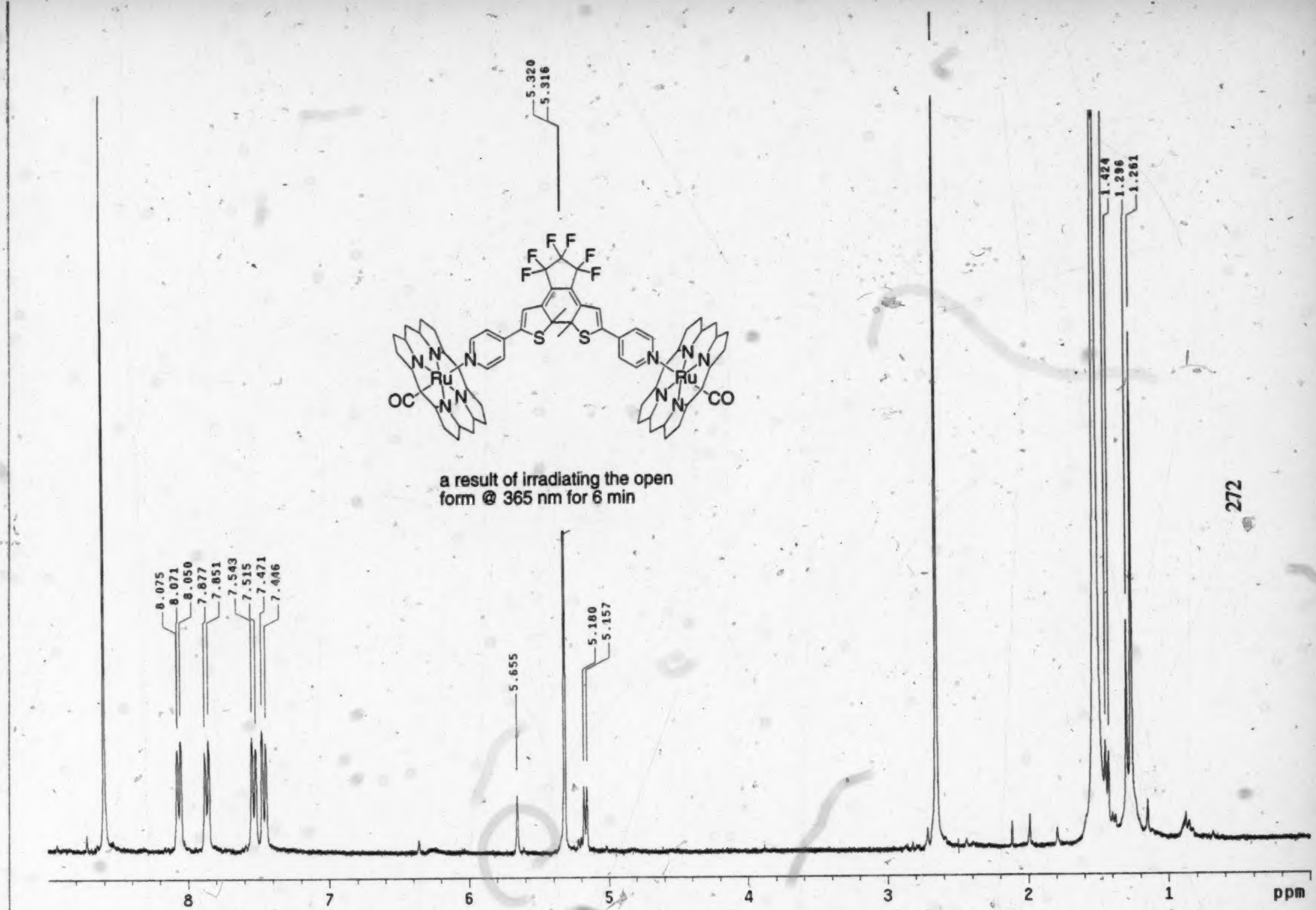

a result of irradiating the open form @ 365 nm for 6 min

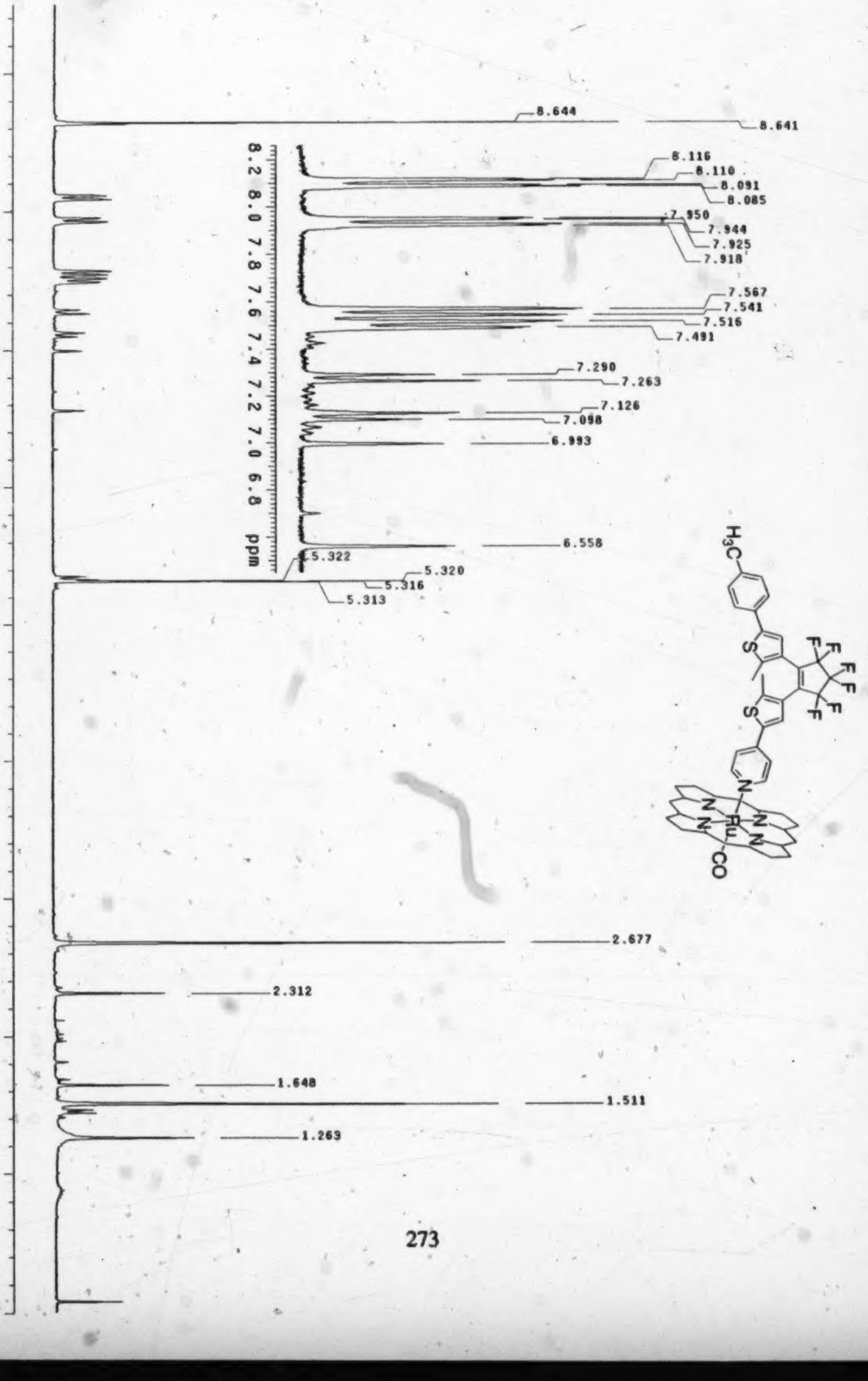
8.644
8.641
8.116
8.110
8.091
8.085
7.950
7.944
7.925
7.918
7.567
7.541
7.516
7.491
7.290
7.263
7.126
7.098
6.993
6.558
5.322
5.320
5.316
5.313
2.677
2.312
1.648
1.511
1.263
8.2 8.0 7.8 7.6 7.4 7.2 7.0 6.8 ppm
9 8 7 6 5 4 3 2 1 ppm
H3C
S
F
N
Ru
CO

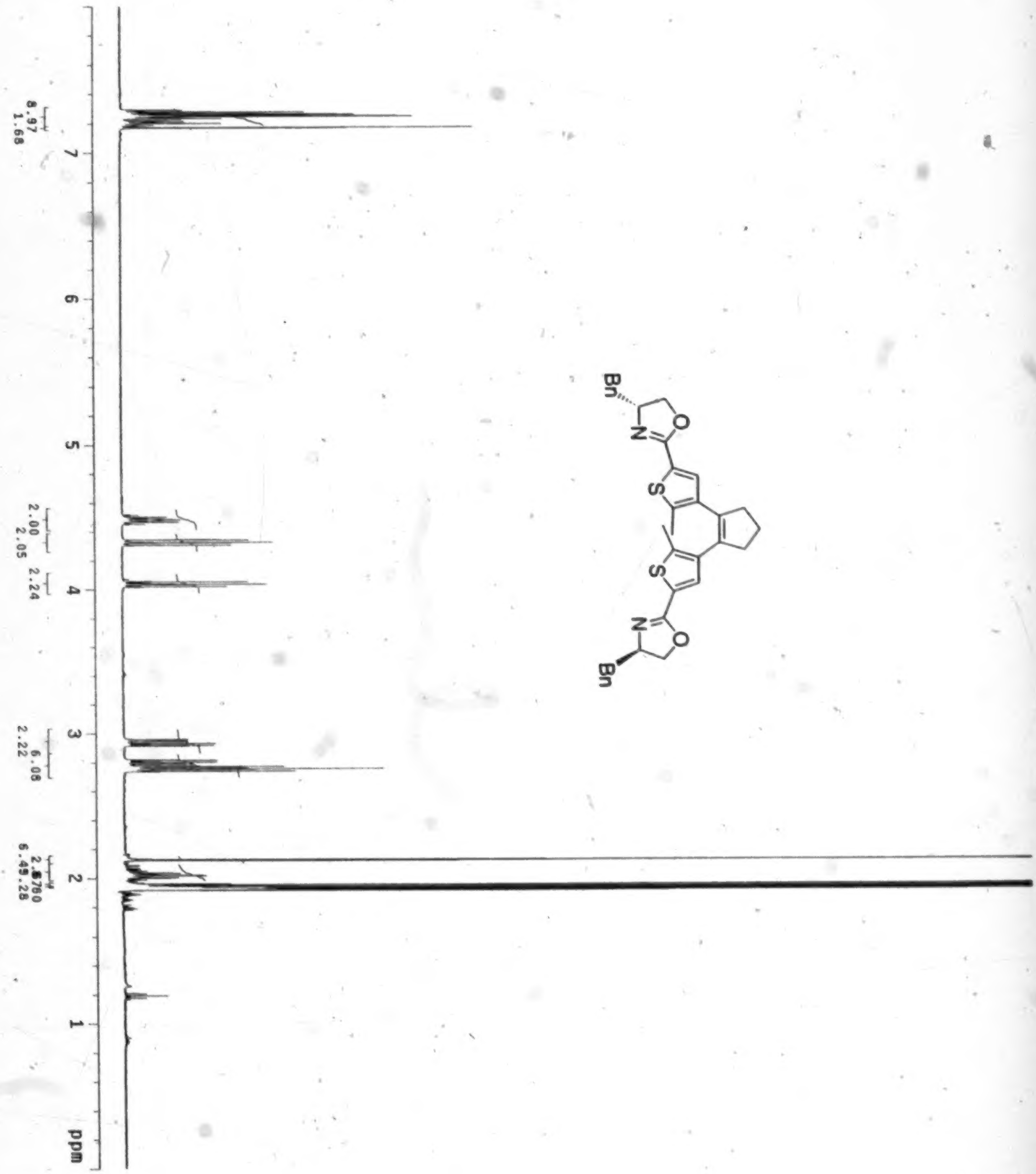
8.97
1.68
2.00
2.05
2.24
2.22
6.08
7
6
5
4
3
2
1
ppm
Bn
O
N
S
S
N
O
Bn

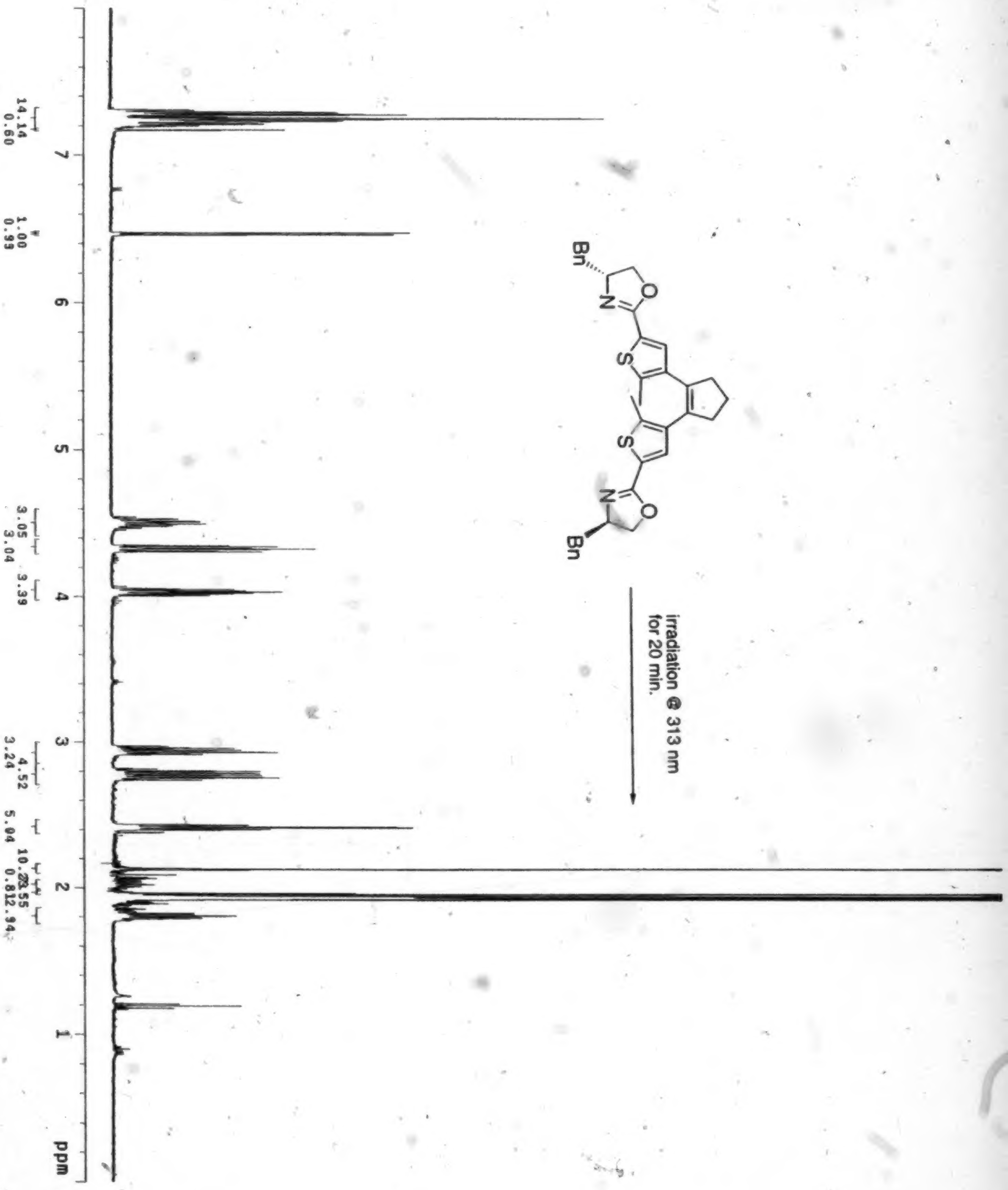
irradiation @ 313 nm
for 20 min.
Bn
N
O
S
S
N
O
Bn
14.14
0.60
1.00
0.99
3.05
3.04
3.39
4.52
3.24
5.04
10.23
3.55
0.81
2.94
7
6
5
4
3
2
1
ppm

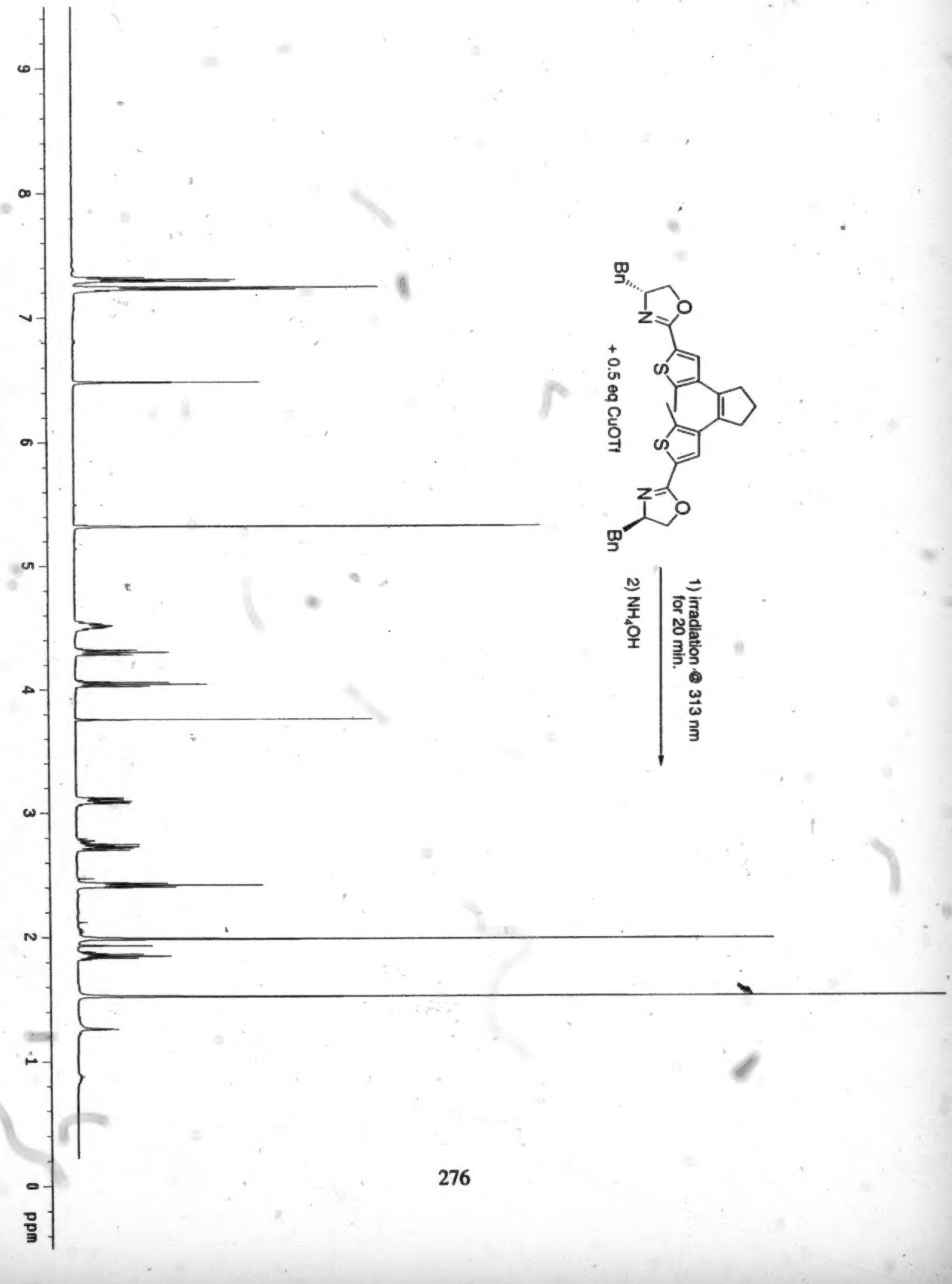
Bn
O
N
S
S
N
O
Bn
+ 0.5 eq CuOTf
1) irradiation @ 313 nm
for 20 min.
2) NH$_4$OH
9
8
7
6
5
4
3
2
1
0
ppm

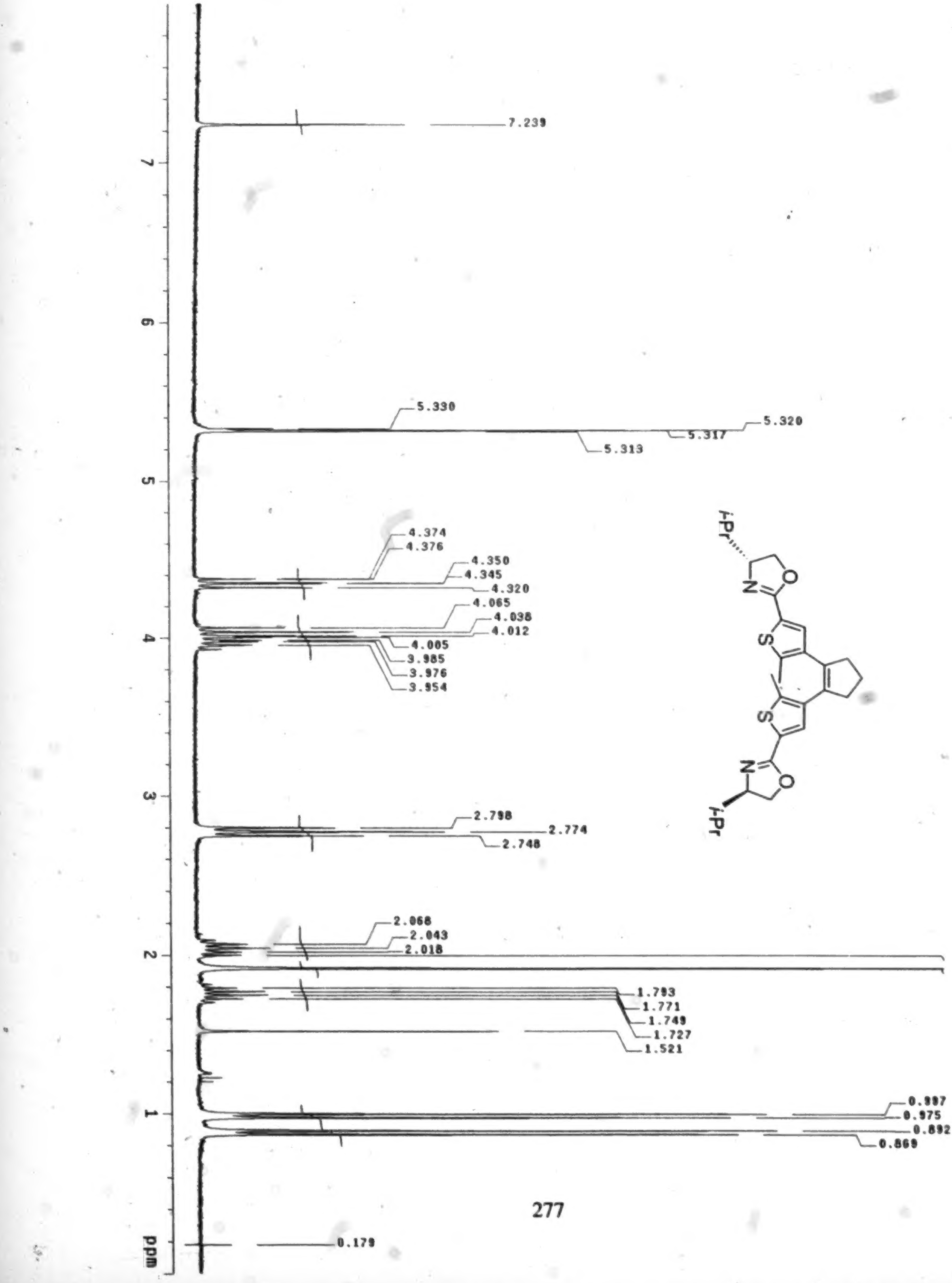
7
6
5
4
3
2
1
ppm
7.239
5.330
5.320
5.317
5.313
4.374
4.376
4.350
4.345
4.320
4.065
4.038
4.012
4.005
3.985
3.976
3.954
2.798
2.774
2.748
2.068
2.043
2.018
1.793
1.771
1.749
1.727
1.521
0.997
0.975
0.892
0.869
0.179
i-Pr
O
N
S
S
N
O
i-Pr

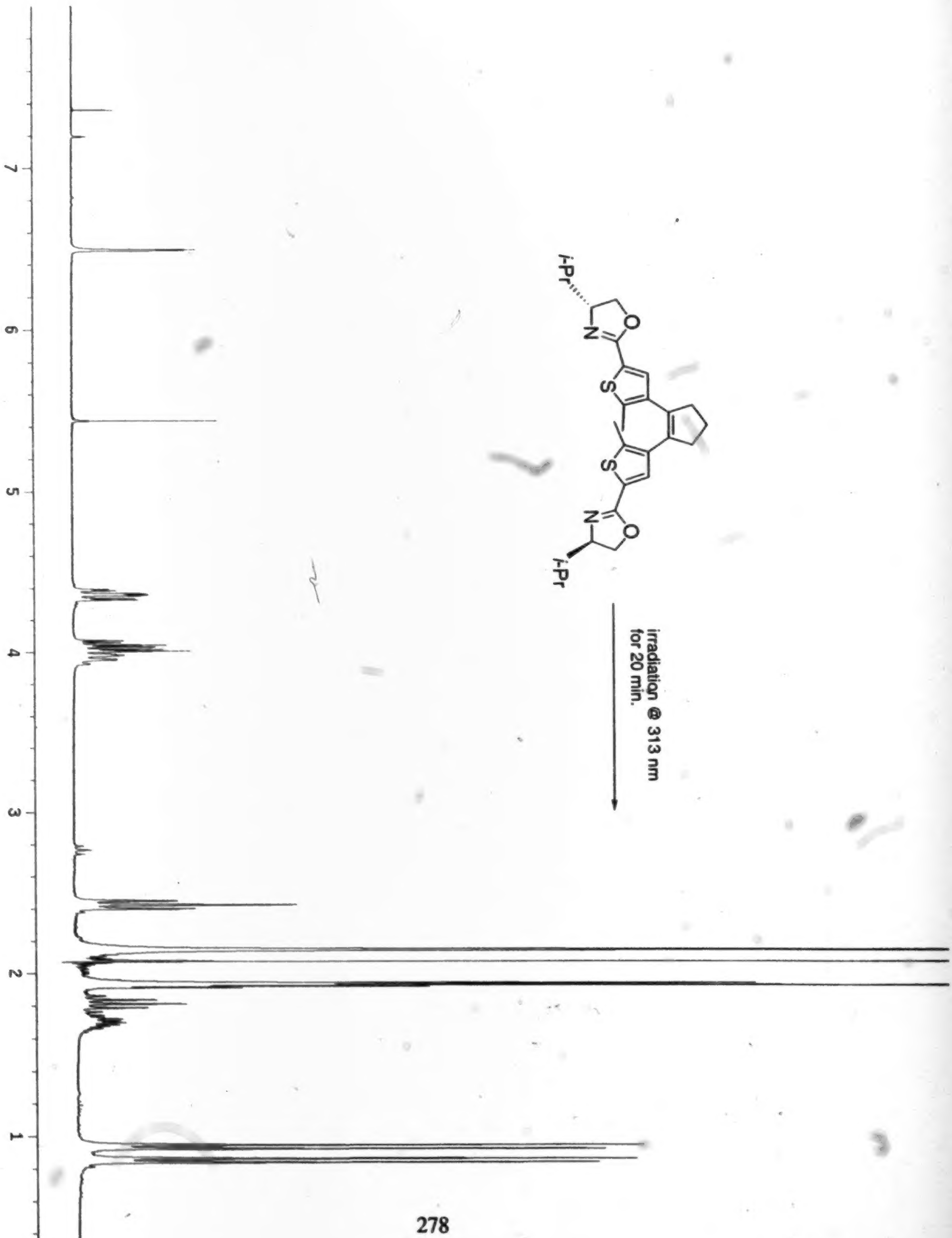

i-Pr
O
N
S
S
N
O
i-Pr
irradiation @ 313 nm
for 20 min.
7
6
5
4
3
2
1
ppm

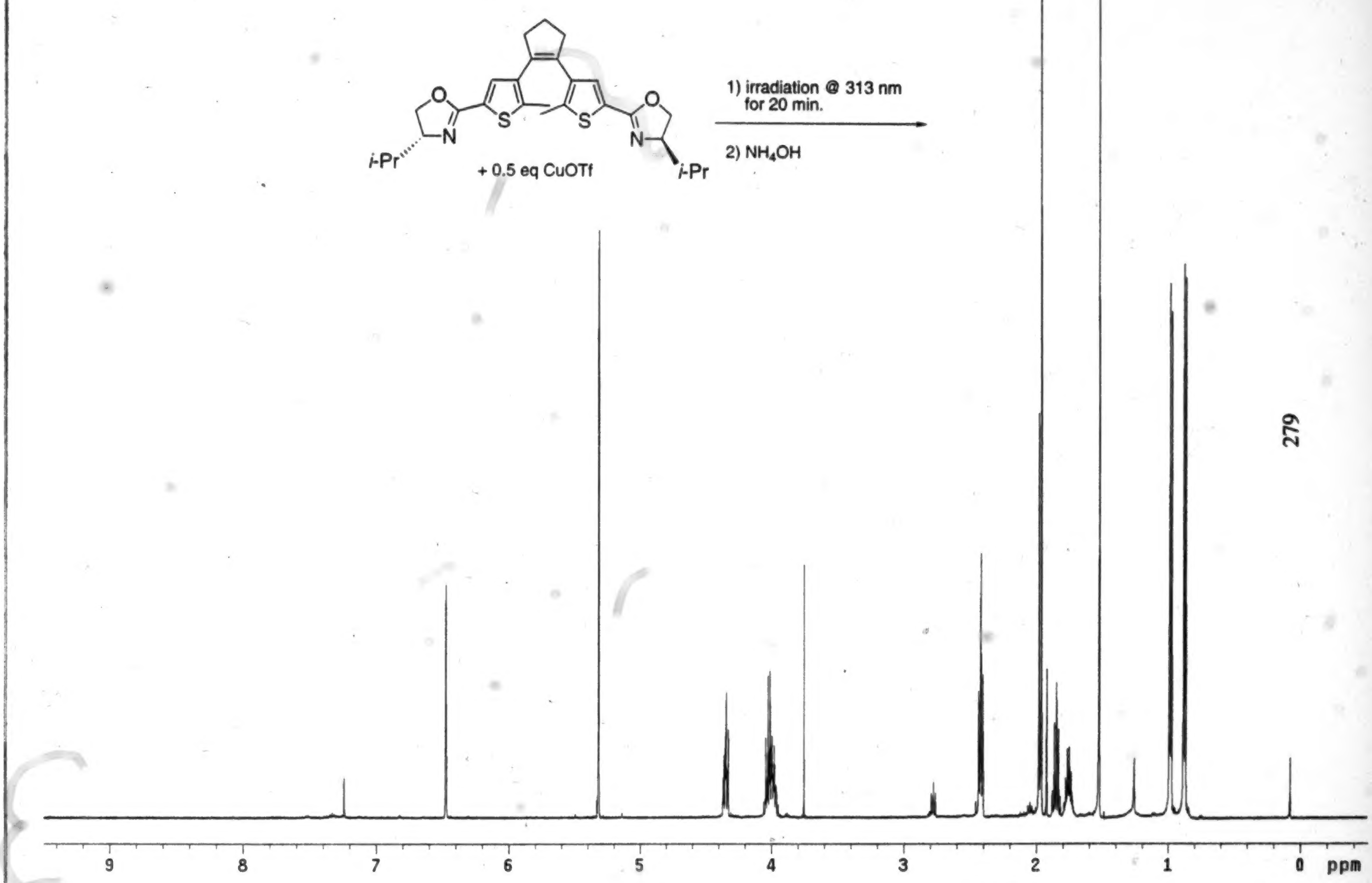

O
N
S
S
O
N
i-Pr
i-Pr
+ 0.5 eq CuOTf
1) irradiation @ 313 nm
for 20 min.
2) NH$_4$OH
9
8
7
6
5
4
3
2
1
0
ppm

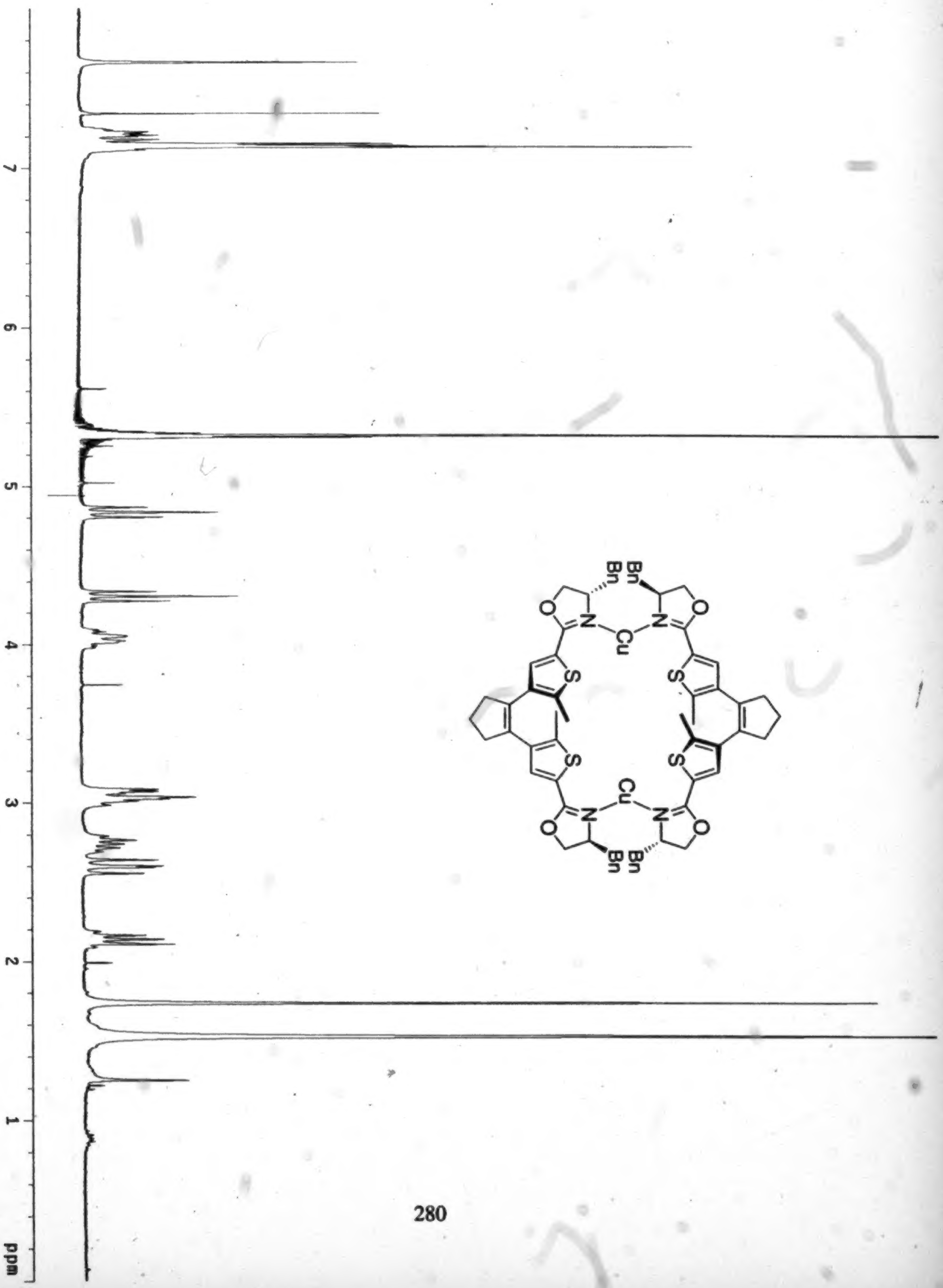
7
6
5
4
3
2
1
ppm
Bn
Bn
O
N
Cu
N
O
S
S
S
S
O
N
Cu
N
O
Bn
Bn

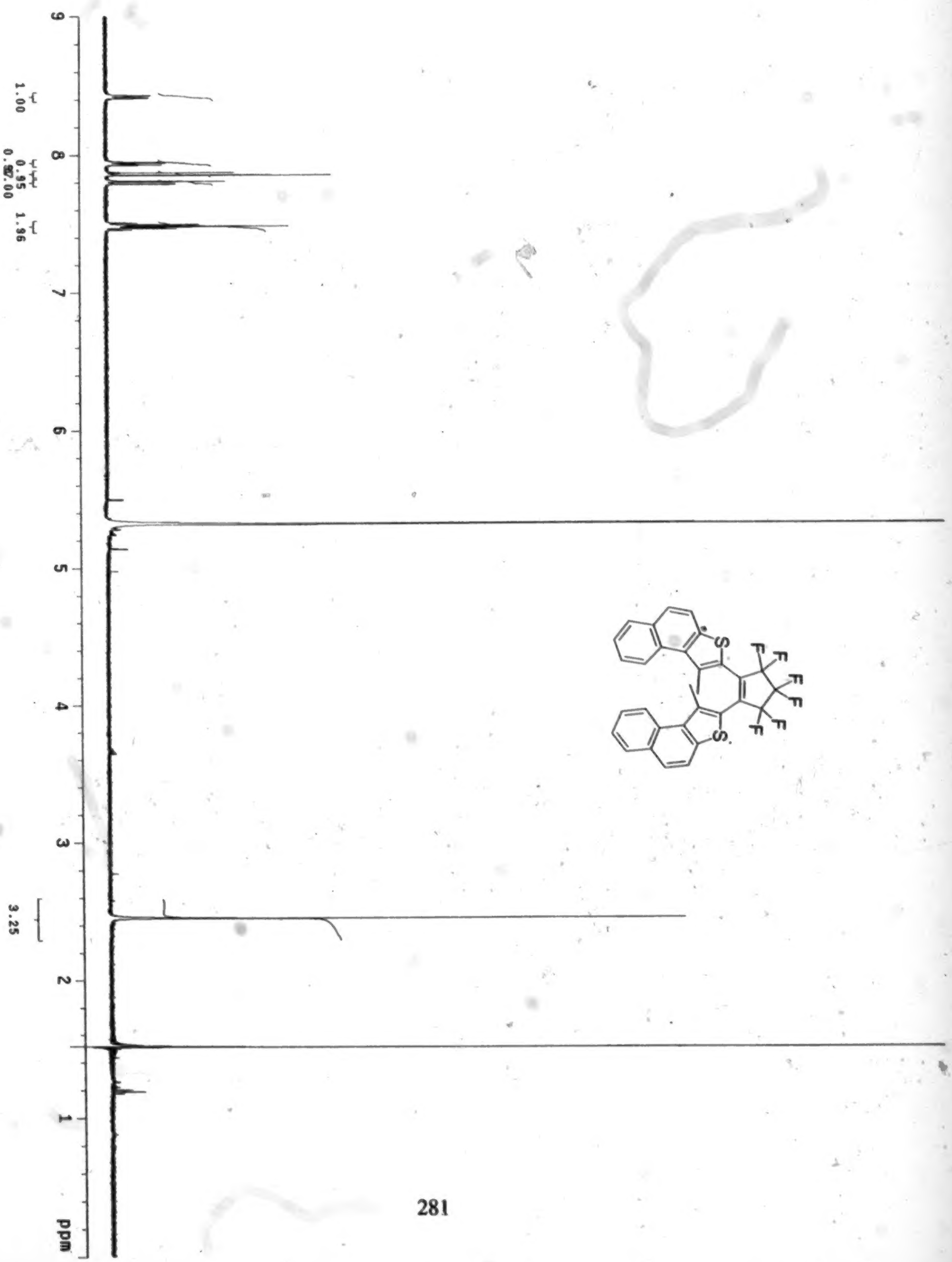
9
8
7
6
5
4
3
2
1
ppm
1.00
0.95
0.97
2.00
1.36
3.25
S
S
F
F
F
F
F
F

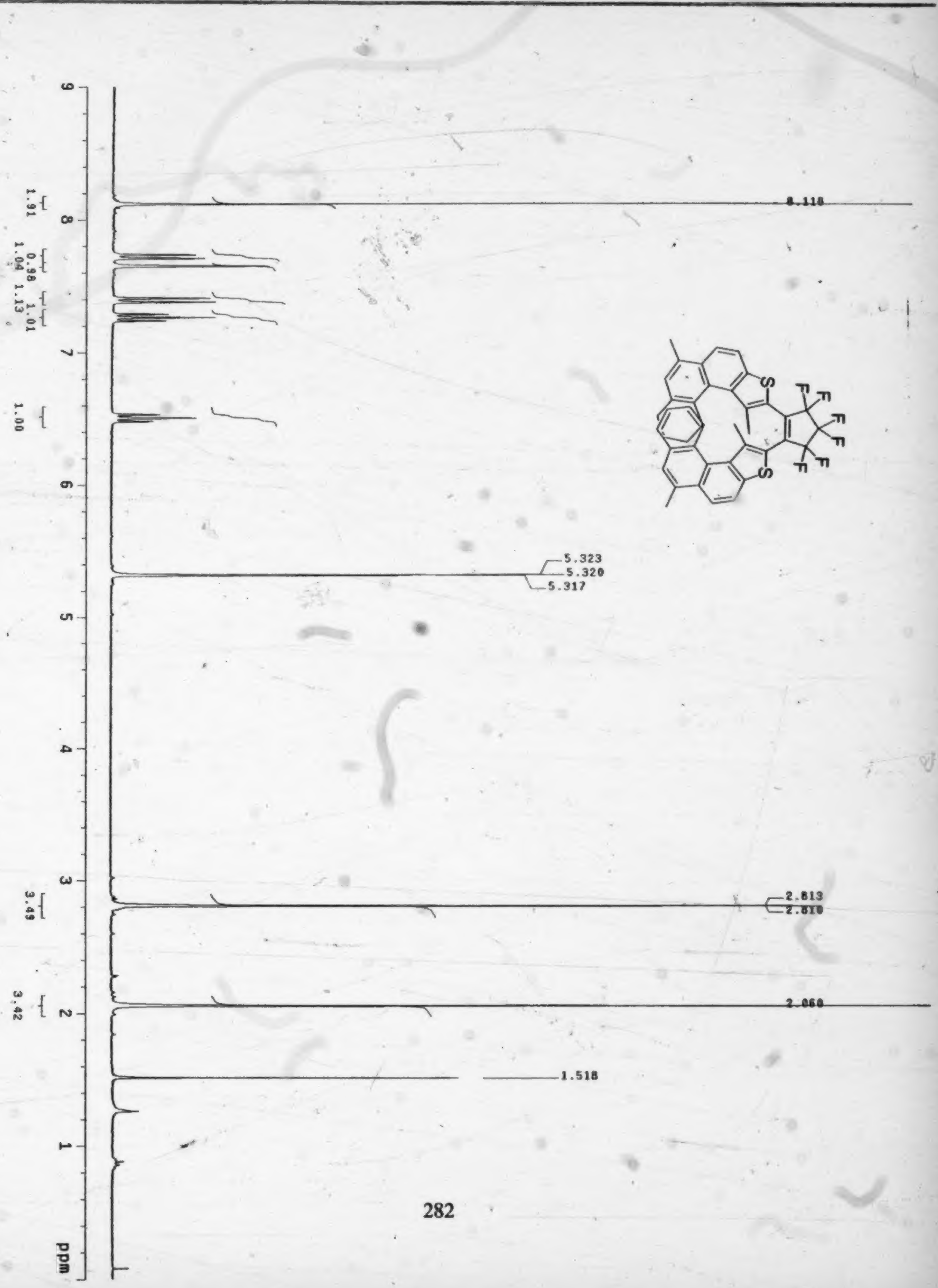
9
8
7
6
5
4
3
2
1
ppm
1.91
0.98
1.04
1.13
1.01
1.00
3.49
3.42
8.118
5.323
5.320
5.317
2.813
2.810
2.060
1.518
S
S
F
F
F
F
F
F

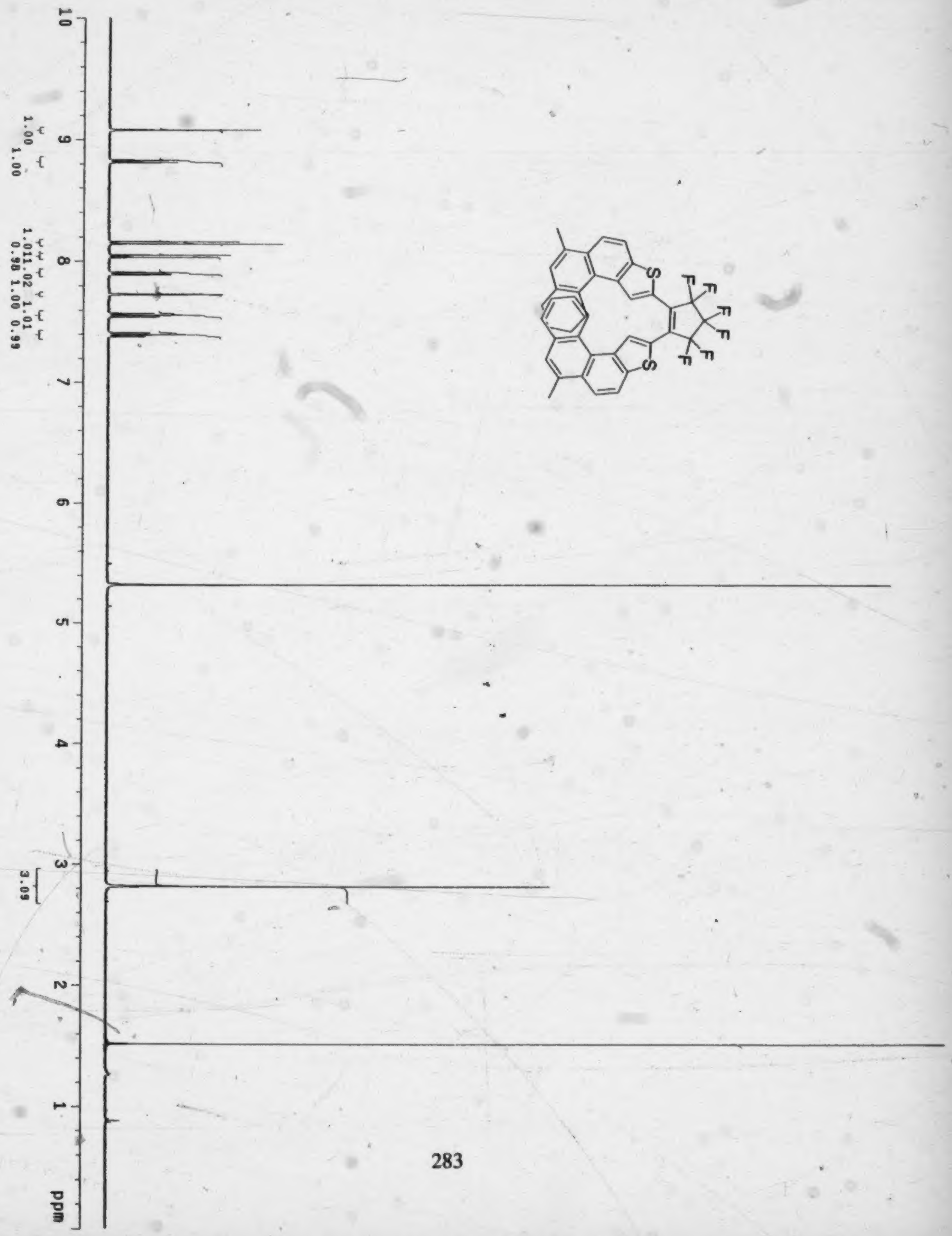
10
9
8
7
6
5
4
3
2
1
ppm
1.00
1.00
1.01
1.02
1.01
0.98
1.00
0.99
3.09
S
S
F
F
F
F
F
F

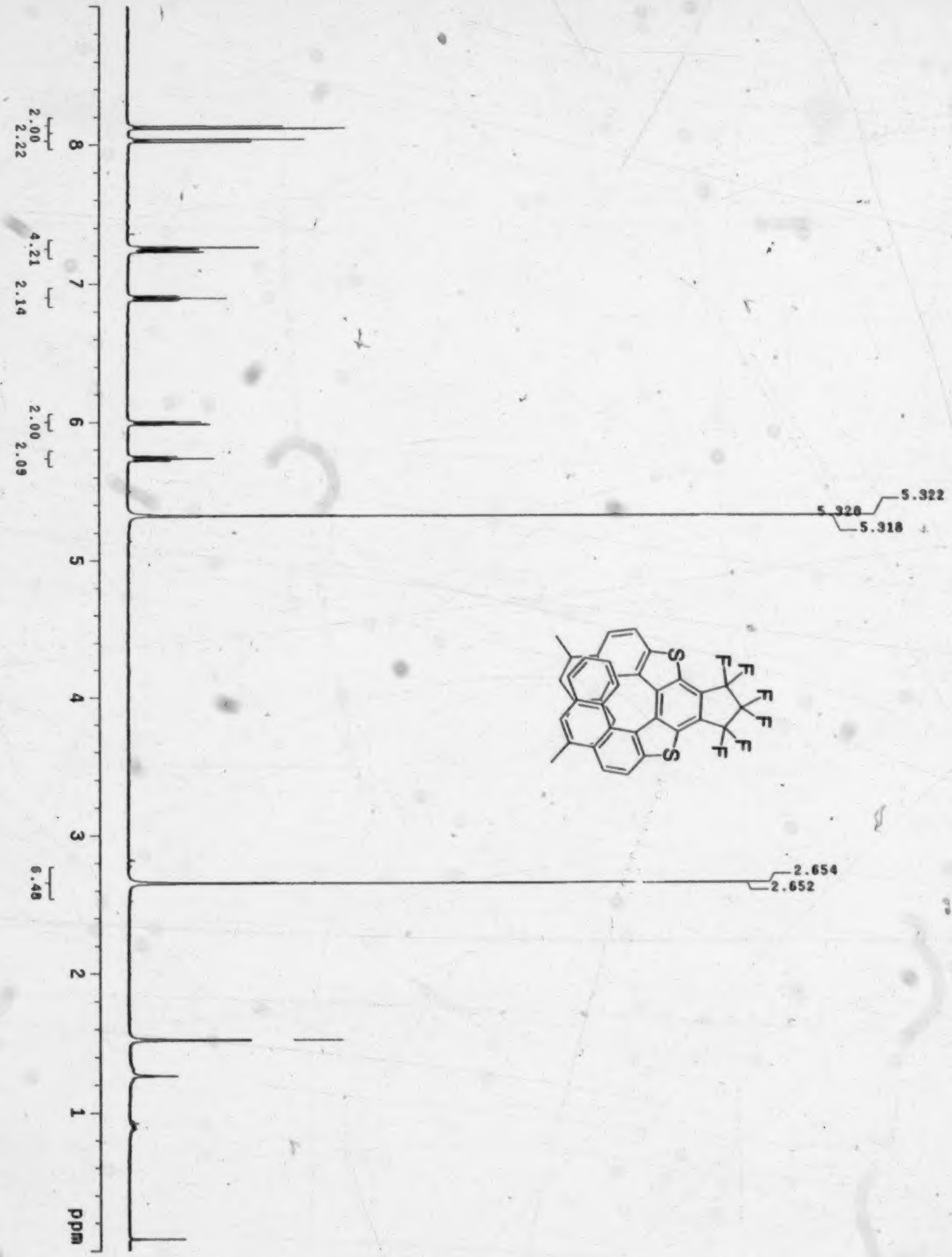
2.00
2.22
4.21
2.14
2.00
2.09
6.48
8
7
6
5
4
3
2
1
ppm
5.322
5.320
5.318
2.654
2.652
S
S
F
F
F
F
F
F

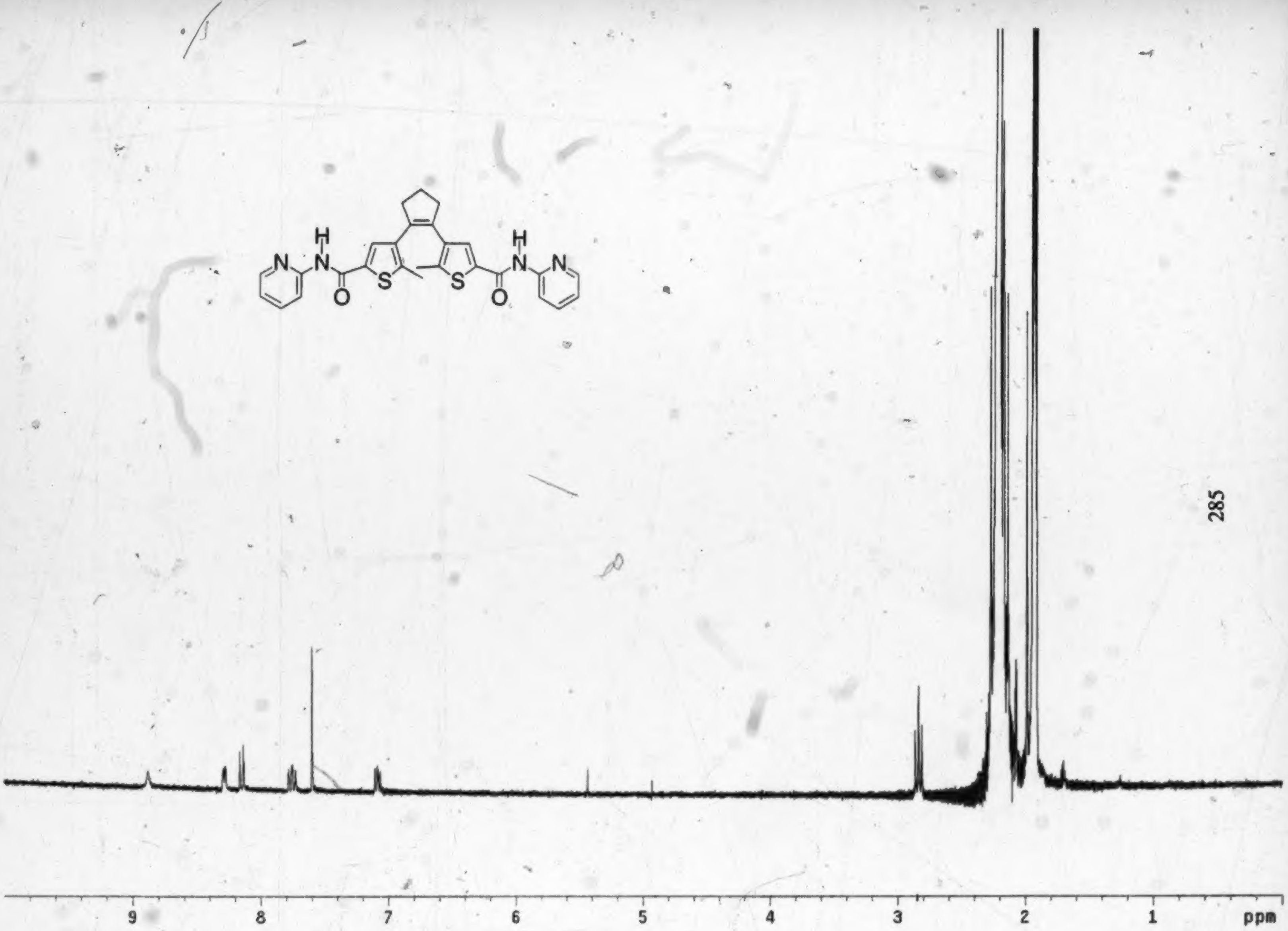

N
H
N
O
S
S
O
H
N
N
9
8
7
6
5
4
3
2
1
ppm

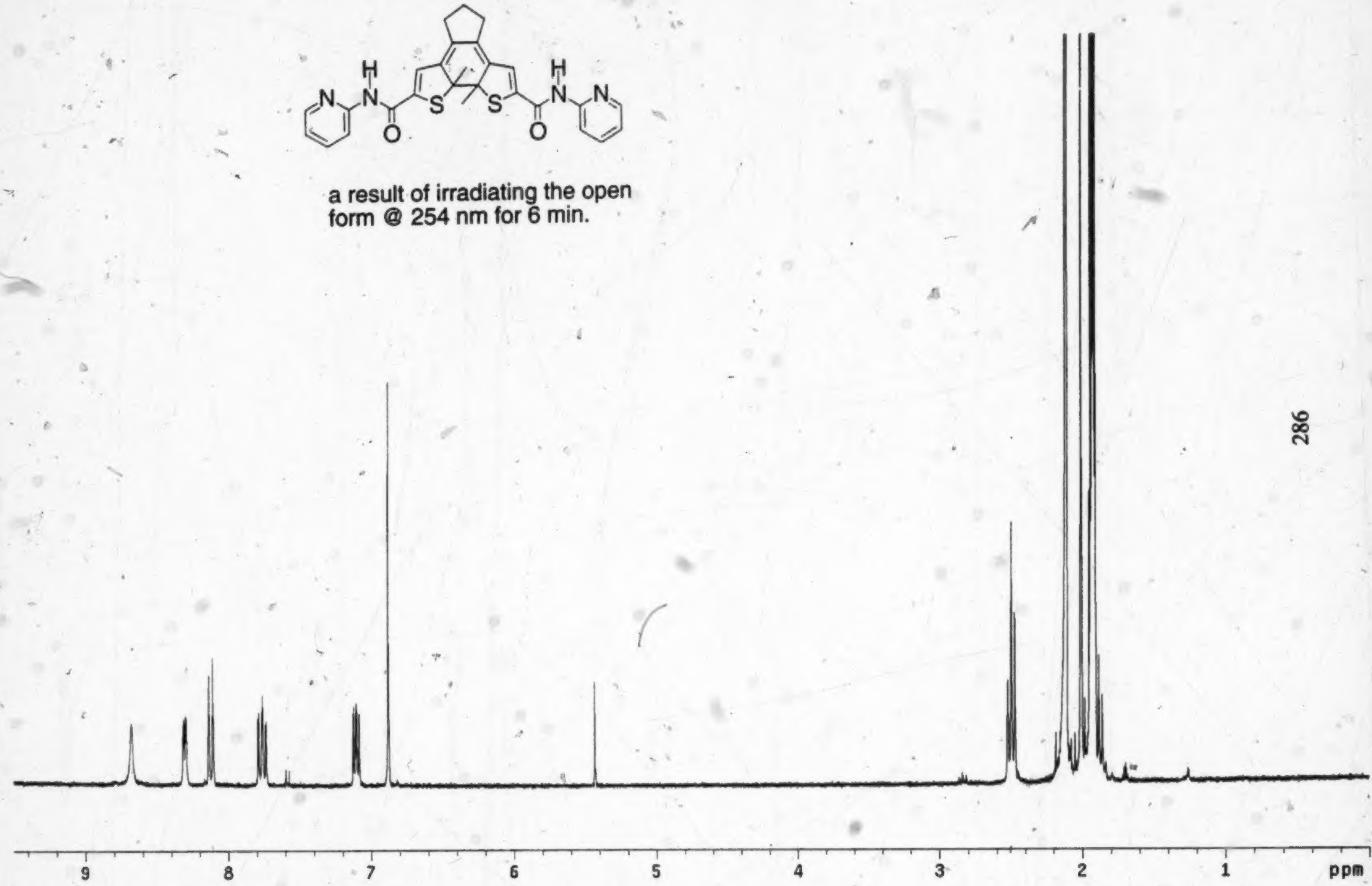

a result of irradiating the open
form @ 254 nm for 6 min.

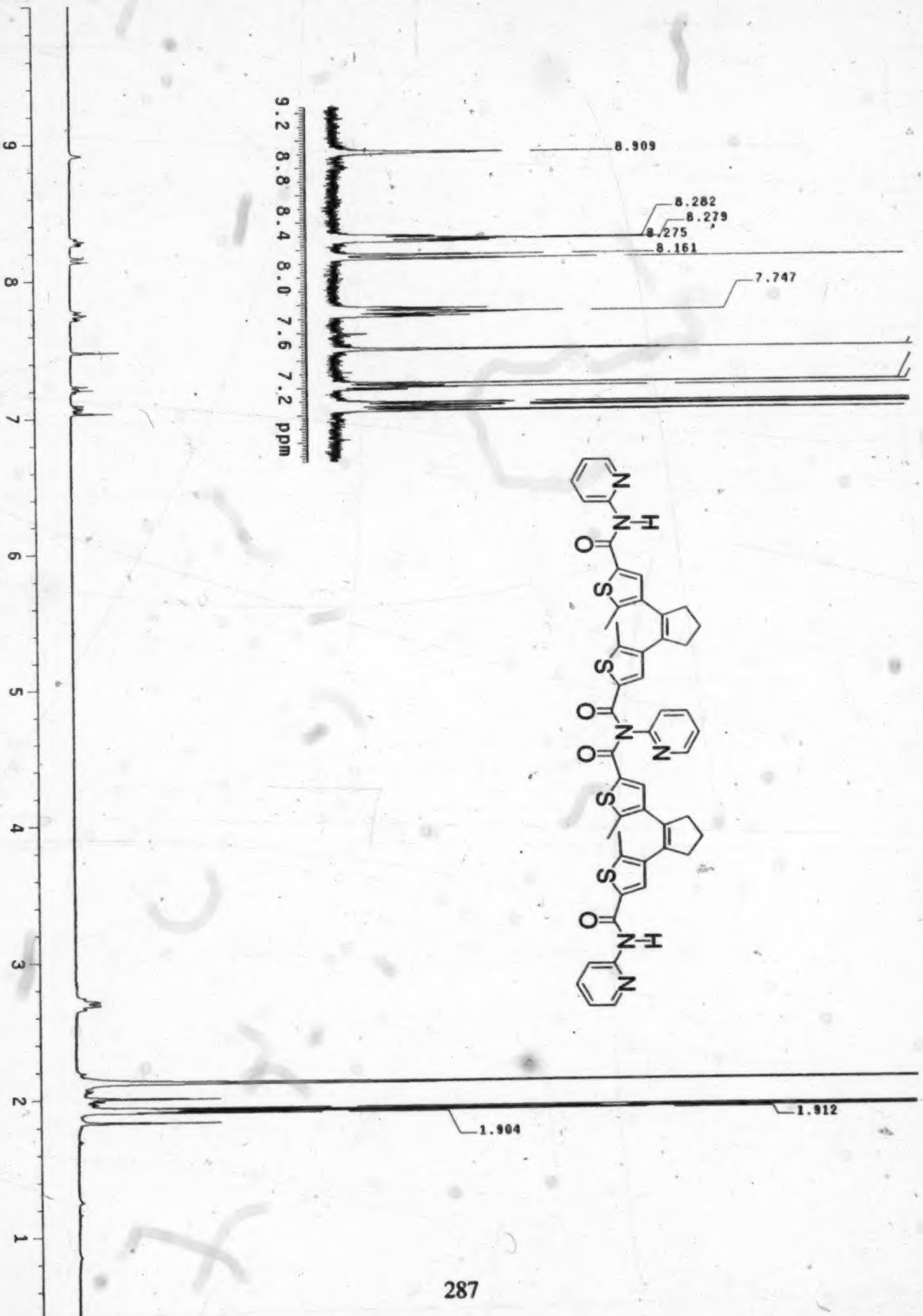
8.909
8.282
8.279
8.275
8.161
7.747
9.2 8.8 8.4 8.0 7.6 7.2 ppm
1.912
1.904
9
8
7
6
5
4
3
2
1
ppm
N
H
O
S

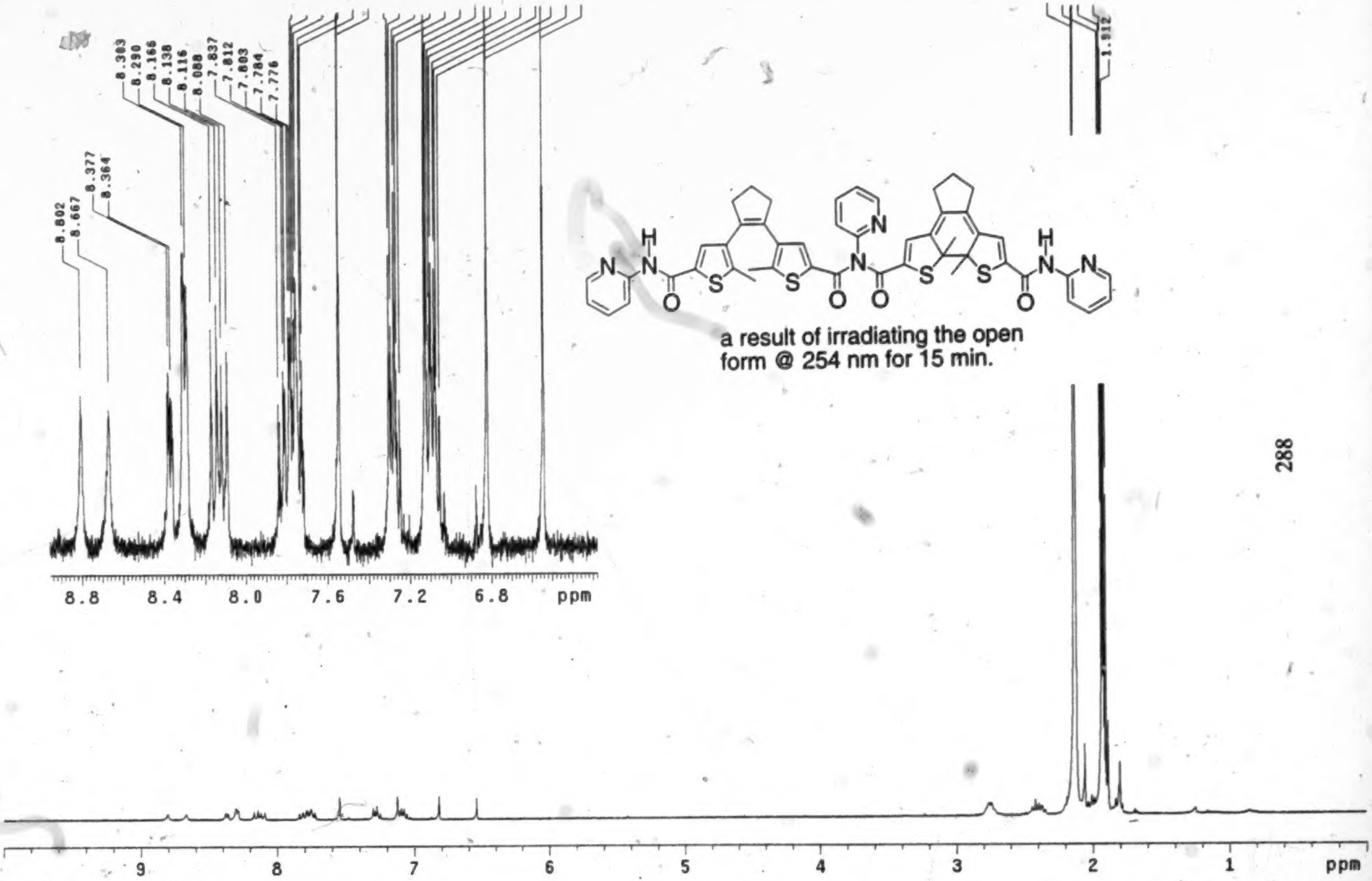

a result of irradiating the open form @ 254 nm for 15 min.

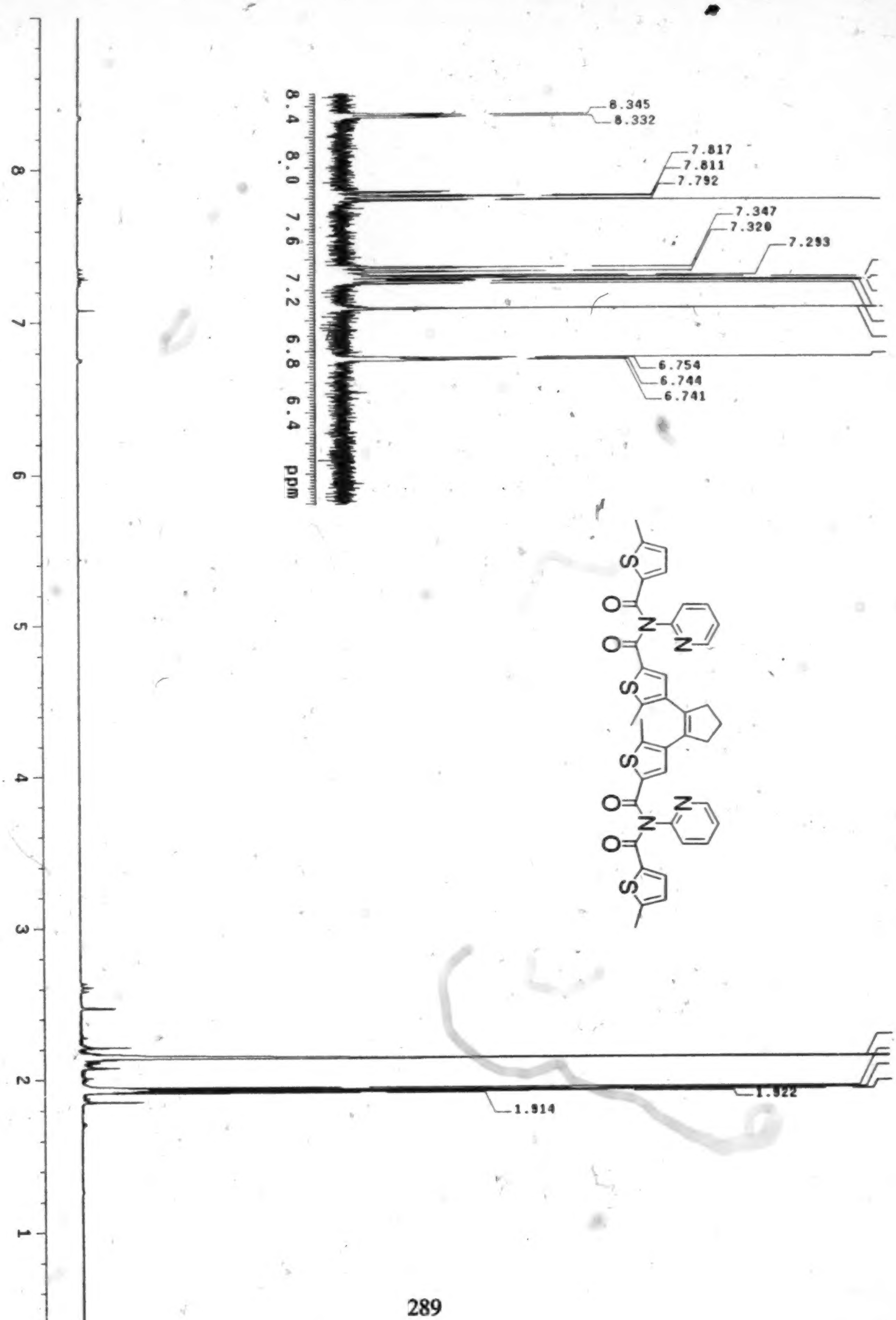
8.345
8.332
7.817
7.811
7.792
7.347
7.320
7.293
6.754
6.744
6.741
8.4
8.0
7.6
7.2
6.8
6.4
ppm
S
O
N
1.914
1.922
8
7
6
5
4
3
2
1
ppm

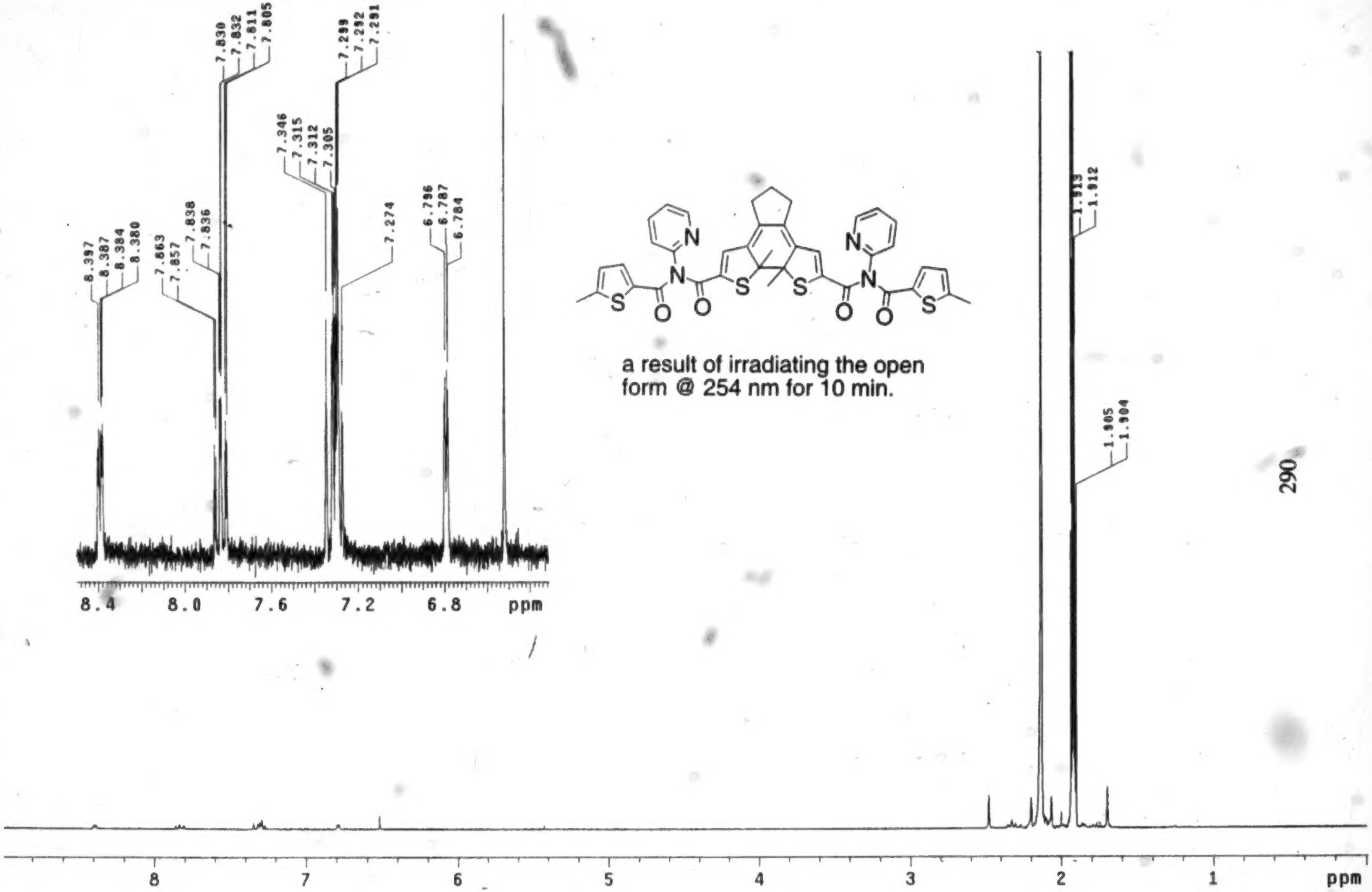

a result of irradiating the open form @ 254 nm for 10 min.

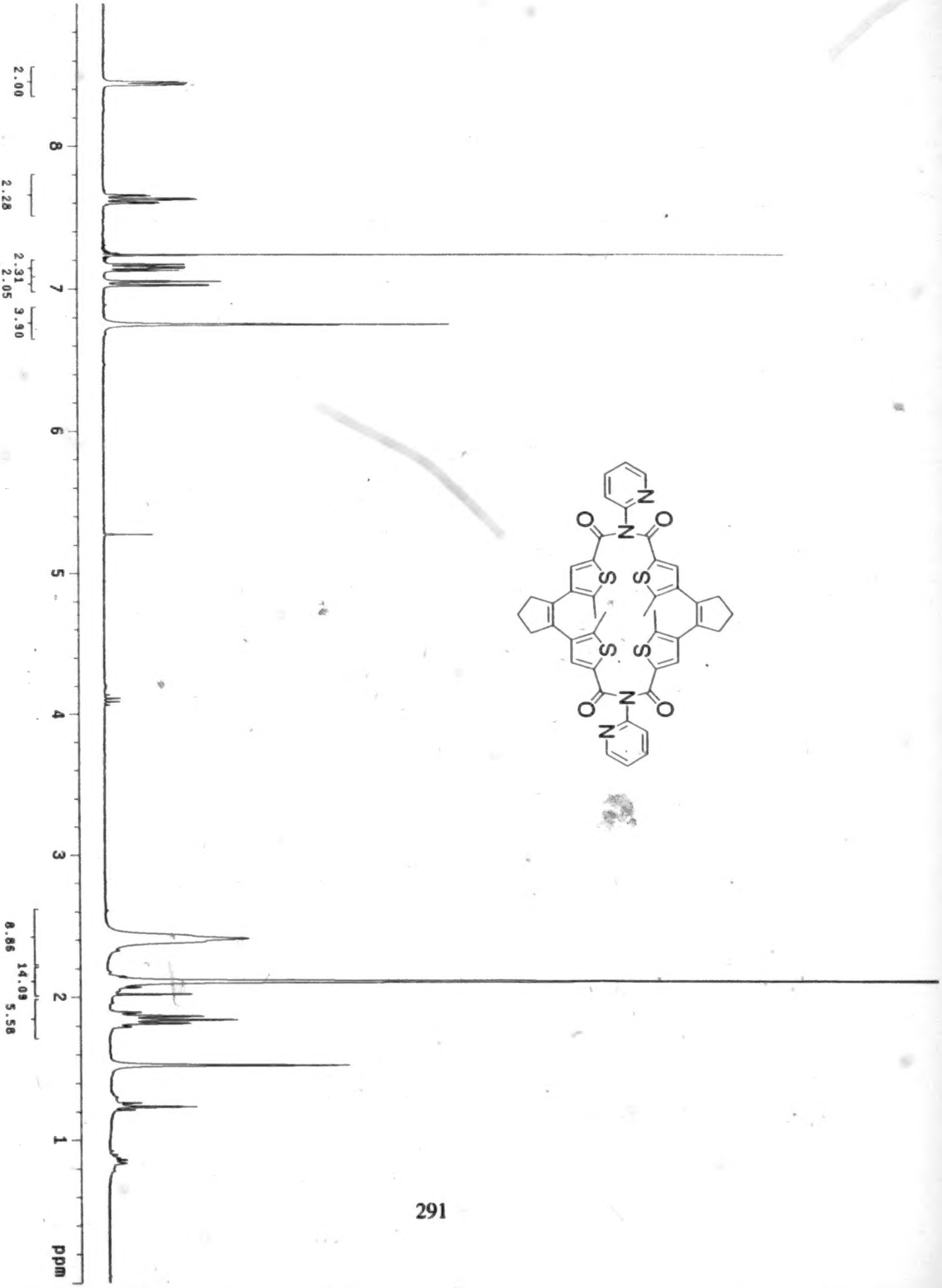

2.00
2.28
2.31
2.05
3.90
8.86
14.09
5.58
8
7
6
5
4
3
2
1
ppm
N
O
S

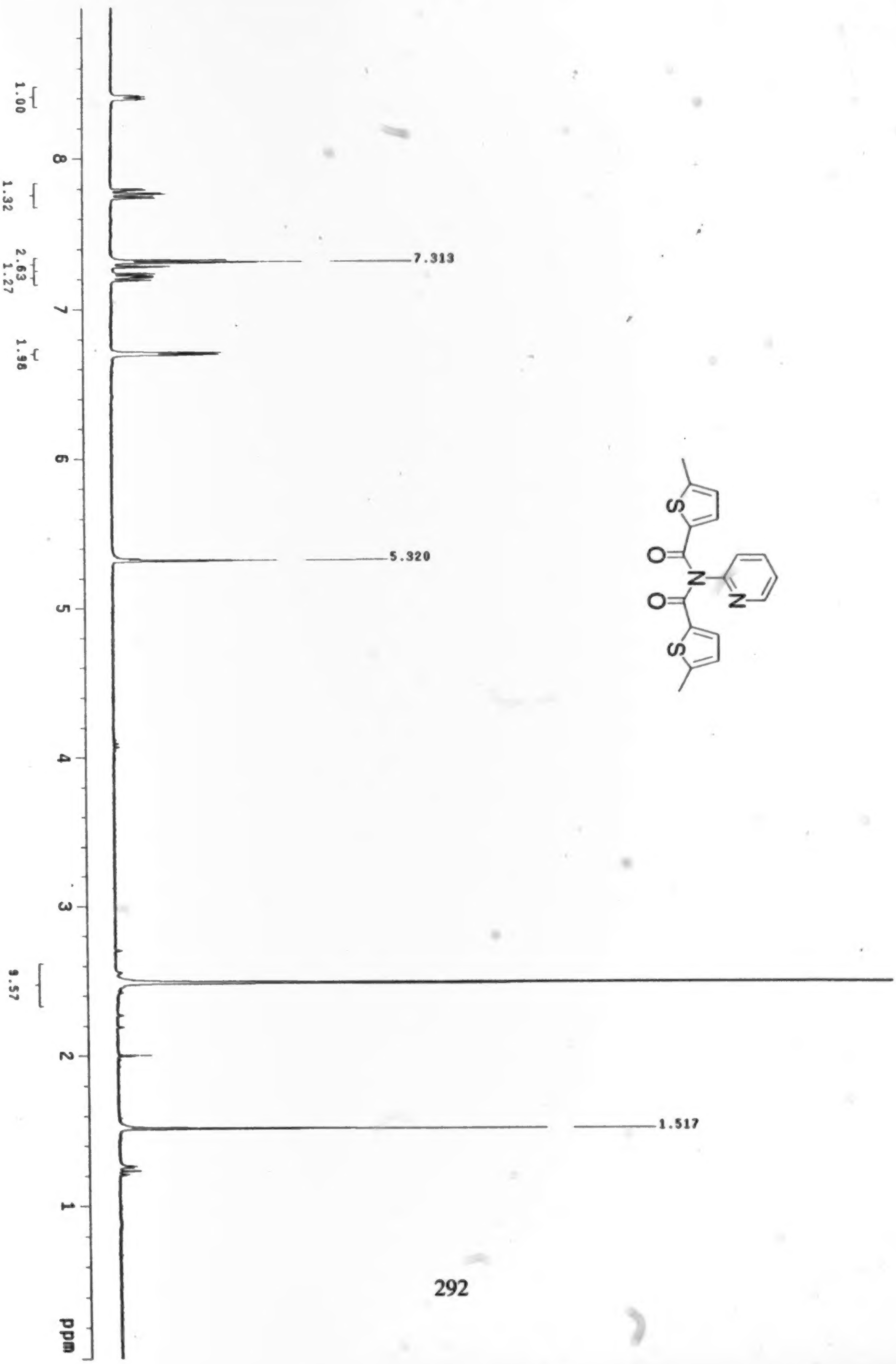
1.00
1.32
2.63
1.27
1.98
9.57
7.313
5.320
1.517
8
7
6
5
4
3
2
1
ppm
S
O
N
O
N
S

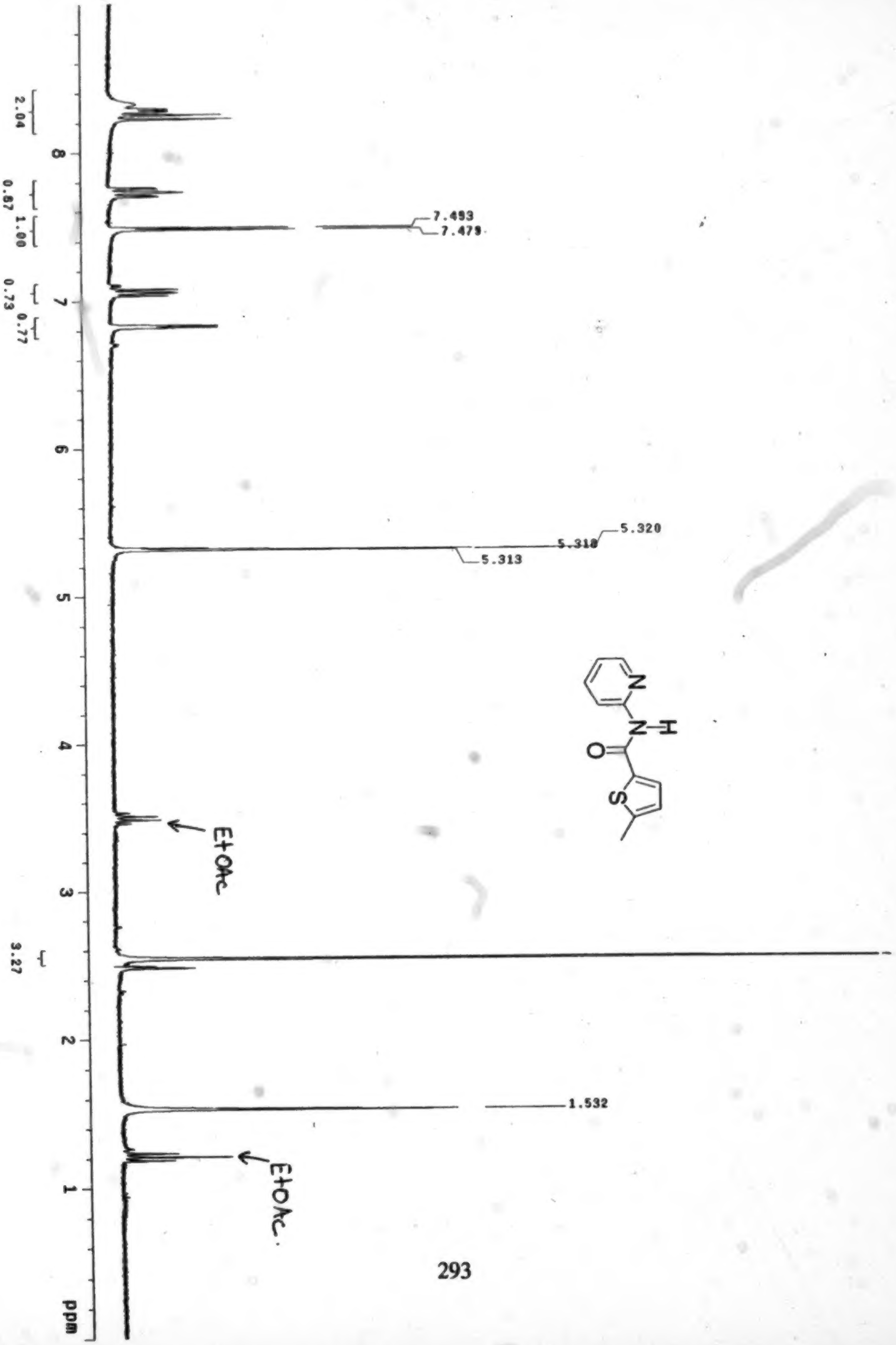
2.04
0.87
1.00
0.73
0.77
3.27
8
7
6
5
4
3
2
1
ppm
7.493
7.479
5.320
5.318
5.313
1.532
EtOAc
EtOAc.
N
N
H
O
S